

Analysis of protein palmitoylation in adipocytes

A thesis presented by

Martin W. Werno

In fulfilment of the requirement for the degree of

Doctor of Philosophy

2014

University of Strathclyde

Strathclyde Institute of Pharmacy and Biomedical Sciences

Declaration of Authenticity and Author's Rights:

This thesis is the result of the author's original research. It has been composed by the author and has not been previously submitted for examination which has led to the award of a degree.

The copyright of this thesis belongs to the author under the terms of the United Kingdom Copyright Acts as qualified by University of Strathclyde Regulation 3.50. Due acknowledgement must always be made of the use of any material contained in, or derived from, this thesis.

Signed:

Date:

Acknowledgments

First and foremost I would like to thank my first supervisor Dr. Luke H. Chamberlain for providing me with the opportunity to work in his fabulous group. Luke, I simply could not have imagined any better supervision. You were always very good to approach and 100% supportive, and at the same time you gave me all the freedom I needed to develop own ideas and interests. I was able to learn very much from you and this would help me for the rest of my career. All over it was an absolutely pleasant experience and my very pleasure to work with you.

I would like to thank all members of the Chamberlain group, for creating a warm, friendly and inspiring atmosphere at work. Thank you Cinta Diez-Ardanuy, Christine Salaun, Jennifer Greaves, Kimon Lemonidis, Maria Sanchez-Perez and Oforiwa Gorleku for not only being colleagues but good friends, for sharing your expertise, for supporting me wherever you could and for the countless good conversations that made me laugh very hard or enriched my understanding of life.

I would also like to thank Prof. Michael J. Shipston and Heather McClafferty from the Centre for Integrative Physiology of the University of Edinburgh for the fruitful and friendly collaboration during the first year of my PhD.

At this occasion I would also like to thank Dr. Edmond Chan who was my second supervisor and provided excellent consultation with his expertise whenever needed.

During my time in Glasgow I encountered many nice and truthful people. Especially within the SIPBS community I found friends, which were not only an endless source of high quality entertainment but also proved themselves as true helpers and supporters in many situation of life. Thank you SIPBS and particularly Alasdair Henry, Leon Williamson, Mark MacAskill, Serge Moudio and Thomas Harwood for being such decent mates and introducing me to Scottish culture so well.

I also want to thank the entire Bellahouston Judo Club for countless brilliant Judo-moments and socials and especially Eric Kane for teaching me to relax.

As well, I would like to thank Samira Barazi for accompanying me for 3 years of my life and helping me back on my feet during difficult times of injury and surgery.

I would not be the person I am today without the support and influence of my dear friends that I know almost the half of my life now. They have always been there for me; they have listened to what I had to say, encouraged me and gave the best possible advice. Thank you, Alexander Zeller, Benedikt Götsch, Holger Funk, Konstanze Gebauer, Maciej Zwoliński, Natalia Zwolińska, Nico Kolesnikow, Peter Straka, Simon Zydek and Van An Du for the very good times together.

And finally I want to thank my immediate family for being the best Brother, Mum and Dad ever possible. Mum and Dad you have provided a harmonic and loving environment I had the pleasure to grow up in, in which I could develop my character, interests and evolve my personal strengths. Without all your endless love and support I would certainly not be where I am now. Dziękuję Wam kolejny raz.

I dedicate this thesis to all of you.

Joy and love only become real when shared.

Poster communications

Protein Acylation: from Mechanism to Drug Discovery, 10-12th September 2014. Martin W. Werno and Luke H. Chamberlain. Investigating the Role of Palmitoylation in Insulin Action. Appendix I

Diabetes UK Professional Conference 2014, 5-7th March 2014. Martin W. Werno and Luke H. Chamberlain. Investigating the Role of Palmitoylation in Insulin Action. Appendix II

Diabetes UK Professional Conference 2013, 13-15th March 2013. Martin W. Werno, Kimon Lemonidis, Heather McClafferty, Michael J. Shipston and Luke H. Chamberlain. Investigating the Role of Palmitoylation in Insulin Action. Appendix III

Regulation of protein trafficking and function by palmitoylation, 23-25th August 2012. Martin W. Werno, Heather McClafferty, Michael J. Shipston and Luke H. Chamberlain. Investigating the Role of Palmitoylation in Insulin Action. Appendix IV

Table of Contents

Acknowledgments.....	II
Poster communications	IV
List of Figures	X
List of Tables.....	XIV
List of Abbreviations	XVI
Abstract	XX
Chapter 1: Introduction.....	1
1.1 Glucose and glucose homeostasis	1
1.2 Glucose transporters.....	5
1.3 Insulin and the insulin receptor	8
1.3.1 Insulin	8
1.3.2 Insulin receptor (IR).....	9
1.4 Vesicle trafficking	11
1.5 Insulin and GLUT4 translocation	14
1.5.1 Endocytosis of GLUT4.....	17
1.6 Insulin-responsive aminopeptidase (IRAP)	19
1.7 Diabetes mellitus.....	21
1.8 Caveolae and caveolins	24
1.8.1 Caveolae	24
1.8.2 Caveolin-1.....	26
1.8.3 Caveolin-2.....	29
1.8.4 Caveolin-3.....	30
1.8.5 Cavins	31
1.8.6 Biogenesis of Caveolae.....	32
1.9 Caveolae and insulin signalling	35
1.10 Palmitoylation	37
1.10.1 zDHHC Palmitoyltransferases (PATs)	39

1.11 Potential role of palmitoylation in insulin signalling	41
1.12 Aims of this study	43
Chapter 2: Materials and Methods	44
2.1 Materials	44
2.1.1 Chemicals	44
2.1.2 Molecular biology reagents	44
2.1.3 Primers	45
2.1.4 Plasmids	47
2.1.5 Electrophoresis and western blot equipment	48
2.1.6 Cell culture plastics and media	48
2.1.7 Antibodies	48
2.1.8 Mammalian cell lines	50
2.2 Mammalian cell culture	50
2.2.1 Culturing 3T3-L1 pre-adipocytes.....	50
2.2.2 Differentiation of 3T3-L1 pre-adipocytes into adipocytes.....	51
2.2.3 Harvesting pre-adipocytes and adipocytes.....	51
2.2.4 Culturing of HEK293T cells	52
2.2.5 Plasmid DNA transfection into mammalian cells.....	52
2.2.6 Harvesting transfected cells for SDS-PAGE	52
2.2.7 Cell fixation and mounting onto microscope slides.....	53
2.3 Molecular Biology	53
2.3.1 Standard molecular biology protocols	53
2.3.2 DNA amplification by polymerase chain reaction (PCR).....	53
2.3.3 Site-directed mutagenesis (SDM)	54
2.3.4 RNA purification	55
2.3.5 Spectrophotometric quantification of DNA and RNA.....	56
2.3.6 Agarose gel electrophoresis.....	56
2.3.7 DNA purification from agarose gels	56

2.3.8 Assessing integrity of purified RNA.....	57
2.3.9 Restriction endonuclease digestion.....	57
2.3.10 Ligation of DNA inserts with plasmid vectors.....	58
2.3.11 Transformation of expression plasmid DNA into One Shot® TOP10 cells	58
2.3.12 Small-scale (miniprep) plasmid purification.....	58
2.3.13 DNA sequencing.....	59
2.3.14 Large scale (maxiprep) plasmid purification.....	59
2.3.15 Reverse transcription of RNA into cDNA.....	59
2.3.16 Quantitative real-time PCR (qPCR).....	60
2.3.17 PCR amplification of targeted protein cDNA and cloning into plasmid expression vector.....	62
2.4 Protein Biochemistry.....	66
2.4.1 Identification of palmitoylated proteins using resin-assisted capture of S- acylated proteins (acyl-RAC).	66
2.4.2 Detection of 17-octadecynoic acid (17ODYA) attachment onto proteins using “Click-Chemistry”.....	68
2.4.2 Sodium dodecyl sulphate polyacrylamide gel electrophoresis (SDS-PAGE)	71
2.4.3 Western blotting.....	72
2.4.4 Isolation of Triton X-100-insoluble membrane fractions.....	73
2.4.5 Comparing protein expression level of proteins in between different cell types.....	74
2.4.6 Blue native polyacrylamide gel electrophoresis (blue native PAGE).....	74
2.4.7 Surface trypsin-digest of membrane-bound proteins.	76
2.5 Confocal Microscopy.....	76
2.5.1 Fixing HEK293T cells on coverslips.....	77
2.5.2 Fixing 3T3-L1 adipocytes on coverslips.....	77
2.5.3 Immunocytochemistry with HEK293T cells and 3T3-L1 Adipocytes.....	78

2.5.4 Mounting coverslips on microscopy slides using ProLong® Gold Antifade Mountant with DAPI	79
2.5.5 Recording images using the confocal microscopy system.....	79
2.6 Brightfield microscopy	80
2.7 Data analysis.....	80
Chapter 3: Isolation and characterisation of the palmitoylome in 3T3-L1 adipocytes.	81
3.1 Introduction	81
3.2 Differentiation of 3T3-L1 adipocytes	82
3.3 Identification of palmitoylated proteins in 3T3-L1 adipocytes using acyl-RAC85	
3.4 Quantification of the palmitoylation levels of identified proteins	88
3.6 Protein palmitoylation following chronic insulin treatment and changes in extracellular glucose concentration.....	91
3.7 Discussion.....	95
Chapter 4: Palmitoylation of the insulin-responsive aminopeptidase IRAP: Identification of palmitoylation sites and analysis of the effect of palmitoylation on intracellular targeting.....	103
4.1 Introduction	103
4.2 Identification of palmitoylated cysteine residues in IRAP	105
4.4 Investigating the effect of palmitoylation on the intracellular localisation of IRAP	111
4.5 Discussion.....	117
Chapter 5: Characterisation of palmitoylation of caveolin-2.	124
5.1 Introduction	124
5.2 Localisation of caveolin-1 and caveolin-2 in mature 3T3-L1 adipocytes.	126
5.3 Palmitoylation of caveolin-2	129
5.4 Identification of the palmitoylation sites in caveolin-2	135
5.5 Effect of palmitoylation on caveolin-2 localisation.....	136

5.5.3 Investigating partitioning of caveolin-1 and caveolin-2 cysteine to alanine mutants into Triton X-100-insoluble membrane microdomains.	142
5.6 Effect of palmitoylation on oligomerisation of caveolin-2.	145
5.6.1 Formation of SDS-resistant oligomers of caveolin-2.	145
5.6.2 Examination of caveolin-2 oligomer formation using blue native PAGE.	147
5.7 Discussion.....	150
Chapter 6: Characterisation of zDHHC enzyme expression profile in the 3T3-L1 cell line and the interaction of zDHHCs with IRAP.	159
6.1 Introduction	159
6.2 Characterisation of zDHHC enzyme expression in the 3T3-L1 cell line	160
6.3 Effect of zDHHC family proteins on IRAP palmitoylation.....	166
6.4 Interaction of IRAP with selected zDHHC enzymes.	170
6.5 Discussion.....	172
Chapter 7: General discussion	179
Chapter 8: References.....	188
Appendices.....	220

List of Figures

Chapter 1

Figure 1.1. Glucose homeostasis	4
Figure 1.2. Insulin-stimulated GLUT4 translocation in adipocytes.....	18
Figure 1.3. Alignment of the amino acid sequences of the caveolin protein family.....	28
Figure 1.4. Formation of caveolae.	34

Chapter 3

Figure 3.1. Differentiation of 3T3-L1 pre-adipocytes into adipocytes.	83
Figure 3.2. Protein expression level of GLUT4 and insulin receptor throughout the differentiation of 3T3-L1 pre-adipocytes in adipocytes.	85
Figure 3.3. Outline of the acyl-RAC procedure to isolate palmitoylated proteins.	86
Figure 3.4. Immunoblotting analysis of acyl-RAC fractions prepared from 3T3L1adipocytes.	87
Figure 3.5. Quantification of 3T3-L1 adipocyte proteins recovered in acyl-RAC fractions.	89
Figure 3.6. Pro-insulin receptor and IR β levels in 3T3-L1 adipocytes treated with varying glucose and insulin concentrations in the culture medium.	92
Figure 3.7. Immunoblotting analysis of acyl-RAC fractions prepared from 3T3-L1 adipocytes treated with insulin and different glucose concentrations.	94
Figure 3.8. Quantification of 3T3-L1 adipocyte proteins recovered in acyl-RAC fractions following cell treatment with different glucose and insulin concentrations.	95

Chapter 4

Figure 4.1.	2D membrane topology of IRAP.	105
Figure 4.2.	Analysis of acyl-RAC fractions prepared from homogenised mouse brain by immunoblotting.	107
Figure 4.3.	Outline of the Click-Chemistry method to detect attachment of 17ODYA onto cysteine residues of proteins.	108
Figure 4.4.	Detection of incorporation of 17ODYA into IRAP constructs in HEK293T cells.	110
Figure 4.5.	Protein stability of IRAP wild type and cysteine to alanine mutants.	112
Figure 4.6.	Analysis of the localisation of IRAP constructs in HEK293T cells using confocal microscopy.	113
Figure 4.7.	Schematic illustration of surface trypsin -digest experiment.....	115
Figure 4.8.	Surface trypsin-digest of IRAP wild type and IRAP 3CA mutant in HEK293T cells..	116

Chapter 5

Figure 5.1.	Localisation of caveolin-1 and -2 isoforms in mature 3T3-L1 adipocytes.	127
Figure 5.2.	Analysis of the co-distribution of caveolin-1 and -2 with Golgi and TGN proteins.	128
Figure 5.3.	2D membrane topology of caveolin-2.	130
Figure 5.4.	Alignment of amino acid sequence of the caveolin protein family.	131
Figure 5.5.	Detection of incorporation of 17ODYA into caveolin-2 constructs in HEK293T cells using click-chemistry.....	132
Figure 5.6.	Incorporation of 17ODYA into caveolin-2 constructs in HEK293T cells detected by click-chemistry combined with immunoprecipitation.	134
Figure 5.7.	Incorporation of 17-ODYA into cysteine to alanine mutants of caveolin-2 in HEK293T cells.....	136

Figure 5.8. Analysis of endogenously expressed caveolin isoforms in HEK293T cells and 3T3-L1 adipocytes.	138
Figure 5.9. Analysis of the localisation of caveolin-2 EGFP fusion proteins in HEK293T cells co-transfected with mCherry caveolin constructs.	139
Figure 5.10. Analysis of localisation of caveolin-2-EGFP WT and 4CA mutant in HEK293T and HeLa cells using confocal microscopy.....	141
Figure 5.11 Isolation of TritonX-100-insoluble fraction from HEK293T cells transfected with caveolin wild type and cysteine-to-alanine mutants.	143
Figure 5.12. Quantification of caveolin-1 and caveolin-2 wild type and cysteine to alanine mutants in Triton X-100-soluble and insoluble fractions in HEK293T cells.	144
Figure 5.13. SDS-PAGE analysis of Triton X-100 soluble and insoluble fractions isolated from HEK293T cells transfected with caveolin-2 constructs.	146
Figure 5.14. Analysis of oligomeric assemblies of caveolin-2 EGFP in HEK293T cells by Blue native PAGE..	149

Chapter 6

Figure 6.1. Analysis of the integrity of total RNA purified from 3T3-L1 pre-adipocytes and adipocytes.....	161
Figure 6.2. Difference in mRNA expression of possible reference genes in 3T3-L1 pre-adipocytes and adipocytes..	162
Figure 6.3. zDHHC mRNA expression profile of 3T3-L1 adipocytes.....	163
Figure 6.4. zDHHC and APT mRNA expression in 3T3-L1 adipocytes relative to 3T3-L1 pre-adipocytes.....	165
Figure 6.5. Effect of zDHHC enzyme co-expression on the incorporation of 17ODYA into IRAP..	167
Figure 6.6. Quantification of incorporation of 17ODYA into IRAP co-expressed with the indicated zDHHCs in HEK293T cells.	169

Figure 6.7. SDS-PAGE analysis of HEK293T cells co-transfected with HA-tagged IRAP constructs and HA-tagged zDHHC7 constructs. 171

List of Tables

Chapter 1

Table 1.1.	Summary of classification and tissue-specific expression of GLUT isoforms.....	7
------------	--	---

Chapter 2

Table 2.1.	Oligonucleotide primers (5'->3') used for amplification of GLUT1 and GLUT4 isoforms from 3T3-L1 adipocyte and mouse brain cDNA.	45
Table 2.2.	Oligonucleotide primers (5'->3') for quantitative real-time PCR (qPCR) from 3T3-L1 pre-adipocyte and adipocyte cDNA.....	45
Table 2.3.	QuantiTect Primer Assay for qPCR with 3T3-L1 pre-adipocyte and adipocyte cDNA.....	46
Table 2.4.	Oligonucleotide primers (5'->3') for site directed mutagenesis (SDM) to mutate cysteine residues into alanine residues in N-terminal triple HA tagged IRAP-wild type EGFP-N1 expression vector.	46
Table 2.5.	Oligonucleotide primers (5'->3') used to replace the triple HA-tag in the IRAP-wild type EGFP-N1 expression vector with a single N-terminal Myc-tag.....	46
Table 2.6.	Oligonucleotide primers (5'->3') for SDM to mutate cysteine residues into alanine residues in the caveolin-2-EGFP-N1 expression vector.	47

Chapter 3

Table 3.1.	CSS-Palm prediction of palmitoylation sites of examined proteins.	90
------------	--	----

Chapter 4

Table 4.1.	CSS-Palm prediction of palmitoylation sites of IRAP	106
------------	---	-----

Chapter 5

Table 5.1	CSS-Palm prediction of palmitoylation sites for caveolin-2.....	130
-----------	---	-----

Chapter 6

Table 6.1. zDHHC enzyme molecular mass sizes according to UniProt..... 168

List of Abbreviations

17ODYA	17-octadecynoic acid
acyl-RAC	resin-assisted capture of S-acylated proteins
ANOVA	one-way analysis of variance
AP2	adaptor protein 2
APT	acyl-protein-thioesterase
Arp-3	actin related protein-3
AS160	AKT substrate 160
ATP	adenosine triphosphate
AU	arbitrary unit
BK	large conductance potassium
Blue native PAGE	blue native polyacrylamide gel electrophoresis
BSA	bovine serum albumin
CAP	c-CBL associated protein
c-CBL	proto-oncogene-c-CBL
CDP138	138 kDa C2 domain-containing phosphoprotein
CNS	central nervous system
CO ₂	carbon dioxide
CSP	cysteine-string protein
DAPI	4',6-Diamidino-2-Phenylindole
DEPC	diethylpyrocarbonate
DMEM	Dulbecco's Modified Eagle Medium
DNA	desoxyribonucleic acid
DTT	dithiothreitol
ECL	enhanced chemiluminescence
EDTA	ethylenediaminetetraacetic acid
ER	endoplasmic reticulum
Fbox	F-box and leucine-rich repeat protein-10
FFA	free fatty acid

FRT	Fisher Rat Thyroid
GAP	GTPase-activating protein
GAPDH	glyceraldehyde 3-phosphate dehydrogenase
GDP	guanosine diphosphate
GEF	guanosine nucleotide exchange factor
GIP	gastric inhibitory peptide
GLP-1	glucagon-like peptide-1
GLUT	facilitative glucose transporters
GM130	cis-Golgi matrix protein 130
GSV	GLUT4 storage vesicle
GTP	guanosine triphosphate
H ₂ O	water
HA	hydroxylamine
HC	heavy chain
HMG	high-mobility group
HMIT	H ⁺ /myo-inositol transporter
HRP	horseradish peroxidase
IBMX	3-isobutyl-1-methylxanthine
IGF	insulin-like growth factor
IPO8	importin 8
IR	insulin receptor
IRAP	Insulin-responsive aminopeptidase
IRS	Insulin receptor substrate
IRβ	Insulin receptor β subunit
LRP6	lipoprotein receptor-related proteins 6
M-MLV RT	Moloney Murine Leukemia Virus Reverse Transcriptase
MDCK	Madin-Darby canine kidney
MMTS	S-methyl methanethiosulfonate
mRNA	messenger RNA
mTORC2	mammalian target of rapamycin complex 2

Munc	mammalian homolog of Unc
MURC	muscle-restricted coiled-coil protein
Na ⁺	sodium ions
NEFA	non-esterified fatty acids
NSF	N-ethylmaleimide-sensitive factor
N-WASP	neural Wiskott-Aldrich syndrome protein
PARP	poly-ADP-ribose polymerase
PARsylation	attachment of poly ADP ribose
PATs	palmitoyl transferases
PBS	phosphate buffered saline
PCR	polymerase chain reaction
PK1	3-phosphoinositide dependent protein kinase-1
PEG	polyethylene glycol
PI3K	phosphatidylinositol 3-kinase
PIP2	phosphatidylinositol 4, 5 bisphosphate
PIP3	phosphatidylinositol 3, 4, 5 trisphosphate
PKB	protein kinase B
P-LAP	oxytocinase/placental leucine aminopeptidase
PM	plasma membrane
PMT	photo tube
PPAR	peroxisome proliferator-activated receptor
Ppia	peptidylprolyl isomerase A
PSD-95	postsynaptic density protein-95
PTM	post-translational modification
PTRF	polymerase I and transcript release factor
PVDF	polyvinylidene difluoride
qPCR	quantitative real-time PCR
RNA	ribonucleic acid
ROS	reactive oxygen species
SDM	site-directed mutagenesis

SDS	sodium dodecyl sulphate
SDS-PAGE	sodium dodecyl sulphate polyacrylamide gel electrophoresis
SEM	standard error of the mean
SH	Src homology
SNARE	soluble NSF attachment protein receptor
SRBC	sdr-related gene product that binds to c-kinase
STREX	stress-regulated exon
SVI	Scientific Volume Imaging
TBTA	tris(benzyltriazolylmethyl)amine
TGN	trans-Golgi-network
TKR	tyrosine kinase receptor
TMD	transmembrane domain
VAMP	vesicle-associated membrane protein
VIP21	vesicular integral-membrane protein of 21 kDa
vp165	vesicle protein of 165 kDa
VSV-G	G protein of vesicular stomatitis virus

Abstract

Blood glucose homeostasis is highly regulated and is essential for survival. A key process is the insulin-stimulated recruitment of the facilitative glucose transporter GLUT4 to the plasma membrane in adipocytes and muscle cells; defects in this pathway can cause insulin resistance and type 2 diabetes. The insulin signalling and GLUT4 trafficking pathways in these cells have been extensively characterised, and a prominent role for protein phosphorylation has been uncovered. In contrast, relatively little is known about the role of other post-translational modifications (PTMs) in these pathways. The aim of this study was to expand existing knowledge of how palmitoylation, a PTM involving reversible attachment of fatty acids onto cysteine residues, affects components of the insulin signalling and GLUT4 trafficking pathways. For this, palmitoylated proteins were isolated from 3T3-L1 adipocytes by resin-assisted capture of S-acylated proteins (acyl-RAC), and screened to identify novel palmitoylated components of the insulin signalling and GLUT4 trafficking pathways. This approach successfully identified the following novel palmitoylated proteins: GLUT4, insulin-responsive aminopeptidase (IRAP) and caveolin-2. Furthermore, click-chemistry confirmed palmitoylation of caveolin-2 and IRAP and also enabled identification of the palmitoylation sites on these proteins.

Palmitoylation has been shown to regulate proteins in many different ways, in particular by modulating protein trafficking, protein stability and protein-protein interactions. Mutation of the palmitoylation sites in caveolin-2 and IRAP had no obvious effect on protein localisation. However, palmitoylation-deficient mutants of caveolin-2 exhibited: (i) a deficit in conversion of monomeric caveolin-2 into low molecular weight oligomeric complexes, and (ii) decreased oligomer stability, revealed by a loss of SDS-resistant caveolin-2 complexes.

Overall, this work has identified novel palmitoylated proteins in 3T3-L1 adipocytes, mapped the palmitoylation sites of these proteins, and determined the effect of this PTM on the localisation and oligomeric status of these proteins. These findings have thus expanded existing knowledge on the potential regulation of insulin signalling and GLUT4 trafficking pathways by PTMs.

Chapter 1: Introduction

1.1 Glucose and glucose homeostasis

Glucose is a hexose and an important source of energy for many eukaryotes and prokaryotes. The energy in its chemical bonds is crucial for the generation of power and warmth in organisms. Eukaryotes and prokaryotes are able to utilise the energy which is released during the oxidation process of glucose to carbon dioxide and water for synthesis of an energy storage molecule called adenosine triphosphate (ATP). A succession of biochemical processes beginning with glycolysis followed by the Krebs-Cycle and the respiratory chain oxidises one mole of glucose ($C_6H_{12}O_6$) into six moles of carbon dioxide (CO_2) and six moles of water (H_2O) to generate up to 36 mole of ATP (Madeira, 2012).

After ingestion in mammals, glucose is absorbed in the intestinal tract and circulates within blood until it is ultimately taken up by cells (Kellett and Helliwell, 2000). The concentration of glucose in the blood serum decreases during fasting and increases significantly after ingestion of carbohydrates and proteins. In order to maintain stable serum glucose levels, a signal peptide based regulatory circuit evolved with the key hormones insulin and glucagon. The process of preserving a constant glucose concentration is called glucose homeostasis and involves a complex interplay of several organs such as brain, pancreas, liver, skeletal muscle and adipose tissue, which secrete peptide hormones or respond to them or both (Jordan et al., 2010; Aronoff et al., 2004). An intact glucose regulatory circuit is able to maintain the blood glucose level between 4-6 mM through fasting and postprandial periods (American Diabetes Association, 2008). When blood glucose concentration is low, the hormone glucagon is secreted by α -cells of the pancreas and results in mobilisation of glucose reserves from liver into the bloodstream (Weir et al. 1974). On the other hand, when blood glucose levels are elevated, the hormone insulin is secreted by β -cells of the pancreas and stimulates glucose depletion from the blood

into insulin-responsive organs such as liver, muscle and adipose tissue (Levine 1981).

Blood glucose concentration below 4 mM (hypoglycaemia) or an increased concentration of above 7 mM (hyperglycaemia) can cause severe medical conditions. Therefore, mechanisms that are able to sense glucose concentration in the blood have evolved in cells of the brain and the pancreas (Oomura and Yoshimatsu, 1984; Yaney and Corkey, 2003). In the pancreas, glucose enters the insulin-secreting β -cells via a glucose-specific transporter (GLUT2) in a concentration gradient dependent manner. The intracellular rise of glucose results in an increased rate of glycolysis and is further metabolised to create ATP by oxidative phosphorylation, which increases the ratio of ATP: ADP. This in turn causes an increase in intracellular potassium due to the closure of ATP-gated potassium channels and leads to depolarisation of the β -cell. As a consequence, voltage-gated calcium channels open and calcium streams into the cell, which triggers the fusion of insulin-containing granules with the plasma membrane (PM) of the β -cell and releases the stored insulin into the bloodstream (Yaney and Corkey, 2003).

Following insulin secretion, glucose is depleted from the blood by its uptake into cells located in insulin-responsive tissues such as liver, adipose tissue and skeletal muscle cells, mediated by specific glucose transporters. Simultaneously, insulin blocks the action of its counter hormone glucagon (Levine, 1981). The liver and skeletal muscles store glucose in the form of the polymer glycogen, which consists of glucose monomers, whereas adipose tissue stores mainly triglycerides, which were previously synthesised by the liver from glucose. While adipose tissue is the major site for energy storage, glucose disposal mainly occurs in skeletal muscles (James et al., 1985).

On the other hand, if the blood glucose concentration is lower than the physiological optimum (<4 mM), α -cells of the pancreas secrete the hormone glucagon, which blocks the action of insulin and stimulates the liver and skeletal muscles to convert glycogen back into glucose, in order to increase glucose levels in the blood or utilise it as energy (Nilsson and Hultman, 1974).

Furthermore, blood glucose level is also controlled by the action of the central nervous system (CNS), which has glucose level sensing cells (Oomura and Yoshimatsu, 1984). Glucose-excited and glucose-inhibited neurons are mainly located in the hypothalamus of the brain close to the blood brain barrier. Together with cells that respond to metabolic hormones such as insulin or leptin, these glucose-sensing cells create a specialised hypothalamic neuronal circuit, which controls a subpopulation of neurons in the CNS, that are involved in the regulation of energy expenditure, glucose homeostasis and food intake (Jordan et al., 2010).

Other hormones are also involved in maintaining constant blood glucose levels. For example, the pancreatic hormone amylin, that is co-secreted together with insulin and complements its function (Moore and Cooper, 1991). Amylin modifies blood glucose dynamics through the suppression of postprandial glucagon secretion and by slowing down the rate of gastric emptying (Gedulin et al., 1997; Samsom et al., 2000). Hormones secreted by the gut also play a role in glucose homeostasis. The incretin hormones gastric inhibitory peptide (GIP) and glucagon-like peptide-1 (GLP-1) stimulate glucose-dependent insulin secretion (Yip and Wolfe, 2000; Lugari et al., 2002). In addition, akin to amylin, GLP-1 inhibits glucagon secretion and slows down the rate of gastric emptying (Matsuyama et al., 1988).

In summary, glucose homeostasis is crucial for the constant energy supply of organisms and to avoid hypoglycaemia or hyperglycaemia. Glucose levels are predominantly controlled by the action of the pancreas, the CNS and the insulin responsive tissues. The two main regulating hormones are insulin and glucagon but other molecules such as the appetite controlling hormones leptin and ghrelin, the pancreatic hormone amylin or the incretin hormones GLP-1 and GIP are also involved in glucose homeostasis (Jordan et al., 2010; Aronoff et al., 2004). A simplified model of the glucose homeostasis is displayed in Figure 1.1.

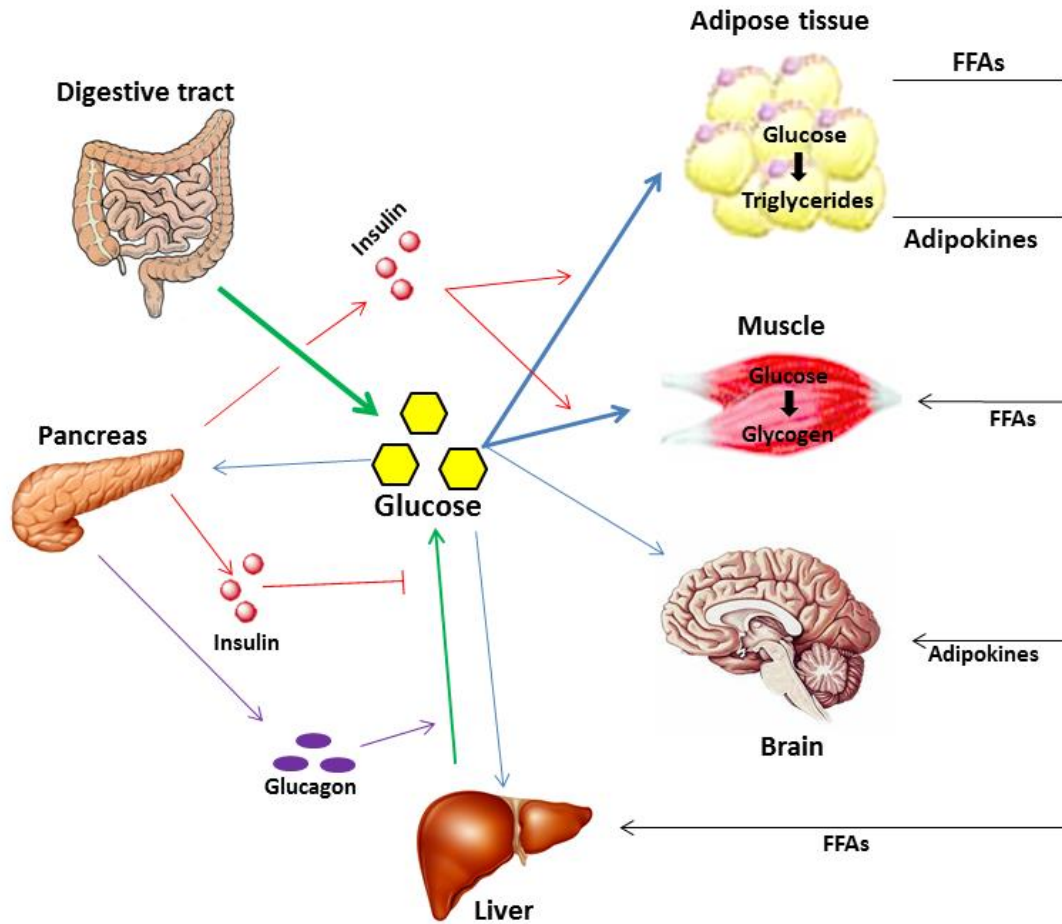


Figure 1.1. Glucose homeostasis. Outline of the interplay between hormones and organs involved in glucose homeostasis is illustrated. Blue arrows indicate the uptake of glucose by organs. Green arrows indicate the release of glucose into the blood. The action of insulin is highlighted with red arrows or lines whereas the action of glucagon is illustrated in purple. Black lines and arrows symbolise released substances from the adipose tissue such as adipokines and free fatty acids (FFAs). Glucose is taken up by the digestive tract and is released into the blood where it is taken up by the liver, pancreas, brain, muscle and adipose tissue. In muscle, glucose is either used as fuel or stored as glycogen, whereas adipocytes store glucose as triglycerides. The uptake of glucose into the pancreas triggers insulin secretion from its β -cells. Insulin stimulates the uptake of glucose into adipose tissue and muscle and simultaneously inhibits the release of glucose from glycogen stores of the liver. Adipose tissue releases FFAs which can be utilised as energy by various organs. Additionally adipose tissue also secretes hormones such as leptin or adiponectin, which can act on the brain to control appetite and contribute to the global energy balance of the body. In the case of low glucose levels, α cells of the pancreas release glucagon, which stimulates the release of glucose from liver stores.

1.2 Glucose transporters

As discussed above, glucose is the primary source of energy for most organisms. In order to utilise glucose as a fuel, cells have to transport it across the hydrophobic PM. Because glucose has a hydrophilic nature, membrane proteins are needed to mediate glucose transport across the PM into the cell cytosol. There are two groups of these transporter proteins. One group of glucose transporting proteins acts as a passive, ATP-independent transporter and facilitates glucose passage across the membrane according to its concentration gradient (Hruz and Mueckler, 2001). Proteins of this group are referred to as facilitative glucose transporters (GLUT). The other type of transporter proteins mediates the movement of glucose across the membrane against its concentration gradient utilising the concentration gradient of sodium ions (Na^+) as a source of energy. These proteins are symporters and are known as sodium-dependent glucose transporters (Mueckler, 1992).

The type of glucose transporter proteins that are mainly involved in glucose homeostasis are the facilitative transporters. 14 different GLUT isoforms including the H^+ /myo-inositol transporter (HMIT) are encoded in the human genome (Wood et al., 2003). The glucose transporter isoforms can vary in their substrate specificity and all have different transport kinetics. They are named according to their chronological discovery, numbered from 1 to 14 (GLUT1-14). Usually cell types express more than one isoform according to the kinetic requirements of the tissue they are located in. The GLUT isoforms share structural similarities and have 12 transmembrane domains (TMDs) with the N-terminus and C-terminus located in the cell cytosol. N-glycosylation sites are located within the first extracellular loop between transmembrane helix one and two or within the fifth extracellular loop (Gould and Holmant, 1993). Five of the TMDs are amphiphatic and potentially cluster together to form a aqueous channel (Mueckler et al., 1985).

The 14 GLUT isoforms are divided into three classes based on the primary sequence and characteristic elements. Class I, also referred to as the classical transporters, comprise the well-characterised GLUT isoforms GLUT1, GLUT2, GLUT3, GLUT4, GLUT14. The remaining odd-numbered GLUT isoforms GLUT5, GLUT7, GLUT9 and

GLUT11 belong to class II. Members of class III are the remaining even-numbered GLUT isoforms GLUT6, GLUT8, GLUT10, GLUT12 and HMIT (or GLUT13). The N-glycosylation site of members of class I and class II isoforms is within the first extracellular loop, whereas the N-glycosylation site of class III GLUT isoforms is located in the fifth extracellular loop between transmembrane helix number 9 and 10 (Augustin, 2010). As already mentioned, the GLUT isoforms expression pattern varies in the body in a tissue-specific manner. The brain for example, expresses GLUT1 and GLUT3 isoforms, which transport the required glucose into brain cells. GLUT1 is expressed in the brain endothelium and enables glucose to pass the blood brain barrier (Pardridge et al., 1990). Insulin-responsive tissues express GLUT4 in addition to other GLUT isoforms. Skeletal muscle for instance expresses GLUT5, GLUT11 and GLUT12 and adipose tissue expresses GLUT1 and GLUT8, but both types of tissue also express GLUT4 (Stuart et al., 2006). Table 1.1 summarises the tissue-specific expression for the GLUT protein family.

GLUT4 is unique among the other GLUT isoforms as it is predominantly stored in intracellular membrane compartments, whereas the other isoforms are predominantly located at the PM (Bryant et al., 2002). GLUT4 was cloned for the first time in 1989 and is encoded by the gene *SLC2A4* (Fukumoto et al., 1989). Its tissue-specific expression is regulated by a region which is located 2.4 kb upstream from the start codon (Liu et al., 1992). The subcellular distribution of GLUT4 is not dependent on the cell type (Haney et al., 1991), which suggests a localisation motif is present within the amino acid sequence of the protein, which is operational in many cell types. Indeed, the N-terminus and the C-terminus of GLUT4 have been reported to contain distinctive sequences capable of controlling the trafficking events of this protein and its localisation within the cell. The C-terminus of GLUT4 contains a characteristic dileucine and acidic motif which can also be found in the C-terminus of the insulin-responsive aminopeptidase (IRAP). Both GLUT4 and IRAP reside in intracellular insulin-responsive vesicles (Martinez-Arca et al., 2000). Within the N-terminus of GLUT4, the tetrapeptide phenylalanine-glutamine-glutamine-

isoleucine (FQQI) was shown to be important for the transporters subcellular localisation (Huang and Czech, 2007).

Table 1.1. Summary of classification and tissue-specific expression of GLUT isoforms.

Isoform	Class	Tissue distribution
GLUT1	1	widely expressed in fetal tissue, erythrocytes, endothelial barrier of brain (also eye, peripheral nerves and placenta), adipocytes
GLUT2	1	hepatocytes, pancreatic β -cells, Kidney (renal tubular cells, small intestine epithelium (basolateral membrane))
GLUT3	1	brain, testis (spermatozoa), placenta, cancer tissues
GLUT4	1	skeletal muscle, heart, brown and white adipose tissue
GLUT5	2	testis, small intestines, muscle, kidney
GLUT6	3	brain, spleen, peripheral leukocytes
GLUT7	2	small intestine (enterocytes), colon, prostate and testis (low level)
GLUT8	3	testis, brain (cerebellum) and adipose tissue (low level)
GLUT9	2	kidney, liver
GLUT10	3	liver, pancreas, brain, placenta, heart, lung, kidney
GLUT11	2	pancreas, kidney, placenta, skeletal muscle, heart,
GLUT12	3	skeletal muscle, heart, small intestine, prostate, breast cancer
HMIT (GLUT13)	3	brain (hippocampus, hypothalamus, cerebellum, brainstem),
GLUT14	1	Testis

GLUT4 is strongly involved in blood glucose homeostasis, which is a major property of the transporter and manifests its special position among the GLUT isoforms. Upon an insulin stimulus, the glucose transporter is recruited to the PM and allows glucose uptake into cells of insulin-sensitive tissues. This translocation of GLUT4 to

the PM is the rate-limiting process in insulin-stimulated glucose uptake (Huang and Czech, 2007). Because of this important physiological role, GLUT4 is related to medical conditions such as insulin resistance, metabolic syndrome and obesity. Some patients suffering from obesity or type 2 diabetes were found to have down-regulated expression levels of GLUT4 (Garvey et al., 1991). Surprisingly, constitutive GLUT4 knock-out in mice does not lead to a disturbed blood sugar level, despite the development of insulin resistance and postprandial hyperinsulinemia (Katz et al., 1995a). Interestingly though, 50% of heterozygous GLUT4 null mice develop diabetes after 6 months. These mice exhibit reduced glucose uptake in muscle which is associated with hyperglycemia and hyperinsulinemia (Stenbit et al., 1997). Furthermore, selective knockout of GLUT4 from either adipose tissue or muscle leads to the development of insulin resistance to the extent as seen in diabetic animals (Abel et al., 2001; Zisman et al., 2000).

1.3 Insulin and the insulin receptor

1.3.1 Insulin

Insulin is a peptide hormone which is secreted by β -cells located in the islets of Langerhans in the pancreas (Houssay et al., 1942). It is one of the most powerful anabolic hormones in the body and stimulates the synthesis of complex carbohydrates, lipids and proteins. At the same time, it prevents the degradation of these molecules. Besides the regulation of blood glucose level, insulin also regulates the turnover of triglycerides in liver and adipose tissue, stimulates amino acid uptake and has a major role in electrolyte homeostasis (Gupta et al., 1992; Clausen, 2008; Czech et al., 2013). The function of insulin is mediated by the modulation of various cellular processes such as vesicle transport, activation of protein transcription or stimulation of protein kinases and phosphates (Saltiel and Pessin, 2002). One of the main functions of insulin in the body is in blood glucose homeostasis. High blood sugar triggers the secretion of insulin from the pancreas, and glucose is taken up into cells of insulin-responsive tissues, which in turn

decreases the glucose blood levels. Simultaneously, the release of additional glucose into the bloodstream from carbohydrate stores within the liver is suppressed, as insulin inhibits the action of its counter hormone glucagon (Saltiel and Kahn, 2001). Moreover, insulin is involved in the regulation of appetite (Schloegl et al., 2011). Insulin also regulates the serum levels of β -hydroxybutyrate, a ketone body which serves as an energy source for the brain during periods of starvation and famine (Vanitallie and Nufert, 1967). Taken together, insulin has a major function in the regulation of metabolism, and homeostasis of glucose and electrolytes.

Insulin was first isolated in 1921 by Frederick Banting. The primary amino acid structure of the 5808 Da protein was determined by Frederick Sanger in the year 1955 (Ryle et al., 1955). It was the first amino acid sequence of a protein to be completely solved. Insulin circulates as a monomer in its active form consisting of a 21 amino acid long A-chain and a 30 amino acid long B-chain. The two chains are linked by two disulphide bridges between the cysteine residues at positions A7-B7 and A21-B30. The A chain contains an N-terminal helix linked to the antiparallel C-terminus, whereas the B-chain has a central helix extended by N- and C-terminal strands (Dodson and Whittingham, 2002). At a micromolar concentration, insulin forms dimers and in the presence of zinc it further associates into a hexamer (Baker et al., 1988). Each monomer has two non-polar surfaces, which are buried when forming a dimer or hexamer. It is hypothesised that these non-polar surfaces interact with the insulin receptor (IR) (De Meyts, 2004).

1.3.2 Insulin receptor (IR)

The IR belongs to the tyrosine kinase receptor (TKR) superfamily. It is present on the PM of all mammalian cell-types including cells of the brain. Although receptor numbers can vary strongly in different cell types, for example erythrocytes exhibit only approximately 40 receptors per cell, whereas 200,000 to 300,000 receptors can be found on the membranes of adipocytes and hepatocytes (Watanabe et al., 1998). The gene encoding the IR is greater than 120 kbp and has 22 exons and 21 introns. The most efficient promoter region was identified as a 247 bp long

fragment stretching from bp positions 276 to 523 upstream of the receptor initiating ATG site, and includes three transcription initiation sites (Seino et al., 1989). Later research revealed that the complete promoter region extends over 1800 bp upstream from the translation initiation site and does not include a TATA-box or CAAT-box resembling promoter features of commonly known housekeeping genes (Brunetti et al., 2001). At present, it is not completely understood how the expression of the IR is regulated. A few factors have been suggested to modulate IR expression levels, such as the medical conditions of insulin-resistance and hyperglycemia, the high-mobility group (HMG) protein family, or the hormone angiotensin II (Brunetti et al., 2001; Venkatesan and Davidson, 1995; Tiwari et al., 2007). Alternative splicing in exon 11 can result in the expression of an isoform lacking 12 amino acids between 717-729 (Seino and Bell, 1989).

Although the receptor consists of different subunits, it is synthesized as a single pro-receptor. A 30 amino acid long signal peptide is cleaved co-translationally, and the pro-receptor undergoes folding and glycosylation under guidance from calnexin and calreticulin in the endoplasmic reticulum (ER) before being transported into the Golgi apparatus (Bass et al., 1998). Subsequently in the Golgi apparatus, the pro-receptor is processed by proteolytic cleavage into its mature subunits. The protease furin recognises the basic tetrapeptide arginine-lysine-arginine-arginine (RKRR) at the amino acid positions 732-735 of the pro-receptor. The furin-mediated cleavage results in the formation of the 740 amino acid long α subunit and the 619 amino acid long β subunit (Nakayama, 1997; Yoshimasa et al., 1988). The α subunit resides extracellularly and bares the insulin binding site. In contrast, the β subunit is inserted into the PM by a predicted 20 amino acid long TMD (amino acids 947-967) and the majority of the protein is intracellular. The juxtamembrane intracellular part of the β subunit is thought to be involved in binding of its interaction partner, IR substrate (IRS) (De Meyts and Whittaker, 2002). The receptor's intrinsic tyrosine kinase domain is predicted to stretch from amino acids 1013-1288 of the β subunit (predicted by UniProt). The two subunits are covalently bound via a disulphide-bridge on the extracellular side, which involves cysteine-647 of the α subunit and

cysteine-872 of the β -subunit (De Meyts and Whittaker, 2002). Furthermore, the two monomers ($\alpha\beta$) consisting of connected subunits are linked via more disulphide-bridges involving cysteine residues of the α subunits, to form the functional IR dimer ($\alpha_2\beta_2$) (Taylor, 1992).

Insulin binding to the receptor activates the intrinsic tyrosine kinase which catalyses the transfer of the γ phosphate of ATP onto a tyrosine residue of its substrates. The first substrate of the receptor kinase is the IR itself. In contrast to other TKRs, the IR resides as a covalently bound dimer even in the absence of insulin, and does not require dimerisation upon ligand binding for its auto-phosphorylation (Hubbard et al., 1994).

1.4 Vesicle trafficking

Vesicles are closed membrane-bound organelles present within all cells. They are crucial for the uptake of nutrients and other molecules into the cell, and for secretion of signalling molecules to the cell exterior. Moreover, there is constant vesicle trafficking within the cell in order to distribute proteins and lipids to different intracellular compartments or to the cell surface (Peer et al., 2011; Keller and Simons, 1997). There are two types of vesicle trafficking. The first is constitutive vesicle trafficking, which occurs constantly within the cytosol and maintains the basic function of the cell. Examples for a common constitutive vesicle trafficking pathway are newly synthesised proteins which travel in vesicles from the ER to the cisternae of the Golgi apparatus where they undergo post-translational modifications. Subsequently, these proteins may be transported from the trans-Golgi-network (TGN) to their final compartment via vesicle trafficking (Ponnambalam and Baldwin, 2003). The second type of vesicle trafficking is regulated. In contrast to the constitutive pathway, regulated trafficking only occurs following a stimulus. Regulated vesicle trafficking is typical in synapses of neurons and mediates neural communication but can also be observed in endocrine and exocrine tissues (Weir et al., 1974; Lin and Scheller, 2000). Furthermore, regulated

exocytosis occurs in adipocytes and striated muscle cells, whereby GLUT4 containing vesicles fuse with the PM upon an insulin stimulus (Govers et al., 2004). Vesicle trafficking can be dissected into three major steps. Firstly, an existing membrane begins to form a cavity followed by budding into a circular, closed membrane which surrounds the molecules and proteins to be transported. The second step comprises the translocation of the vesicle, which is mediated by motor proteins along the cytoskeleton. The final and third step is the fusion with the target membrane and the release of the vesicle interior into the target compartment or the cell exterior (Bonifacino and Lippincott-Schwartz, 2003; Bonifacino and Glick, 2004).

The budding process requires the interaction of several proteins in order to facilitate curvature of the membrane and to anchor the correct cargo proteins to the vesicle. There are three types of protein-coated vesicles each of which regulate characteristic trafficking pathways. The COPI coats mediate intra-Golgi trafficking and retrograde transport from the Golgi apparatus to the ER (Letourneur et al., 1994). COPII coated vesicles travel from the ER to the Golgi passing the ER-Golgi intermediate compartment (Barlowe et al., 1994). The third type of vesicle coats are clathrin coats, which mediate the transport from the TGN to the cell surface and the endocytic pathways (Boettner et al., 2011). Assembly of the coat complex is similar for all vesicle coats and will therefore be explained using the COPII coat proteins as an example. Firstly a guanosine triphosphate (GTP)ase (Sar1) of the Ras superfamily is recruited by a guanosine nucleotide exchange factor (GEF) (Sec 12) to the membrane and loaded with GTP. The Ras GTPase Sar1 then recruits a protein sub-complex (Sec23 and Sec24), the Sar1-Sec23-Sec24 complex is also referred to as the pre-budding complex and functions as an adaptor for cargo proteins (Bi et al., 2002). Within this protein sub-complex, Sec23 interacts directly with Sar1 and functions as a GTPase-activating protein (GAP). Once the pre-budding complex is assembled at the membrane it acts as a polymerisation site for further coat proteins (Sec13 and Sec31) (Lederkremer et al., 2001). With completion of the assembly of the protein complex consisting of the membrane-proximal layer (Sar1, Sec23,

Sec24) and the membrane-distal layer (Sec13, Sec31) the membrane is ready for budding. Upon vesicle formation, the GTP hydrolysis activity of Ras-like GTPase Sar1 is stimulated by its GAP (Sec23), which induces the disassembly of coat proteins from the vesicle. The GAP activity of Sec23 increases significantly with the binding of the membrane-distal layer. This mechanism prevents premature or delayed disassembly of the protein coat (Antonny et al., 2001). Clathrin coat assembly is more complex than for COPI and COPII coats, as apart from the Ras GTPase, phosphoinositides are also able to recruit a variety of clathrin adaptors from the cytosol (Bonifacino and Lippincott-Schwartz, 2003).

After the vesicles translocate into the proximity of the target membrane, an interplay of various proteins is required for vesicle fusion with the target membrane. In particular, soluble NSF attachment protein receptor (SNARE) proteins (where NSF stands for N-ethylmaleimide-sensitive factor), that reside either on the vesicle membrane (referred to as R-SNAREs) or the target membrane (Q-SNAREs) play an essential role in vesicle fusion (Chen and Scheller, 2001). Vesicle-associated membrane proteins (VAMPs) are R-SNAREs that bind to cognate Q-SNAREs on the target membrane. The pairing of cognate R- and Q-SNAREs ensures that vesicles fuse with the correct target membrane. Common Q-SNARE proteins are syntaxin and 23 kDa synaptosome-associated protein (SNAP23) and SNAP25. Most SNARE proteins are anchored to the membrane by a C-terminal TMD while the N-terminus is facing the cytosol exposing one or two SNARE motifs. Exceptions are SNAP23 and SNAP25, which are anchored to the membrane through palmitate groups attached to cysteine residues of the protein (Veit et al., 1996; Vogel and Roche, 1999). During fusion of the target and vesicle membrane, a 4-helix SNARE bundle is formed. One helix is derived from the R-SNARE and three from the Q-SNAREs. At the beginning of the fusion process, the alpha helix bundle is formed through SNAREs located on opposing membranes. This transient topology of the SNARE complex is referred to as a trans-SNARE complex (Jahn et al., 2003). Other proteins are thought to be involved in the transformation of the trans-SNARE complex into a post-fusion cis-SNARE complex, where the SNAREs making up the helical bundle are situated on

one membrane. One suggested protein that regulates the transition of the trans- to the cis-SNARE complex is the calcium sensing protein synaptotagmin (Collins and Wickner, 2007). The formed 4-helical bundle is stable and the individual SNARE proteins remain attached together after membrane fusion. In order to recycle the SNARE proteins, NSF is recruited to the 4-helix bundle by the soluble NSF attachment protein (alpha SNAP). NSF uses the energy from ATP hydrolysis to disassemble the cis-SNARE complex back into free R-SNAREs and Q-SNAREs (Rice and Brunger, 1999).

Vesicle fusion is tightly regulated and there are many more proteins involved in this process than are described above. Higher specificity of the fusion process is achieved by the assembly of Rab GTPases onto the vesicle membrane (Jahn et al., 2003). Munc18 prevents premature fusion via its interaction with syntaxin and is involved in the priming of the fusion reaction (Rickman and Duncan, 2010).

1.5 Insulin and GLUT4 translocation

The peptide insulin is a key hormone regulating glucose homeostasis, and a major function of insulin is to stimulate the translocation of GLUT4 from intracellular stores to the PM (see section 1.3). GLUT4 is sequestered intracellularly within the endosomal system and also in specialised, highly insulin-responsive, GLUT4 storage vesicles (GSVs). Insulin released from pancreatic β -cells stimulates the translocation of GLUT4-containing vesicles to the PM and the subsequent fusion of these two membrane compartments (Govers et al., 2004). The major pool of GLUT4 recruited to the PM is derived from GSVs, although there is also an increased movement of GLUT4 from recycling endosomes (Lampson et al., 2001; Bryant et al., 2002). As insulin-stimulated GLUT4 vesicle translocation and fusion is rate limiting for glucose uptake into the cell, it has been a subject of intense interest for many researchers in the past decades.

The activation of intracellular insulin signalling pathways is induced by the binding of insulin to the α -subunit of the IR on the cell surface. This results in the activation of the intrinsic tyrosine kinase activity, which leads to the auto-phosphorylation of

the receptor. Following activation of the receptor, its tyrosine kinase phosphorylates IRS proteins (Gammeltoft and Vanobberghen, 1986). The phosphorylated IRS proteins then recruit the p85 regulatory subunit of phosphatidylinositol 3-kinase (PI3K) through Src homology (SH)2 and SH3 domains. PI3K catalyses the transfer of phosphate from ATP to phosphatidylinositol 4, 5 bisphosphate (PIP₂) to form phosphatidylinositol 3, 4, 5 trisphosphate (PIP₃) on the cytosolic side of the PM. The pleckstrin homology domain of protein kinase B (PKB; also known as AKT) binds to PIP₃ at the membrane. AKT is then activated through dual phosphorylation at serine-473 and threonine-308 by 3-phosphoinositide dependent protein kinase-1 (PDK1) and mammalian target of rapamycin complex 2 (mTORC2) (Alessi et al., 1996; Sarbassov et al., 2005). Once the protein kinase AKT is activated, it triggers several events that result in the translocation of intracellular GSVs to the PM. The fusion of the GSVs with the PM exposes the GLUT4 transporter to the extracellular environment and enables glucose uptake into the cell.

The pathway downstream of AKT activation has not yet been fully dissected, and is the subject of intense investigation. However, several important targets of AKT have been identified. AKT phosphorylates a protein known as AKT substrate of 160 kDa (AS160; also referred to as TBC1/4), which is a Rab GTPase-activating protein (Kane et al., 2002). AS160 is thought to be a negative regulator of GLUT4 translocation by maintaining several Rab proteins (such as Rab-8, -10 and -14) in their inactive/guanosine diphosphate (GDP)-bound state (Mîinea et al., 2005). Upon its phosphorylation by AKT, AS160 dissociates from the Rab proteins and binds the chaperone protein 14-3-3. This enables the Rab proteins to be in an active/GTP-bound form because of the removal of the AS160 G activity (Sakamoto and Holman, 2008). As Rab proteins are involved in vesicle trafficking and were shown to reside in GSVs (Ishikura et al., 2008), this phospho-regulation of AS160 by AKT is thought to play a crucial role in GLUT4 trafficking. The action of AKT is not only restricted to the phosphorylation of AS160 and the regulation of GLUT4 translocation to the PM, it is also involved in regulating the fusion of GSVs with the PM. Phosphorylation of Synip by AKT enables fusion to proceed by initiating the dissociation of Synip from

the SNARE protein syntaxin 4 (Yamada et al., 2005). Furthermore, AKT phosphorylates another SNARE regulatory protein called 138 kDa C2 domain-containing phosphoprotein (CDP138), which in a phosphorylated state positively impacts the GSV fusion event with the PM (Xie et al., 2011). Thus, several mechanisms linking the activation of AKT with GLUT4 vesicle translocation and fusion in response to insulin stimulation are beginning to emerge.

Although the activation of AKT through the PI3K-dependent pathway is sufficient to cause GLUT4 translocation in 3T3-L1 adipocytes (Ng et al., 2008), insulin is also thought to act via other signalling pathways. A PI3K-independent pathway functions in parallel to the PI3K-dependent pathway to couple insulin stimulation to the translocation of intracellular GSVs to the PM. This pathway is initiated by the binding of the adaptor protein APS to the activated IR and its subsequent phosphorylation by the receptor (Hu et al., 2003). Phosphorylated APS in turn serves as a binding site for the SH2 domain of the proto-oncogene-c-CBL (c-CBL) and the c-CBL associated protein (CAP) and this is important for the phosphorylation of c-CBL by the IR (Liu et al., 2002). Once phosphorylated, c-CBL can recruit the adaptor protein CRKII together with the GEF C3G to lipid raft domains of the PM (Chiang et al., 2001). C3G activates the small GTPase TC10, which also resides in lipid raft microdomains of the PM, via its GEF activity (Watson et al., 2001). Once TC10 is activated, it interacts with several effector proteins that are involved in the translocation and tethering of GSVs to the PM. One of the identified downstream targets of TC10 is EXO70, which assembles together with other proteins into the "exocyst" protein complex upon activation by TC10. The exocyst complex is thought to play an important role in guiding and tethering GSVs to appropriate domains in the PM in order to facilitate their fusion with the PM (Inoue et al., 2003). Other effectors of TC10 are the actin related protein-3 (Arp-3) and the actin-regulatory neural Wiskott-Aldrich syndrome protein (N-WASP), which participate in shaping the dynamic actin network within cells (Jiang et al., 2002). Interestingly, insulin-stimulated GLUT4 trafficking involves cytoskeleton proteins, as GLUT4 vesicles have been shown to associate with actin filaments and microtubules (Fletcher et al.,

2000). Following insulin stimulation, the cytoskeleton protein actin is remodelled into a cortical mesh, and blocking this mesh formation by application of a G-actin polymerisation inhibitor inhibits GLUT4 translocation (Lopez et al., 2009). Movement of GLUT4 vesicles along the actin filament, which is mediated by the motor protein myo1, was suggested to also be controlled by the Ca^{2+} /calmodulin-dependent protein kinase II (Yip et al., 2008). Although the remodelling of the cytoskeleton was shown to be important for GLUT4 translocation in both muscle cells and adipocytes, the involvement of the PI3K-independent pathway in this process is mainly limited to adipocytes (JeBailey et al., 2004).

1.5.1 Endocytosis of GLUT4

The amount of GLUT4 at the PM is determined by the net rate of its exocytosis and endocytosis. It is well established that insulin increases the net rate of exocytosis in muscle and adipose tissue (see section 1.5). In contrast the effect of insulin on the rate of GLUT4 endocytosis is debated and less well studied. Internalisation of GLUT4 is mediated by at least by two independent pathways. Clathrin-mediated endocytosis is one of the GLUT4 internalisation pathways and takes place in both muscle and adipose tissue (Antonescu et al., 2008; Blot and McGraw, 2006). An alternative GLUT4 internalisation mechanism in adipocytes is thought to involve a cholesterol-dependent pathway but this mechanism has not been identified in muscle cells (Blot and McGraw, 2006; Lajoie and Nabi, 2010; Antonescu et al., 2008). After internalisation via both clathrin- and cholesterol-dependent pathways, the endocytosed GLUT4 containing vesicles are likely to be trafficked to the sorting endosome compartment (Leto and Saltiel, 2012). Both internalisation mechanisms require dynamin for vesicle abscission (Henley et al., 1998; Mettlen et al., 2009), and subsequent migration of the formed vesicles towards the cell interior is mediated by microtubule-associated dynein motors (Huang et al., 2001). The FQQI motif in the N-terminus of GLUT4 has been found to be important for clathrin-mediated internalisation. This motif interacts with adaptor protein 2 (AP2), which

functions as an endocytic adaptor and coordinates the packaging of GLUT4 into clathrin-coated vesicles (Blot and McGraw, 2006).

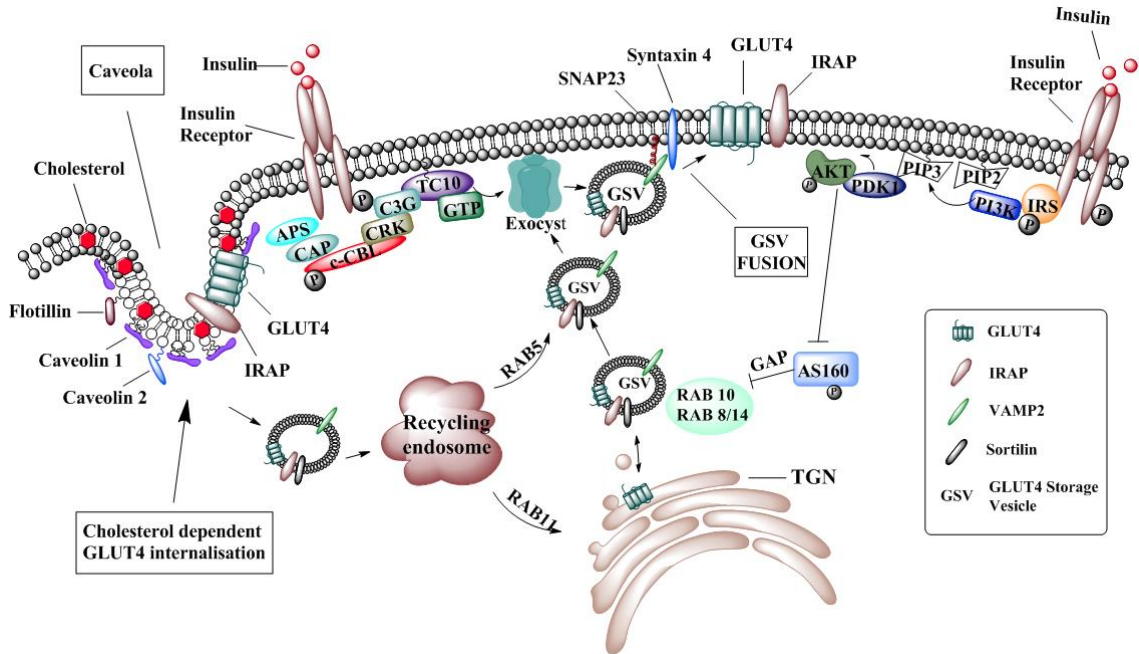


Figure 1.2. Insulin-stimulated GLUT4 translocation in adipocytes. Insulin-stimulated GLUT4 translocation is mediated by two separate pathways in adipocytes. On the left hand side of the figure, the PI3K-independent pathway is illustrated. IR auto-phosphorylation is stimulated by insulin binding and recruits APS (adaptor protein with pleckstrin homology and Src homology). APS in turn recruits c-CBL and CAP (c-CBL associated protein), which results in tyrosine phosphorylation of c-CBL by the IR. Phosphorylation of c-CBL stimulates the recruitment of the adaptor protein CRK and GEF C3G to the PM. C3G then activates the small GTPase TC10, and activated TC10 (GTP-bound) creates targeting sites for GSVs by interaction with the exocyst complex. On the right hand side the PI3K-dependent pathway is shown. Insulin stimulation triggers auto-phosphorylation of the IR which in turn phosphorylates IRS (IR substrate). Phosphorylated IRS serves as a docking site for PI3K, which catalysis synthesis of phosphatidylinositol 3, 4, 5 trisphosphate (PIP3) from phosphatidylinositol 4, 5 bisphosphate (PIP2) at the PM. PIP3 serves as a binding site for PDK1 (phosphoinositide-dependent kinase 1) and protein kinase AKT. PDK1 together with mTORC2 (mammalian target of rapamycin complex 2) activate AKT through phosphorylation. Activated AKT in turn phosphorylates AS160 (AKT substrate 160 of kDa), which then stops acting as a GAP (GTPase activating protein) for several Rab proteins (Rab8, Rab10 and Rab14). As a consequence these Rab proteins become active and contribute to the translocation of GSVs to the PM. Cholesterol-dependent GLUT4 internalisation is also illustrated on the far left hand side.

In turn, the cholesterol-dependent internalisation of GLUT4 in adipocytes is thought to be mediated by specific invaginated microdomains of the PM called caveolae, which are enriched with the protein caveolin and cholesterol (Shigematsu et al.,

2003). Evidence for this notion derives from work showing that the depletion of both caveolin and cholesterol resulted in a reduced rate of GLUT4 internalisation (Ros-Baro et al., 2001; Shigematsu et al., 2003; Blot and McGraw, 2006). Furthermore, GLUT4 was found in some studies to be localised in caveolae, however not all studies support this idea (Antonescu et al., 2009).

The role of insulin in the regulation of GLUT4 internalisation is currently unclear. Insulin does not affect the rate of GLUT4 endocytosis in muscle cells (Antonescu et al., 2008). In contrast, a decrease in the rate of GLUT4 internalisation upon insulin stimulation was reported in adipocytes (Czech and Buxton, 1993). This decrease in GLUT4 endocytosis is thought to be caused by a switch from the potentially faster cholesterol-dependent internalisation mechanism to the slower clathrin-mediated and AP2-dependent GLUT4 endocytosis pathway (Blot and McGraw, 2006). In agreement with this finding, the accumulation of GLUT4 into clathrin-coats of the PM was stimulated by insulin (Huang et al., 2007).

1.6 Insulin-responsive aminopeptidase (IRAP)

The insulin-responsive aminopeptidase (IRAP) was originally identified in low density microsomal fractions from adipocytes and muscle cells. It was found that IRAP resides in the same vesicles as GLUT4 and translocates to the PM upon an insulin stimulus (Keller et al., 1995; Ross et al., 1998). Because of its molecular weight and origin it was originally named vesicle protein of 165 kDa (vp165 (Mastick et al., 1994). An alternative name was glycoprotein of 160 kDa (Kandror et al., 1994). Characterisation of IRAP classified it as a type II membrane protein with a single TMD, an N-terminal cytosolic domain comprising 109 amino acids and a large extracellular C-terminal domain with 894 amino acids. IRAP is detected on SDS-polyacrylamide gels at a molecular weight of 165 kDa in most tissues and this exceeds the predicted molecular weight of 117.3 kDa. It is suggested that this difference originates from post-translational processing in the form of multiple glycosylation of the extracellular C-terminal domain (Keller et al., 1995). Indeed, protein databases such as UniProt predict 17 glycosylation sites for mouse IRAP.

Analysis by northern and western blotting demonstrated that IRAP messenger RNA (mRNA) and protein can be found in striated muscle, brain, spleen, lung, kidney and white adipose tissue (Keller et al., 1995). In brain, IRAP was detected at the apparent molecular size of only 140 kDa on SDS gels, which is suggested to originate from alternative glycosylation. Furthermore, structural analysis showed that parts of the extracellular domain share homology with the catalytic domain of the aminopeptidases A and N and thyrotropin-releasing hormone degrading enzyme. Hence, IRAP was classified as a member of the group of zinc-dependent aminopeptidases (Keller et al., 1995). Correspondingly, subsequent research identified IRAP as a homolog of the human oxytocinase/placental leucine aminopeptidase (P-LAP) (Rogi et al., 1996). Potential substrates of IRAP are vasopressin, oxytocin, lys-bradykinin and angiotensin III and IV, as these molecules are cleaved by IRAP *in vitro* (Herbst et al., 1997). In addition to its function as an aminopeptidase, IRAP was also identified as a receptor of angiotensin IV (Albiston et al., 2001). Because IRAP can potentially exert multiple functions (aminopeptidase for several signal peptides, angiotensin IV receptor) and is expressed in brain, it was suggested to be involved in memory and learning. Indeed, a study proposed that inhibition of IRAP enhanced memory and cognitive function (Albiston et al., 2001). Congruently, mice with a knockdown of IRAP exhibit an age-specific deficit in spatial memory (Albiston et al., 2010).

In contrast to other members of the zinc-dependent aminopeptidases, the majority of IRAP molecules do not reside at the PM of adipocytes and muscle cells. IRAP shares several similarities in its subcellular localisation and trafficking dynamics with GLUT4. Only approximately 10% of total IRAP proteins can be detected at the PM and the remaining 90% are found in intracellular vesicles and the endosomal recycling compartments (Karylowski et al., 2004; Ross et al., 1998). As mentioned above, IRAP co-resides in the same intracellular vesicles as GLUT4 in muscle cells and adipocytes. Furthermore, it was reported that 50% of IRAP molecules translocate to the PM within 5 minutes following stimulation with insulin, as reported for GLUT4 (Ross et al., 1997). Amino acid residues between 56-84 in the

cytosolic N-terminal domain were identified to be essential for intracellular retention and insulin-stimulated translocation of IRAP (Johnson et al., 2001). Together, these observations have classified IRAP as cargo and marker protein for GSVs. Subsequent research highlighted a role of IRAP beyond being simply a cargo molecule of GSVs and demonstrated that IRAP is implicated in processes such as the retention of GLUT4 in intracellular vesicles and translocation of GSVs to the PM. Overexpression of cytosolic regions of IRAP, including amino acids 1-52 or 55-82, caused an increase in GLUT4 translocation to the PM independently of insulin (Waters, 1997). Furthermore, knockdown of IRAP or its interaction partner tankyrase in cultured adipocytes impaired insulin-stimulated movement of GLUT4 to the PM (Yeh et al., 2007). Furthermore, knockdown of IRAP was shown to result in a three-fold increase of GLUT4 at the PM of unstimulated cells (Jordens et al., 2010).

1.7 Diabetes mellitus

Diabetes mellitus is a common metabolic disease characterised by hyperglycaemia and polyuria. The name derives from the Greek word for “siphon” (diabetes) and the Latin word for “honey sweet” (mellitus). The name diabetes mellitus was established by Thomas Willis in 1675, before the disease was referred to simply as diabetes. In the UK, 3.2 million people have been diagnosed to have Diabetes mellitus in the year 2013, which makes up 4.99% of the whole UK population and the numbers are rising. Additionally, it is estimated that approximately 600,000 people live with that condition but were not diagnosed (www.diabetes.org.uk). The prevalence of diabetes is not only rising in the UK, at the beginning of this century 171 million people world-wide had the condition. At this time, studies estimated the numbers of affected individuals to double by 2030 (Wild et al., 2004). However, recent studies reported that in 2013, 382 million people had diabetes, which already had exceeded the estimation for 2030 made in 2004, and current projections suggest the numbers will rise to 592 million people by 2035 (Guariguata et al., 2014). The main characteristic of this disease is hyperglycaemia, although

patients with diabetes mellitus exhibit more symptoms such as polyuria, increased thirst and fatigue (American Diabetes Association, 2004). Long-term effects of hyperglycaemia can result in damage to and dysfunction of nervous tissue, blood vessels or kidney, and can also lead to retinopathy with potential loss of vision. These effects are primarily caused by the unregulated and excessive uptake of glucose into endothelial cells, which supply these tissues with oxygen and nutrients. Endothelial cells are not able to reduce their glucose uptake in response to high blood glucose concentration, and therefore exhibit an elevated intracellular glucose concentration in the case of hyperglycaemia (Kaiser et al., 1993). The increased intracellular glucose is excessively oxidised in the mitochondria of these cells and generates cell damaging reactive oxygen species (ROS) due to an overstressed respiratory chain. The oxidative damage can lead to death of the affected endothelial cells, which then fail to supply the tissues they surround, which in turn can result in the dysfunction of these tissues (Brownlee, 2005).

Diabetes mellitus is subdivided into two types according to the pathophysiology and the cause of the disease. Type 1 diabetes is characterised by the insufficient secretion of insulin (see section 1.3.1 Insulin). The insulin secreting β -cells of the islets of Langerhans in the pancreas are attacked by an autoimmune reaction. Symptoms of Diabetes mellitus occur when over 70% of the β -cells are degraded, which is mediated by the T-helper 1 cells of the immune system (Katz et al., 1995b). A common treatment for patients with type 1 diabetes is the subcutaneous injection of insulin. The insulin responsive tissues such as liver, muscle and adipose tissue are not affected in this type of diabetes and are capable of insulin-stimulated glucose clearance from the blood. This treatment of type I diabetes only became possible with the isolation of insulin in 1921 by Frederick Banting. Before this achievement, type I diabetes was lethal. Because insulin is crucial for the survival of the patients, this type of diabetes is also referred to as insulin-dependent diabetes mellitus.

Type 2 diabetes is by far the more common type of diabetes and accounts for approximately 90-95% of all diabetes cases (American Diabetes Association, 2004).

As the number of people with diabetes is rapidly rising world-wide, type 2 diabetes has become a global health challenge. In contrast to type 1 diabetes, the secretion of insulin is not affected at early stages in type 2 diabetes. Hyperglycaemia is caused by a loss of insulin-stimulated glucose uptake by the insulin-responsive tissues (American Diabetes Association, 2004). Because insulin is not needed for treatment (in the early stages) of this disease, type 2 diabetes is also referred to as non-insulin dependent diabetes. Neither the exact underlying mechanisms of the genesis of insulin resistance and the associated hyperglycemia, nor the factors that cause its onset are known, and are the subject of ongoing research. It is believed the onset of type 2 diabetes has its origin in a combination of genetic predisposition and environmental factors (Zimmet et al., 2001; O'Rahilly et al., 2005). For example, point mutations in the IR gene, which disable its correct processing, have been identified to cause insulin resistance (Yoshimasa et al., 1988). Insulin resistance and hyperglycemia can be also caused by an inappropriate diet and lack of exercise and commonly coexists with obesity. There are several suggested mechanisms and shared physiological observations that link obesity to type 2 diabetes (Kahn et al., 2006). Both obesity and type 2 diabetes are accompanied by a disturbed blood lipid profile due to the increased release of non-esterified fatty acids (NEFA) from adipose tissue (Reaven et al., 1988). At least two different mechanisms are proposed to explain how the elevated NEFA in the blood serum contributes to the development of insulin resistance and hyperglycemia. Elevated NEFAs interfere with glucose metabolism, as they lead to the inhibition of enzymes that are involved in the oxidation of glucose such as pyruvate dehydrogenase, phosphofructokinase or hexokinase II, and hence slow down the oxidation of glucose (Randle et al., 1963). There is also evidence that the fatty acid metabolites diacylglycerol, fatty acyl-coenzyme A and ceramides accumulate as a consequence of increased intracellular NEFA levels. These metabolites in turn can lead to the phosphorylation of serine and threonine residues of IRS and decrease the activation of PI3K or impede the kinase activity of AKT via a protein-phosphatase-2A dependent pathway (Shulman, 2000; Mahfouz et al., 2014). Furthermore, akin to obese individuals, patients with

type 2 diabetes have reduced levels of GLUT4 expression and an impaired GLUT4 recruitment to the PM following an insulin stimulus (Sinha et al., 1991). Collectively, the above listed observations can be interpreted that type 2 diabetes can be partially caused by a defect in the pathway of insulin-induced GLUT4 translocation. In addition to the faulty pathway of insulin-dependent GLUT4 recruitment to the PM, abnormalities in the levels of hormones other than insulin can be observed in type 2 diabetes. The secretion of the pancreatic hormone amylin is impaired and the postprandial level of the incretin hormone GLP-1 is decreased (Young, 1997; Lugari et al., 2002). Both hormones were shown to complement and enhance the action of insulin (see section 1.1) (Young, 1997; Lugari et al., 2002; Aronoff et al., 2004).

1.8 Caveolae and caveolins

1.8.1 Caveolae

Caveolae are specialised membrane compartments, typically forming flask-shaped invaginations in the PM. They were first discovered by electron microscopy over a half century ago (Palade, 1953; Yamada, 1955) and were described as “smooth uncoated pits”. The nature, composition and function of these membrane invaginations remained largely unknown until the identification of a caveolae marker protein named vip-21, which was later renamed caveolin-1 (Rothberg et al., 1992). The flask-shaped invaginations have a diameter varying from 50-100 nm, and can be dynamic structures that can fuse or transform in order to form multi-caveolar assemblies. Conglomerations of caveolae were reported in several different shapes and seem to be cell type specific. At the PM of adipocytes, caveolae can be found in a circular assembly of numerous caveolae often referred to as circular or caveolar “rosettes” (Parton et al., 1994). In contrast, grape-like clusters of caveolae are mostly found in developing muscle cells (Parton, 1997) and the caveolae of endothelial cells can form detached tubular structures (Simionescu

et al., 1975). It is likely that these different structures are linked to specific physiological roles within these cell types.

As more research has been conducted, caveolae have been linked to various cellular processes such as transportation of molecules across the PM via transcytosis or endocytosis (Montesano et al., 1982; Schnitzer, 2001), cholesterol homeostasis (Fielding and Fielding, 1995) and signal transduction (Lisanti et al., 1994). Major insights into the function of caveolae, and particularly its effect on whole organism physiology, were generated by Razani and colleagues in studies examining mice lacking caveolae (Razani et al. 2002). These mice were lean, resistant to high fat diet-induced obesity and exhibited a disturbed blood lipid profile. Additionally, these mice suffered from vascular abnormalities due to irregular functioning of epithelial cell, which is thought to be linked to disturbed caveolae. Another study that examined a different mouse model with defects in caveolar formation and function found that these mice had elevated triglycerides, were insulin resistant and overly lean (Liu et al., 2008). These studies suggested an important involvement of caveolae in lipid metabolism, specifically for lipid deposition into adipocytes, but also questioned the general importance of caveolae in global (whole organism) physiology.

Caveolae can be found in the vast majority of cells, although the number and structure of caveolae varies widely from cell type to cell type. Adipocytes, smooth and striated muscle cells, endothelial cells, fibroblasts, and type I pneumocytes were reported to be the richest in caveolae (Napolitano, 1963; Gabella, 1976; Mobley, 1975; Palade, 1953; Gil, 1983). In adipocytes for example, caveolae can account for up to 30-50% of the surface of the PM (Fan et al., 1983; Thorn et al., 2003). The lipid composition of caveolae is thought to differ from the bulk PM. Specifically, caveolae are thought to be enriched in cholesterol, sphingolipids and saturated glycerophospholipids (Razani et al., 2002c), and to have a similar lipid profile as lipid “raft” microdomains. The lipid composition of caveolae and lipid raft microdomains is thought to lead to relative insolubility of these structures in the non-ionic detergent Triton X-100 at 4°C (Brown and London, 1998). Despite

caveolae and lipid rafts sharing similarities in their lipid composition they are distinct, as some proteins associate with one or the other type of microdomain but not with both (Liu et al., 1997).

Although caveolae were originally described as smooth invaginations, later research revealed that a striated and rough layer coated the caveolae suggesting the involvement of structural proteins (Izumi et al., 1989). Various proteins have been identified to reside in the caveolar coat such as its marker protein caveolin-1 (Rothberg et al., 1992), caveolin-2 (Scherer et al., 1996) and, more recently, cavins (Hill et al., 2008). The exact molecular composition of the caveolar coat is as yet unknown and the current subject of ongoing research. Like the composition of the molecular coat, the detailed mechanism of caveolar biogenesis is not yet fully deciphered. Certain proteins and molecules have been identified to play a crucial role in the formation of caveolae. Not surprisingly, this includes the proteins residing in the molecular coat (caveolins and, cavins) and also membrane lipids, specifically cholesterol. Before discussing the formation of caveolae in more detail, it is important to introduce the proteins in this process.

1.8.2 Caveolin-1

Caveolin-1 was originally discovered as a 22 kDa substrate of the v-Src tyrosine kinase (Glenney, 1989). This protein was later identified as a marker protein of caveolae and therefore named caveolin (Rothberg et al., 1992). At the same time Kurzchalia and colleagues isolated a protein from a CHAPS insoluble membrane fraction and named it vesicular integral-membrane protein of 21 kDa (VIP21) (Kurzchalia et al., 1992). Subsequently, caveolin and vip-21 were shown to be the same protein (Glenney, 1992). The names of both proteins were unified to “vip21-caveolin” which later was simplified to just caveolin. With the discovery of more isoforms of this protein family, caveolin has been renamed as caveolin-1 (Scherer et al., 1996; Tang et al., 1996). Caveolin-1 is expressed in most major tissues including brain (Li et al., 2001). It is encoded by a single gene (Glenney, 1992) and can be found in a larger 24 kDa alpha- and a smaller 21 kDa beta- isoform. These isoforms differ only in their N-terminal region and are produced as the result of an

alternative initiation of translation. The start of translation at the first start codon of caveolin-1 mRNA results in production of the alpha isoform with a total amount of 178 amino acids. The alpha isoform has a second methionine at position 32 which is the first amino acids of the shorter beta isoform (Figure 1.3). These isoforms were reported to have an overlapping but partially different subcellular localisation (Scherer et al., 1995). Furthermore, some research indicates that the ratio of alpha to beta isoform can determine caveolar morphology (Fujimoto et al., 2000).

Caveolin-1 and other members of the caveolin family (caveolin-2 and caveolin-3) exhibit a nonconventional membrane topology. The N- and the C-termini are both localised within the cytosol (Dupree et al., 1993) and are separated by a 32-amino acid long intramembrane domain. Membrane insertion of this domain takes place co-translationally in the ER (Monier et al., 1995). Analysis of caveolin-1 by Lisanti and colleagues suggested that this central hydrophobic intramembrane domain (amino acids 102-134) forms an incomplete hairpin loop within the lipid bilayer. In contrast, the protein database UniProt predicts an intramembrane domain of only 20 amino acids (105-125). After translation and insertion of caveolin-1 into the membrane, caveolin-1 undergoes several PTMs. The N-terminal tyrosine at the position 14 and serine at position 80 are important phosphorylation sites (Seitz, 1996; Fielding et al., 2004). The C-terminal domain has been reported to be palmitoylated at all three cysteine residues 133, 143 and 156, of which cysteine 133 is thought to be the major site of palmitoylation (Dietzen et al., 1995). Although palmitoylation plays a well-defined role in membrane association of soluble proteins and in the targeting of proteins to caveolae and lipid rafts, it was found that palmitoylation of caveolin-1 was not required either for membrane attachment nor to direct caveolin into detergent resistant membrane microdomains (Dietzen et al., 1995).

Caveolin-1 is essential for many aspects of caveolar physiology. As mentioned above, it is a major component of the caveolar coat. Indeed, overexpression of caveolin-1 in caveolae-deficient cells is sufficient to initiate *de novo* synthesis of caveolae (Fra et al., 1995). Concordantly, mice with a knockout of caveolin-1 gene,

showed a loss of caveolae (Razani et al. 2002). Furthermore, these mice were reported to have a disturbed lipid metabolism. Caveolin-1 has also been proposed to be involved in the transportation of fatty acids across the PM into cells independent of caveolae. Caveolin-1 was demonstrated to bind long chain fatty acids in HEK293T and cells with high expression levels of caveolin-1 showed increased fatty acid uptake (Meshulam et al., 2006). Moreover, caveolin-1 was demonstrated to bind to cholesterol in the ratio of 1:1 (Murata et al., 1995) and cholesterol transport from the ER to the PM was increased by overexpression of caveolin-1 (Meshulam et al., 2006). Hence, there is evidence that caveolin-1 is involved in cholesterol transport and metabolism in addition to its implication in fatty acid uptake.

1	MSGGKYVDSEGHLYTVPIREQGNIYKPNNKAMADEVTEKQ	caveolin-1
1	MGLETEKADVQLFMADDDAYSHH	caveolin-2
1	MMTEEHTDLE	caveolin-3
41	---VYDAHTKEIDLV-NRDPKHLNDDVVKIDFEDVIAEPE	caveolin-1
23	SGVDYADPEKYVDSSHDRDPHQLNSHL-KLGFEDLIAEPE	caveolin-2
11	ARI IKDIHCKEIDLV-NRDPKNINEDIVKVD FEDVIAEPE	caveolin-3
77	GTHSFDGIWKASFTTFTVTKYWFYRLLS TIFGIPMALIWG	caveolin-1
62	TTHSFDKVWI CSHALFEISKYVMYKFLTVFLAIP LAFIAG	caveolin-2
51	GTYSFDGVWKSFTTFTVSKYWCYRLLS TLLGVPLALLWG	caveolin-3
117	IYFAILSFLHIWAVVP C IKSFLIEIQ C ISRVYSIYVHTFC	caveolin-1
102	ILFATLS LHIWILMPFVK T LMVLP SVQTIWKSVDVVI	caveolin-2
91	FLFACISFCHI WAVVP C IKSFLIEIQ C ISHIYSLCIRTF C	caveolin-3
161	DPLFEAIGKIFSNIRISTQKEI	caveolin-1
142	GPL C TSVGRSFSSVSMQLSHD	caveolin-2
131	NPLFAALGQVCSNIKVVLRREG	caveolin-3

Figure 1.3. Alignment of the amino acid sequences of the caveolin protein family. Initiating methionines are highlighted in blue. Oligomerisation domain is shaded grey and predicted intramembrane domain highlighted in yellow (membrane prediction by Lisanti and colleagues). Palmitoylated cysteines of caveolin-1 and caveolin-3 are highlighted in red. The cysteine residues of caveolin-2 are highlighted in green. Amino acid position is indicated on the left side of the alignment panel.

However, Lisanti and colleagues found evidence that the amino acids localised between positions 82 and 101 exert function as a scaffold-domain. Moreover, caveolin-1 was shown to form homo-oligomers and the amino acids from 61 to 102 were identified as an oligomerisation domain, as deletion of this domain prevented its assembly into oligomeric structures (Sargiacomo et al., 1995).

1.8.3 Caveolin-2

Caveolin-2 is an additional member of the caveolin gene family, which was identified by microsequencing of a caveolin-enriched membrane preparation from murine adipose tissue (Scherer et al., 1996). Caveolin-2 was demonstrated to reside in caveolae, as it co-purified in these membrane microdomains with caveolin-1 (Scherer et al., 1996). Moreover, analysis by confocal microscopy revealed co-localisation of caveolin-1 and caveolin-2 (Scherer et al., 1997). Caveolin-2 was initially reported to be abundantly expressed in adipose and lung tissue (Scherer et al., 1997). Although later studies expanded this knowledge about tissue-specific expression, and reported that caveolin-2 was also detected in kidney, small intestines, colon, heart, uterus and to a lesser extent in muscle (Li et al., 2001). Unlike caveolin-1, caveolin-2 could not be detected in brain. Two different isoforms, alpha and beta, of caveolin-2 were identified, of which the alpha isoform is the more abundantly expressed (Scheiffele et al., 1998). Similar to caveolin-1, it is thought that these two isoform originate from the use of different translation start sites, as caveolin-2 has two methionines in the N-terminus which could potentially both function as the start of translation (Figure 1.3). In contrast to caveolin-1, only a small amount of research has been conducted to elucidate the membrane topology of caveolin-2, but it was also suggested to have cytosolic N- and C-termini, separated by an intramembrane domain forming an incomplete hairpin structure in the lipid bilayer. Like caveolin-1, caveolin-2 has been reported to be phosphorylated (Scheiffele et al., 1998), and phosphorylation sites identified as tyrosine at positions 19 and 27, and serine at positions 23 and 26 (Lee et al., 2002; Wang et al., 2004;

Sowa et al., 2003). Although caveolin-2 has 4 cysteines at the positions 72, 109, 122 and 145, no palmitoylation of these residues has been reported yet.

The importance of caveolin-2 for cell and organism physiology has been studied to a far lesser extent than caveolin-1. Mice deficient in the caveolin-2 gene had membranes with normal caveolae in all examined tissues and no disturbed vascular responses or lipid homeostasis could be observed. Regardless of the fact that regular caveolae structures formed within lung parenchyma, caveolin-2 deficient mice exhibited pulmonary dysfunction manifested in hypercellularity with thickened aveolar septa within lung parenchyma. This abnormality renders the knockout mice intolerant to exercise (Razani et al., 2002b). Hence, caveolin-2 seems to exert a physiological role independent of caveolin-1. As the expression of caveolin-2 is initiated throughout the differentiation of 3T3-L1 pre-adipocytes into adipocytes and is abundant in adipose tissue, caveolin-2 is thought to play a role in adipocyte physiology (Scherer et al., 1997). It is speculated that caveolin-2 functions together with caveolin-1, as they were found to form hetero-oligomers (Scherer et al., 1997) and mice deficient of caveolin-1 expressed lower levels of caveolin-2 and vice versa (Razani et al., 2002a; b). Additionally, there is some evidence that caveolin-2 is involved in formation of caveolae. Although caveolin-2 knockout mice had regular caveolae, caveolin-2 seems to be required for the formation of caveolae on the basolateral surface of Madin-Darby canine kidney (MDCK) cells (Scheiffele et al., 1998; Lahtinen et al., 2003).

1.8.4 Caveolin-3

Caveolin-3 is the third member of the caveolin family and was isolated from muscle cells where it localises in caveolae of the sarcolemma (Parton, 1997). The expression of caveolin-3 differs from the expression pattern of caveolin-1 and caveolin-2 as it is mostly limited to the cells of heart and skeletal muscle tissue and can be only found to a significantly lower extent in lung, stomach and small intestine (Li et al., 2001). Hence, caveolin-3 is predominantly expressed in striated and smooth muscle tissue. The structural properties of caveolin-3 are thought to be very similar to the ones of caveolin-1, and indeed these proteins share 85%

similarity and 65% identity at the amino acid level. As depicted in Figure 1.3, caveolin-3 is slightly shorter than caveolin-1 and has only 151 amino acids in comparison to the 178 in caveolin-1. In general, it is thought that caveolin-3 is the equivalent of caveolin-1 in muscle cells. In agreement with this notion, the caveolin-3 derived caveolae are enriched with the same signalling proteins as caveolin-1 derived caveolae (Feron et al., 1996; Song et al., 1996). In addition, the expression of caveolin-3 also drives the formation of caveolae (Shengwen et al., 1998). Furthermore, the three palmitoylated cysteines in caveolin-1 are conserved in caveolin-3 and are also palmitoylated (Tang et al., 1996; Couet et al., 2001).

1.8.5 Cavins

The cavin protein family is a group of cytosolic proteins with 4 members, which have been linked to caveolae. The individual members of this group were discovered unrelated to their involvement in the formation and physiology of caveolae. Cavin-1 for example was discovered as the polymerase I and transcript release factor (PTRF) (Jansa et al., 1998) and later identified to be associated with caveolae (Vinten et al., 2005). Akin to cavin-1, cavin-2 was originally discovered as a phosphatidylserine binding protein and a substrate of protein kinase C (Burgener et al., 1990), and later found to localise in caveolae (Mineo et al., 1998). Cavin-3 and cavin-4 were also originally discovered unrelated to caveolae and have alternative names whereby cavin-3 was originally named sdr-related gene product that binds to c-kinase (SRBC) and the alternative name of cavin-4 is muscle-restricted coiled-coil protein (MURC) (Briand et al., 2011). The sizes of cavin proteins vary, with cavin-2 being the largest (418 amino acids) and cavin-3 the smallest (260 amino acids). It is thought that cavins undergo extensive post-translational modifications, as their detected molecular size by SDS-PAGE is up to 15 kDa higher than the predicted molecular weight (Hill et al., 2008; Vinten et al., 2005; Hansen et al., 2009; Liu and Pilch, 2008). All members of the cavin family are cytosolic and have a conserved N-terminal domain with a repeating heptad of hydrophobic amino acids, which are likely to form a coiled-coils (Bastiani et al., 2009). Cavin proteins have a broad tissue expression profile and, in contrast to caveolin-1, their expression can be found in

both muscle tissue and in adipose tissue. Cavin-4 is an exception however, as its expression is confined to muscle cells (Bastiani et al., 2009). There is evidence that members of the cavin protein family play an essential role in caveolae formation, as mice lacking cavin-1 expression were not able to form caveolae and displayed a similar phenotype as caveolin-1 and caveolin-3 double knockout mouse (Liu et al., 2008). Additionally, cultured cells with a loss of cavin-2 expression also lacked caveolae (Hansen et al., 2009). Complementary to these knockout studies, the overexpression of cavin-1 was demonstrated to correlate with an increased number of caveolae (Hansen et al., 2009). Cavin-3 and cavin-4 are less well studied than the other cavin proteins, although they have also been linked to the formation or function of caveolae (McMahon et al., 2009; Bastiani et al., 2009).

1.8.6 Biogenesis of Caveolae

The exact mechanism of caveolar biogenesis is not yet known and the subject of ongoing research. The current model is based on the trafficking pathway of caveolin-1. Caveolin-1 is synthesised in the rough ER and inserted into the membrane co-translationally (Monier et al., 1995). Shortly after its biosynthesis, caveolin-1 begins to assemble within the ER into homo-oligomeric structures with the size of approximately 150-200 kDa corresponding to the size of 8S on velocity gradients (Hayer et al., 2010; Monier et al., 1995). It is estimated that these oligomers consist of 7 to 10 caveolin-1 monomers (Fernandez et al., 2002). If caveolin-2 is co-expressed, this isoform is also incorporated into the oligomeric assemblies, although the amount of caveolin-1 is at least twice as much as caveolin-2 in those hetero-oligomers (Scheiffele et al., 1998). Indeed homo-oligomers of caveolin-1 and hetero-oligomers of caveolin-1 and caveolin-2 have been reported in various studies and are thought to play an essential role in caveolae formation (Sargiacomo et al., 1995; Scherer et al., 1997; Fernandez et al., 2002; Lahtinen et al., 2003; Hayer et al., 2010). The N-terminal region of caveolin-1 from amino acid 61-102 was identified to be essential for oligomerisation (Sargiacomo et al., 1995). Furthermore, the C-terminus of caveolin-1 was demonstrated to interact with both

the C- and the N-terminus of caveolin-1 in homo-oligomers to enhance oligomeric assemblies (Song et al., 1997).

These caveolin oligomers traffic via COPII-dependent transport from the ER to the Golgi apparatus, where they assemble into larger oligomers of an approximate size of 70S (Hayer et al., 2010). In the compartments of the Golgi apparatus, these larger oligomers acquire a resistance to solubilisation by certain detergents such as Triton X-100 (Scheiffele et al., 1998). It is thought that the special membrane environment, including the presence of membrane microdomains in the Golgi apparatus, plays an important role in the maturation of the caveolin oligomers. Moreover, it is proposed that in the Golgi apparatus caveolin-1 and caveolin-2 undergo post-translational modifications (Parat and Fox, 2001). As mentioned above, caveolin-1 was identified to be palmitoylated at all three of its cysteine residues (Dietzen et al., 1995), and this attachment of long chain fatty acids to caveolin-1 stabilised its oligomeric assemblies (Monier et al., 1996). Besides long chain fatty acids, caveolin-1 has been demonstrated to tightly bind cholesterol in an approximate ratio of one mole cholesterol per mole of caveolin-1 (Murata et al., 1995). The binding of cholesterol to caveolin-1 plays a crucial role in the biogenesis of caveolae, as treatment of cells with cholesterol depleting drugs such as filipin or nystatin resulted in flattening of the caveolar invaginations and the disassembly of the caveolar coat (Rothberg et al., 1992). In agreement with these findings, cholesterol was demonstrated to stabilise oligomeric structures of caveolin-1 (Monier et al., 1996) and to accelerate the export of the protein from the Golgi apparatus towards the PM (Pol et al., 2005).

Following assembly and maturation, the 70S caveolin oligomers exit the Golgi apparatus and translocate to the PM, where they assemble with proteins from the cavin family to form mature caveolae (Hayer et al., 2010). It is not clear whether the 70S large caveolin oligomers in the Golgi apparatus correspond to the caveolar scaffold which together with cavins forms mature caveolae. Recent estimations revealed that the 70S caveolin oligomer consists of approximately 160 caveolin monomers (Hayer et al., 2010), which is consistent with previous studies where 144

± 39 caveolin monomers per caveolae had been suggested (Pelkmans and Zerial, 2005). The transport vesicles in which the caveolin oligomers exit the Golgi apparatus have been termed caveolar carriers and these vesicles seem to leave the Golgi apparatus through the medial Golgi complex and not through the TGN (Hayer et al., 2010). Furthermore, it was found that fusion of the caveolar carriers require the SNARE protein Syntaxin 6 (Choudhury et al., 2006). Once the caveolar carriers have reached the membrane it is not clear how recruitment and attachment of cavins to the caveolins is mediated. Cavin complexes can form independently of caveolin-1 in the cytosol and reach the size of 60S, but they only associate with caveolin once the caveolin assemblies have reached the PM (Hayer et al., 2010). At present, it is thought that the incorporation of the caveolin oligomer together with the peripheral association of members of the cavin protein family forms mature caveolae.

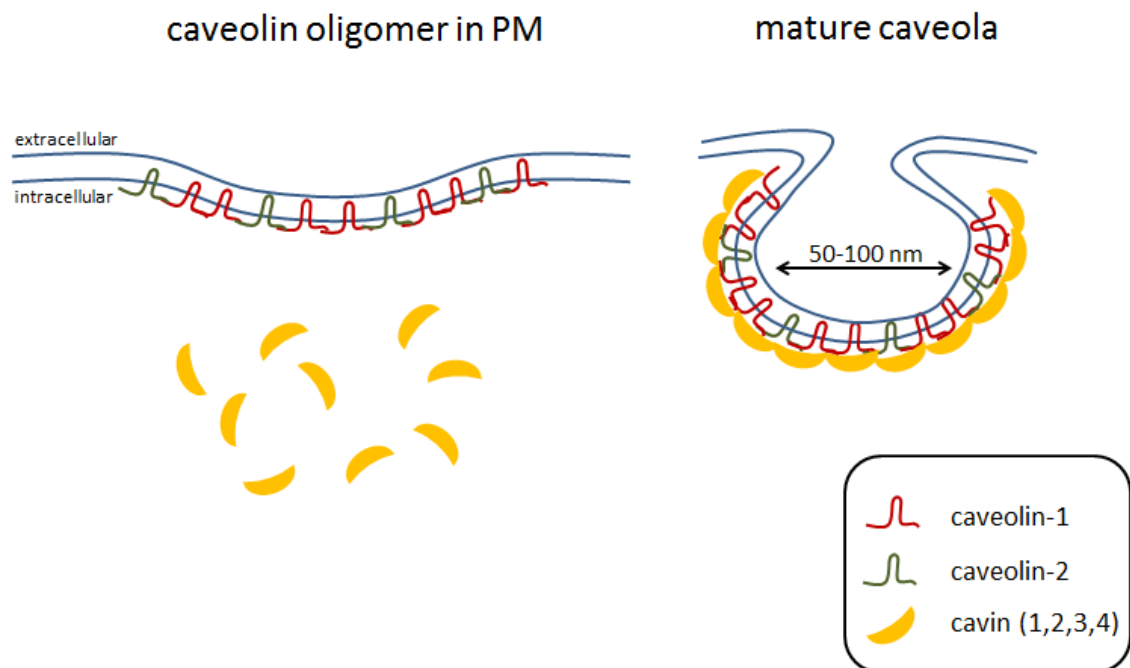


Figure 1.4. Formation of caveolae. The current model for the formation of caveolae is illustrated. The panel at the left hand side shows the PM-integrated caveolin hetero-oligomer with an estimated size of 70S and cytosolic cavin monomers. The caveolin hetero-oligomer consists of caveolin-1 and caveolin-2 in the ratio of 2:1 in favour of caveolin-1 and is not sufficient to induce strong membrane curvature. The panel on the right hand side shows a mature caveola, where cavins are oligomerised and bind to the caveolin hetero-oligomer scaffold. The outer cavin-coat with an estimated size of 60S together with the caveolin hetero-oligomer scaffold induce the typical membrane curvature and are considered mature caveolae. Phospholipids, cholesterol and sphingolipids are not shown.

1.9 Caveolae and insulin signalling

There is growing evidence that caveolae and caveolin proteins are involved in insulin signalling. The IR has been shown to mainly reside in caveolae at the PM, especially in adipocytes (Gustavsson et al., 1999; Foti et al., 2007), and it has been proposed that a specified subset of caveolae harbour several IRs per caveola (Thorn et al., 2003). Upon insulin binding and autophosphorylation, it is thought that the IR undergoes rapid internalisation through caveolae into “caveosomes”, the IR is then dephosphorylated and recycled back to the PM. Endocytosis of the IR through caveolae is thought to be mediated by phosphorylation of caveolin-1 at tyrosine 14, as phosphorylated caveolin-1 and IR were co-immunocaptured from endosomes (Fagerholm et al., 2009). In support of this notion, caveolin-1 has been previously reported to be a substrate of the IR kinase activity (Kimura et al., 2002). Additional evidence linking caveolae with the IR was highlighted by studies in caveolin-1 knockout mice, which are insulin resistant and had a reduced expression of the IR (Cohen et al., 2003). Moreover, loss of caveolin-1 function increased IR and GLUT4 degradation in cultured adipocytes (González-Muñoz et al., 2009). Similar observations have been made in muscle tissue from caveolin-3 knockout mice (Capozza et al., 2005).

Aside from the role of caveolin and caveolae in the localisation, endocytosis and stability of the IR, caveolae are also involved in the regulation of the insulin signalling cascade. IRS1 expression levels are regulated by caveolin-1 and overexpression of caveolin-1 and caveolin-3 in HEK293T cells enhanced insulin-stimulated IRS1 phosphorylation without altering auto-phosphorylation levels of the IR (Chen et al., 2008; Yamamoto et al., 1998). Moreover IRS1 and PI3K are suggested to be recruited to caveolin-enriched domains in liver cells after insulin stimulation (Balbis et al., 2004). β -cyclodextrin treatment of 3T3-L1 adipocytes depleted caveolae and inhibited IRS1 phosphorylation and activation of AKT, without affecting insulin binding to the IR and receptor auto-phosphorylation (Parpal et al., 2001). A similar observation was made in primary human adipocytes,

where depletion of cholesterol from the PM blocked insulin-stimulated AKT activation and the translocation of GLUT4 to the plasma membrane (Karlsson et al., 2004).

Unlike the IR, the localisation of GLUT4 in caveolae has not been demonstrated unequivocally in the currently available literature. However, studies exist showing that the majority of GLUT4 at the PM resides in caveolae after insulin stimulation (Karlsson et al., 2002). Furthermore, it is not clear which mechanism mediates GLUT4 endocytosis from the PM after its insulin-stimulated translocation to the PM. It was suggested that GLUT4 is mainly internalised via clathrin-mediated endocytosis, as GLUT4 containing vesicles did not contain caveolin-1 (Kandror et al., 1995). However, knock-down of clathrin in myoblasts and adipocytes reduced the endocytosis of GLUT4 by only 50%, suggesting that there might also be a clathrin-independent endocytosis pathway for GLUT4. In adipocytes it is suggested that this internalisation mechanism is cholesterol-dependent and mediated by caveolae (Ros-Baro et al., 2001; Shigematsu et al., 2003; Blot and McGraw, 2006). Irrespective of whether GLUT4 is internalised via caveolae-mediated endocytosis, caveolae seem to have a stabilizing effect on GLUT4. Knock-down of caveolin-1 and cavin-1 resulted in increased GLUT4 degradation and a lower total amount of the protein in 3T3-L1 adipocytes (González-Muñoz et al., 2009; Liu et al., 2008). Furthermore, it was demonstrated that glucose uptake correlates with a slow translocation of GLUT4 into caveolae (Gustavsson et al., 1996).

Taken together, there is a substantial amount of evidence for the involvement of caveolae in insulin signalling, including effects on IR cycling and stability, regulation of the IR-stimulated phosphorylation cascade, and the stability of GLUT4. These findings are underpinned by the fact that mice which are not able to form caveolae exhibit insulin resistance and dyslipidemia (Liu et al., 2008; Cohen et al., 2003). Furthermore, IRs of some patients with extreme types of insulin resistance have been shown to contain mutations in the caveolin-1 binding motif (Iwanishi et al., 1993).

1.10 Palmitoylation

S-Palmitoylation is a post-translational protein modification whereby a saturated C16 fatty acid is attached to a cysteine residue of a protein by a thioester bond. S-Palmitoylation or simply “palmitoylation” belongs to a group of lipid modifications, which includes N-myristoylation and prenylation. In mammals, palmitoylation is mediated by a family of 24 enzymes which are characterised by the amino acid sequence motif DHHC (aspartic acid-histidine-histidine-cysteine) present within a 51-amino acid cysteine-rich domain of the protein (Fukata et al., 2004). These palmitoyl transferases (PATs) are polytopic membrane proteins and hence palmitoylation occurs in proximity to membrane surfaces within the cell.

In contrast to other covalent lipid modifications, palmitoylation is dynamic as the attachment of the palmitic acid to a cysteine residue is reversible. Depalmitoylation is mediated by acyl-protein-thioesterase (APT) enzymes (Duncan and Gilman, 1998; Zeidman et al., 2009). The rate of depalmitoylation varies from protein to protein. For example, the half-life time of palmitoylation on the Src family kinase Fyn has been shown to be 1.5-2 h (Wolven et al., 1997), whereas palmitoylation of syntaxin 1a was suggested to be a static modification (Kang et al., 2008). Palmitoylation and depalmitoylation dynamics can vary even for isoforms of the same proteins, as demonstrated for H- and N-Ras (Baker et al., 2003; Magee et al., 1987). Suggested factors that affect protein depalmitoylation rate are the interaction specificity with APT enzymes, the accessibility of modified cysteines to these enzymes, and the number of palmitoylated cysteines within the protein (Salaun et al., 2010). It is likely that APTs are well distributed throughout the cell rather than being confined to one cell compartment, as depalmitoylation can be observed in many locations of the cell (Rocks et al., 2005).

Palmitoylation has many important effects on modified proteins. For proteins that lack a TMD, palmitoylation can be essential for membrane recruitment (Vogel and Roche, 1999). Some soluble proteins are modified by myristoylation or prenylation together with palmitoylation. These myristoyl and prenyl chains increase the hydrophobicity of the protein, sufficient to allow transient membrane interaction,

which then enables membrane-bound PATs to palmitoylate the protein and mediate stable membrane attachment (Shahinian and Silvius, 1995). Thus, palmitoylated cysteine residues often occur adjacent to myristoylation and prenylation sites. For transmembrane proteins or soluble proteins that lack other lipid modifications, palmitoylated cysteine residues are often surrounded by hydrophobic or basic amino acids or are located adjacent to or within TMDs, however as yet no known consensus sequence for palmitoylation has been reported (Salaun et al., 2010).

It was shown that palmitoylation is involved in processes beyond the membrane anchoring of soluble proteins. One particular aspect that palmitoylation often affects is the regulation of protein sorting and trafficking. The specific intracellular compartmentalization of small GTPase Ras isoforms (H- and N-Ras) is regulated by a constitutive cycle of palmitoylation and depalmitoylation, which enables coordinated trafficking from the Golgi apparatus to the PM and back (Rocks et al., 2005). Transmembrane protein trafficking is also frequently regulated by palmitoylation. For example the dendritic targeting of AMPA and NMDA glutamate receptors is regulated by palmitoylation, as is their cycling between the PM and endosomes within dendrites (Hayashi et al., 2005, 2009). Furthermore, palmitoylation can regulate protein localisation in response to signal transduction and neuronal cell activity. This is seen with the palmitoylation of the postsynaptic density protein-95 (PSD-95), which is decreased upon activation of the glutamate receptor, leading to a loss of synaptic localisation (El-Husseini Ael et al., 2002).

Another important role of palmitoylation is the partitioning of proteins into cholesterol-rich membrane microdomains, such as caveolae and lipid rafts. Both soluble and transmembrane proteins have been shown to be targeted into membrane microdomains in a palmitoylation dependent manner (Bhattacharyya et al., 2013; Prior et al., 2001). Interestingly however, the palmitoylation of caveolin-1 does not appear to be important for its localisation to detergent-insoluble domains or caveolae (Dietzen et al., 1995).

Other effects of palmitoylation include regulating protein stability (Linder and Deschenes, 2007; Delandre et al., 2009). This effect of palmitoylation can often reflect interplay between this modification and ubiquitination; for example palmitoylation of the yeast SNARE protein Tlg1 was shown to be important to prevent the ubiquitination of an adjacent lysine residue and subsequent degradation of the protein at the yeast vacuole (Valdez-Taubas and Pelham, 2005). Interplay between palmitoylation and phosphorylation has also been observed for proteins such as the beta2-adrenergic receptor (Moffett et al., 1996) and BK potassium channels (Tian et al., 2008). The interplay between palmitoylation and other post-translational modifications is not restricted to phosphorylation and ubiquitination, as recent work also highlight reciprocal regulation of PSD-95 by palmitoylation and S-nitrosylation of the same cysteine residues (Ho et al., 2011).

1.10.1 zDHHC Palmitoyltransferases (PATs)

The detailed mechanism of palmitoylation was not clear for many years following the identification of this process. It was observed that incubation of various proteins such as rhodopsin or SNAP25 with palmitoyl-CoA was sufficient for auto-palmitoylation to occur *in vitro* (Veit et al., 1998; Veit, 2000). These observations together with the lack of knowledge about palmitoylation enzymes led many investigators to suggest that palmitoylation was likely a spontaneous event *in vivo* that did not require a specific enzymatic activity (Linder et al., 2000). However, major breakthroughs came in 2002 with the identification of enzymes responsible for palmitoylation in yeast. Erf2p and Erf4p were found to palmitoylate Ras (Lobo et al., 2002), and Akr1p was shown to palmitoylate yeast casein kinase (Roth et al., 2002). Importantly, Erf2p and Akr1p were found to share a common “DHHC cysteine-rich” domain, which was critical for PAT activity. These studies served as a catalyst for subsequent studies in mammalian cells that identified a whole family of PAT enzymes, which includes 24 members (Fukata et al., 2004). All members of this protein group have a conserved cysteine rich 51 amino acid long zinc finger-like domain with a tetrapeptide aspartic acid, histidine, histidine, cysteine (DHHC) motif (Lobo et al., 2002; Mitchell et al., 2006), hence members of this protein group are

referred to as “zDHHC” proteins. Isoforms of the zDHHC enzyme family share structural similarities and have four to six TMDs with the DHHC motif located in a cytoplasmic loop (Mitchell et al., 2006). Studies examining mutations within this DHHC tetrapeptide showed that an intact DHHC motif is essential for PAT activity (e.g. Roth et al. 2002). Palmitoylation catalysed by zDHHC PATs is thought to consist of two steps, first the cysteine within the DHHC motif undergoes auto-palmitoylation to create a DHHC-palmitoyl intermediate, followed by the transfer of this palmitate onto the cysteine residue of its substrates (Mitchell et al., 2010).

The localisation of mammalian zDHHCs varies within the cell and individual members of the zDHHC family reside in different compartments of the cell. One of the first studies addressing the subcellular distribution of zDHHCs revealed that the majority of the zDHHC enzymes reside at membranes of the ER or Golgi apparatus and only a few zDHHCs were found to be elsewhere within the cell (Ohno et al., 2006). As this study was based on expression of N-terminally His₆ and Myc-tagged zDHHC isoforms in HEK293 cell, some of the reported localisations could have been affected by high expression levels. Indeed, zDHHC2 for example, which was found to localise in ER and Golgi apparatus by Ohno, was subsequently reported to localise at the PM and recycling endosomes of PC12 cells and hippocampal neurons (Greaves et al., 2011; Fukata et al., 2013). Another example is zDHHC4, which was reported to localise in the Golgi apparatus in the examination by Ohno, but was isolated at the ER in a different study (Gorleku et al., 2011). There is very little information available about how subcellular localisation of zDHHC enzymes is regulated (Gorleku et al., 2011; Greaves et al., 2011). Furthermore, whether zDHHC enzymes exhibit substrate specificity or how this potential specificity is regulated is currently debated (Huang et al., 2009; Rocks et al., 2010). Most evidence on this subject is gathered either from co-overexpression experiments of zDHHC enzymes together with substrates or in experiments where specific zDHHCs were knocked down. With this methodology, substrate specificity of some zDHHC enzymes was demonstrated for substrates such as the SNAP25 protein family and the protein huntingtin. Additionally these studies identified motifs within both substrates and

zDHHC enzymes which mediated the enzyme-substrate specificity (Huang et al., 2009; Greaves et al., 2010). However other studies failed to show strict specificity in the interaction of zDHHC enzymes with substrate proteins or to identify a consensus sequence or conserved feature within the substrate for recognition by a specific zDHHCs (Hou et al., 2009; Rocks et al., 2010). These studies suggest either an overlapping substrate specificity of zDHHC enzymes or propose that zDHHCs function promiscuously as PATs for many substrates at the same time.

1.11 Potential role of palmitoylation in insulin signalling

As described above (section 1.5), insulin-stimulated recruitment of GLUT4 to the PM involves multiple phosphorylation steps and various protein kinases, vesicle translocation from inside the cell towards the PM, and finally vesicle fusion with the PM. The various phosphorylation steps involved in the insulin signalling/GLUT4 translocation pathways have been extensively studied, whereas our knowledge of how other types of PTM impact on these pathways is less well-defined. It is clear that palmitoylation is important for the operation of these pathways but existing knowledge on the role of this PTM is very limited. Proteins in the initial steps of the insulin signalling pathways such as the IR and the small GTPase TC10 are palmitoylated (Magee and Siddle, 1988; Watson et al., 2003). However, neither the extent nor the role of palmitoylation of the IR is known. The palmitoylation of TC10 is better characterised and it is suggested that attachment of palmitate on two cysteine residues of TC10 is required for its partitioning into caveolin and cholesterol-enriched membrane domains (Watson et al., 2003). This is physiologically relevant, as localisation of TC10 in these specialised membrane compartments is essential for its role in insulin stimulated GLUT4 translocation in adipocytes (Watson et al., 2001, 2003). In addition to acting in the initial steps of the insulin signalling cascade, palmitoylation is also known to be required for fusion of GLUT4 vesicles with the PM. As described in section 1.4 and 1.5, fusion of GSVs with the PM is mediated by proteins of the vesicle fusion machinery. Proteins regulating vesicle fusion such as SNAP23, cysteine-string protein (CSP) or VAMP2 have been reported to be palmitoylated (Gundersen et al., 1994; Vogel and Roche,

1999; Veit et al., 2000). The palmitoylation of these exocytotic proteins is essential for their membrane attachment or correct protein trafficking or both (Vogel and Roche, 1999; Greaves and Chamberlain, 2006; Prescott et al., 2009). Apart from the initial steps of the insulin signalling pathway and membrane fusion, palmitoylation could also be involved in many other steps of these pathways. For example, recent research has suggested that the substrate of AKT, AS160, is palmitoylated in cultured adipocytes and in adipose tissue (Ren et al., 2013b). As described in section 1.5 AS160 is thought to regulate the intracellular retention of GSVs, however it is not known how palmitoylation of AS160 impacts its function in this process. More evidence for the role of palmitoylation in GLUT4 translocation was found in a recent study where silencing of the PAT zDHHC17 was demonstrated to impede insulin-stimulated GLUT4 translocation (Ren et al., 2013a). This effect is thought to be mediated by the palmitoylation of the zDHHC17 substrate ClipR-59. Palmitoylation of ClipR-59 regulates its association with the PM and this in turn also modulates the PM attachment and compartmentalisation of the protein kinase AKT (Ding and Du, 2009). Another process where palmitoylation could be potentially involved is the assembly of GSVs. Sortilin is a major component of GSVs and was reported to be palmitoylated (McCormick et al., 2008). The palmitoylation of sortilin is thought to be necessary for the correct trafficking from endosomes to compartments of the Golgi apparatus and affects its protein stability (McCormick et al., 2008; Dumaresq-Doiron et al., 2013). Stable sortilin with a correct cellular localisation may be important for the formation of GSVs, as sortilin is thought to be required for the association of GLUT4 with GSVs (Shi and Kandror, 2005).

Yet a comprehensive and detailed analysis of protein palmitoylation of components of the insulin signalling/GLUT4 trafficking pathways has not been undertaken. The initial phosphorylation steps in the insulin signalling cascade are in proximity to the PM and involve proteins that lack TMDs, and it is therefore possible that some of these membrane interactions are mediated by palmitoylation. Furthermore, palmitoylation is able to affect phosphorylation; it is thought that this effect is mediated by altering accessibility of kinases to their substrates (Moffett et al., 1993;

Tian et al., 2008). Thus, the interplay between palmitoylation and phosphorylation could be another potential mechanism of how palmitoylation might impact insulin signalling. Furthermore, palmitoylation was demonstrated to affect protein-protein interaction (Delandre et al., 2009), hence it is also possible that the attachment of palmitate onto components of the signalling pathway regulate their interaction.

When the present project was initiated, there was very little other information published on palmitoylated proteins in adipocytes. However, during the course of this PhD, a proteomics study was published identifying a number of other palmitoylated proteins in adipocytes (this is discussed further in section 3.7).

1.12 Aims of this study

The major aim of this PhD project is to identify novel palmitoylated proteins in 3T3-L1 adipocytes that might be involved in insulin signalling and/or GLUT4 trafficking. This will be followed by a detailed analysis of how palmitoylation impacts the properties of the identified proteins. Collectively, these analyses will provide more detailed information on the role of this important PTM in the pathways relevant to insulin-stimulated glucose transport. It is hoped that this analysis will identify potential new points of intervention to treat insulin resistance and type 2 diabetes. Overall, the individual aims of the project are to:

1. Identify novel palmitoylated proteins involved in insulin signalling and GLUT4 trafficking.
2. Determine the palmitoylation sites of these novel palmitoylated proteins.
3. Determine the effects of palmitoylation on protein trafficking and protein-protein interactions.
4. Identify the zDHHC proteins that are expressed in 3T3-L1 adipocytes, and that are potentially important for adipocyte physiology.
5. Identify the zDHHC enzymes that modify newly identified palmitoylated proteins in adipocytes.

Chapter 2: Materials and Methods

2.1 Materials

2.1.1 Chemicals

If not declared otherwise, chemicals were obtained as the purest grade available from Sigma-Aldrich Company (Dorset, U.K.) and Life Technologies (Paisley, U.K.).

2.1.2 Molecular biology reagents

One Shot® TOP10 Chemically Competent *E.coli*, PureLink™ Quick Plasmid Miniprep Kit, PureLink™ Gel Extraction Kit, TOPO® TA Cloning® Kit TA Cloning® Kit, SYBR® Safe desoxyribonucleic acid (DNA) gel stain, DNA ladder (1 kb) and Lipofectamine™ 2000 transfection reagent were purchased from Life Technologies (Paisley, U.K.). RNeasy® Mini kit, QIAquick gel extraction kit and QuantiTect Primer Assay were obtained from Qiagen (Sussex, U.K.) FastStart Universal SYBR Green Master, Transcriptor First Strand cDNA Synthesis kit and High Pure ribonucleic acid (RNA) Isolation kit were supplied by F. Hoffmann-La Roche Ltd. (Basel, Swiss). Oligonucleotide primers were synthesised by Sigma-Aldrich (Dorset, U.K.). GoTaq® DNA Polymerase, *pfu* polymerase, Oligo (dT)₁₅ primer, M-MLV Reverse Transcriptase, recombinant RNasin® Ribonuclease inhibitor, dNTPs (dATP, dCTP, dGTP, dTTP), restriction endonucleases, and T4 DNA Ligase were obtained from Promega (Southampton, U.K.). KOD hot Start DNA polymerase was supplied from Novagen, Merck Millipore (Billerica, MA, USA). FastDigest DpnI restriction enzyme was obtained from Thermo Scientific (Waltham, MA, U.S.A.) NucleoBond® Xtra Maxi kit was purchased from Macherey-Nagel (Düren, Germany). BCA Protein Assay Reagent Kit was supplied by Pierce Biotechnology (Rockford, IL, U.S.A.).

2.1.3 Primers

Table 2.1. Oligonucleotide primers (5'->3') used for amplification of GLUT1 and GLUT4 isoforms from 3T3-L1 adipocyte and mouse brain cDNA. Restriction sites used for cloning are underlined.

Primer Name	Forward Sequences	Reverse Sequences
GLUT1_E GFPC2	GATCAGAATTCATGGATCCCAGCAGC AAGAAG	GATCAGTCGACTCACACTTGGGAGTC CGCCCC
GLUT4_E GFPC2	GATCAGAATTCATGCCGTCGGGTTTCC AGCAG	GATCAGTCGACTCAGTCATTCTCATCT GGCCC
GLUT4_E GFPN1	GATCAAAGCTTATGCCGTCGGGTTTCC AGCAG	GATCAGTCGACCAGTCATTCTCATCT GGCCC

Table 2.2. Oligonucleotide primers (5'->3') for quantitative real-time PCR (qPCR) from 3T3-L1 pre-adipocyte and adipocyte cDNA

Primer Name	Forward Sequences	Reverse Sequences
DHHC1	CGCATAGAGGACCAGAAACCAG	CGCATAGAGGACCAGAAACCAG
DHHC2	ACACGGAACAGATAAGAACG	CGCATAGAGGACCAGAAACCAG
DHHC3	CGCATAGAGGACCAGAAACCAG	CGCATAGAGGACCAGAAACCAG
DHHC4	GGAAATGAACGCAAAAGGTG	CAGATCAGGACAACACAAATC
DHHC5	TGTTATCCAACCTTTGTCCATCAAGAG	GCAGTCCTCGTCTCTTTCCG
DHHC6	GCTTTATAATCGGCTCTCCTTTGG	GCCAATCCAAGGCAAACAAG
DHHC7	GAGTGCAGCGACTTCTCTCC	ATGACTGCGGTGAAGGTGAAG
DHHC9	GCTATGCTCTTTCTTTCTCC	CATTGGTGGCTTCTATTTC
DHHC12	CAGCTACGCCAATGGGAAGAG	GGTCCATGAGTGACACAGC
DHHC13	GGACAGAGTGTGAATATGACAGATG	AGAGGAGTGTCTGATGTGTTTTATC
DHHC14	TGTCATATTGTGCCACCATG	GTATACAGATCAAGAAAATAACAGAGG
DHHC15	GGTGCCAGTGCTCGTTATTG	AAAATGGCATGATAGAGTATGAGGTAG
DHHC16	TCTGATCCTCATCGTCTTCCATTAC	ACTTCTTACAGATGGAGACAGTAGC
DHHC17	CAAGCGAAAGGGTATGACAAACC	TTAATGAGCCAAGAATCAATGTCTAGG
DHHC20	CTCAAATCAACCTTTTCTATCAAACC	ACTCCTTCTCAGCTCCATTCTC
DHHC21	TCCCTACCACTTTGCCAATCAC	TTCATAAAACCTGTAACGCATTTCC
DHHC22	GCTGTCCTTTCCATCTCCTTCG	CAAACCAGAGGTAGAGCATGAGG
DHHC24	TCTGGTTCTGGCCTTTTCTAGC	AAGTTCTCAGTTCGATCCTCTGC

Table 2.3. QuantiTect Primer Assay for qPCR with 3T3-L1 pre-adipocyte and adipocyte cDNA

Target Protein	QuantiTect Primer Assay (200)	Catalogue Number
DHHC8	Mm_Zdhhc8_2_SG	QT01041257
DHHC11	Mm_Zdhhc11_2_SG	QT01078637
DHHC19	Mm_Zdhhc19_1_SG	QT00174650
DHHC23	Mm Zdhhc23 1 SG	QT01077545
DHHC25	Mm_1700030J15Rik_1_SG DHHC25	QT00255731
Ipo8	Mm_Ipo8_2_SG	QT01057518
Kdm2b	Mm_Kdm2b_2_SG	QT01044365
GLUT4	Mm_Slc2a4_2_SG	QT01538334

Table 2.4. Oligonucleotide primers (5'->3') for site directed mutagenesis (SDM) to mutate cysteine residues into alanine residues in N-terminal triple HA tagged IRAP-wild type EGFP-N1 expression vector. Mismatches to introduce mutations are underlined; reverse primers were synthesised as the reverse complementary sequence of forward primers

Target cysteine residue	Forward Sequence
35	GGTAGATTTAGCCAAAGAACCT <u>G</u> CTTTACATCCTCTGGAACC
103	CAGGCAGAGTCCAGATGGGACT <u>G</u> CTTCATTACCCTCTGCCAG
114	CTGCCAGGACCTTAGTGATCGCTGTTTTTGTTCATTGTGGTTGC

Table 2.5. Oligonucleotide primers (5'->3') used to replace the triple HA-tag in the IRAP-wild type EGFP-N1 expression vector with a single N-terminal Myc-tag. Restriction sites are underlined; Myc-tag coding sequence is in italic.

Target cysteine residue	
Forward Sequence	GGTAG <u>T</u> CGAC <i>ATGGAACAAAACTTATTTCTGAAGAAGATCTG</i> <i>ATGGAGTCCTTACCAATGATCGG</i>
Reverse Sequence	CGAT <u>G</u> GATCCGATCAATGATCATATGATATC CTACAGCCACTGGGAGAGCG

Table 2.6. Oligonucleotide primers (5'→3') for SDM to mutate cysteine residues into alanine residues in the caveolin-2-EGFP-N1 expression vector. Mismatches to introduce mutations are underlined; reverse primers were synthesised as the reverse complementary sequence of forward primers.

Target cysteine residue	Forward Sequence
72	CTTTGACAAAGTGTGGATCG <u>CC</u> CAGCCATGCTCTCTTTG
109	CCTGTTTGCTACCCTCAG <u>CG</u> CTCTGCACATCTGGATCC
122	CCTGATGCCTTTTGTGAAGAC <u>CG</u> CCCTAATGGTCTTGC
145	GTTGTCATTGGCCATTG <u>G</u> CTACAAGTGTGGGCCGAG

2.1.4 Plasmids

The plasmid vectors pEGFP-N1 and pEGFP-C2 were obtained from Clontech Laboratories Inc. (California, U.S.A.). The vectors express a red shifted variant of wild type GFP which has its excitation maximum at 488 nm and its emission maximum at 507 nm. DNA cloned in the pEGFP-N1 vector is expressed as a fusion protein to the N-Terminus of EGFP as the multiple cloning site is located in between the immediate early promoter CMV and the EGFP coding region. In contrast, the multiple cloning site of the pEGFP-C2 vector is located after the immediate early promoter CMV and the EGFP coding region. Thus genes cloned into the pEGFP-C2 vector will be expressed as a fusion protein to the C-terminus of EGFP. Both vectors express a kanamycin resistance cassette for selection in *E.coli*.

The pMa or pMa-T plasmid expression vectors were supplied by GeneArt®, Life Technologies (Carlsbad, CA, USA). The inserted DNA was N-terminal triple HA-tagged-IRAP, caveolin-1, caveolin-2, caveolin-1 3CA mutant and caveolin-2 4CA mutant. The inserted coding sequences were flanked with restriction enzyme sites and were subsequently cloned into pEGFP-N1, pEGFP-C2 or mCherry vector as described in the following sections.

Modified EGFP-N1 plasmids encoding mCherry-tagged constructs were generated by excising the coding region of EGFP from EGFP-N1 using *Age*1 and *Bsr*G1 restriction enzymes and replacing with the coding region of mCherry flanked by the

same restriction sites. This generated mCherry constructs that were in the same backbone as EGFP-N1 and had mCherry instead of EGFP.

EGFP- and RFP-tagged TC10 plasmids were kindly provided by Dr. Dolores Perez-Sala (Centro de Investigaciones Biologicas, CSIC Ramiro de Maeztu, 9, 28040 Madrid, Spain).

2.1.5 Electrophoresis and Western blot equipment

Gel-plates, electrophoresis tanks, protein transfer-tanks, power supplies and Polyvinylidene difluoride (PVDF) membranes were purchased from Bio-Rad Laboratories (California, U.S.A). Protran Nitrocellulose Membrane was obtained from Whatman (Maidstone, U.K.).

2.1.6 Cell culture plastics and media

All plasticware used to culture 3T3-L1 adipocytes (10 cm, 6-well, 12-well and 24-well plates) were purchased from BD Falcon™ VWR International (Radnor, Pennsylvania, U.S.A.). Rectangular Canted Neck Cell Culture Flask (75 cm²) were obtained from Corning (Tewksbury, Massachusetts, U.S.A.) All other cell culture plasticware was supplied by Greiner Bio-One (Kremsmünster, Austria). Gibco® DMEM GlutaMAX™, Newborn Calf Serum, Fetal Bovine Serum, penicillin-streptomycin, and Trypsin-EDTA were purchased from Life Technologies (Paisley, U.K.). 12 mm pre-coated poly-D-lysine coverslips were obtained from BD Biosciences (Oxford, U.K.).

2.1.7 Antibodies

Primary Antibodies

A rabbit polyclonal glucose transporter GLUT1 antibody was obtained from Merck Millipore (Billerica, Massachusetts, U.S.A.). This antibody is directed against a 12 amino acid long peptide in the C-terminus of GLUT1.

Glucose Transporter GLUT4 and cyclophilin b antibodies were purchased from Abcam plc (Cambridge, U.K.). The rabbit polyclonal GLUT4 antibody is directed against an immunogen located in the C-terminus of the protein. The rabbit

polyclonal cyclophilin b antibody was raised against a C-terminal peptide of human cyclophilin b.

BD Biosciences (Oxford, U.K.) supplied the polyclonal caveolin-1 antibody, which was raised in rabbit using a human caveolin-1 as the immunogen, and the polyclonal caveolin-2 antibody from mouse immunized with human caveolin-2 amino acids 42-162.

The following rabbit antibodies were purchased from Cell Signalling Technologies (Danvers, MA, U.S.A.):

 Polyclonal flotillin-1 antibody raised against a synthetic peptide corresponding to residues surrounding isoleucine-368 of human flotillin-1.

 Monoclonal flotillin-2 antibody raised against a synthetic peptide derived from residues surrounding phenylalanine-157 of human flotillin-2.

 Monoclonal antibody recognising the amino acid residues around tyrosine-960 residue of the IR β .

 Monoclonal antibody against IGF-I Receptor β raised in rabbit and recognising the carboxy-terminal residues of IGF-1 Receptor β .

 Polyclonal antibody recognising the carboxy-terminus of phosphoinositide-dependent protein kinase 1 (PDK-1).

Monoclonal mouse antibody raised against the total insulin-responsive aminopeptidase protein (IRAP) was purchased from Cell Signalling Technologies (Danvers, MA, U.S.A.).

The polyclonal rabbit antibody against Cysteine-string Protein (CSP) was raised against the C-terminus of the protein and supplied by Enzo life sciences (Farmingdale, NY, U.S.A.).

Anti Syntaxin-4 polyclonal rabbit antibody was purchased from Synaptic Systems (Goettingen, Germany).

Anti GFP JL-8 monoclonal mouse antibody was obtained from Clontech (Mountainview, CA, U.S.A.).

Anti HA-Biotin monoclonal rat antibody recognises the HA peptide sequence and was purchased from Roche (Basel, Switzerland).

Secondary Antibodies

Sheep anti-mouse IgG, donkey anti-rabbit IgG and goat anti-rat IgG conjugated to horseradish peroxidase (HRP) were purchased from GE Healthcare (Little Chalfont, Buckinghamshire, U.K.). HRP-conjugated antibodies were used at dilution ratio of 1:2000 for immunoblotting.

IRDye®-conjugated secondary antibodies were used to detect immune signals with the LI-COR Odyssey® Imager. IRDye® 680rd-conjugated goat anti-rat antibody, which has its excitation wavelength at 680 nm and its emission wavelength at 694 nm, was supplied by LI-COR Biosciences (Lincoln, NE, U.S.A.). DyLight 680-conjugated goat anti-mouse antibody, DyLight 680-conjugated rabbit anti-goat antibody, DyLight 680-conjugated goat anti-rat and DyLight 800 conjugated goat anti-rabbit antibody were supplied by Thermo Fischer Scientific (Waltham, MA, U.S.A.). IRDye® and DyLight conjugated antibodies were used at dilution ratio of 1:10 000 for immunoblotting.

2.1.8 Mammalian cell lines

3T3-L1 pre-adipocytes were either purchased from ATCC (Manassas, VA, U.S.A.) or from ZenBio (Triangle Park, NC, U.S.A.). HeLa cells and HEK293T cells were purchased from ATCC.

2.2 Mammalian cell culture

2.2.1 Culturing 3T3-L1 pre-adipocytes

Mouse 3T3-L1 pre-adipocytes were grown in 75 cm² cell culture flasks in Dulbecco's Modified Eagle Medium (DMEM) GlutaMAX™ supplemented with 10% newborn calf serum and 1% penicillin/streptomycin. Controlled conditions were maintained in a cell incubator including a temperature of 37° C, a gas mixture containing 10% CO₂ and saturated humidity.

3T3-L1 pre-adipocytes were sub-cultured approximately every 5 days when the cells were at approximately 60%-80% confluence. For this, the cell media was completely removed and the flask was washed with 5 ml of 0.05% Trypsin-ethylenediaminetetraacetic acid (EDTA) in order to remove residual media and detached cells. Subsequently, 2 ml of 0.05% Trypsin-EDTA was added and incubated for 2-3 min at 37°C in order to detach cells from the surface of the flask. To aid the process of cell detachment, the flask was flicked from the side. After ensuring all cells were detached, cell media was added to a final volume of 15 ml. Cells were then reseeded in dilutions of 1:10 or 1:20 in 75 cm² culture flasks or 1:5 in 100 mm culture dishes for further analysis or differentiation into adipocytes. All cells were maintained by replacing the media every third day.

2.2.2 Differentiation of 3T3-L1 pre-adipocytes into adipocytes

3T3-L1 is an established pre-adipocyte cell line, capable of differentiation into adipocytes (Green and Kehinde, 1975). The differentiation was induced by adding differentiation media consisting of DMEM GlutaMAX™ containing 10% fetal bovine serum, 1% penicillin/streptomycin, insulin (170 nM), troglitazone (1 µM), 3-isobutyl-1-methylxanthine (IBMX) (500 µM) and dexamethasone (0.25 µM) to pre-adipocytes which had been confluent for approximately 48 h. After three days the media was replaced with differentiation media without IBMX and dexamethasone. Differentiating cells were fed every three days by replacing the differentiating media with DMEM GlutaMAX™ containing 10% fetal bovine serum, 1% penicillin/streptomycin (adipocyte media) and collected 10 days after initiation of differentiation.

2.2.3 Harvesting pre-adipocytes and adipocytes

In order to collect cells, the culture media was aspirated completely from culture dishes followed by two washes with 10 ml phosphate buffered saline (PBS) (136 mM NaCl, 2.7 mM KCl; 10 mM Na₂HPO₄; 1.76 mM KH₂PO₄; pH 7.4). The cells were then transferred into 1.5 ml reaction tubes using a cell scraper and pelleted by a centrifugation step at 1,500 x g for 3 min. The cell pellets were stored at -80 °C for

further analysis. Pre-adipocytes were generally collected 10 days after plating in 100 mm culture dishes. Adipocytes were collected 10 days after the initiation of the differentiation.

2.2.4 Culturing of HEK293T cells

HEK293T cells were cultured in 75 cm² tissue culture flasks in DMEM GlutaMAX™ containing 10% fetal bovine serum and sub-cultured depending on the density of growth according to the procedure explained in section 2.2.1. Cells were reseeded at 1:20 dilution for culturing in flasks, in 1:6 dilution for culturing in pre-coated poly-D-lysine 24-well plates for biochemical analysis at a 1:12 dilution on pre-coated poly-D-lysine coverslips for subsequent analysis by confocal microscopy.

2.2.5 Plasmid DNA transfection into mammalian cells

Plasmid DNA was introduced into HEK293T cells using Lipofectamine™ 2000 Transfection Reagent (Life Technologies).

Lipofectamine™ 2000 reagent was added into 50 µl serum free media in sterile 1.5 ml reaction tubes and was used at a ratio of 2 µl/µg DNA for transfections. The required amount of DNA was pipetted into a separate 50 µl of serum free media. The solutions containing plasmid DNA and Lipofectamine™ 2000 were then combined and incubated for 25 minutes at room temperature. Subsequently the plasmid-Lipofectamine mixture was added to the cells. Cells were incubated with transfection mixture for 24 h in a cell incubator and then used for either immunofluorescence microscopy, for cell lysis followed by SDS-PAGE and western blotting or other biochemical based analysis.

2.2.6 Harvesting transfected cells for SDS-PAGE

Cells were washed two times with PBS and subsequently incubated for 10 minutes at room temperature in 200 µl SDS-Sample-Buffer (0.1% m/v bromphenol blue, 50 mM TrisBase, 10% v/v glycerol, 69.3 mM SDS, 25 mM DTT). The SDS-Sample-Buffer cell mixture was then heated to 95°C for 5 min and stored at -20°C for subsequent analysis.

2.2.7 Cell fixation and mounting onto microscope slides

In order to avoid any cell media contamination, cells were washed twice with PBS. To achieve fixation of the cells they were incubated in 4% v/v of formaldehyde in PBS for 30 minutes at room temperature followed by two washes with PBS. The coverslips were then air-dried and mounted onto microscope slides using 15 µl of ProLong Gold Antifade Reagent with DAPI (4',6-Diamidino-2-Phenylindole) mounting medium (Life Technologies (Paisley, U.K.)) per coverslip. Mounted coverslips were allowed to dry for at least 12 h and protected from light before they were analysed by fluorescence microscopy.

2.3 Molecular Biology

2.3.1 Standard molecular biology protocols

All bacterial liquid cultures were grown in autoclaved Luria-Bertani broth (LB) media (10 g/L NaCl, 10 g/L tryptone (Merck), 5 g/L yeast extract (Bacto™ Yeast Extract, BD)). For growth on solid media, LB agar was prepared containing LB media and 20 g/L agar. The LB media was supplemented with appropriate antibiotics (100 µg/ml ampicillin or 30 µg/ml kanamycin) prior to use.

DNA and RNA were kept in diethylpyrocarbonate (DEPC)-treated water, which was prepared by adding 0.1% DEPC to ultra-pure water and incubating overnight, prior to autoclaving in order to remove traces of DEPC.

2.3.2 DNA amplification by polymerase chain reaction (PCR)

Polymerase chain reaction (PCR) was used to amplify specific DNA sequences. PCR was also used as a method to introduce targeted mutations into DNA.

For amplification of a specific DNA sequence, sense and antisense oligonucleotide primers were designed and synthesised by Sigma-Aldrich. The PCR reaction mix contained 50 ng template DNA or cDNA, 300 nM of each primer (forward and reverse), 5 µl of 10X PCR Buffer for KOD Hot Start DNA Polymerase, 200 µM dNTPs (50 µM each of dATP, dCTP, dGTP and dTTP), 2.5 mM MgSO₄ and 1 µl of KOD Hot

Start DNA Polymerase (1.0 U/ μ l). DEPC treated water was added to bring the PCR mixture to a final volume of 50 μ l and then the PCR-mix was heated to 94°C for two minutes in order to denature the DNA and heat-activate the KOD Hot Start DNA Polymerase. Subsequently, 30 cycles followed consisting of a 30 second denaturation step at 94°C, a 30 second annealing step with the temperature chosen 5°C below the melting temperature (T_M) of the primers and an elongation step at 68°C. The duration of the elongation step was adjusted according to the length of the amplification product with approximately 30 seconds for 1 kilobase pair of DNA. PCR products were stored at - 20°C until required. This PCR protocol was used for amplifying coding regions from cDNA.

2.3.3 Site-directed mutagenesis (SDM)

Site-directed mutagenesis (SDM) was used to introduce target specific mutations into DNA of expression plasmids.

For this, oligonucleotide primers were designed to have a specific mismatch of up to two base pairs with the target DNA of the expression plasmid. The sequence with the mismatching base pairs would then be amplified in each following PCR cycle and eventually outnumber the original sequence of the expression plasmid. The oligonucleotide primers consisted of approximately 15-20 nucleotides up-and downstream of the specific mismatch and thus had a total length between 30 and 45 nucleotides. The final length of the SDM oligonucleotide primers was adjusted to result with a melting temperature T_M of approximately 78°C or higher of the oligonucleotide. The sequence of the antisense primer was the reverse complementary sequence of the sense primer.

The SDM PCR reaction mix concentrations and reagents used were according to the reaction mix of the standard PCR described in 2.3.2. The reaction mix was heated at 95°C for two minutes for initial denaturation of the DNA and heat activation of the KOD hot start DNA Polymerase, followed by 18 cycles comprising of a 30 second denaturation step at 95°C, a 15 second annealing step at 55°C and an elongation step at 68°C. The length of the elongation step was adjusted according to the size of

the expression plasmid with approximately 30 seconds for 1 kilobase pair of plasmid DNA.

The template expression vector was isolated from the bacterial strain *E. coli*. As the replication of plasmid DNA in *E. coli* results in DNA methylation, it was possible to selectively digest the template plasmid using a methylation sensitive restriction enzyme. For this, 1 μ l of the restriction enzyme FastDigest DpnI was added to 9 μ l of the plasmid DNA amplified by SDM and incubated for two hours at 37°C. The DNA solution containing the mutated expression plasmid was then processed further or stored at -20°C until needed.

2.3.4 RNA purification

Total RNA was purified using RNeasy Mini Kit (Qiagen Ltd.) according to the manufacturer's protocol. 3T3-L1 pre-adipocytes or adipocyte cell pellets were collected as described in section 2.2.3 and lysed in 600 μ l RLT-buffer containing 1% v/v β -Mercaptoethanol (β -ME) by passing the pellet 10 times through a 26g needle with an inner diameter of 0.26 mm. The lysed pellets could be stored at -80°C for up to one month before continuing with the RNA purification. Subsequently 600 μ l of 70% v/v ethanol was added to the lysed cells and mixed well by pipetting. The mixture was then immediately transferred onto an RNeasy mini column and centrifuged at 10,000 x g for 30 seconds to pass through the unbound solution and to allow binding of the RNA to the column. The RNA-bound column was then washed with 700 μ l RW1-buffer (composition proprietary) followed by a wash with 500 μ l RPE-buffer (composition proprietary), applying centrifugation at 10,000 x g for 30 seconds for both washing steps. The wash with RPE-buffer was repeated followed by centrifugation at 10,000 x g for 2 minutes to dry the column in order to avoid carrying over ethanol into the RNA elution. After the centrifugation, the column was placed in a fresh collection tube and RNA was eluted by adding 50 μ l of DEPC-treated water directly onto the column and centrifugation at 10,000 x g for 1 minute. The concentration of the eluted RNA was measured by spectrophotometric quantification. RNA was either immediately processed by reverse transcription into cDNA or stored at -80°C.

2.3.5 Spectrophotometric quantification of DNA and RNA

Purines and pyrimidines in nucleic acids have absorption maxima at approximately 260 nm wavelength (eg. dTTP: 259 nm; dGTP: 253 nm; dATP: 259 nm; dCTP: 272 nm). This property of nucleic acids enables UV spectrophotometric-based analysis to determine the concentration and purity of purified DNA and RNA. Contaminants like proteins or phenol have an absorbance maximum around 280 nm whereas organic solvents containing aromatic compounds absorb light at a wavelength of 230 nm. The ratios of OD_{260}/OD_{230} and OD_{260}/OD_{280} therefore determined the grade of purity of the samples. An OD_{260}/OD_{280} ratio of 1.8-2.0 and an OD_{260}/OD_{230} ratio of 2.0 – 2.2 indicate sufficient purity of the samples for downstream processing. The amount of DNA/RNA was quantified using following formula:

Absorbance (OD) * dilution factor * 50 = DNA concentration (ng/ μ l)

Absorbance (OD) * dilution factor * 40 = RNA concentration (ng/ μ l)

2.3.6 Agarose gel electrophoresis

Agarose gel electrophoresis was used to determine the integrity of purified RNA, for visualisation or purification of DNA fragments amplified by polymerase chain reaction (PCR) or to visualise and separate DNA fragment which were digested by restriction enzymes. Samples were electrophoretically separated in a 1% (w/v) agarose gel in TAE buffer (40 mM Tris, 1 mM thylenediaminetetraacetic acid (EDTA), pH8) supplemented with SYBR[®] Safe (1:10,000). The nucleic acids were visualised under ultraviolet illumination.

2.3.7 DNA purification from agarose gels

After subjecting PCR amplification products to agarose gel electrophoresis (see section 2.3.6), DNA was visualised under UV light and DNA bands were excised from the agarose gel in a minimum volume of agarose. The DNA-containing agarose was then transferred into a 1.5 ml reaction tube and DNA was purified using a QIAquick Gel Extraction kit (Qiagen Ltd). First, three volumes of QG buffer was added to the gel slice (100 mg of gel slice corresponds to a 100 μ l volume) followed by melting

the agarose by heating to 50°C for 10 minutes with occasional vortexing. Subsequently, one gel volume of isopropanol was added and gently mixed by pipetting. The mixture was then transferred to a QIAquick Spin Column and centrifuged for one minute at 13,000 x g to bind the DNA to the column. In order to remove any residual agarose from the column, it was washed with first 500 µl and then 750 µl RPE buffer by centrifuging the column for one minute at 13,000 x g. The column was cleared of any residual buffer by centrifugation for one minute at 13,000 x g. Subsequently, the column was transferred into a fresh 1.5 ml reaction tube and the bound DNA was eluted by adding 30 µl of DEPC-treated water onto the column followed by centrifugation for one minute at 13,000 x g. To examine success or otherwise of the purification, one tenth of the elution volume was resolved on a 1% agarose gel, compared against a 100 bp or 1 kb DNA ladder (see 2.3.6).

2.3.8 Assessing integrity of purified RNA

In order to determine the extent of degradation of the purified RNA an integrity test was performed. For this, 5 µl of the purified RNA was electrophoretically separated as described above (see 2.3.6.) The RNA integrity was assessed as good if the signal ratio for 28S ribosomal RNA (at approximately 5 kbp) to the signal for the 18S ribosomal RNA (at approximately 2 kbp) was around 2:1 (Sambrook et al., 1989). Only RNA with an appropriate ratio and clear bands was processed further and used for cDNA synthesis.

2.3.9 Restriction endonuclease digestion

In order to digest DNA with site-specific restriction endonucleases, 1-2 µg vector DNA was mixed with 1 µl of each FastDigest® restriction enzymes (Fermantas Life Sciences), 2 µl of 10X FastDigest® Buffer and finally DEPC-treated water was added to give a final volume of 20 µl. The mixture was then incubated for one hour at 37°C. The success of the digestion was determined by agarose gel electrophoresis.

2.3.10 Ligation of DNA inserts with plasmid vectors

Following restriction digestion, the DNA was ligated to the plasmid vector to obtain the final construct. To ensure high efficiency of the ligation, it was important to use a higher concentration of the DNA insert than the plasmid DNA. The appropriate amount of DNA, 10 μ l of 2X ligation buffer, and 1 μ l of T4 ligase were added and made up to a final volume of 20 μ l with DEPC-treated water. The ligation mix was then incubated for 30 minutes at room temperature. Following the ligation, a transformation into chemically-competent cells (see 2.3.11) and a miniprep (see 2.3.12) was performed to amplify the newly-formed plasmid DNA. The purified plasmid DNA was then sequenced to determine the success of the ligation (GATC Biotech).

2.3.11 Transformation of expression plasmid DNA into One Shot® TOP10 cells

In order to replicate plasmid DNA, the expression vector was transformed into a chemically competent *E. coli* strain (TOP10; Life Technologies). The plasmid DNA was subsequently purified from the cells to yield a higher copy number of the plasmid.

For this, one to 5 μ l of DNA was added into a vial of One Shot® TOP10 cells (50 μ l) and incubated for 30 minutes on ice followed by a 30 second incubation at 42°C and then immediately placed on ice for at least two minutes. The transformed cells were then incubated in 250 μ l SOC medium (Tryptone 2% (w/v), Yeast extract 0.5% (w/v), 8.6 mM NaCl, 2.5 mM KCl, 20 mM MgSO₄, 20 mM Glucose) for one hour at 37°C in an orbital shaker set to 200 rpm, and subsequently plated on pre-warmed agar plates (see 2.3.1) containing 50 μ g/ml ampicillin or 30 μ g/ml kanamycin . The plates were then incubated overnight at 37°C.

2.3.12 Small-scale (miniprep) plasmid purification

Small-scale plasmid purification was performed to screen bacterial colonies for the presence of the appropriate plasmid DNA. The miniprep was carried out according

to the protocol of the supplier (PureLink™ Quick Plasmid Miniprep Kit; Life Technologies).

2.3.13 DNA sequencing

In order to assure the accuracy of plasmid vectors, the generated plasmids were sequenced on both strands by GATC Biotech (Konstanz, Germany).

2.3.14 Large scale (maxiprep) plasmid purification

After confirming the fidelity of plasmid DNA constructs by sequencing, large scale plasmid purification was performed to obtain sufficient quantities of the expression vector construct for use in downstream analyses. The maxiprep was carried out following the protocol of the used kit (Machery Nagel, Nucleo Bond Xtra Maxi).

2.3.15 Reverse transcription of RNA into cDNA

The purified total RNA from either 3T3-L1 pre-adipocytes or adipocytes was reverse transcribed into cDNA and was used either for quantitative real-time PCR (qPCR) or for amplification of specific coding sequences by conventional PCR. Dependent on the intended use of the cDNA, different reverse transcription kits were used.

Reverse transcription for quantitative real-time PCR (qPCR)

Purified RNA from 3T3-L1 pre-adipocytes and adipocytes was reverse transcribed into cDNA for later analysis by qPCR. For this, the Transcriptor First Strand cDNA Synthesis Kit (Roche) was used. Pre-adipocyte and adipocyte RNA concentrations were equalised prior to reverse transcription which was conducted according to the manufacturer's protocol. 10 µl of RNA was combined with 1 µl of anchored oligo (dT)₁₈ primer (50 pmol/µl) and 2 µl of random hexamer primer (600 pmol/µl) followed by an incubation at 65°C for 10 minutes, to denature the template-primer mixture, and especially the secondary structure of the RNA. Subsequently, other components required for the reaction were added to the template-primer mix, which were: 4 µl Transcriptor Reverse Transcriptase Reaction Buffer 5X, 8 mM MgCl₂, 0.5 µl Protector RNase Inhibitor 40 U/µl, 2 µl Deoxynucleotide Mix 10 mM each (final concentration 1 mM each); 0.5 µl Transcriptor Reverse Transcriptase 20

U/ μ l. The sample mix was then incubated in a thermocycler for 60 min at 50°C. The reaction was stopped by inactivating the reverse transcriptase enzyme by incubation at 85°C for 5 minutes. The synthesised cDNA was stored at -20°C or immediately used for qPCR. For each RNA sample a non-enzyme control was performed by replacing the reverse transcriptase with water, and one non-template control was performed by replacing the RNA with water.

Reverse transcription for amplifying coding sequences by PCR

For reverse transcription, 2 μ l of RNA was combined with 0.5 μ g of Oligo (dT)₁₅ primer and DEPC treated water was added to a final volume of 15 μ l. Secondary structures of RNA and primers were denatured by incubating the primer-RNA mix at 70°C for 5 minutes. Following the denaturation, remaining reaction components were added to the RNA-primer mix: 10 μ l of M-MLV Reverse Transcriptase 5X Reaction Buffer (Promega); 0.625 μ l of RNasin® Ribonuclease Inhibitors (Promega); 5 μ l Deoxynucleotide Mix 10 mM each (final concentration 1 mM each); 1 μ l Moloney Murine Leukemia Virus Reverse Transcriptase (M-MLV RT, Promega); DEPC treated water to a final volume of 50 μ l. The reaction mix was gently mixed and incubated at 42 °C for 60 minutes. The cDNA was either used directly in PCR amplifications using gene-specific primers or stored at -20°C for future use.

2.3.16 Quantitative real-time PCR (qPCR)

Primers designed for DNA amplification were obtained from Sigma-Aldrich. Prior to use, the primers were validated to ensure sufficient efficiency and specificity. For this, cDNA derived from mouse brain tissue was used as a template and three dilutions with the ratios of template to water 1:10, 1:100 and 1:1000 were prepared. Each primer was tested for every dilution ratio in triplicate. In addition to 2.5 μ l template, each reaction mix contained 12.5 μ l SYBR Green Master, 1 μ l each of forward and reverse primer (100 μ M) and 8 μ l of DEPC treated water. The qPCR mix was heated to 50°C for two minutes and then heated further to 95°C for 10 minutes in order to denature the DNA template. This was followed by 40 cycles consisting of a DNA denaturation step at 95°C for 15 seconds and a annealing and

extension step at 60°C for one minute. Finally the dissociation of double-stranded DNA into single-stranded DNA was initiated by one cycle consisting of 15 seconds at 95°C, 20 seconds at 60°C and 15 seconds at 95°C. This final dissociation step was performed to assess the specificity of the used primers. Dissociation curves with one peak indicate the amplification of one specific PCR product. In order to determine the efficiency of the primers, Ct values for each dilution ratio of the template were measured and the Ct values were plotted against the concentration of the template to form a standard curve. The slope of the standard curve was then used to calculate the efficiency using the following equation:

$$\text{primer_efficiency} = 10^{(-1/\text{slope})} - 1$$

Primers with an efficiency of 1 ± 0.1 were further used for qPCR analysis.

The template cDNA for qPCR analysis was obtained from RNA which was purified from 3T3-L1 pre-adipocytes and corresponding adipocytes and then reverse transcribed into cDNA as described in section 2.3.4 and 2.3.15. Template cDNA was diluted 1:10 in DEPC-treated water before adding to the qPCR mix. Conditions applied for the qPCR analysis of target genes were identical with the conditions used for primer validation (see above). The measured Ct values for all target genes were analysed relative to a control gene. The fold expression of each gene was calculated by forming the ΔCt value of the control gene and the target gene ($\Delta\text{Ct} = \text{ct}(\text{control gene}) - \text{ct}(\text{target gene})$). The relative fold expression change of target gene to control gene was calculated by following equation.

$$\text{fold_exp_ression} = 2^{\Delta\text{Ct}}$$

When comparing the relative expression levels of target genes derived from two different cell types (eg. 3T3-L1 pre-adipocytes and 3T3-L1 adipocytes) a $\Delta\Delta\text{Ct}$ was formed by subtracting the ΔCt of a target gene derived from one cell type (eg. adipocytes) from the ΔCt from the other cell type (eg. pre-adipocytes). The relative fold change of the relative expression between two cell types was calculated using following equation:

$$\text{fold_exp_ression} = 2^{\Delta\Delta\text{Ct}}$$

2.3.17 PCR amplification of targeted protein cDNA and cloning into plasmid expression vector

This section describes how cDNA of targeted proteins was amplified either from plasmid DNA or from purified mRNA using PCR (see 2.3.2) and subsequently cloned into an expression plasmid vector. If not differently stated, forward and reverse primers for the amplification with PCR were designed to introduce restriction sites upstream and downstream of the targeted cDNA. The resulting PCR amplification product and the target expression plasmid were then subjected to digestion by appropriate endonucleases as described in 2.3.9. The digested amplification product and plasmid vector were then subjected to gel electrophoresis, to separate the DNA fragments (see 2.3.6). Bands corresponding to targeted DNA fragments were excised and purified according to section 2.3.7. Following gel purification, both DNA fragments were ligated together according to 2.3.10 Ligation of DNA inserts with plasmid vectors¹⁰ and transformed into One Shot[®] TOP10 (see 2.3.11). In order to amplify the ligated expression vector, small-scale plasmid purification was performed (see 2.3.12). Subsequently, fidelity of the DNA plasmids was confirmed by DNA sequencing and large scale plasmid purification was performed (See 2.3.13 and 2.3.14). Amplified expression vectors were stored at -20 °C until used.

2.3.17.1 PCR amplification of GLUT1 and GLUT4 coding sequences and cloning into pEGFP-C2 and pEGFP-N1 vectors

For amplification of the coding sequences of GLUT1 and GLUT4, RNA was purified from 3T3-L1 adipocytes and mouse brain tissue and reverse transcribed into cDNA, as described in sections 2.3.4 and 2.3.15. Subsequently, the cDNA was used as a template to amplify the GLUT1 and GLUT4 coding sequences using PCR with conditions described in section 2.3.2.

For cloning into the pEGFP-C2 vector, forward primers were designed to insert a restriction site for *EcoRI* and the reverse primers were designed to insert a restriction site for *Sall*. For cloning GLUT4 into a pEGFP-N1 expression vector, the forward primer was designed to create a restriction site for *HindIII* and the reverse

primer was designed to create a *Sall* restriction site. Sequences of these oligonucleotide primers are shown in Table 2.1. Oligonucleotide primers (5'→3') used for amplification of GLUT1 and GLUT4 isoforms from 3T3-L1 adipocyte and mouse brain cDNA. The PCR amplification was then subjected to agarose gel electrophoresis (see 2.3.6). Bands corresponding to GLUT1 or GLUT4 amplification product were excised from the gel. Subsequently the DNA contained in the gel piece was purified according to section 2.3.7. The purified plasmid was then sub-cloned into a pCR®2.1 TOPO® Cloning Vector as described below.

Sub-cloning of PCR amplification products into a pCR®2.1 TOPO® Cloning Vector and transformation into One Shot® TOP10 Competent Cells

For increased cloning efficiency, amplified GLUT1 and GLUT4 coding sequences were first cloned into the pCR®2.1 TOPO® Cloning Vector. TOPO® cloning is based on an adenine overhang of the PCR product, which anneals with the help of topoisomerase I with the thymidine overhang of the vector. To add the required adenine at the 3' phosphate of the PCR product, 20 µl of the gel purified PCR product was incubated with 0.5 units of *Taq* DNA-polymerase, 2 µl of TOPO® *Taq* polymerase buffer and 0.4 µl dNTPs (40 mM; 10mM each dATP, dTTP, dCTP, dGTP) at 72°C for 20 minutes. Subsequently, 2 µl of the *Taq* polymerase treated PCR product was added to 1 µl TOPO® salt solution, 1 µl TOPO® Cloning Vector and 1 µl of DEPC-treated water and incubated for 5 minutes at room temperature to clone the PCR product into the TOPO® Cloning Vector. The TOPO® cloning Vector including the PCR product was then transformed into One Shot® TOP10 Competent Cells (see 2.3.11).

For subsequent cloning of GLUT1 and GLUT4 cDNA in EGFP-N1 or EGFP-C2 vectors, the TOPO® Cloning Vector amplified DNA (see above) was digested using the appropriate restriction enzymes. Cloning into pEGFP-N1 vector required digestion with restriction enzymes *HindIII* and *Sall*. For cloning constructs into the pEGFP-C2 vector restriction enzymes *EcoRI* and *Sall* were used. The digested DNA fragments were further processed as described above (see 2.3.17).

2.3.17.2 Cloning IRAP cDNA into the EGFP-N1 expression vector

Expression plasmid with pMA vector backbone and IRAP wild type (wt) cDNA was supplied by GeneArt®. The IRAP wild type cDNA had the sequence of three HA-tags upstream the ATG of IRAP. The whole construct was flanked with restriction enzyme site for *Sall* upstream the triple HA-tag and *BamHI* immediately downstream of the stop codon of IRAP.

The IRAP cDNA containing pMA vector and the empty EGFP-N1 vector were digested with *Sall* and *BamHI* restriction enzymes and cloned into the EGFP-N1 vector as described in section 2.3.17.

Introducing cysteine to alanine mutations in 3HA-IRAP-EGFP-N1 plasmid using SDM.

Cysteine residues at positions 35, 103 and 114 were mutated to alanine using SDM according to section 2.3.3. For this the triplet codon TGT for cysteine was changed into GCT which encodes alanine. The sequences of the oligonucleotide primers used for each mutation are listed in Table 2.4.

Changing the triple HA-tag upstream of IRAP to single Myc-tag to create Myc-IRAP-EGFP-N1 expression vector.

The sequence of three HA-tags upstream the ATG of IRAP cDNA in the 3HA-IRAP-EGFP-N1 plasmid were replaced with the sequence of a single Myc-tag. For this oligonucleotide primers were ordered from Integrated DNA Technologies (Coraville, IA, U.S.A) to insert the required sequence changes using PCR. The forward primer was designed to anneal to 24 nucleotides starting from the ATG. Additionally the forward primer was comprised of an overhang upstream the ATG which included the sequence of the Myc-tag, the restriction site for *Sall* and a four nucleotide long spacer sequence upstream the *Sall* restriction site to enable binding of the restriction enzyme. The reverse primer was designed to anneal with 20 nucleotides upstream from the stop codon of IRAP and included an overhang comprising a spacer sequence and the sequence for the restriction enzyme *BamHI*. The detailed

sequence of both oligonucleotide primers can be seen in Table 2.5. After performing the PCR with the specified oligonucleotide primers, the PCR product was digested with *DpnI* followed by a digestion using the restriction enzymes *SalI* and *BamHI*. The remaining steps of the cloning were carried out according to section 2.3.17.

2.2.17.3 Cloning caveolin-1 and caveolin-2 cDNA constructs into EGFP-N1 expression vector.

Expression plasmid with pMA-T vector backbone and various caveolin cDNA as inserts were ordered from GeneArt®. The inserts were the cDNA encoding for: Caveolin-1 wild type, caveolin-2 wild type, caveolin-1 mutant with amino acid alanine instead of cysteine residues named caveolin-1 3CA and caveolin-2 mutant with amino acid alanine instead of cysteine residues named caveolin-2 4CA. The stop codons of all four caveolin constructs were removed in order to express EGFP once cloned in the EGFP-N1 expression vector. The caveolin insert was flanked upstream the N-terminus by the restriction site for enzyme *SalI* and downstream the C-terminus with an in frame restriction site for enzyme *BamHI*. The plasmids were digested with *SalI* and *BamHI* and cloned into EGFP-N1 vector according to 2.3.17.

2.2.17.4 Cloning caveolin-1 and caveolin-2 cDNA from EGFP-N1 into the mCherry -N1 vector expression vector.

The expression vectors caveolin-1-EGFP-N1, caveolin-2-EGFP-N1 and the mCherry were digested with the restriction enzymes *SalI* and *BamHI*. Subsequent ligation, transformation into chemo competent cells, small scale plasmid purification, DNA sequencing and large scale purification was performed as described in section 2.3.17.

Introducing cysteine to alanine mutations in caveolin-2-EGFP-N1 plasmid using SDM.

The protein caveolin-2 has four cysteine residues at the amino acid positions 72, 109, 122 and 145. Oligonucleotide primers were designed (see Table 2.6.) to change

the cysteine encoding triplet codon TGC into the alanine encoding triplet codon GCC using SDM of each cysteine separately in caveolin-2. The procedure for the SDM was carried out as described in section 2.3.3. Following the SDM the plasmids were amplified according to sections 2.3.11 - 2.3.14.

2.4 Protein Biochemistry

2.4.1 Identification of palmitoylated proteins using resin-assisted capture of S-acylated proteins (acyl-RAC).

Purification of palmitoylated proteins using resin-assisted capture of S-acylated proteins (acyl-RAC) was used to investigate palmitoylation in adipocytes. This method allows analysis of the level of palmitoylation of known palmitoylated proteins, or identification of novel palmitoylated proteins. Furthermore, it can be used to detect changes in palmitoylation during various processes of cell signalling.

2.4.1.1 Purification of membrane-associated proteins by differential centrifugation.

As the majority of palmitoylated proteins are membrane-associated, a membrane fraction was used as the starting material for acyl-RAC. In order to separate proteins associated with membranes from proteins localised in the cytosol or nucleus, differential centrifugation was applied. 3T3-L1 adipocytes were collected at day 10 post-differentiation initiation and pelleted by centrifugation at 1,000 x g for 2 minutes, and subsequently resuspended in 1 ml buffer A (25 mM HEPES, 25 mM NaCl, 1 mM EDTA, pH 7.4 and protease inhibitor cocktail). The resuspended pellet was passed five to ten times through a 26G needle (inner diameter 0.26 mm) in order to disrupt the cells. Following disruption, the cell fraction was centrifuged at 800 x g for 5 minutes at 4°C to pellet the nuclei; the supernatant was then subjected to further centrifugation at either 16,000 x g for 50 min at 4°C or 136,000 x g for 60 min at 4°C. The supernatant containing the cytosolic fraction was removed and the pellet containing the membrane fraction was resuspended in 100 µl buffer A containing 0.5% Triton X-100 (v/v).

2.4.1.2 Blocking free cysteines with S-methyl methanethiosulfonate (MMTS)

Proteins which do not undergo post-translational S-acylation or other cysteine modifications contain unmodified cysteine residues with free SH groups. As the generation of free SH groups is a key step in the acyl-RAC protocol to purify palmitoylated proteins, free SH groups present on non-palmitoylated proteins first need to be blocked. For this, S-methyl methanethiosulfonate (MMTS) was used. MMTS blocks free SH-groups by adding a thiomethyl group via formation of a mixed disulphide bond. In order to block free SH groups with MMTS, 200 µl of blocking buffer (100 mM HEPES, 1 mM EDTA, 87.5 mM SDS and 1-1.5% MMTS) was added to the resuspended proteins and incubated for 4 h at 40 °C with frequent vortexing.

2.4.1.3 Acetone precipitation of proteins

Following the blocking treatment, the proteins were precipitated using acetone. For this, 3 volumes of cold 100% acetone was added to the blocking protein mixture and incubated for 20 minutes at -20 °C. Following the incubation, the precipitated proteins were sedimented by centrifugation at 5,000 x g for 10 minutes. The supernatant was removed and the pellet was air-dried. Subsequently, the pellet was washed five times by resuspending in 1 ml of 70% (v/v) acetone and vortexing, followed by centrifugation at 5000 x g for 10 min.

2.4.1.4 Hydroxylamine treatment and resin capture

During this step, the post-translational modification consisting of palmitoylation, is cleaved off by treatment with hydroxylamine (HA). HA reduces the thioester bond of the proteins resulting in free SH-groups. These free thiol groups can then bind to Thiopropyl Sepharose® beads forming disulphide bonds, allowing separation of S-acylated and non-S-acylated proteins.

For the HA treatment and resin capture, the Thiopropyl Sepharose® was activated by adding dH₂O and shaking for 15 minutes. After pelleting the beads by centrifugation at 1,000 x g for 5 min, excess dH₂O was removed and the activated beads were resuspended in the appropriate amount of binding buffer (0.1 g beads in 1 ml binding buffer (100 mM HEPES, 1 mM EDTA, 35 mM SDS)). 200 µl of the

beads/binding buffer slurry was then aliquoted into 1.5 ml reaction tubes and centrifuged for three minutes at 800 x g. Excess binding buffer was removed. The previously precipitated proteins (see above) were resuspended in 400 µl binding buffer and 160 µl was added into two separate tubes each, containing the previously prepared Thiopropyl Sepharose® beads. The remaining 40 µl were kept as the **total input** control.

For treatment with HA, 2 M HA pH 7.5 was added into the reaction tube containing the beads/protein-binding buffer solution to a final concentration of 0.5 M. For a negative control HA was replaced with the same concentration of Tris. These samples were then incubated overnight at room temperature with end-over-end mixing. In order to separate the beads from the unbound solution, the tubes were then centrifuged at 800 x g for 5 minutes. The supernatant was removed and retained as the **unbound** fraction. The remaining beads were washed five times with 1 ml binding buffer by vortexing and pelleting the beads by centrifugation at 1,000 x g for 30 seconds. Subsequently, the proteins were eluted from the beads by two consecutive incubations in 100 µl 1x Laemmli buffer containing 50 mM dithiothreitol (DTT) for 15 minutes at room temperature and then 5 minutes at 95 °C. The eluted proteins were the **bound** fraction. The **bound** fraction was separated from the beads by centrifugation 1,000 x g for 2 min and the supernatant transferred into a fresh reaction tube. Before subjecting all samples to SDS-PAGE, the final volumes of the bound and unbound fractions were equalised.

2.4.2 Detection of 17-octadecynoic acid (17ODYA) attachment onto proteins using “Click-Chemistry”

The detection of 17-octadecynoic acid (17ODYA) incorporated in proteins with the use of click-chemistry was used in order to characterise the palmitoylation of identified palmitoylated proteins. The click-chemistry method is based on a chemical reaction termed Azide-alkyne Huisgen cycloaddition, where an azide forms covalent bonds with an alkyne and results in a 1,2,3-triazole. In this thesis, the term click-chemistry refers to the entire process of detection of 17ODYA incorporation in

proteins. This method in combination with SDM enabled the identification of palmitoylation sites of proteins. Furthermore, characterisation of zDHHC substrate specificity was possible, when substrates were co-overexpressed with zDHHC enzymes followed by the application of click-chemistry.

2.4.2.1 Metabolic labelling of HEK293T cells with 17ODYA.

The method of click-chemistry relies on the incorporation of 17ODYA onto cysteine residues of proteins within examined cells. For this, 17ODYA was provided to the cells in the culture media. After being taken up by the cell, palmitoyl transferases can attach the 17ODYA onto cysteine residues via a thioester linkage. This is possible because 17ODYA does only differ from palmitic acid by an alkyne at the omega end of the fatty acid and an additional carbon.

In order to examine the palmitoylation of specific proteins, HEK293T cells were transfected with expression vectors containing the cDNA of the protein of interest. 24 hours post-transfection, the culture medium was replaced with serum-free medium containing 1% (w/v) fatty acid-free bovine serum albumin (BSA) for 30 minutes. For the metabolic labelling, cells were incubated in serum free culture medium containing 1% (w/v) fatty acid-free BSA and 15 μ M 17ODYA for 4 hours. All incubations of the cells were carried out in a cell culture incubator with saturated humidity, 5% CO₂ and at 37°C.

2.4.2.2 Cell-lysis and Azide-alkyne Huisgen cycloaddition reaction

After the transfected cells were metabolically labelled, it was possible to detect 17ODYA attached to proteins of interest by the addition of an infrared fluorescent dye conjugated with an azide. Under the appropriate conditions (see below), and with divalent copper ions as a catalyst, the alkyne group of 17ODYA and the azide of the dye undergo an azide-alkyne cycloaddition to form a 1,2,3-triazole. With the help of infrared imaging (LI-COR) it is possible to visualise the dye which is covalently bound to 17ODYA.

For this, cells were transferred onto ice following the 4 hour metabolic labelling and washed twice with ice cold PBS. Subsequently cells were lysed in 100 μ l of click-chemistry lysis buffer (50mM Tris, 17 mM SDS, pH 8.0 containing protease inhibitors) and transferred into 1.7 ml reaction tubes. For the click-reaction, 80 μ l of the click reaction mix (5 mM CuSO₄, 500 μ M Tris(benzyltriazolylmethyl)amine (TBTA), 25 μ M IRDye 800 CW azide in dH₂O) was added to the lysed cells and vortexed. The click reaction mix was then immediately supplemented with 20 μ l of ascorbic acid (4 mM) and incubated for one hour at room temperature with end-over-end mixing.

2.4.2.3 Acetone protein precipitation and sample preparation for SDS-PAGE

For detection of the infrared fluorescent dye with the Odyssey[®] infrared imaging system, the proteins within the lysate were precipitated and separated by SDS-PAGE. The proteins were then transferred to nitrocellulose membrane and imaged.

Following the click-reaction three volumes (600 μ l) of ice cold 100% acetone was added to the mix, vortexed and incubated at -20°C for 20 minutes. To pellet the precipitated proteins, the mixture was centrifuged for 5 minutes at 13,000 x g at 4°C. In order to wash out any unbound infrared dye residing in the mixture, the supernatant was aspirated and the protein pellet was washed 3 times. For this, the pellet was resuspended in 70% ice cold acetone and centrifuged for 5 minutes at 13,000 x g at 4°C. The pellet was then dissolved in 100 μ l 1 x SDS sample buffer (15 μ M bromphenol blue, 200mM Tris; 40% (v/v) glycerol, 2.7 mM Sodium dodecyl sulfate [SDS], 25 mM DTT at pH 6.8) and heated for 5 minutes at 95°C. The samples were then ready for analysis by SDS-PAGE and Western blotting.

2.4.2.4 Click-chemistry combined with immunoprecipitation using anti GFP MicroBeads

As palmitoylation occurs constitutively in cells on various proteins, the attachment of 17ODYA was not exclusively limited to the overexpressed proteins. Hence, the azide conjugated IRDye 800 CW was also attached to a number of other proteins

within the cell which resulted in a background “click-signal”. In order to minimize this background signal an optional immunoprecipitation was incorporated into the procedure of click-chemistry when required.

The protein to be immunoprecipitated (caveolin-2) had an EGFP protein attached to its C-terminus. The μ MACS™ Epitope Tag Protein Isolation Kit with anti-GFP MicroBeads was used for immunoprecipitation of the GFP epitope of caveolin-2.

For this, metabolically labelled cells were washed with ice cold PBS, collected into 1.7 ml reaction tubes and pelleted at 10,000 x g for 5 minutes at 4°C. Subsequently, the cells were lysed in 100 μ l lysis-buffer (3.4 mM SDS, 1% (v/v) Triton x-100 with protease inhibitors) by passing them through a 26G needle and incubating for 30 minutes on ice. To magnetically label the EGFP-tagged protein, 5 μ l of the anti-GFP MicroBeads solution was added to the lysate and incubated for 30 minutes on ice. This was followed by the addition of 80 μ l of the click-reaction mix and 20 μ l of ascorbic acid (4 mM) as described in section 2.4.2.2. The mix was then incubated for 1 hour at room temperature with end-over-end mixing. To bind the beads to the μ Column, the columns were placed on a magnetic platform and equilibrated with 200 μ l of lysis-buffer (see above). The protocol of the μ MACS™ Epitope Tag Protein Isolation Kit was followed strictly except that the Washing Buffer 1 solution was replaced by lysis-buffer. The immunopurified proteins were then kept at -20°C until analysing them by SDS-PAGE and detection with the Odyssey® infrared imaging system.

2.4.2 Sodium dodecyl sulphate polyacrylamide gel electrophoresis (SDS-PAGE)

SDS-PAGE was performed according to Laemmli (Laemmli, 1970) with a 4% (v/v) acrylamide stacking- gel. The acrylamide concentration of the resolving gel was varied between 8% and 12% according to the size of proteins being investigated. The applied voltage for the stacking gel was 80 mV and for the resolving gel 150 mV.

2.4.3 Western blotting

After electrophoresis, the proteins were transferred to a nitrocellulose membrane. To achieve this, the gel and the nitrocellulose membrane were soaked in transfer buffer (48 mM Tris, 39 mM glycine, 1.3 mM SDS, 20% methanol v/v) and placed together in between several layers of filter paper and sponges. This assembly was finally placed in a holding cassette to maintain a tight contact of the nitrocellulose membrane and gel. The cassette was placed into a transfer tank with the nitrocellulose membrane facing the anode and a current of 120 mA was applied overnight. The nitrocellulose membranes were then washed with PBST buffer (PBS with 0.02% (v/v) Tween-20,) and blocked in 5% non-fat milk (5% (w/v) skim milk powder in PBST) for 60 minutes at room temperature. After washing the membranes three times for 10 minutes with PBST, the blots were probed with the primary antibody targeted against the protein of interest using dilutions recommended by the manufacturer or determined experimentally. In order to remove non-specifically bound primary antibodies, the membranes were washed three times for 10 minutes with PBST. The immunoblots were subsequently incubated for 1 h at room temperature with the secondary antibody.

2.4.3.1 Visualising immunoreactive protein bands using enhanced chemiluminescence (ECL) Western blotting detection system.

For this purpose a horseradish peroxidase conjugated secondary antibody was used according to the supplier's recommendation. The probed nitrocellulose membranes were then washed three times for 10 minutes with PBST and subsequently evenly covered with the ECL solution. The ECL solution was an equal mix of ECL Solution1 (100 mM TrisBase (pH 8.5), 2.45 μ M luminol, 0.9 μ M coumaric acid) and ECL Solution2 (100 mM TrisBase (pH 8.5) 0.061% (v/v) H₂O₂). The resulting chemoluminescence was scanned and digitalised with a Fujifilm LAS-3000 imaging system, or detected using light sensitive film and an X-OMAT developer (Konica SRX-101A, Medical Film processor, Konica Corporation, Tokyo, Japan). The images were saved as TIFF files for further analyses.

2.4.3.2 Visualising protein bands using Odyssey ® infrared imaging system (LI-COR)

In order to visualise protein bands using infrared imaging, secondary antibodies conjugated with the infrared dyes IRDye® 680rd, DyLight 680 or DyLight 800 were used. The secondary antibodies were diluted 1:10,000 in PBST and incubated for one hour at room temperature. After washing the membranes three times with PBST for 10 minutes the membranes were scanned with the LI-COR Odyssey ® infrared imager with the appropriate channel for each conjugated dye.

2.4.4 Isolation of Triton X-100-insoluble membrane fractions.

Some membrane microdomains such as lipid “rafts” or caveoale, are rich in cholesterol and sphingolipids and are resistant to solubilisation by the detergents such as Triton X-100. Some membrane-bound proteins could be selectively associated with these membrane microdomains. In order to isolate proteins from these specialised membrane microdomains, cells were collected 24 h post transfection and pelleted by centrifugation at 5000 x g for 5 min at 4°C. Cell pellets were resuspended in PBS containing 1% (v/v) Triton X-100 and protease inhibitor and lysed by passing through a 26G needle. After 30 min incubation on ice, the lysates were subjected to centrifugation at 16400 x g for 20 min at 4°C. A fraction of the lysate before centrifugation was kept as **T=Total input**. Following the centrifugation, the resulting supernatant was transferred into a fresh reaction tube with the appropriate amount of 4x Laemmli sample buffer with 100 mM DTT and corresponded to the **soluble fraction=S**. The pellet was resuspended in 1x Laemmli sample buffer with 25 mM DTT and corresponded to the **insoluble fraction=IS**. The volume of 1x sample buffer of IS fraction was adjusted to the volume of the S fraction. Samples were stored at -20 °C or directly analysed by SDS-PAGE followed by Western blotting.

2.4.5 Comparing protein expression level of proteins in between different cell types.

Expression of proteins can be cell type-specific. In order to compare protein level of a particular protein in between selected cell types (HEK293T cells and 3T3-L1 adipocytes) cells were collected when confluent (HEK293T) or when fully differentiated (3T3-L1 adipocytes). Subsequently, the cells were lysed by addition of 200 µl lysis buffer containing 25 mM HEPES; 25 mM NaCl; 1 mM EDTA; 17 mM SDS, Triton X-100 1% (v/v) and protease inhibitor and the passage through a 26G needle. Cell lysates were then incubated on ice for 20 min and cell nuclei and debris were separated by centrifugation at 10,000 x g at 4 °C for 10 minutes. Protein concentration of the supernatant was measured using a BCA protein assay and normalised to the lowest obtained protein concentration. An appropriate amount of 4x Laemmli buffer with 100 mM DTT was added and samples were analysed by SDS-PAGE followed by Western blotting (as described in section 2.4.2 and 2.4.3) or stored at -20 °C until further analysis.

2.4.6 Blue native polyacrylamide gel electrophoresis (blue native PAGE)

Proteins do not only exist as monomers, but also form multi-protein complexes such as homo-dimers, homo-oligomers or hetero-dimers and hetero-oligomers within cells (Hurtley and Helenius, 1989). As sodium dodecyl sulphate (SDS) disrupts most of such multi-protein complexes, blue native PAGE was applied to examine whether the protein of interest formed multi-protein complexes. The detergent digitonin, used in blue native PAGE, allows the proteins to remain in their multi-protein complex structure while being separated in a polyacrylamide gel.

For the blue native PAGE the NativePAGE™ Bis Tris Gel System was used (Life Technologies).

2.4.6.1 Sample preparation

HEK293T cells were collected 24 hours after transfection with the expression vector encoding proteins to be examined. For this, the cells were washed with ice cold PBS, transferred into 1.7 ml reaction tubes and pelleted at 10,000 x g at 4°C for 10

minutes. In order to lyse the cells, lysis buffer containing 1% (v/v) of the detergent digitonin, 25 µl NuPAGE® LDS Sample Buffer (4X), 1 µl protease inhibitor cocktail 100X, and 20 µl 5 % (w/v) digitonin were mixed and made up with dH₂O to a final volume of 100 µl. The cell pellet was then solubilised in 100 µl of lysis-buffer and incubated for 30 minutes on ice. Following cell lysis, the samples were centrifuged at 20,000 x g and 4°C for 30 min and the supernatant was transferred into a fresh reaction tube. The supernatant was stored in -20°C for further analysis.

2.4.6.2 Gel electrophoresis

For gel electrophoresis, the protocol of the manufacturer was followed. Precast NativePAGE Novex 4-16% (v/v) Bis-Tris Protein Gels, 1.0 mm were used. Before loading the samples on the gel, 5 µl of 5% (w/v) G-250 Sample additive was added to 100 µl sample so the final Coomassie G-250 concentration was 0.25% (v/v). Anode buffer, light blue- and dark blue cathode buffer were mixed according to the manufacturer's protocol. After loading 15 µl sample in each well, the inner chamber of the electrophoresis tank was filled with dark blue cathode buffer and proteins were separated by applying a voltage of 150 mV for 30 minutes. Then the dark blue cathode buffer was replaced with light blue cathode buffer and a voltage 150 mV were applied for additional 60 minutes.

2.4.6.3 Transfer of separated proteins onto polyvinylidene fluoride (PVDF) membrane and immunodetection.

Following gel electrophoresis, the gel was washed in 3.5 mM SDS for 15 minutes. PVDF membranes were soaked for two minutes in 100% methanol and then placed into transfer buffer (48 mM Tris, 39 mM glycine, 1.3 mM SDS, 20% methanol (v/v)) for another two minutes before being used. The transfer has been carried out according to section 2.4.3. After completing the transfer, membranes were washed with 8% (v/v) acetic acid for 15 minutes to fix the proteins, followed by two washes with demineralised water for two minutes. In order to wash the Coomassie G-250 dye out of the membranes, the PVDF membranes were air dried and then re-

hydrated with 100% methanol for two minutes and soaked in water for another two minutes before proceeding with immunodetection. Blocking the membrane with 5% (w/v) non-fat milk, and incubation with primary and secondary antibodies were carried out according to section 2.4.3. Protein bands were visualised with ECL Western blotting detection system. When secondary antibodies was conjugated with DyLight 800 the Odyssey[®], infrared imaging system was used.

2.4.7 Surface trypsin-digest of membrane-bound proteins.

This experiment was conducted to examine the association of proteins with the PM. It is based on the proteolytic properties of the serine protease trypsin, which cleaves proteins at lysine and arginine residues. Addition of trypsin to the cell culturing media, results in the digestions of proteins at their extracellular side. In contrast, proteins residing in intracellular are not digested by trypsin, as it is not able to cross the PM. Hence, comparing total protein levels of the examined proteins of trypsin-treated and untreated cells by immunoblotting allowed quantification of their association with the PM.

For this, cells were transfected for 24 h with plasmids encoding the protein of interest. Following 2 washes with PBS, trypsin-EDTA (0.05%) or HEK293T culture media (control) was added and incubated for 30 min in a cell culture incubator. Subsequently, the cells were transferred into reaction tubes and pelleted by centrifugation at 16,000 x g at 4°C for 10 min. The cell pellets were then washed twice by adding 1 ml PBS followed by centrifugation at 16,000 x g at 4°C for 5 min. Following the washing steps the cell pellets were resuspended in 200 µl 1x Laemmli buffer with 25 mM DTT and subjected to SDS-PAGE on 8% (v/v) acrylamide gels followed by immunoblotting.

2.5 Confocal Microscopy

Confocal Microscopy was used in order to determine localisation of either endogenously expressed proteins or over-expressed wild type or mutated proteins within fixed cells. In confocal microscopy, out-of-focus light is eliminated by point

illumination and a spatial pinhole which is in an optical plane in front of a detector. With this technique it was possible to achieve high resolution images of whole cells as only light from one fluorescent point of the object is detected at a time.

For confocal microscopy in this thesis, the Leica SP5C Spectral Confocal Laser Scanning Microscope was used (Leica Microsystems GmbH, Wetzlar, Germany). Following laser lines were available: 405 blue diode (excitation wavelength 405 nm); Argon (excitation wavelength 488 nm); Helium Neon 1 (excitation wavelength 543 nm); Helium Neon 3 (excitation wavelength 633 nm).

2.5.1 Fixing HEK293T cells on coverslips

For this, HEK293T cells were plated on poly-D-lysine coated coverslips (VWR) in 24-well plates at a dilution of 1:12 when passaging cells from a 75 cm² culture flasks (see 2.2.4). 24 hours after plating the cells onto coverslips, transfections were carried out according to section 2.2.5. Expression of the transfected expression vector proceeded for 24 hours. In order to fix the cells, they were washed twice with ice cold PBS and incubated with 4% (v/v) formaldehyde for 30 min at room temperature. Afterwards, fixed cells were washed twice with PBS. Depending on the protein encoded by the expression plasmids the cells were then either subjected to immunocytochemistry or mounted directly on microscopy slides with an antifade mounting medium (mowiol). Immunocytochemistry was not required if the over-expressed protein was conjugated with a fluorescent protein like EGFP or mCherry.

2.5.2 Fixing 3T3-L1 adipocytes on coverslips

In order to culture 3T3-L1 adipocytes on coverslips 3T3-L1 pre-adipocytes were plated first and then differentiation initiated on the coverslips into mature 3T3-L1 adipocytes.

For this, 3T3-L1 pre-adipocytes were reseeded 1:5 on coverslips placed in 24-well plates in accordance with section 2.2.1. Differentiation was initiated two days after cells became 100% confluent according to section 2.2.2. Mature 3T3-L1 adipocytes were washed twice with PBS, and then fixed with 4% (v/v) formaldehyde for 30

minutes at room temperature and immediately washed twice with PBS again. The fixed 3T3-L1 adipocytes were then subjected to immunocytochemistry for further analysis.

2.5.3 Immunocytochemistry with HEK293T cells and 3T3-L1 Adipocytes

Endogenously expressed proteins in 3T3-L1 adipocytes were visualised using immunocytochemistry combined with confocal microscopy to examine their localisation within the cell and relative to other proteins within the cell. Furthermore, localisation of over-expressed proteins within HEK293T cells was investigated. For this the over-expressed proteins, which were either wild type or cysteine to alanine mutants of the proteins, were tagged with either a HA-tag or Myc-tag. Primary antibodies recognising these tags were used.

In order to reduce non-specific binding of the primary and secondary antibodies, all washes and incubations of the fixed cells on coverslips were performed with PBS containing 0.3% (w/v) of bovine serum albumin (PBS/BSA).

For immunocytochemistry, the fixed cells were washed twice with PBS/BSA. The membranes of the cells were then permeabilised by incubating with PBS/BSA containing 0.25% (v/v) Triton X-100 for 10 minutes at room temperature. Permeabilisation of the membranes enables antibodies to access epitopes localised within the cytoplasm or membrane surrounded cell organelles. The detergent Triton X-100 was washed off by two rinses with PBS/BSA. For the incubation with the primary antibody, coverslips were placed on parafilm (with the cells facing side down) containing a 30 µl drop of primary antibody solution (1:50 dilution of primary antibody in PBS/BSA), and incubated for one hour at room temperature. To avoid evaporation of the antibody solution, the incubation was held in a box with high humidity. The coverslips were then washed three times with PBS/BSA and incubated with the secondary antibody (diluted 1:400 in PBS/BSA) on parafilm in a box protected from light and with high humidity as described for the primary antibody incubation. Secondary antibodies were conjugated with the fluorophore Alexa Fluor® Dyes and could be detected with the appropriate laser of the confocal microscope system. To avoid photobleaching of the fluorophore it was important to

work protected from light. Following the incubation with the secondary antibody the coverslips were washed three times with PBS/BSA and one times with demineralised water and subsequently air-dried with the cells facing up and protected from light. The dry coverslips were mounted on glass slides with an antifade mounting media.

2.5.4 Mounting coverslips on microscopy slides using ProLong® Gold Antifade Mountant with DAPI

As the fluorescence of the fluorophores that were used to label proteins for confocal microscopy decreases with time and is susceptible to photobleaching, a mounting media with antifade properties was used to mount the coverslips on microscopic slides. For this, ProLong® Gold Antifade Mountant with DAPI was used. This mountant comprised the nucleus-staining dye DAPI which intercalates with DNA and binds to the small groove of adenosine-thymidine sites. Thus, it was possible to visualise the nucleus of the cells in addition to the stained proteins of interest.

For this, the air-dried coverslips were placed (cell facing side down) on a drop of 15 µl ProLong® Gold Antifade Mountant with DAPI. For ideal mounting the mountant was allowed to cure for at least 24 hours. The mounted coverslips were kept in the dark at 4°C until used for confocal microscopy.

2.5.5 Recording images using the confocal microscopy system

A Leica SP5C Spectral Confocal Laser Scanning Microscope was used to detect the fluorophores introduced in 3T3-L1 Adipocytes or HEK293T cells. The images were taken with 63 x/1.40 oil Plan Apochromat objective. Fluorophores were excited with following laser lines: 405 blue diode (excitation wavelength 405 nm); Argon (excitation wavelength 488 nm); Helium Neon 1 (excitation wavelength 543 nm); Helium Neon 3 (excitation wavelength 633 nm). The fluorescent emission was recorded by 3 different photo multiplier tubes (PMTs). Image stacks were collected reaching from top to bottom of the cells with pinhole set to 1 Airy unit. Afterwards

Hygens Scientific Volume Imaging (SVI) was used to deconvolve the recorded images.

2.6 Brightfield microscopy

Brightfield microscopy was used to image live cells of the 3T3-L1 cell line. For this a LEICA DMIRB inverted microscope equipped with the digital camera LEICA DC 200 was used. Imaging was performed on living cells cultured in 100 mm culturing dishes with a 20 x/0.4 objective. Culture dishes were placed back into the cell incubator immediately after imaging.

2.7 Data analysis

In order to measure relative protein expression levels, protein bands on immunoblots were quantified. When ECL detection system was used for visualising protein bands, Western blots were scanned and intensity of the signal was quantified by densitometry using the software ImageJ (Image Processing and Analysis in Java). The software Image Studio™ Lite V3.1 (LI-COR Biosciences, Lincoln, NE, U.S.A.) was used for quantification of immunoblots when detection was carried out with Odyssey® infrared imaging system. The mean of the measured values was presented with the standard error of the mean (SEM). In order to assure statistical significance one-way analysis of variance (ANOVA) in conjunction with a Tukey's Test or unpaired two samples Student's t-test were performed (GraphPad Prism® software).

Chapter 3: Isolation and characterisation of the palmitoylome in 3T3-L1 adipocytes.

3.1 Introduction

The recent development of techniques such as acyl-biotin exchange, acyl-RAC and click-chemistry have facilitated the proteomic characterisation of palmitoylated proteins in a range of different cell and tissue types (Roth et al., 2006; Martin and Cravatt, 2009; Yount et al., 2010; Forrester et al., 2011; Ren et al., 2013b). When the current project was initiated, there had been no reported studies examining the palmitoylome in adipocytes. The main goal of this study was to examine the effect of palmitoylation on proteins that function in key aspects of adipocyte physiology, including the insulin signalling pathway, regulated trafficking of GLUT4 containing storage vesicles, or fatty acid transport. The insulin signalling cascade is regulated at multiple levels by phosphorylation. However, how other post-translational modifications, such as palmitoylation, impact the insulin signalling cascade and its link to GLUT4 vesicle trafficking is less well established. Previous work has identified palmitoylated proteins involved in the initial stages of insulin signalling to GLUT4 trafficking such as the IR or the small GTPase TC10 (Magee and Siddle, 1988; Watson et al., 2003). Also, proteins involved in the terminal step of the translocation pathway such as the vesicle fusion protein SNAP23 are palmitoylated (Vogel and Roche, 1999). In addition, the caveolae/lipid raft structural proteins caveolin-1 and flotilin-1/flotilin-2 are also palmitoylated (Dietzen et al., 1995; Morrow et al., 2002; Neumann-Giesen et al., 2004), and these membrane microdomains have been linked to insulin signalling, GLUT4 trafficking and fatty acid transport (Karlsson et al., 2002; Liu et al., 2008; Fagerholm et al., 2009).

To generate a more detailed understanding of palmitoylation in adipocytes, I sought to purify and characterise the palmitoylome from 3T3-L1 adipocytes. The 3T3-L1 cell line is derived from mouse embryonic fibroblasts and has been used as a model cell line to study adipocyte physiology for three decades (Green and Kehinde, 1975, 1972). Hence, the application of recently developed techniques to study

palmitoylation in 3T3-L1 adipocytes would allow a more detailed analysis of the palmitoylation of components of the insulin signalling/GLUT4 trafficking pathways.

3.2 Differentiation of 3T3-L1 adipocytes

The 3T3-L1 cell line is fibroblastic, and hence the 3T3-L1 fibroblasts/ pre-adipocytes need to be induced to differentiate into mature adipocytes prior to analysis. Differentiation was induced by addition of insulin, troglitazone, dexamethasone and IBMX into the cell culture media (see Material and Methods 2.2). Optical, molecular and biochemical approaches were taken to ensure that the differentiation protocol was successful. First, changes in cell morphology throughout the differentiation protocol were monitored using phase contrast microscopy. As can be seen in Figure 3.1, the cells undergo various changes in morphology during different stages of differentiation from pre-adipocytes into fully matured adipocytes. Day 0 corresponds to pre-adipocytes before initiation of differentiation; the shape of these cells is elongated and narrow at this stage. From day 1 to day 4 after initiation of differentiation, it can be observed that the cells start to lose their elongated shape and become rounder; at day 4, small, round droplets inside the cell can be observed. The images at day 5 to day 7 post-differentiation show that the cells become rounder towards a circular shape and that fat droplets inside the cell become more prominent. From day 8 onwards the shape of the cells is circular and fat droplets are clearly visible and increase in size until day 10.

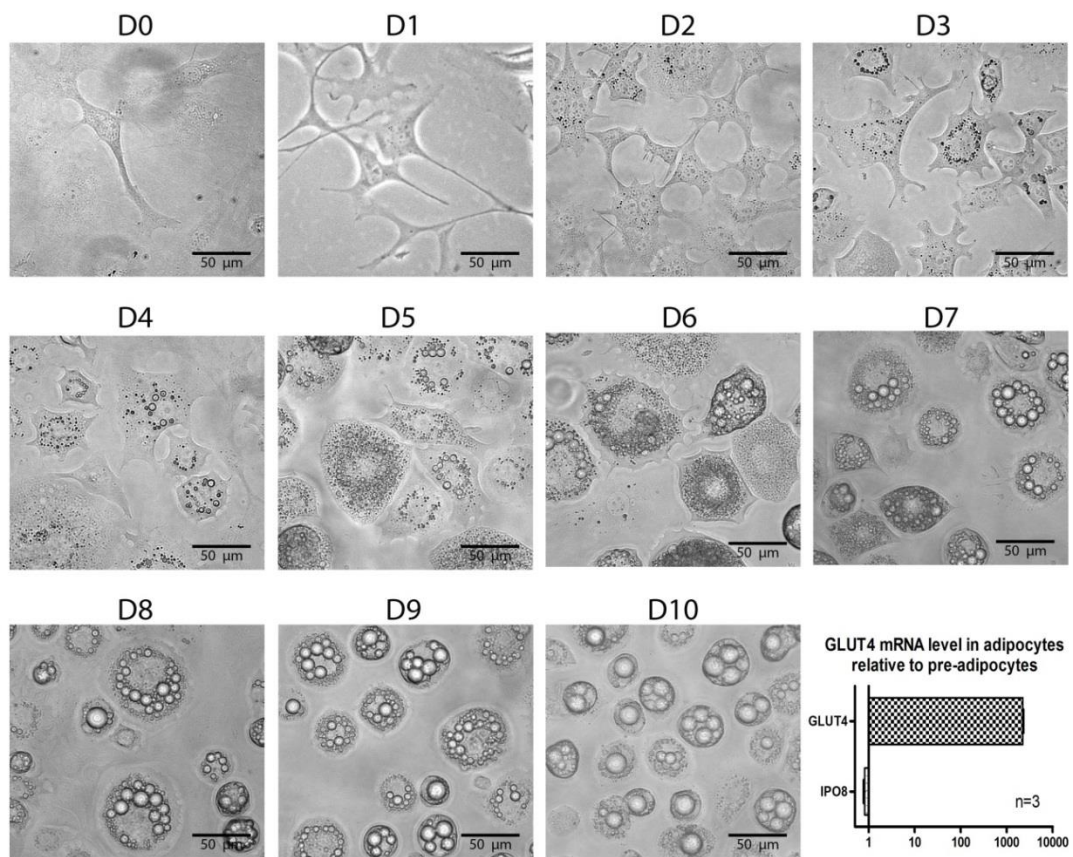


Figure 3.1. Differentiation of 3T3-L1 pre-adipocytes into adipocytes. Differentiation was initiated by addition of insulin (170 nM), troglitazone (1 μ M), 3-isobutyl-1-methylxanthine (IBMX) (500 μ M) and dexamethasone (0.25 μ M) to confluent cultures of 3T3-L1 pre-adipocytes. Representative cells are shown at indicated days post differentiation initiation from day 0 to day 10. In the bottom right corner of the panel, the results of qPCR analysis of pre-adipocytes and adipocytes is shown. GLUT4 mRNA levels and mRNA levels of IPO8 before and after differentiation were quantified. These mRNA levels were normalised to the mRNA levels of FBOX protein.

In addition to this morphological analysis, a molecular approach was taken to confirm the development into mature adipocytes. As adipocytes but not pre-adipocytes express GLUT4, the mRNA of GLUT4 should only be detectable after differentiation. Quantitative real-time PCR was applied to compare mRNA levels of GLUT4 before and after the differentiation procedure. The qPCR analysis showed an approximately 2000-fold increase of mRNA level of GLUT4 in adipocytes compared to pre-adipocytes (see bottom right corner of Figure 3.1).

To confirm that the increase of GLUT4 mRNA in adipocytes resulted in increased levels of GLUT4 protein, lysates from cells at selected days post initiation of differentiation were analysed by SDS-PAGE and Western blotting. As can be seen in Figure 3.2, from day one to day 3 post initiation of differentiation, there is little immunoreactivity corresponding to GLUT4 at the apparent molecular weight of approximately 50 kDa. Protein levels of GLUT4 begin to be detectable from day 4 and the intensity of the bands increases with each day until the intensity of the GLUT4 protein bands reaches a maximum at day 10. The presence of multiple immunoreactive bands is due to the glycosylation of GLUT4 (Zaarour et al., 2012). The expression of the IR was also determined as a second marker for differentiation. As mentioned in the introduction (1.3.2), the IR is synthesised as a single polypeptide pro-receptor with the approximate size of 180-200 kDa and is subsequently cleaved into α - and β subunits, which then form one subunit of the functional IR dimer. The top panel of Figure 3.2 displays the immunoreactivity of the cleaved IR β subunit (IR β) and the pro-receptor during the differentiation process. The intensity of the protein band corresponding to the insulin pro-receptor (indicated by an arrow) decreases from day one to day 10 post differentiation initiation, although the signal is the strongest at day 4 and 5. In contrast, the intensity of the band at the apparent molecular weight of approximately 90 kDa corresponding to IR β increases from day one to day 10. Thus, the increase in the amount of the processed IR β together with the simultaneous decrease of the pro-receptor polypeptide suggests an increased cleavage of the insulin pro-receptor into its functional α - and β subunits. Collectively, the morphological, molecular and biochemical analysis demonstrate that the differentiation of 3T3-L1 cells was successful and complete for the large majority of cells in the culture.

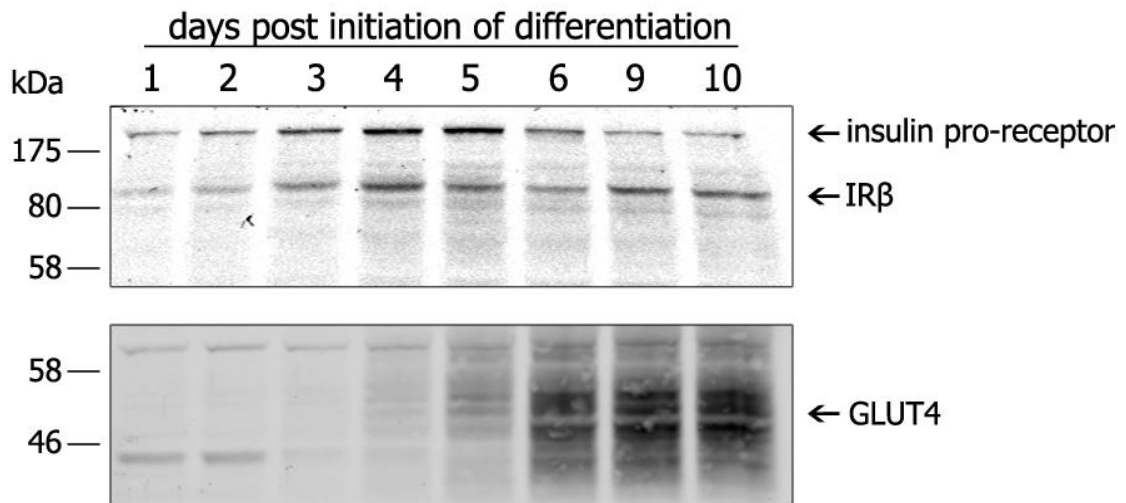


Figure 3.2. Protein expression level of GLUT4 and IR throughout the differentiation of 3T3-L1 pre-adipocytes in adipocytes. Confluent 3T3-L1 pre-adipocytes or adipocytes were collected at the indicated days post initiation of differentiation. Cells were lysed in 200 μ l of lysis buffer containing 1% (v/v) Triton X-100 and 3.5 mM SDS and were incubated for 30 min on ice. Lysates were centrifuged at 16,000 \times g for 20 min at 4°C and the protein concentration of the supernatants was measured using a BCA assay and normalised to 600 μ g/ml. 4x Laemmli sample buffer with 100 mM DTT was added. 20 μ l of each sample was subjected to SDS-PAGE using 12% polyacrylamide gels followed by immunoblotting. The figure shows immunoblots probed with antibodies against GLUT4 and IR β . Protein bands of interest are indicated with arrows on the right hand side and position of molecular weight markers are shown on the left hand side of the panel.

3.3 Identification of palmitoylated proteins in 3T3-L1 adipocytes using acyl-RAC

Having confirmed that the differentiation of 3T3-L1 cells into mature adipocytes was successful, I next set out to isolate and characterise the palmitoylome from adipocytes. For this, 3T3-L1 adipocytes were collected 10 days post-differentiation and subjected to resin-assisted capture of S-acylated proteins (acyl-RAC). This method enables the quantification of palmitoylation levels of known proteins or the identification of novel palmitoylated proteins. An outline of the experimental procedure used in acyl-RAC is shown in Figure 3.3, a more detailed description can be found in the methods section.

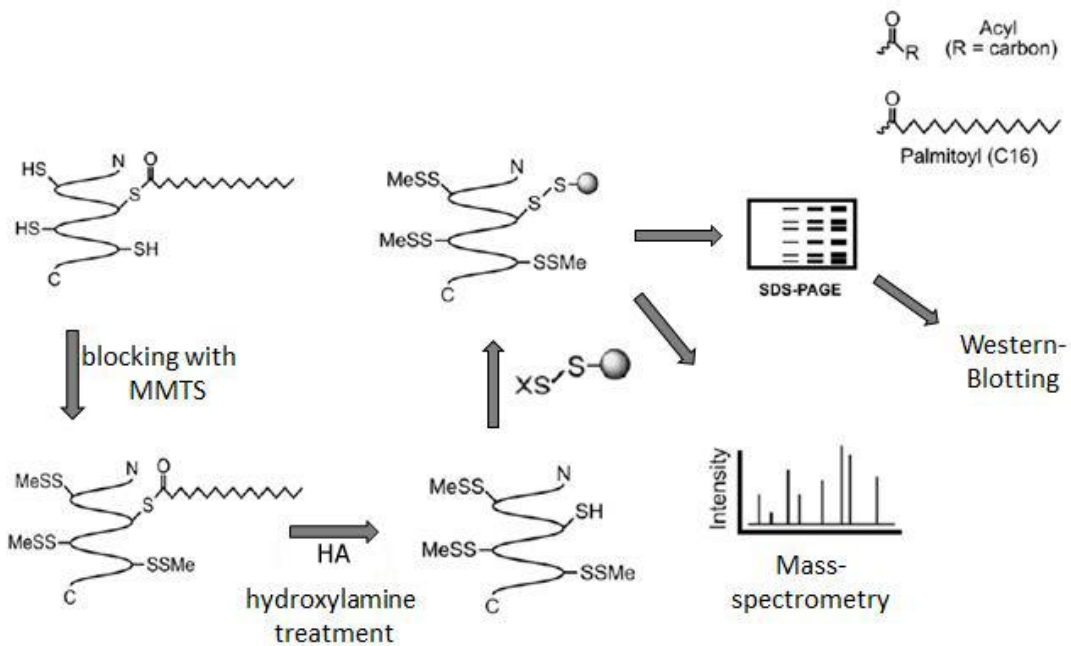


Figure 3.3. Outline of the acyl-RAC procedure to isolate palmitoylated proteins. Illustration of resin-assisted capture of *S*-acylated proteins. Free cysteines are blocked by adding 1.5% *S*-methyl methanethiosulfonate (MMTS) in 100 mM HEPES, 1.0 mM EDTA, 85 mM SDS. The addition of MMTS results in the transfer of a thiomethyl group onto a free cysteine forming a mixed disulfide bond. During the next step *S*-acylation is cleaved off by treatment with 0.5 M hydroxylamine (HA) (pH 7.5 in 100 mM HEPES, 1.0 mM EDTA, 35 mM SDS) resulting in free SH-groups. Proteins with free SH-groups bind to thiopropyl sepharose beads via a disulphide bond and can be pelleted by centrifugation once bound to the beads. The isolated proteins can be then subjected to either SDS-PAGE followed by immunoblotting or analysed by mass-spectrometry.

Acyl-RAC was performed on 3T3-L1 adipocytes as described in the Methods section and the isolated proteins were subjected to SDS-PAGE and immunoblotting. Probing with a panel of antibodies against known components of the insulin signalling/GLUT4 trafficking pathways revealed that caveolin-1, caveolin-2, flotillin-1, flotillin-2, SNAP23 and IRAP were highly palmitoylated (see Figure 3.4). IR β , IGF-1 receptor β subunit and GLUT4 were also found to be palmitoylated albeit at relatively low levels. In contrast, GLUT1, syntaxin 4, PKD-1, cyclophilin b and clathrin heavy chain (HC) were palmitoylated either at very low levels or not at all, as indicated by the lack of bands corresponding to these proteins in the bound fraction treated with HA.

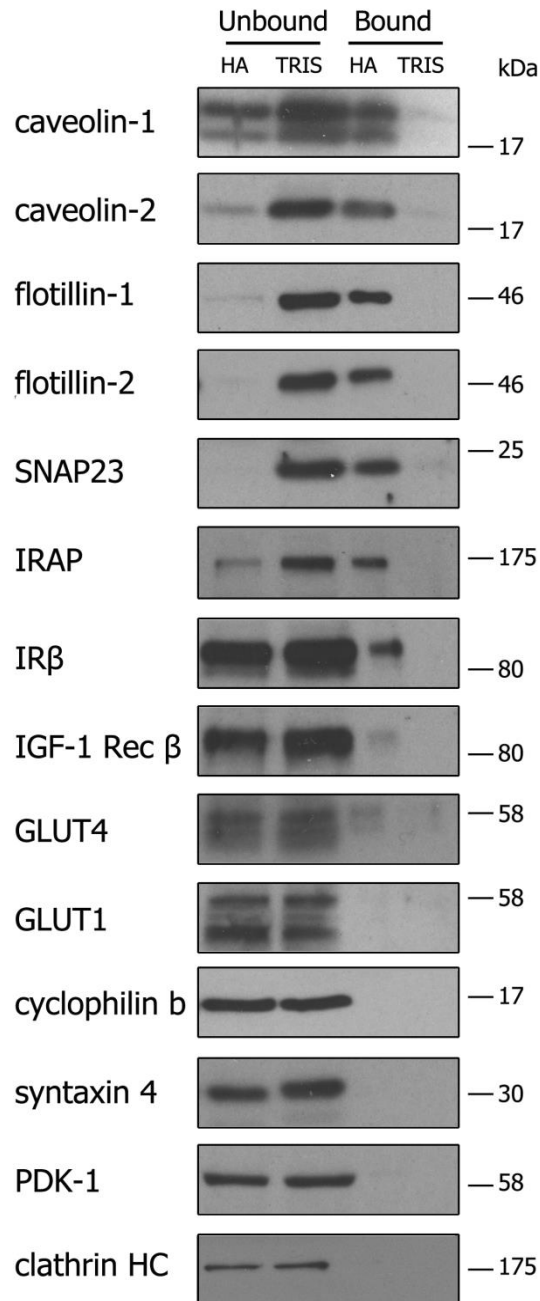


Figure 3.4. Immunoblotting analysis of acyl-RAC fractions prepared from 3T3-L1 adipocytes. Cells were collected on day 10 post differentiation initiation. Nuclei were pelleted by centrifugation for 5 min at 800 x g. A membrane fraction was isolated by centrifugation of the resulting supernatant for 50 min at 16,000 x g. The membrane fraction was incubated with MMTS (1.5% v/v) and subsequently proteins were precipitated with acetone. The isolated proteins were then incubated with either 0.5 M hydroxylamine (HA) or 0.5 M Tris together with free thiol group binding beads. Proteins were eluted from the beads using 1x Laemmli sample buffer with 50 mM DTT. The figure shows immunoblots using the indicated antibodies. HRP conjugated secondary antibodies were used. Chemiluminescence was detected with ECL system. Signal from immunoreaction in the bound/HA lane corresponds to palmitoylated proteins. The position of molecular weight marker is indicated on the right side of the. The blots shown are representative of an experiment that was performed at least three times.

3.4 Quantification of the palmitoylation levels of identified proteins

As the thiopropyl sepharose beads bind quantitatively to free thiol groups and the bound and unbound fractions were visualised using the same antibody, it was possible to determine the level of palmitoylation for each protein using densitometry. The quantification of the palmitoylation of each protein is shown in Figure 3.5. According to this quantification, approximately 80% of caveolin-2, flotillin-1, flotillin-2 and SNAP23 molecules are palmitoylated. In contrast, the percentage of palmitoylation of caveolin-1 is around 38%. The difference between the calculated palmitoylation of the highly palmitoylated proteins and caveolin-1 is statistically significant ($p < 0.001$). Approximately 55% of IRAP is palmitoylated and the level of palmitoylation of IR β , IGF-receptor β subunit and GLUT4 varies between 7% (IGF-1 receptor β) and 14% (GLUT4). Finally, the percentage of GLUT1, cyclophilin b, syntaxin 4, PDK-1 and clathrin HC recovered in the HA bound fraction was below 5%.

Level of palmitoylation of selected proteins

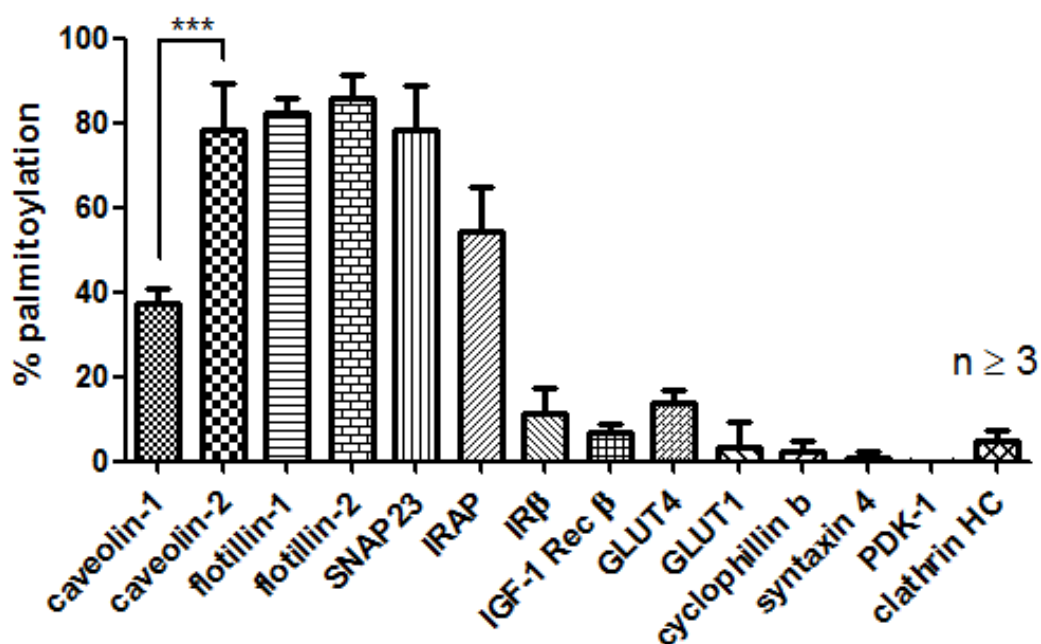


Figure 3.5. Quantification of 3T3-L1 adipocyte proteins recovered in acyl-RAC fractions. Levels of palmitoylation were assessed using densitometry of immunoblots obtained from acyl-RAC experiments (see Figure 3.4). The following equation was used to calculate the percentage of palmitoylation:

Percentage of palmitoylation = $[\text{Bound}_{\text{HA}} / (\text{Bound}_{\text{HA}} + \text{Unbound}_{\text{HA}})] - [\text{Bound}_{\text{Tris}} / (\text{Bound}_{\text{Tris}} + \text{Unbound}_{\text{Tris}})]$

All quantified data was from a minimum of three experimental repeats. One way ANOVA followed by Tukey's multiple comparison test was applied for statistical analysis *** $P \leq 0.001$.

In the previous sections, palmitoylated proteins were identified experimentally. Although the extent of palmitoylation of the identified proteins was determined, it was not clear where the palmitoylation sites were likely to be located within these proteins. In order to assess the localisation of the palmitoylation sites, an *in silico* analysis was undertaken. For this, CSS-Palm software was used. This software utilises an algorithm based on experimental data from 583 palmitoylation sites from 277 different proteins, to predict palmitoylation sites using the linear amino acid sequence of a protein (Ren et al., 2008). Table 3.1 shows the probability (score) of palmitoylation of cysteine residues of examined proteins according to CSS-Palm prediction. Furthermore, the right column of the table displays predicted protein domains surrounding the examined cysteine residues according to UniProt (SwissProt).

Table 3.1. CSS-Palm prediction of palmitoylation sites of examined proteins. The numbers in the column which is labelled “Position” indicate the position of the amino acid. Amino acids surrounding the examined cysteine are indicated in column “Amino acid sequence”. Values which express how likely a cysteine is to undergo palmitoylation can be found in column “Score”, where small values correspond to a low probability and high values a high probability of palmitoylation. The protein predicted domain in which the examined cysteines are located is displayed in column “Domain”. CSS-Palm 4.0 was used for this analysis.

Protein	Position	Amino acid sequence	Score	Domain
caveolin-1	133	HIWAVVPCIKSFLIE	1.503	Cytosolic/Juxtamembrane
	143	SFLIEIQCISRVSYSI	2.139	
	156	SIYVHTFCDFLFEAI	0.95	
caveolin-2	72	SFDKVVICSHALFEI	5.731	Oligomerisation domain
	109	ILFATLSCLIHWILM	13.761	Cytosolic/Juxtamembrane
	122	LMPFVKTCMLVLPVS	12.003	Cytosolic/Juxtamembrane
	145	DVIGPLCTSVGRSF	1.329	cytosolic
clathrin HC	736	FKYQAACKTGQIKE	1.001	Cytosolic
	1565	LQEEKRECFGACLFT	4.122	
	1569	KRECFGACLFTCYDL	3.91	
cyclophilin b	-	-	-	No site predicted
flotillin-1	5	***MFFT ^C GPNEAMV	39.752	Cytosolic
	17	AMVVSGFCRSPPVMV	28.887	
	34	GRVFLPCIQIQRI	1.971	
	203	QEKVSAQCLSEIEMA	3.788	
flotillin-2	4	****MGNCHTVGPNE	39.437	Cytosolic
	19	ALVVS ^{CG} CGSDYKQ	14.364	
	20	LVS ^{CG} CGSDYKQY	18.607	
GLUT1	207	QCILLPFCPESPRFL	2.078	Juxtamembrane intracell.
	421	GLAGMAGCAVLMTIA	5.471	Transmembrane intr.
GLUT4	361	LLGLAGMCGCAILMT	3.191	Transmembrane intr.
	363	GLAGMCGCAILMTVA	6.096	Transmembrane intr.
	430	AGFSNWT ^C NFIVGMG	6.325	Transmembrane intr.
IGF-1 Receptor β	1143	RDLAARN ^C MVAEDFT	2.845	Tyrosine Kinase
	1250	LFELMRMCWQYNPKM	5.079	
IR β	1251	YLDPPDN ^C PERLTDL	4.107	Tyrosine Kinase
	1262	LTDLMRMCWQFNPKM	5.995	
IRAP	35	VDLAKEPCLHPLEPD	7.201	Cytosolic
	103	RQSPDGTCSLPSART	7.487	Juxtamembrane intracell.
	114	SARTLVICVFVIVVA	7.324	Juxtamembrane intracell.
PDK1	330	DATKRLGCEEMEGYG	6.053	Protein Kinase
SNAP23	79	TLTELNKCCGLCICP	13.822	Cytosolic, between coiled- coil homology 1 and 2
	80	LTELNKCCGLCICPC	6.272	
	83	LNKCCGLCICPCNRT	11.04	
	85	KCCGLCICPCNRTKN	11.438	
	87	CGLCICPCNRTKNFE	4.283	
syntaxin 4	141	FVELINK ^C NSMQSEY	3.708	Cytosolic

3.6 Protein palmitoylation following chronic insulin treatment and changes in extracellular glucose concentration

Palmitoylation levels of specific proteins involved in the insulin signalling pathway have been determined in 3T3-L1 adipocytes. These cells were cultured under standard conditions with high glucose (25.5 mM) and a low concentration of insulin in the culture medium (2.2.1). Under these conditions 3T3-L1 adipocytes respond to an insulin stimulus with recruitment of GSVs to the PM to facilitate glucose uptake into the cell. Hence, palmitoylation levels of identified palmitoylated proteins were determined in insulin sensitive 3T3-L1 adipocytes. I next sought to investigate whether palmitoylation levels of the identified proteins change when cells become insulin resistant or when cells are cultured with different glucose concentrations in the culture medium. For this, cells were treated with 500 nM insulin for 24 hours in culture medium containing either 25.5 mM glucose (high glucose) or 5.5 mM glucose (low glucose). In order to confirm that the chronic insulin treatment had an effect on the treated 3T3-L1 adipocytes, the protein levels of the IR β were estimated by western blotting. Previous studies have shown that chronic insulin treatment of 3T3-L1 adipocytes leads to insulin resistance of the cells and down regulation of total IR protein levels (Knutson et al., 1982). Immunoblots derived from whole cell 3T3-L1 adipocytes treated under the indicated conditions were probed with an antibody against the IR β subunit. As can be seen in Figure 3.6A, the intensity of bands corresponding to the insulin pro-receptor (apparent molecular weight of approximately 190 kDa) was constant regardless of the cell treatment. In contrast, the intensity of the bands corresponding to IR β at an apparent molecular weight of approximately 80 kDa varied, and was higher when cells were treated without additional insulin. Densitometry was used to quantify the intensity of the protein bands, shown in Figure 3.6B. For calculation of the ratio of processed receptor to pro-receptor, the determined values for the insulin pro-receptor were divided by the values obtained for IR β . The ratio was approximately 3.2, when cells were treated with high glucose in culture medium without added insulin. Addition of insulin decreased the ratio to approximately 1.2. This decrease by circa three-fold

was statistically significant with a P value of 0.035. Under low glucose conditions, the ratio also decreased when insulin was added (from 3.5 to 1.3), although the difference between this pair of values was not found to be statistically significant ($p= 0.0735$). Calculated values were comparable when cells were treated without insulin in the culture media irrespectively of the concentration of glucose. The same could be observed for values when cells were treated with added insulin in the culture media under high and low glucose conditions. Thus, the ratio of pro-receptor to processed receptor appears to be sensitive to insulin levels but not to glucose levels in the extracellular solution.

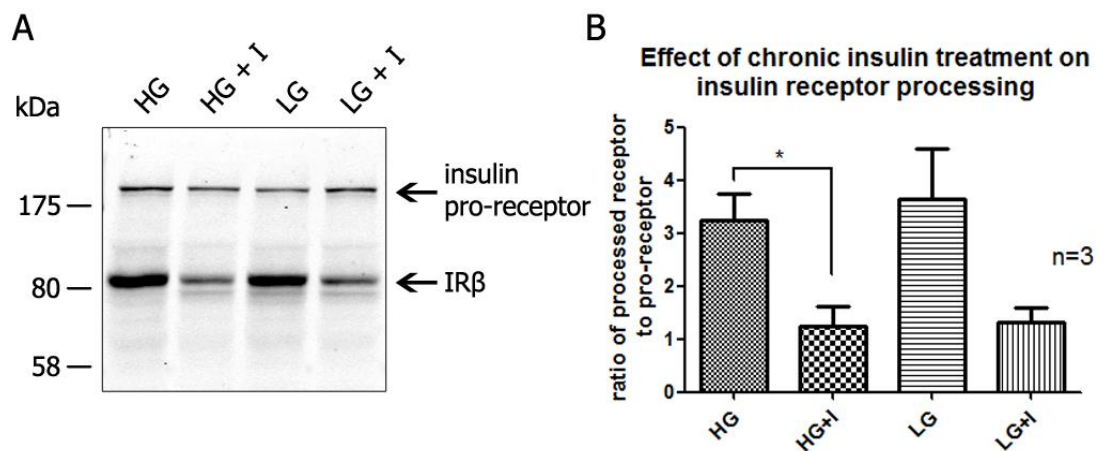


Figure 3.6. Pro-insulin receptor and IR β levels in 3T3-L1 adipocytes treated with varying glucose and insulin concentrations in the culture medium. Cells were collected on day 10 post initiation of differentiation. For the last 24 hours, cells were cultured in media as follows: **HG** = containing 25.5 mM d-glucose and **HG+I** = containing 25.5 mM d-glucose with 500 nM insulin; **LG** = containing 5.5 mM d-glucose; **LG+I** = containing 5.5 mM d-glucose with 500 nM insulin. Cells were lysed in 400 μ l lysis buffer (PBS with 1% (v/v) Triton X-100 and 3.5 mM SDS) and incubated for 30 min on ice. Lysates were centrifuged at 16,000 \times g for 20 min at 4 $^{\circ}$ C and protein concentration of the supernatant was measured using a BCA assay and normalised to 390 μ g/ml. 4x Laemmli sample buffer with 100 mM DTT was added and 20 μ l of each sample were subjected to SDS-PAGE on 8% polyacrylamide gels followed by immunoblotting with antibodies against IR β . **(A)** A representative immunoblot is shown of an experiment conducted 3 times. Arrows indicate differently processed forms of the IR β subunit. Positions of the molecular weight markers are indicated on the left hand side. **(B)** Intensity of protein bands were determined by densitometry using Image Studio software from LI-COR. Values of the protein bands corresponding to IR β were divided by the values for pro-insulin receptor to create a ratio. * indicates a P value of < 0.05 determined by Student's *t*-test.

The experiment above confirmed that 3T3-L1 adipocytes responded to chronic insulin treatment with a decrease in the processing of IR β subunit. The next step was to investigate whether insulin treatment or different glucose concentrations in the culture media had an effect on the palmitoylation levels of the palmitoylated proteins identified in Figure 3.4. Therefore, acyl-RAC was performed on 3T3-L1 adipocytes that had been previously treated with insulin under low glucose or high glucose conditions, followed by analysis by SDS-PAGE. Immunoblots with antibodies against selected proteins are shown in Figure 3.7. Palmitoylation levels of the proteins caveolin-1, caveolin-2, flotillin-2, IRAP, IR β , GLUT4, cyclophilin b and syntaxin 4 appear to be constant throughout varying culture media conditions, as no major changes in protein band intensities in the bound HA fraction could be observed. To quantify this result, the immunoblots were subjected to analysis using densitometry.

Quantification of the protein band intensities from the acyl-RAC analysis (see Figure 3.7) using Image Studio software are shown in Figure 3.8. According to the quantification, changes in the percentage of palmitoylation could be observed for some of the examined proteins. Despite detectable changes of palmitoylation levels for some proteins in cells treated under specified conditions, these changes were not statistically significant. Flotillin-2 and caveolin-2 were the most highly palmitoylated proteins out of all the examined proteins, with an estimated percentage of palmitoylation of approximately 90% and 80% respectively. Palmitoylation levels of flotillin-2 and caveolin-2 remained constant throughout the different treatment conditions.

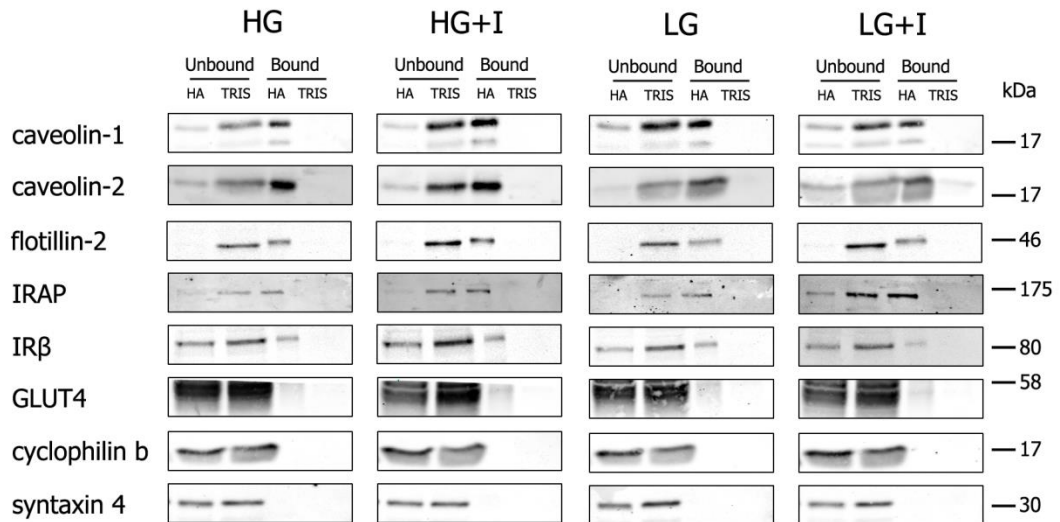


Figure 3.7. Immunoblotting analysis of acyl-RAC fractions prepared from 3T3-L1 adipocytes treated with insulin and different glucose concentrations. Cells were collected on day 10 post differentiation initiation. For the last 24 hours, cells were cultured in media: **HG** = containing 25.5 mM d-glucose and **HG+I** = containing 25.5 mM d-glucose with 500 nM insulin; **LG** = containing 5.5 mM d-glucose; **LG+I** = containing 5.5 mM d-glucose with 500 nM insulin. A membrane fraction was isolated by differential centrifugation (800 x g for 5 min, 136,000 x g for 1 h), and proteins were incubated with MMTS (1.5% v/v). Following the MMTS treatment, proteins were precipitated with acetone and incubated with either 0.5 M hydroxylamine (HA) or 0.5 M Tris (Tris) together with free thiol group binding beads. Proteins were eluted from the beads using 1x Laemmli sample buffer with 50 mM DTT. The figure shows immunoblots using the indicated antibodies. The positions of molecular weight marker are indicated on the right side of the blots. The blots shown are representative of an experiment that was performed three times.

In contrast the palmitoylated fraction of caveolin-1 varies from approximately 50% (LGI) to 68% (LG). IRAP has its lowest palmitoylation levels at approximately 42% (HG) and the highest at 63% (LG). The percentage of palmitoylation of IR β subunit varies from approximately 23% (LGI) to approximately 60% (HGI). As mentioned above however the changes in palmitoylation of IR β were not statistically significant ($P=0.1917$). The fraction of palmitoylated GLUT4 was the highest at approximately 17% (HGI) and lowest at approximately 5% (LGI). Cyclophilin b and syntaxin 4 were found to be recovered in HA bound samples to a very low level, with a maximum for syntaxin 4 of approximately 3.5% (LG) and cyclophilin b at 1.2% (LG).

Palmitoylation levels of indicated proteins under varying glucose and insulin levels in culture medium

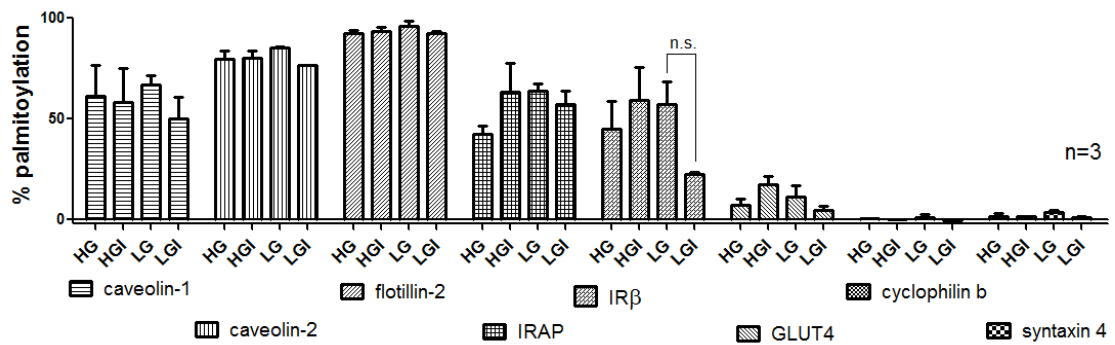


Figure 3.8. Quantification of 3T3-L1 adipocyte proteins recovered in acyl-RAC fractions following cell treatment with different glucose and insulin concentrations. Levels of palmitoylation were assessed using densitometry of immunoblots obtained from acyl-RAC experiments (Figure 3.7). The following equation was used to calculate the percentage of palmitoylation:
 Percentage of palmitoylation = $\frac{[\text{Bound}_{\text{HA}} / (\text{Bound}_{\text{HA}} + \text{Unbound}_{\text{HA}})] - [\text{Bound}_{\text{Tris}} / (\text{Bound}_{\text{Tris}} + \text{Unbound}_{\text{Tris}})]}{1}$
 All quantified data was from n=3 (Except caveolin-2 LG N=2; caveolin-2 LGI N=1). One way ANOVA followed by Tukey's multiple comparison test was applied for statistical analysis.

3.7 Discussion

3T3-L1 cells have played a fundamental role in defining the pathways involved in insulin signalling and GLUT4 translocation, and offer a similarly valuable system to probe the potential roles of palmitoylation in regulating these pathways. However, it is essential that robust differentiation of 3T3-L1 pre-adipocytes into adipocytes is demonstrated. This was achieved by monitoring changes in morphology, and through the application of molecular and biochemical methods which measured mRNA and protein levels of GLUT4 (Figure 3.1 and Figure 3.2). Acyl-RAC-mediated isolation of palmitoylated proteins from differentiated 3T3-L1 cells was successfully applied and allowed the identification of a set of palmitoylated proteins involved in insulin action (Figure 3.4). Furthermore, this method allowed the estimation of the extent of palmitoylation for these identified proteins (Figure 3.5). Additionally, the effects of chronic insulin treatment and glucose concentration of the extracellular

medium was investigated, albeit with no significant changes in palmitoylation detected under these conditions (Figure 3.7 and Figure 3.8).

The morphology of mature 3T3-L1 adipocytes and the monitored morphological changes throughout the differentiation process agree with published data available about this cell line (Russell and Ho, 1976). The increase in size of lipid droplets during the course of differentiation is likely to originate from fusion of the initially small and numerous lipid droplets with each other and through incorporation of *de novo* synthesised triglycerides. This process is accompanied by rising protein levels of GLUT4 from day four onwards (Figure 3.2). The detection of GLUT4 protein agreed with the detection of GLUT4 mRNA which is present in high copy numbers in mature 3T3-L1 adipocytes but not in pre-adipocytes (Figure 3.1). Furthermore, an increase of the ratio of the processed IR β subunit to the pro-receptor form of the IR could be observed. Although insulin-induced GLUT4 translocation or glucose transport assays were not conducted, the collected data conforms to previously published data, and hence I interpret that the differentiation procedure resulted in fully functional and mature 3T3-L1 adipocytes (Chang and Polakis, 1978; Wu et al., 1998).

Application of acyl-RAC allowed the identification of a number of known and novel palmitoylated proteins in 3T3-L1 adipocytes (Figure 3.4). The captured palmitoylated proteins were separated by SDS-PAGE and probed with selected antibodies, against proteins which are either involved in the insulin-induced GLUT4 trafficking pathway or are known non-palmitoylated proteins (serving as negative control for this assay). Caveolin-2 was identified as a novel palmitoylated protein. The palmitoylation of caveolin-1, flotillin-1, flotillin-2, SNAP23, IR β and IGF-1 receptor β subunit has been reported in previous work (Dietzen et al., 1995; Vogel and Roche, 1999; Magee and Siddle, 1988; Morrow et al., 2002; Neumann-Giesen et al., 2004). When the current study was initiated, palmitoylation of IRAP and GLUT4 had not been reported, but in 2013 palmitoylation of these proteins was demonstrated in a separate study (Ren et al., 2013b). Although palmitoylation has been reported for all proteins except caveolin-2, no data is available about the

extent of palmitoylation for each individual protein, and this analysis was an important part of the current study. The thiopropyl beads, which were used for acyl-RAC, bind quantitatively to free SH groups. Hence, it was possible to determine the fraction of palmitoylated species within a population of proteins. This analysis revealed several interesting observations, including a difference in palmitoylation of the two members of the caveolin family with caveolin-2 being palmitoylated somewhat higher as caveolin-1.

At present it is not known what the exact function of palmitoylation is in the physiology of caveolin-1, as the only described effect was the stabilisation of caveolin-1 oligomeric assemblies (Monier et al., 1996). Although both caveolin-1 and -2 have a similar structure and membrane topology, none of the three palmitoylated cysteines in caveolin-1 are conserved in caveolin-2 (see Figure 1.3) (Monier et al., 1996). *In silico* analysis using CSS-Palm resulted in higher scores for the cysteine residues of caveolin-2 when compared to scores of caveolin-1 (Table 3.1). This finding agreed with the experimentally calculated palmitoylation levels of both caveolin isoforms, when membrane fraction was isolated by differential centrifugation with the maximum centrifugation speed of 16,000 x g. In that experiment the palmitoylated fraction of caveolin-2 (~80%) was assessed as approximately twice as much as for caveolin-1 (~38%) (see Figure 3.4 Figure 3.5) and this difference was statistically significant. However, this difference in palmitoylation levels was strongly decreased in a different experiment, where membrane fractions were isolated by ultracentrifugation with a maximum centrifugation speed of 136,000 x g. With the centrifugation at a speed of 16,000 x g predominantly membrane fractions from cell compartments such as lysosomes, peroxisomes and the PM are isolated, while with at the centrifugation at higher speed (e.g. 136,000 x g), achieves the isolation of additional membrane compartments including low density vesicles such as microsomes or endosomes and fractions of the ER (Lodish et al., 2007). Therefore, the variance in palmitoylation of caveolin-1 between the two different experiments could be explained by presence

of palmitoylated caveolin-1 molecules in low density vesicles, which raised the total fraction of palmitoylated caveolin-1 molecules from 38% to approximately 60%.

CSS-Palm prediction software contradicts the experimental approach in the case of GLUT4 and IRAP. Predicted scores for both of these proteins are in a similar range but the experimentally estimated percentage of palmitoylated molecules is approximately threefold higher for IRAP (55%) than for GLUT4 (14%). Despite the different extent of palmitoylation, both proteins have three cytosolic cysteine residues and both co-localise and translocate within GSVs to the PM upon insulin stimulation in a similar fashion (Ross et al., 1997). This suggests that palmitoylation may not be involved in insulin-stimulated translocation of GLUT4 and IRAP, although it has not been studied how cysteine-deficient mutants of these proteins respond to insulin stimulation in cells.

GLUT4 was detected as multiple bands stretching from the apparent molecular weight of approximately 46 to 55 kDa (Figure 3.2 and Figure 3.4). It is thought, that this band pattern originates from a combination of other PTMs such as glycosylation or ubiquitination and from partial degradation of GLUT4 (Zaarour et al., 2012). Interestingly, the isolated palmitoylated GLUT4 molecules appear only at the higher molecular weights of the GLUT4 band spectrum, which can be seen in the HA bound fraction in Figure 3.4. Thus, it is possible that there is selective palmitoylation of a subset of GLUT4 molecules which undergo a specific combination of PTMs or that only the non-degraded form of GLUT4 gets palmitoylated. It is also possible that palmitoylation protects GLUT4 from partial degradation and therefore remains in the higher molecular weight state. However, it is unlikely that the appearance of palmitoylated GLUT4 in the upper bands is caused by the molecular weight of palmitic acid itself. GLUT4 has only three putative palmitoylation sites, hence a maximum of three palmitate molecules could be attached to one molecule of GLUT4, resulting in a potential molecular weight increase of 3×0.256 kDa. Further research needs to be conducted to clarify whether palmitoylation is targeted towards higher molecular processed forms of GLUT4 or if palmitoylation itself increases protein stability of GLUT4. For example, transient expression of GLUT4

wild type and cysteine-deficient mutants in cell lines and subsequent pulse-chase analysis using ^{35}S -methionine could reveal whether palmitoylation protects GLUT4 from protein degradation. Another possibility could be the addition of lysosome and proteasome inhibitors in the cell culture medium and subsequent analysis by SDS-PAGE.

The previously reported palmitoylation of IR β and IGF-receptor β has been confirmed in this study (Magee and Siddle, 1988), although only a small fraction of the IGF-receptor β (approximately 7%) was found to be palmitoylated. Akin to caveolin-1, the estimated levels of palmitoylation of IR β were dependent on which method for the isolation of the membrane fractions was used. When centrifugation at lower speed (16,000 x g) was applied, the estimated palmitoylated fraction of IR β was approximately 12%, in contrast application of ultracentrifugation (136,000 x g) resulted with an estimated palmitoylated fraction of approximately 50% of the total IR β molecules. As described for caveolin-1 (see above), it is likely that this increase in palmitoylation of IR β is due to palmitoylated IR β molecules, that reside in low density vesicles, and that are only isolated by ultracentrifugation. It is possible that low density vesicles, which are enriched in palmitoylated caveolin-1 and IR, might play a role in moving newly synthesised IR molecules to the PM.

The IR resides mainly in caveolae at the PM of adipocytes (Gustavsson et al., 1999; Foti et al., 2007). Furthermore, caveolin-1, which is a major coat protein of caveolae, was identified as a substrate of IR kinase activity (Kimura et al., 2002). Moreover, endocytosis and recycling of the IR is believed to be mediated at least partly by caveolae (Strålfors, 2012). This internalisation and recycling pathway is thought to involve insulin-stimulated phosphorylation of caveolin-1 by the tyrosine kinase activity of the IR (Fagerholm et al., 2009). As both these proteins are palmitoylated, it can be speculated that palmitoylation regulates or stabilises the interaction between these two proteins (Delandre et al., 2009) and therefore facilitates their joint endocytosis and recycling. An argument supporting this assumption is that there is evidence that palmitoylated molecules of both, the IR and caveolin-1 are enriched in low density vesicles such as microsomes and

endosomes (see above). As the internalisation of the IR increases after stimulation with insulin (Fagerholm et al., 2009), it would be interesting to test whether there is an immediate but transient increase in palmitoylation of IR and caveolin-1 upon insulin stimulation.

Both cysteine residues which are likely to undergo palmitoylation are located intracellularly within the IR β kinase domain at the amino acid positions 1251 and 1262. Hence it is possible, that palmitoylation interferes with or regulates the kinase activity of the receptor. Auto-phosphorylation by the receptor kinase domain was previously demonstrated to regulate the activity of the IR (Wilden et al., 1992). Previous research has shown that palmitoylation can regulate phosphorylation of adjacent amino acid residues (Moffett et al., 1996). There would be potential for such a mode of regulation within the IR as a tyrosine residue resides only 7 amino acids away from cysteine-1251 towards the C-terminus. However, this tyrosine-1246 was not predicted to undergo auto-phosphorylation (UniProt). To address the question of whether palmitoylation has an effect on the IR, palmitoylation deficient mutants of the receptor need to be examined in respect to activity and endocytosis. For example, cysteine to alanine mutants of the IR could be expressed in 3T3-L1 adipocytes, followed by the examination of insulin-stimulated phosphorylation of the receptors immediate substrates such as IRS or its own auto-phosphorylation.

In silico analysis using CSS-Palm 4.0 did not always correlate with the experimental data. For example the score for cysteine residues of PDK-1 (score= 6) or clathrin HC (score = 3.9 and 4.1) were sufficiently high to suggest that they might be targets for palmitoylation, but experimental data demonstrated that there was no or only very little palmitoylation of both proteins. On the other hand, the predicted scores for the cysteine residues of caveolin-1 (score= 1.5, 2.1 and 0.9) were lower than for PDK-1 and clathrin HC, and yet this protein was robustly palmitoylated. In contrast, high predicted values for flotillin-1, flotillin-2, SNAP23 and caveolin-2 palmitoylation were confirmed experimentally with high levels of palmitoylation of these proteins. A possible source for the discrepancy of the results between *in silico*- and experimental analysis may be that the experimental procedure was limited to 3T3-

L1 adipocytes in this study. The origin of the database, which the algorithm of CSS-Palm 4.0 is based on, is not specified. Hence, it is possible that the prediction by CSS-Palm would agree with experiments conducted in other cell types but not with 3T3-L1 adipocytes. However, as quantification of the palmitoylated population of a protein is not examined in the majority of the studies in the field, it remains unknown whether the extent of palmitoylation of the proteins examined in this study is cell type specific.

The quantification of palmitoylation levels for the identified proteins was conducted at first under standard 3T3-L1 culture conditions. These conditions included a glucose concentration of 25.5 mM and an unspecified low level of insulin, which originated from the fetal bovine serum in the medium. As mentioned in the introduction, physiological glucose serum levels are between 4-6 mM, and patients with type 2 diabetes and insulin resistance have significantly elevated blood glucose and insulin levels (Alberti and Zimmet, 1998). Thus, adipocytes from these patients are surrounded by a different glucose and insulin concentration in the interstitial fluid than in non-diabetic individuals. Therefore, I examined the palmitoylation of a panel of proteins in 3T3-L1 adipocytes cultured with varying glucose concentrations in the media combined with chronic insulin treatment. Chronic insulin treatment was reported to result in the down-regulation of IR levels (Ronnett et al., 1982; Knutson et al., 1982), and indeed this effect could be observed when 3T3-L1 adipocytes were treated for 24 h with 500 nM insulin in the culture medium (Figure 3.6). In contrast, variation of the glucose concentration did not have any effect on IR levels. The palmitoylation level of all examined proteins did not change significantly under any of the tested conditions (Figure 3.7 and Figure 3.8). It could be concluded that the down regulation of the IR level was independent of palmitoylation. Furthermore, chronic insulin treatment leads to insulin resistance of cultured adipocytes (Thomson et al., 1997), and hence the results also suggest that palmitoylation changes in the examined proteins are not likely to be involved in the development of insulin resistance in this cell type. In contrast to the results presented in this thesis, elevated palmitoylation of IRAP was demonstrated in 3T3-

L1 adipocytes cultured with high glucose in the medium (22.5 mM) and in fat tissue from obese mice assayed using acyl-RAC (Ren et al., 2013b). However, the demonstrated increase of palmitoylation was subtle and the estimation of palmitoylation was presented showing only the bound fraction of the acyl-RAC experiment without analysis of the unbound fraction; there was also no quantified data presented for these analyses. Estimation of the palmitoylation levels from such an analysis is difficult as the input of total protein is not normalised. A different study reported that phosphorylation of caveolin-2 was increased in fat tissue of mice with preliminary insulin resistance (Gómez-Ruiz et al., 2011). As mentioned above, such an effect could not be observed with palmitoylation of caveolin-2.

Collectively, this chapter has identified novel palmitoylated proteins in 3T3-L1 adipocytes (caveolin-2, IRAP and GLUT4) and confirmed the palmitoylation of other proteins, including caveolin-1 and IR β subunit. An important aspect of this study was the ability to estimate the pool of a particular protein that is likely to be palmitoylated. This analysis highlighted a broad range of palmitoylation levels, from >80% for proteins such as SNAP23 and caveolin-2 down to 7% for proteins including IGF-1 receptor β and GLUT4 (14%). Although palmitoylation is a dynamic modification, no effect on palmitoylation levels of any of these proteins was observed following chronic insulin treatment or changes in extracellular glucose concentration. Important follow-up studies will include mapping the palmitoylation sites in novel palmitoylated proteins and investigating how palmitoylation regulates these proteins.

Chapter 4: Palmitoylation of the insulin-responsive aminopeptidase IRAP: Identification of palmitoylation sites and analysis of the effect of palmitoylation on intracellular targeting.

4.1 Introduction

Diabetes is a condition where the regulation of blood glucose levels is disturbed. In the case of type I diabetes the pancreas is not capable of insulin production and in type II diabetes the individuals are resistant to insulin but still may be able to produce it. In both cases glucose levels in the blood can be elevated and medication may be required to maintain blood glucose at stable levels (Alberti and Zimmet, 1998).

The underlying mechanisms of insulin resistance are not clear and this is being intensively studied. The main organs responsible for glucose clearance from the blood are the liver, skeletal muscle and adipose tissue. In muscle and adipose tissue, glucose is transported into the cell through GLUT4 (Stuart et al., 2006). Under basal conditions, approximately 75% of the total GLUT4 resides intracellularly in so-called GSVs; these vesicles translocate to the PM upon stimulation with insulin (Bryant et al., 2002). Fusion of GSVs with the PM enables the increased transportation of glucose into the cell through GLUT4 in a concentration gradient-dependent manner. GLUT4 is then recycled back into intracellular vesicles via endocytosis. Although the mechanisms regulating biogenesis of GSVs and their translocation to the PM are not yet fully characterised, several resident GSV proteins have been identified, such as the SNARE protein VAMP2, sortilin and the IRAP. IRAP is an integral protein with a single membrane-spanning domain, that has zinc-dependent aminopeptidase activity and has been identified as one of the major component of GSVs (Keller et al., 1995). IRAP is the main protein that is known to traffic together with GLUT4 and the two proteins exhibit a high degree of co-localisation in various intracellular compartments (Martin et al., 1996; Hashiramoto and James, 2000). The specific

function of IRAP in adipocytes and muscle cells or other cell types is not known. A potential function as an aminopeptidase is suggested as IRAP was demonstrated to cleave signal peptides *in vitro* such as vasopressin, oxytocin and several other hormones (Herbst et al., 1997). Additionally, IRAP has been identified as a receptor for angiotensin IV and therefore research proposes a possible role for IRAP in spatial memory (Albiston et al., 2010). IRAP is not only considered as just cargo protein of GSVs but also has a function in GSV trafficking, as overexpression of specific cytosolic fragments of the protein resulted in an insulin-independent translocation of GSVs to the PM (Waters, 1997). Furthermore, depletion of IRAP in unstimulated adipocytes caused a threefold increase of GLUT4 at the PM (Jordens et al., 2010), suggesting a possible role for IRAP in the intracellular retention of GSVs.

IRAP consist of a total of 1025 amino acids and has been reported to undergo several PTMs. It has 17 predicted glycosylation sites and these are thought to undergo tissue-specific glycosylation, since the detected molecular weights from brain (140kDa) differed to those of other tissues (165kDa)(Keller et al., 1995). Another potential PTM of IRAP is the attachment of poly ADP ribose. IRAP was reported to interact with the protein tankyrase, a protein that has a poly-ADP-ribose polymerase (PARP) activity and has been shown to attach poly ADP ribose onto other proteins (Cook et al., 2002; Sbodio and Chi, 2002).

In this thesis, I was specifically interested in the PTM palmitoylation. At the outset of my PhD project, there was no information published regarding palmitoylation of IRAP, however in 2013 IRAP was identified in a proteomic screen for palmitoylated proteins in cultured adipocytes, epididymal fat tissue and brain (Ren et al., 2013b). Furthermore, the same group demonstrated that palmitoylation of IRAP was increased in cultured cells under high glucose conditions and in fat tissue from obese mice. In Chapter 3 of this thesis, 55% of IRAP molecules were shown to be palmitoylated in 3T3-L1 adipocytes via analysis of purified acyl-RAC fractions. In this chapter, I set out to deepen the knowledge about IRAPs palmitoylation by identifying the palmitoylation sites and determining how palmitoylation impacts IRAP localisation.

4.2 Identification of palmitoylated cysteine residues in IRAP

In Chapter 3, IRAP was identified as a palmitoylated protein in 3T3-L1 adipocytes assayed by using acyl-RAC. Additionally, palmitoylated IRAP was determined to account for approximately 55% of the total IRAP pool. Having shown palmitoylation of IRAP by acyl-RAC, I next set out to confirm this palmitoylation by using an independent technique, and to identify the likely sites of palmitoylation in IRAP.

Palmitoylation has been identified on many transmembrane proteins (Dietzen et al., 1995; Magee and Siddle, 1988; Abrami et al., 2006), and is usually observed to occur on cysteine residues present at a juxtamembrane position (i.e. adjacent to TMDs) (Levental et al., 2010; Delandre et al., 2009). Although IRAP is a large protein, it has a relatively short cytoplasmic domain. IRAP has three cysteine residues in this domain at amino acid positions 35, 103 and 114, as illustrated in Figure 4.1. According to the membrane topology prediction of SwissProt, cysteine-103 and cysteine-114 are localised in a juxtamembrane position, whereas cysteine-35 is localised further away from the TMD towards the N-terminus of the protein.

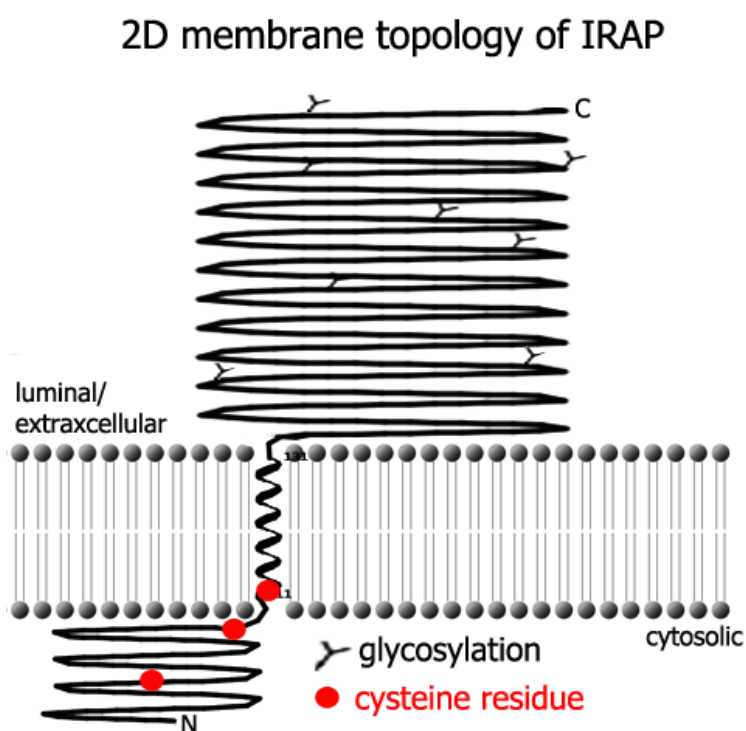


Figure 4.1. 2D membrane topology of IRAP. The transmembrane domain was defined by SwissProt and the image was created using TMRPres2D software. Cysteine residues and glycosylation sites are highlighted as indicated in the legend.

To examine the potential for the three cysteine residues in the cytoplasmic domain of IRAP to undergo palmitoylation, *in silico* analyses were carried out using CSS-Palm palmitoylation site prediction software (see Chapter 3). The software predicted a score of approximately 7 for all three cytosolic cysteine residues with the highest score for cysteine-103 and the lowest for cysteine-35 was (see Table 4.1).

Table 4.1. CSS-Palm prediction of palmitoylation sites of IRAP

Protein	Position	Amino acid sequence	Score	Domain
IRAP	35	VDLAKEPCLHPLEPD	7.201	Cytosolic
	103	RQSPDGTCSLPSART	7.487	Juxtamembrane intracell.
	114	SARTLVICVFVIVVA	7.324	Juxtamembrane intracell.

The identification of palmitoylated proteins shown in Chapter 3 was carried out in 3T3-L1 adipocytes. However, the expression of IRAP is not confined to adipocytes, but is present in all major tissues (Keller et al., 1995). Since IRAP was also suggested to be involved in memory and spatial learning (Chai et al., 2004), I examined whether IRAP is palmitoylated in mouse brain by using acyl-RAC. As shown in Figure 4.2, palmitoylation of IRAP in brain tissue is indicated by the protein band migrating at an apparent molecular weight of approximately 140 kDa in the lane loaded with HA treated bound fraction. Furthermore, when comparing the intensities of the protein bands corresponding to IRAP in the unbound fractions, it is noticeable that the signal is stronger in Tris unbound fraction than in the HA unbound fraction. Altogether, examining the immunoblot of the acyl-RAC analysis from mouse brain indicates a robust palmitoylation of IRAP in brain.

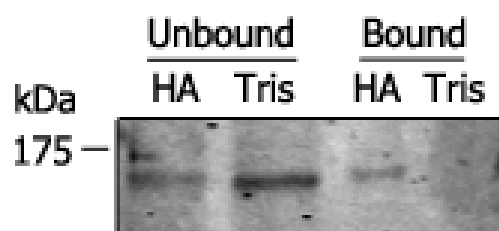


Figure 4.2. Analysis of acyl-RAC fractions prepared from homogenised mouse brain by immunoblotting. Brain samples of mouse were homogenised in lysis buffer (25 mM HEPES, 25 mM NaCl, 1 mM EDTA, pH 7.4 and protease inhibitor cocktail) using a Dounce homogeniser. The homogenate was then subjected to centrifugation to isolate the membrane fraction and proteins were precipitated with acetone. Following a treatment with MMTS (1.5% v/v), the isolated proteins were incubated with either 0.5 M HA or 0.5 M Tris together with free thiol group binding beads. Beads were pelleted by centrifugation and the supernatant was transferred into an appropriate amount of 4x Laemmli buffer = **Unbound**. Proteins were eluted from the beads using 1x Laemmli sample buffer with 50 mM DTT = **Bound**. The figure shows a representative immunoblot using an antibody against IRAP. Position of molecular weight marker is shown on the left.

In order to study the palmitoylation of IRAP in more detail and to identify the individual palmitoylation sites of IRAP, click-chemistry was applied. This method allows the incorporation of an alkynyl derivative of palmitic acid (17ODYA) onto cysteine residues of a protein to be detected using the principle of the Azide-alkyne Huisgen cycloaddition. Specifically, incorporated 17ODYA is reacted with an azide-linked infra-red dye in a copper-catalysed reaction, allowing proteins labelled with 17ODYA to be visualised by in-gel fluorescence using a LICOR Odyssey infra-red imaging system. This click-chemistry approach was used to compare palmitoylation of wild type and cysteine mutants of IRAP. An outline of the click-chemistry method is illustrated in Figure 4.3. A more detailed description of the experimental procedure can be found in the method section.

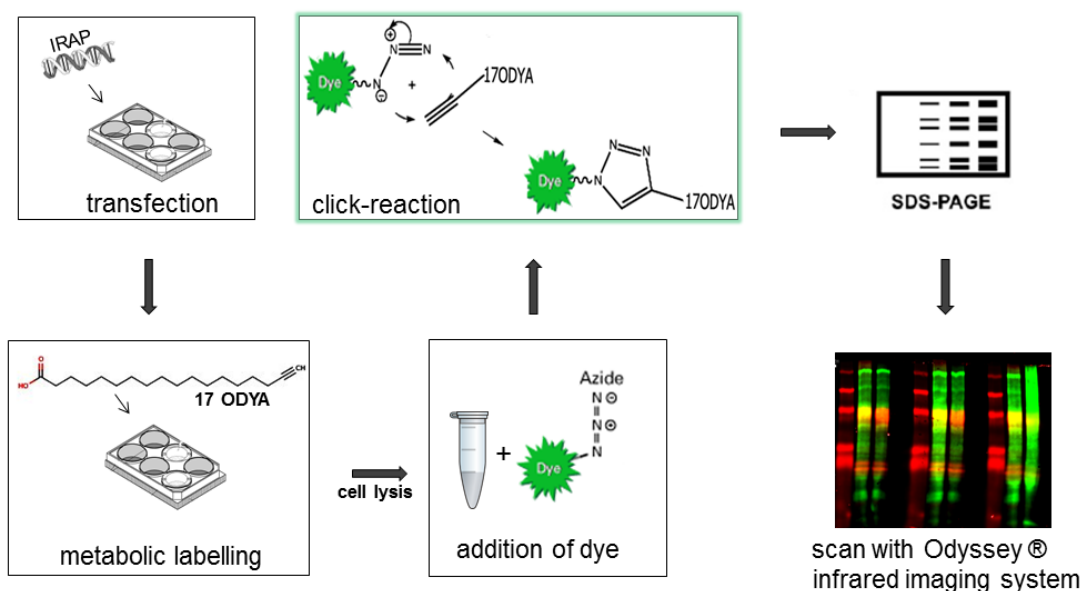


Figure 4.3. Outline of the click-chemistry method to detect attachment of 17ODYA onto cysteine residues of proteins. HEK293T cells were transfected with an expression vector containing the cDNA encoding the proteins of interest. After 24 h, cells were metabolically labelled with 15 μM 17ODYA for 4 h and subsequently lysed in 50 mM Tris; 0.5% SDS; pH 8.0 containing protease inhibitors. Click reaction mix was added including 10 μM of IRDye 800 CW azide and incubated for 1 h at room temperature. After precipitating the proteins with acetone, they were solubilised in 1x Laemmli buffer, separated by SDS-PAGE and transferred onto nitrocellulose for immunoblotting analysis and detection of click-signal. Dye and proteins of interest (HA- or GFP-tagged) were visualised using the LICOR Odyssey[®] infrared imaging system.

In order to identify palmitoylated cysteine residues in IRAP, cDNA encoding 3xHA-tagged wild type and cysteine-to-alanine mutants of IRAP were cloned in the EGFP-N1 expression vector (see section 2.3.17.2). As the cysteine-103 and cysteine-114 residues were predicted to reside close to the membrane interface, they were mutated either individually or together into alanine. A cysteine-to-alanine mutant of IRAP with all three cytosolic cysteines mutated was also generated. HEK293T cells were then transfected with the IRAP cDNA expression vectors and analysed by 17ODYA labelling and click-chemistry. The result of this experiment is shown in Figure 4.4A. The immunodetection of HA-tagged IRAP constructs in the left panel and shows a doublet protein band migrating at the apparent molecular weight of 175 kDa, which is the predicted size of IRAP. Samples from untransfected HEK293T

cells were also prepared as a negative control and as can be seen no immunoreactive signal could be detected for these samples.

In the middle panel of Figure 4.4A the click-signal corresponding to incorporation of 17ODYA into cellular proteins can be seen. There is a clear click-signal at the apparent molecular weight of approximately 175 kDa, corresponding to the protein bands immunolabelled with the HA-tag antibody (see merge image in right hand panel). This indicates that incorporation of 17ODYA into IRAP wild type, IRAP C103A and IRAP C114A has clearly occurred. The intensity of the click-signal is comparable for these three IRAP constructs. In contrast, no incorporation of 17ODYA could be detected in IRAP mutants with two or three cysteine to alanine mutations (103/114 CA and 35/103/114 CA) nor in untransfected cells. Furthermore, background signal from the IRDye 800cw is detectable at all molecular weights in each lane; in particular, there is a strongly labelled band at approximately 80 kDa in all lanes. The right panel displays a merge of both detected protein expression and click-signal.

To analyse these results in more detail, the intensity of the bands recorded with both channels were quantified by densitometry using Image Studio software. For calculation of the incorporation of 17ODYA into each IRAP constructs, the obtained value for the specific click-signal of the IRAP constructs was normalised to the corresponding expression levels of each IRAP construct. The resulting value for 17ODYA attachment in wild type IRAP was set to one and all mutants are expressed relative to this. The graph displayed in Figure 4.4B shows that incorporation of 17ODYA in the single cysteine to alanine IRAP mutants, C103A (1.05 AU) and IRAP C114A (0.94 AU), is comparable to the IRAP wild type. The incorporation of 17ODYA into the double cysteine to alanine IRAP mutant 103/114CA (0.05 AU) and the triple IRAP mutant 35/103/114CA (0.03 AU) was substantially and significantly ($p < 0.001$) lower than wild type IRAP and the two single cysteine mutants.

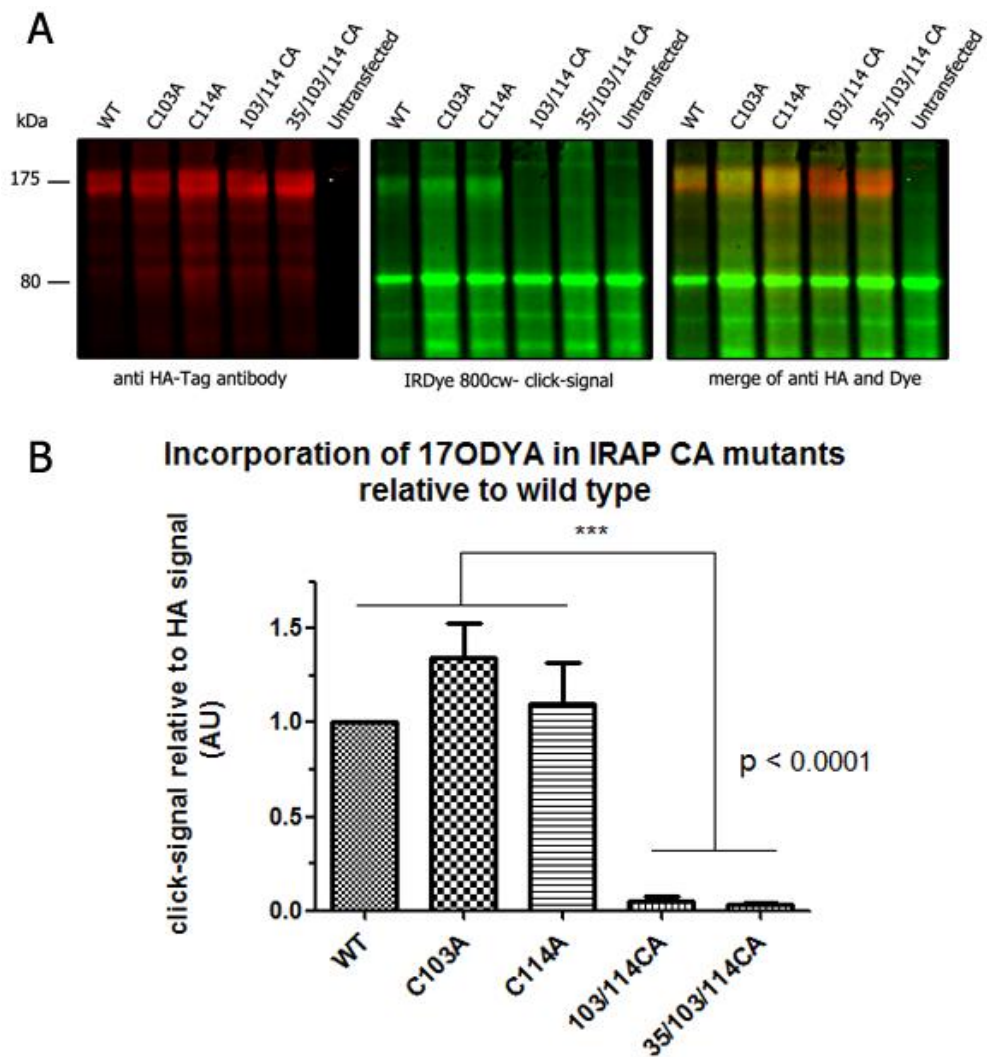


Figure 4.4. Detection of incorporation of 17ODYA into IRAP constructs in HEK293T cells. HEK293T cells were transfected with plasmids encoding the indicated HA-tagged IRAP constructs for 24 h. Cells were then serum-starved in DMEM culture medium containing 1% fatty acid-free (FAF) BSA for 30 min and metabolically labelled with 15 μ M 17ODYA for 4 h. Incorporation of 17ODYA was detected by reaction with IRDye 800 CW azide (as described in Section 2.4.2). Samples were subjected to SDS-PAGE on 8% acrylamide gels. Proteins were transferred onto nitrocellulose membranes and probed with HA antibody. Anti-HA antibody binding and IRDye were visualised using the Odyssey[®] infrared imaging system. **(A)** Representative LICOR images are shown of an experiment that was conducted 5 times. **(B)** Image Studio software was used to quantify 17ODYA incorporation into IRAP constructs from click-chemistry experiments. Quantified values of click-signal from IRAP constructs were divided by the value for the HA-tagged IRAP constructs. The calculated value of 17ODYA incorporation of the wild type IRAP was set to 1. Calculations were carried out with values obtained from 5 separate experiments. One way ANOVA followed by Tukey's multiple comparison test was applied for statistical analysis. *** $P \leq 0.001$. AU = arbitrary unit.

As follow-up experiments were conducted using the triple mutant IRAP 35/103/114CA, this mutant will be abbreviated to IRAP 3CA throughout the remainder of the thesis.

4.4 Investigating the effect of palmitoylation on the intracellular localisation of IRAP

Palmitoylation of IRAP was demonstrated using the techniques acyl-RAC and click-chemistry in previous sections. Furthermore, the fraction of palmitoylated IRAP in 3T3-L1 adipocytes was determined and the palmitoylated cysteine residues of IRAP were identified. In this section, I set out to characterise the effect of palmitoylation has on IRAP. As mentioned before (see section 1.10), palmitoylation can alter the biochemical properties of proteins in several ways. Most notably, attachment of palmitate increases the hydrophobicity of proteins and it has been reported that this can result in the insertion of soluble proteins into phospholipid bilayers (Vogel and Roche, 1999). Furthermore, palmitoylation of both soluble and transmembrane proteins can change their partitioning into membrane microdomains (Levental et al., 2010). Other effects of palmitoylation include regulating protein stability and the trafficking of proteins to various intracellular organelles (Salaun et al., 2010; Linder and Deschenes, 2007).

To examine if palmitoylation of IRAP had any major effect on protein stability, the expression level of the various cysteine mutants was compared to that of the wild type protein. As can be seen in Figure 4.5, there was no significant difference in the expression levels of any of the mutant proteins compared with wild type IRAP. This result suggests that palmitoylation probably does not exert a major effect on IRAP stability.

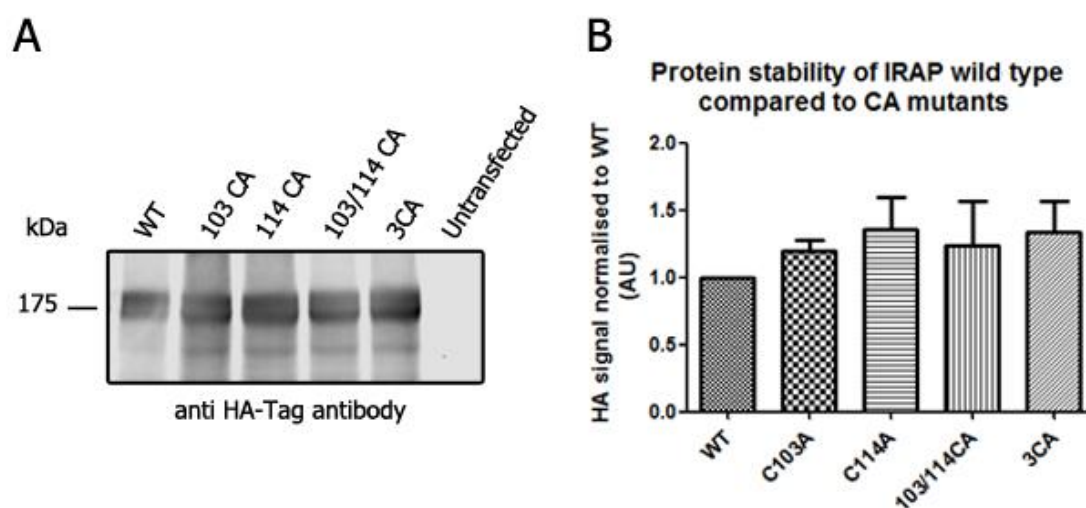


Figure 4.5. Protein stability of IRAP wild type and cysteine to alanine mutants. HEK293T cells were transfected with plasmids encoding the indicated HA-tagged IRAP constructs for 24 h. Cells were lysed in lysis buffer 50mM Tris, 17 mM SDS, pH 8.0 containing protease inhibitors, After addition of 4x Laemmli buffer samples boiled and subsequently subjected to SDS-PAGE on 8% acrylamide gels. Proteins were transferred onto nitrocellulose membranes and probed with HA antibody. Anti-Ha antibody binding visualised using the Odyssey[®] infrared imaging system. **(A)** Representative image is shown of an experiment that was conducted 5 times. **(B)** Image Studio software was used to quantify HA antibody binding and IRAP expression levels were normalised to IRAP wild type. Calculations were carried out with values obtained from 5 separate experiments.

In order to investigate whether palmitoylation of IRAP affects its trafficking within cells, the steady-state localisation of IRAP was examined by immunofluorescence labelling and confocal microscopy. For this, HEK293T cells were co-transfected with Myc- and HA-tagged IRAP constructs, which allows a direct comparison of wild type and cysteine mutant (3CA) IRAP to be made in the same cell. As can be seen in Figure 4.6 (top two panels), both HA- and myc-tagged IRAP wild type constructs reside mainly at the PM of HEK293T cells and are also detected in a perinuclear location.

The second panel from the top displays images of cells which were co-transfected with myc-tagged wild type IRAP and HA-tagged IRAP 3CA mutant. No major difference could be detected between these constructs, and both wild type and 3CA mutant were well expressed at the PM.

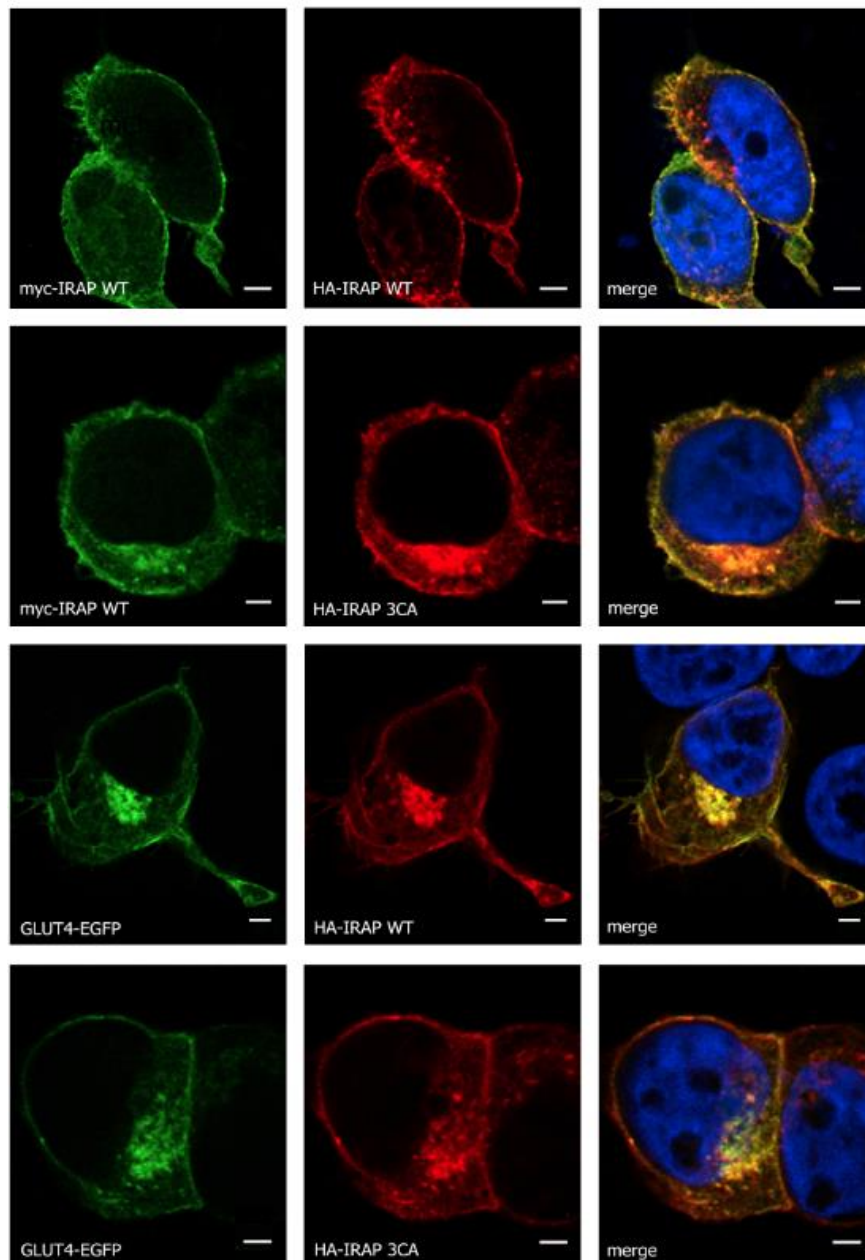


Figure 4.6. Analysis of the localisation of IRAP constructs in HEK293T cells using confocal microscopy. HEK293T cells were co-transfected with HA-tagged IRAP constructs together with myc-tagged wild type IRAP or GLUT4-EGFP as indicated. After 24 h, cells were fixed in 4% formaldehyde and subsequently permeabilised with PBS containing 0.3% (w/v) of bovine serum albumin (PBS/BSA) and 0.25% (v/v) Triton X-100 for 10 minutes at room temperature. Following washing with PBS/BSA, the cells were incubated with primary antibodies diluted 1:50 in PBS/BSA for 1 h at room temperature in a humid chamber. Primary antibodies were used against the myc and HA tags. Secondary antibodies used were: Alexa Fluor® 647-conjugated anti-mouse and Alexa Fluor® 647-conjugated anti-rabbit and were used at 1:400 dilution. Cells were mounted in ProLong Gold Antifade mounting medium containing DAPI. Whole cell image stacks were acquired by confocal microscopy and representative sections of a typical cell were chosen. Separate channels displaying myc-tagged IRAP WT or GLUT4-EGFP (green) and HA-tagged IRAP WT or 3CA mutant (red) and a merge of both channels including DAPI staining are shown. Images were deconvolved using Huygen's Essential software. Scale bar = 5 μ m.

As mentioned in section 1.7, IRAP co-localises and traffics together with GLUT4 in GSVs in myocytes and adipocytes; hence the localisation of IRAP constructs was also examined relative to the co-expressed GLUT4-EGFP fusion protein. The bottom two panels of Figure 4.6 show cells co-expressing GLUT4-EGFP and HA-tagged IRAP constructs. The expression pattern of GLUT4-EGFP was very similar to the localisation of both IRAP constructs and indeed the merge on the right panel of the figure confirms co-localisation of both proteins. As described for IRAP, GLUT4-EGFP localises at the PM and at an area adjacent to the nucleus of the cell. Thus, confocal microscopy analysis of wild type and 3CA mutant IRAP constructs in HEK293T cells suggests that there is no major effect of palmitoylation on the localisation of IRAP either in the absence or presence of GLUT4.

Complementary to the optical based localisation analysis using confocal microscopy, a biochemical approach was also undertaken. For this, a method called trypsin surface-digest was applied. This experiment is based on the proteolytic properties of the enzyme trypsin, a serine protease that cleaves proteins at lysine and arginine residues. When trypsin is added to the cell culturing media, it digests proteins only at the extracellular side of the PM, as it is not able to cross the PM. IRAP has a large extracellular domain (see Figure 4.1) with 54 predicted trypsin cleavage sites (according to ExPASy), and hence the extracellular domain of IRAP is expected to be digested by trypsin if integrated into the PM. For this experiment, N-terminal HA-tagged IRAP constructs were expressed in HEK293T cells. As the N-terminal HA-tag is intracellular, the digested IRAP would then be detected as a smaller protein fragment on an immunoblot, or the remaining IRAP protein fragment would be degraded by the cell. Therefore, comparing protein level and protein fragment sizes of the IRAP wild type and IRAP cysteine to alanine mutants in the absence and presence of trypsin treatment, could reveal a different incorporation of IRAP constructs into the PM. A cartoon illustrating the surface trypsin digest experiment is displayed in Figure 4.7.

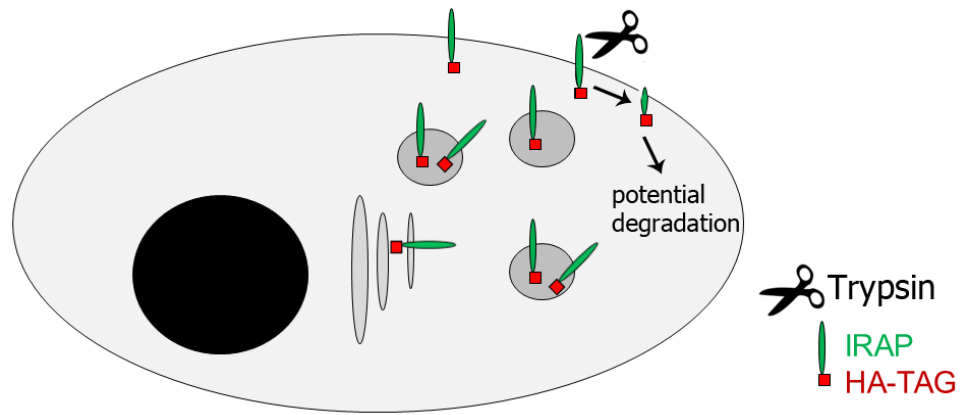


Figure 4.7. Schematic illustration of the surface trypsin-digest experiment. A schematic cartoon of a cell with nucleus (black circle), Golgi Apparatus (grey ovals), vesicles (grey circles) and PM (oval boarder of cell) is shown. HA-tagged IRAP and trypsin are indicated as in legend. IRAP is shown in the Golgi apparatus, at the membranes of vesicles and at the PM. Addition of trypsin to the culture medium digests the IRAP only on the extra-cellular side of the PM. The remaining IRAP fragments are potentially subjected to protein degradation through the proteasome or lysosome pathway.

The result of such a surface trypsin-digest experiment is shown in Figure 4.8. zDHHC5 was selected as a positive control in these experiments as it is known to associate with the PM (Greaves et al., 2010; Kokkola et al., 2011). A substantial decrease in the intensity of protein bands corresponding to zDHHC5 could be detected when cells were treated with trypsin. In contrast, trypsin treatment has no effect on the immunoreactivity of β -actin, demonstrating that trypsin did not affect protein levels of cytosolic proteins. As expected from the results shown in Figure 4.6, IRAP protein levels decreased when cells were incubated with trypsin compared to cells treated without trypsin. This effect was seen for both wild type and 3CA mutant IRAP. Immunoblots were subjected to densitometry using the software Image Studio, and protein levels normalised to corresponding β -actin. The calculated percentage of protein remaining after digestion with trypsin for IRAP constructs and zDHHC5 are shown in Figure 4.8B. zDHHC5 was selected as the positive control for a PM associated protein and indeed only approximately 23% of the total protein was detected after treating cells with trypsin. Approximately 42% of IRAP wild type was still detectable following the surface digest with trypsin.

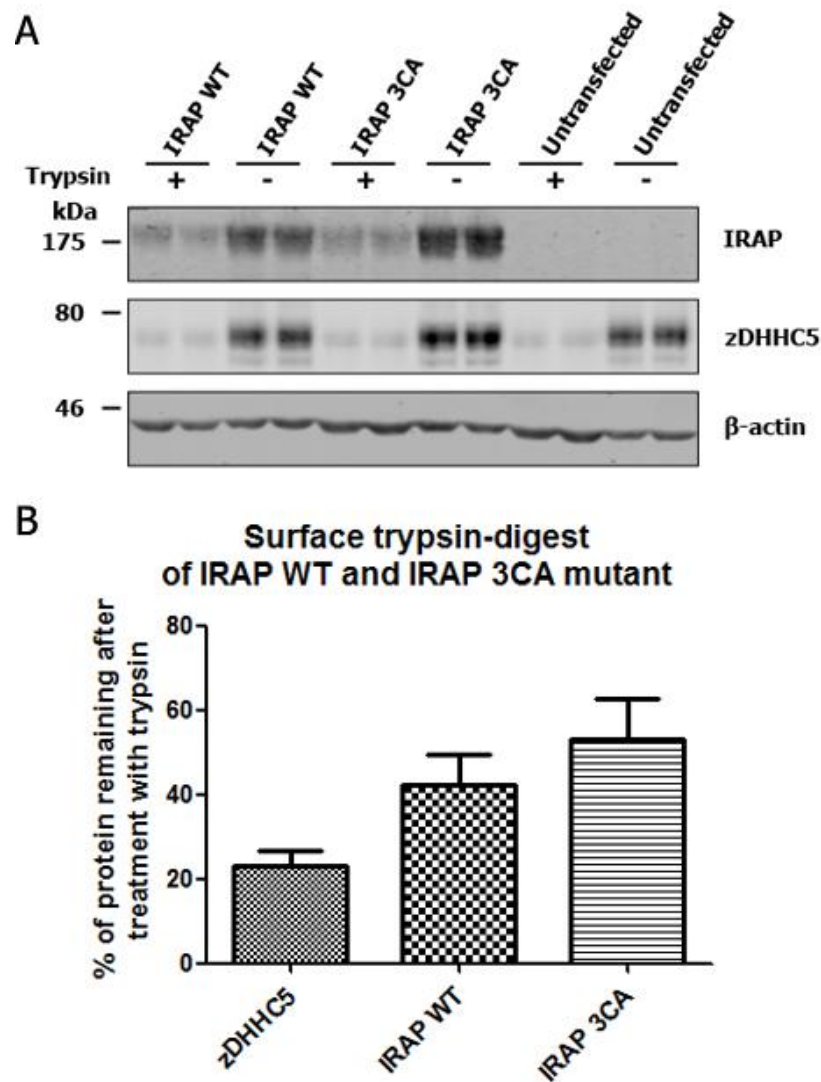


Figure 4.8. Surface trypsin-digest of IRAP wild type and IRAP 3CA mutant in HEK293T cells. Cells were transfected for 24 h with plasmids encoding N-terminal HA-tagged IRAP wild type or IRAP cysteine to alanine mutant (3CA). Following 2 washes with PBS, trypsin-EDTA (0.05%) (+) or HEK293T culture media (-) was added and incubated for 30 min in a cell culture incubator. Cells were transferred into reaction tubes and pelleted by centrifugation at 16,000 x g at 4°C for 10 min. The cell pellets were washed twice by adding 1 ml PBS followed by centrifugation at 16,000 x g at 4°C for 5 min. The washed cell pellets were then resuspended in 200 µl 1x Laemmli buffer with 25 mM DTT and subjected to SDS-PAGE on 8% acrylamide gels followed by immunoblotting with the indicated antibodies. Samples were loaded in duplicate. **(A)** Representative immunoblots are shown from an experiment conducted 7 times. Position of molecular weight markers are indicated on the left. **(B)** Densitometry was applied using Image Studio software from LICOR. All protein band intensities were normalised to the corresponding β-actin signal. Furthermore, normalised values of trypsin-treated cells were divided by normalised values of non-trypsin treated cells and the result was multiplied by 100 to obtain a percentage value. Calculated trypsin-digested fractions are shown for the proteins zDHHHC5, IRAP wild type and IRAP 3CA cysteine to alanine mutant. N=7. Student's *t*-test revealed no significant difference between trypsin digestion of IRAP wild type and 3CA mutant ($p=0.387$).

The calculated percentage for IRAP 3CA mutant was approximately 53%. Although the calculations revealed that 10% more of IRAP wild type was digested when compared to IRAP 3CA, there was no statistical significance ($p=0.387$) when the results were analysed by Student's *t*-test.

4.5 Discussion

In Chapter 3, approximately 55% of IRAP molecules were identified to be palmitoylated at steady state in 3T3-L1 adipocytes. In this chapter, experiments were undertaken in order to advance the knowledge about the palmitoylation sites on IRAP and the potential role that palmitoylation has in regulating IRAP stability and localisation. Results in this chapter demonstrate that IRAP palmitoylation is not restricted to adipocytes but also occurs in brain (Figure 4.2). Furthermore, *in silico* analysis revealed that all three intracellular cysteines of IRAP have the potential to be palmitoylated (Table 4.1). However, as cysteine-103 and cysteine-114 were localised in a juxtamembrane position it was considered that these sites are most likely to be palmitoylated *in vivo*. Click-chemistry experiments revealed that mutation of neither of these sites alone affected incorporation of 17ODYA, whereas mutation of both sites led to an almost complete loss of labelling. No palmitoylation-dependent change in the localisation of IRAP could be observed when subcellular targeting of wild type and cysteine mutant IRAP constructs was examined by confocal microscopy in HEK293T cells. Congruently, application of the biochemical method surface trypsin-digest showed no significant difference of protein levels at the cell surface between IRAP WT and the cysteine-deficient IRAP (3CA) mutant. Finally, no major difference in the stability of wild type and cysteine mutant IRAP was observed when expression levels of transfected constructs was examined.

For *in silico* analysis of the potential palmitoylation sites of IRAP, the prediction software CSS-Palm version 4.0 was used (see Table 4.1). The predicted score for all three cysteine was similar and had values of approximately 7. These are updated values, as version 4.0 of CSS-Palm was released in 2013. A previous version of CSS-

Palm (version 3.0) which was used originally in this thesis predicted somewhat different values with an approximately 7 fold lower value for cysteine-35 compared to the values predicted for cysteine-103 and cysteine-114. Because cysteine-35 is predicted to be present at some distance from the TMD (Figure 4.1) and the originally predicted score by CSS-Palm V3.0 was negligible, cysteine-35 was not further investigated in this thesis. The discrepancy between the values of version 4.0 and 3.0 is likely to originate from different algorithms which were used from palmitoylation prediction.

Palmitoylation of IRAP in brain was confirmed by the application of acyl-RAC with homogenised mouse brain samples. Hence, it was demonstrated that palmitoylation of IRAP is not only limited to cultured 3T3-L1 adipocytes but also occurs *in vivo* in mouse brain. This finding conforms with recently published research in which the palmitoylation of IRAP was demonstrated to be found in 3T3-L1 adipocytes, HEK293 cells, hepatoma FAO cells, epididymal fat and brain (Ren et al., 2013b). Furthermore, it could be estimated from Figure 4.2 that 30-50% of IRAP molecules undergo palmitoylation in brain to a similar extent to the calculated values seen for adipocytes in Figure 3.4.

IRAP cDNA used for expression studies was tagged with three consecutive HA epitopes upstream of the first methionine of the protein and was detected using an anti-HA antibody. A single HA tag comprises 9 amino acids and hence a triple HA tag would add 27 additional amino acids resulting in an increase of the total molecular weight by approximately 4.3 kDa. Indeed IRAP was detected with an slightly higher apparent molecular weight in this thesis than the previously reported apparent molecular weight of 165 kDa (Keller et al., 1995). Moreover, IRAP appeared as a doublet band Figure 4.4 (left panel) which does not conform to detected IRAP in 3T3-L1 adipocytes and brain where it appeared as a single band with the molecular weight just under 175 kDa or 140 kDa, respectively (Figure 3.4 and Figure 4.2.) The doublet band may originate from either proteolytic cleavage in HEK293T cells or differential modification by PTMs in this cell type. I favour the latter possibility, as IRAP has 17 predicted glycosylation sites in the extracellular domain and has also

been reported to undergo the attachment of poly ADP ribose (PARsylation) (Chi and Lodish, 2000). Furthermore, the size at which IRAP is detected in brain (140 kDa) and muscle and adipose tissue (165 kDa) varies by approximately 25 kDa, which is thought to be due to different extent of glycosylation (Keller et al., 1995). However, the click-signal for IRAP results in a single band which corresponds more strongly to the upper band of the IRAP doublet seen in the middle and right panel of Figure 4.4. As palmitic acid has the molecular weight of 0.256 kDa and a maximum of two or three molecules of palmitic acid are attached to one molecule of IRAP, it can probably be excluded that palmitoylation causes the association of the click-signal band with the upper band of the IRAP doublet. Assuming that the doublet band originates from differently processed IRAP, it is possible that the higher molecular weight IRAP molecules are preferably palmitoylated. However, it is unknown how this selectivity is regulated. Glycosylation is unlikely to have a direct effect on palmitoylation, as all glycosylation sites are localised in the extracellular/luminal domain of IRAP, whereas palmitoylation of IRAP takes place at the cytosolic side of the membrane. Instead, it may be that differential glycosylation of IRAP reports a specific intracellular localisation of the protein for example, that the upper band represents IRAP that has trafficked through the Golgi complex.

Incorporation of 17ODYA into the various IRAP constructs was quantified in order to gain information about the potential sites of palmitoylation. Single cysteine to alanine mutation of cysteine-103 and cysteine-114 did not change the level of 17ODYA incorporation when compared to wild type protein. In contrast, the double mutant 103/114 cysteine mutant and triple mutant 35/103/114 CA (3CA) of IRAP displayed a near complete loss of incorporation of 17ODYA (Figure 4.4). The cysteine residue pair consisting of cysteine-103 and cysteine-114 therefore seem to be essential for IRAP palmitoylation, as simultaneous loss of cysteine-103 and cysteine-114 was sufficient to block 17ODYA incorporation. Interestingly, the presence of only one of both cysteines was sufficient for full 17ODYA attachment. A similar observation was made in the lipoprotein receptor-related proteins 6 (LRP6). Like IRAP, LRP6 has a large extracellular domain that is connected with a smaller

cytosolic domain through one membrane-spanning domain and has two cytosolic juxtamembrane cysteines. Simultaneous replacement of both juxtamembrane cysteines in LRP6 to alanine resulted in a substantial loss of palmitoylation, but individual cysteine replacement had nearly an unaltered palmitoylation when compared to the wild type (Abrami et al., 2008). A possible explanation to this observation could be that only one cysteine (cysteine-103 or cysteine-114) undergoes palmitoylation at a time but not both simultaneously. Perhaps the cysteine residues are recognised by different zDHHC enzymes and palmitoylation at one site prevents recognition of the other site. Further experiments to investigate the stoichiometry of IRAP palmitoylation could shed light on whether only a single cysteine residue is palmitoylated at any one time. The use of “PEGylation” with polyethylene glycol (PEG)-maleimide would represent a suitable approach to investigate the number of free cysteines following HA treatment. As mentioned above, the originally predicted palmitoylation score for cysteine-35 was much lower than for the two other cysteines, and 17ODYA attachment to IRAP 3CA mutant was nearly identical to the attachment of 17ODYA to IRAP double mutant 103/114 CA. For these two reasons the examination of single C35A mutant was not considered.

As mentioned above, palmitoylation can regulate many aspects of a proteins life-cycle, including its intracellular trafficking (Salaun et al., 2010). To investigate whether palmitoylation of IRAP has an effect on its trafficking in the cell, analysis of IRAP WT and the IRAP 3CA mutant were undertaken using confocal microscopy. Comparing the localisation of myc-tagged IRAP WT with HA-tagged IRAP 3CA mutant within the same cell enables the detection of subtle effects of palmitoylation on the localisation of IRAP (Greaves and Chamberlain, 2011b). As IRAP was shown to co-localise and translocate to the PM together with GLUT4 in muscle and adipose tissue (Kandror et al., 1994; Ross et al., 1998), the localisation of both IRAP constructs was also examined relative to GLUT4. The localisation of IRAP 3CA mutant was neither changed relative to IRAP WT nor to GLUT4 in HEK293T cells. The majority of IRAP constructs and GLUT4 were localised adjacent to the nucleus and at the PM. In each case, there was a strong co-localisation between

both transfected IRAP constructs and the IRAP constructs and GLUT4. Furthermore, the distribution of the proteins within the cell was similar to previously published studies (Thoidis and Kandror, 2001; Hosaka et al., 2005; Xie et al., 2011).

In addition to microscopy-based localisation studies, IRAP association with the PM was investigated biochemically. Application of surface trypsin-digest (illustrated in Figure 4.3), confirmed the findings obtained by confocal microscopy and suggested that palmitoylation of IRAP has no significant effect on its targeting to and insertion into the PM (Figure 4.8). Surface trypsin-digestions have been applied successfully in previous publications to identify PM localisation of other proteins, such as the anthrax toxin receptor, which has a similar membrane topology to IRAP (Abrami et al., 2006). In this thesis the functionality of this assay was confirmed by examination of the PM-localised zDHHC5 protein. Although zDHHC5 has only one predicted trypsin digestion site located in an extracellular loop, 80% of DHHC5 was degraded by treatment with trypsin, highlighting the efficiency of this method; intracellular β -actin was not affected by trypsin treatment. As mentioned above, IRAP has 54 predicted extracellular-localised trypsin digestion sites. Following surface trypsin-digestion only 42% of IRAP WT and 53% the IRAP 3CA mutant was detected. The HA-tag of the IRAP constructs is in the cytosolic N-terminal part of IRAP, and hence it was possible that the entire cytosolic domain of IRAP (amino acids 1-109) could have been detected after the trypsin digest as a smaller fragment with an approximate size of 10 kDa. No fragment with this size was detected (data not shown), suggesting that upon trypsin treatment the remaining IRAP protein was subjected to protein degradation. Collectively the results of the trypsin digest agree with the confocal analysis, in which no difference in the intracellular localisations was found.

At the present stage it is not clear what role palmitoylation exerts on IRAP. It will be interesting to perform follow-up experiments to investigate whether palmitoylation affects the localisation of IRAP in 3T3-L1 adipocytes. However, these experiments are more time-consuming as they require viral transduction of adipocytes for protein expression. It is interesting to note that palmitoylation of

IRAP was reported to be increased in 3T3-L1 adipocytes cultured in medium with high glucose (22.5 mM) and also in adipose tissue obtained from obese mice (Ren et al., 2013b). However, neither the mechanism of regulation of palmitoylation nor the physiological relevance for its regulation by glucose and fat metabolism is yet known in adipose or in any other tissue. In this thesis, no effect of palmitoylation on the stability or localisation of IRAP was identified. Besides regulating the localisation and stability of proteins, palmitoylation is also thought to be capable of influencing other protein properties, such as protein-protein interactions, their association with membrane microdomains, and the modification of proteins by other PTMs (Delandre et al., 2009). Although, none of these other possible functions of palmitoylation were examined here, it would be interesting to perform further studies in this area. Interestingly AS160 and GLUT4, which are key proteins involved in insulin-stimulated glucose uptake, are both interaction partners of IRAP. IRAP is thought to interact with GLUT4 in the lumen of the GSV through its luminal domain (Shi et al., 2008) and with AS160 through its cytoplasmic domain (Peck et al., 2006). Both, GLUT4 and AS160 were demonstrated to undergo palmitoylation (Ren et al., 2013b) and the palmitoylation of GLUT4 was confirmed in this thesis. Although palmitoylation of GLUT4 and AS160 could have various functions, it is also possible that it may facilitate the interaction between those proteins.

IRAP also undergoes the PTM PARsylation, which is mediated by tankyrase. Tankyrase exerts the catalytic function of a poly-ADP-ribose polymerase (PARP) and interacts with IRAP through its ankyrin-repeat domain (Chi and Lodish, 2000). Ankyrin-repeat domains are known to mediate protein-protein interaction (Li et al., 2006) and some zDHHC enzymes use this motif for their substrate recognition (Huang et al., 2009; Lemonidis et al., 2014). The region in the cytosolic N-terminus of IRAP comprising the amino acids 96-101 was identified to correspond to the ankyrin-repeat domain binding motif (Sbodio and Chi, 2002). Interestingly, two amino acids away from this putative ankyrin-repeat binding domain resides a cysteine (cysteine-103) which undergoes the attachment of palmitic acid as demonstrated in this thesis. It is possible that palmitoylation of cysteine-103 could

affect the interaction of tankyrase with IRAP. This could be potentially relevant for the insulin induced translocation of GSVs to the PM as depletion of tankyrase or inhibition of its PARP activity resulted in an attenuated association of GSVs with the PM (Yeh et al., 2007).

Chapter 5: Characterisation of palmitoylation of caveolin-2.

5.1 Introduction

Caveolin-2 is a 162 amino acid long protein which has been identified to be one of the major coat proteins of specialised cholesterol rich membrane micro domains called caveolae. Caveolae, meaning “little caves”, are flask shape invaginations of the PM; they have a diameter ranging from 50 to 100 nm and can be mostly found at the surface of epithelial cells, striated muscle cells and adipocytes (Napolitano, 1963; Palade, 1953; Gil, 1983). Originally discovered by electron microscopy in epithelial cells, they were described as smooth uncoated pits (Palade, 1953; Yamada, 1955). Later research revealed that caveolae do not have just a smooth surface, as caveolar coat proteins such as caveolin-1 and caveolin-2 were identified (Rothberg et al., 1992; Scherer et al., 1996). The knowledge about the caveolar coat was complemented approximately 10 years later with the discovery of the family of cavin proteins, which are thought to form the outer coat of caveolae (Vinten et al., 2005). Although the detailed mechanism of biogenesis of caveolae is not known yet, a model has been suggested, which is based on the trafficking pathway of its major coat proteins, caveolin-1 and caveolin-2. According to this model, caveolin-1 and caveolin-2 form hetero-oligomers shortly after their protein biosynthesis in the ER (Scheiffele et al., 1998). These oligomers are estimated to consist of approximately 7 to 10 caveolin monomers and are subsequently transported to the compartments of the Golgi apparatus, where they continue their maturation into larger oligomeric assemblies. The extended oligomerisation within the Golgi apparatus is dependent on cholesterol and the oligomeric assemblies reach a size of approximately 70S. The estimated number of caveolin monomers in these hetero-oligomers are approximately 160 (Hayer et al., 2010) which corresponds well to the estimated amount of caveolin monomers (144 ± 39) in mature caveolae (Pelkmans and Zerial, 2005). The assembly is then thought to leave the Golgi apparatus through the medial Golgi complex, to translocate and be subsequently inserted into the PM

(Choudhury et al., 2006; Hayer et al., 2010). At present it is suggested that biogenesis of caveolae is finalised with the peripheral association of cavin proteins to the caveolin oligomers scaffold which is inserted in the PM.

Caveolae were found to exert physiological functions at cellular and whole organism level. They have been identified to play a role in cellular transport such as endocytosis and transcytosis and are involved in cholesterol homeostasis (Fielding and Fielding, 1995; Schnitzer, 2001). Furthermore, caveolae are important for lipid metabolism especially for uptake and incorporation of triglycerides into adipose tissue (Liu et al., 2008).

Caveolin-2 is expressed in most major tissues and as briefly mentioned above, it is a major component of the caveolar coat. The detailed role of caveolin-2 in the biogenesis of caveolae is not known yet; it is not essential for formation of caveolae, as caveolae are still present in caveolin-2 deficient mouse (Razani et al., 2002b). It is speculated that caveolin-2 is involved in the regulation of the shape of caveolae, as the presence of caveolin-2 was necessary for the formation of deep caveolae (Fujimoto et al., 2000). Independently of its role in caveolae, caveolin-2 has been shown to be important for correct pulmonary function, as lung parenchyma of mouse showed thickened aveolar septa due to hypercellularity in mouse deficient in caveolin-2 (Razani et al., 2002b).

The structure and membrane topology of caveolin-2 is similar to the remaining members of the caveolin family caveolin-1 and caveolin-3. The cytoplasmic N and C-termini are separated by a 32 amino acid long intra membrane domain which forms an incomplete hairpin structure in the lipid bilayer. Although palmitoylation has been reported for caveolin-1 and caveolin-3, no data regarding the palmitoylation of caveolin-2 is available yet (Dietzen et al., 1995; Galbiati et al., 1999). In Chapter 3 of this thesis I identified that approximately 80% of caveolin-2 molecules are palmitoylated in 3T3-L1 adipocytes. In this chapter I set out to identify the palmitoylation sites of caveolin-2 and the potential effect of caveolin-2 palmitoylation on its localisation, membrane partitioning and oligomerisation.

5.2 Localisation of caveolin-1 and caveolin-2 in mature 3T3-L1 adipocytes.

As discussed in Section 5.1, caveolae can account for up to 50% of the PM surface area in adipocytes (Thorn et al., 2003). Caveolae play an important role in adipocyte physiology, and are thought to be involved in transmembrane transport of fatty acids into cells (Meshulam et al., 2006; Razani et al., 2002a). Before undertaking further analysis of caveolin-2 palmitoylation, the intracellular localisation of this isoform was compared with caveolin-1 in 3T3-L1 adipocytes using immunocytochemistry and confocal microscopy.

3T3-L1 adipocytes were probed with antibodies against caveolin-1 and caveolin-2. Alexa Fluor® 647-conjugated anti-rabbit antibody was used for the detection of caveolin-1 (shown as red, Figure 5.1), whereas an Alexa Fluor® 488-conjugated secondary antibody was used to label the caveolin-2 antibody (Figure 5.1, shown as green). The top panel of Figure 5.1 shows a section from the bottom of the cell. As can be seen, both caveolin proteins were observed to form “circular rosette” structures, which have previously been described for caveolin-1 (Parton et al., 1994), and which are believed to represent higher-order caveolar assemblies. These circular structures vary in their diameter from approximately 0.5 μm to 2.5 μm . The merge of caveolin-1 and caveolin-2 indicates that the proteins are strongly co-distributed within these structures.

The bottom panel of Figure 5.1 shows a section from the middle of the same cell. This image shows that caveolin-1 is strongly enriched at the PM, with very little protein detected inside the cell. Caveolin-2 also localises at the PM, but in contrast to caveolin-1 a substantial amount of caveolin-2 can be detected at a perinuclear location and throughout the cell cytoplasm. The detection of caveolin-2 in the intracellular compartments also reveals large dark circular structures, which are likely lipid droplets for triglyceride storage.

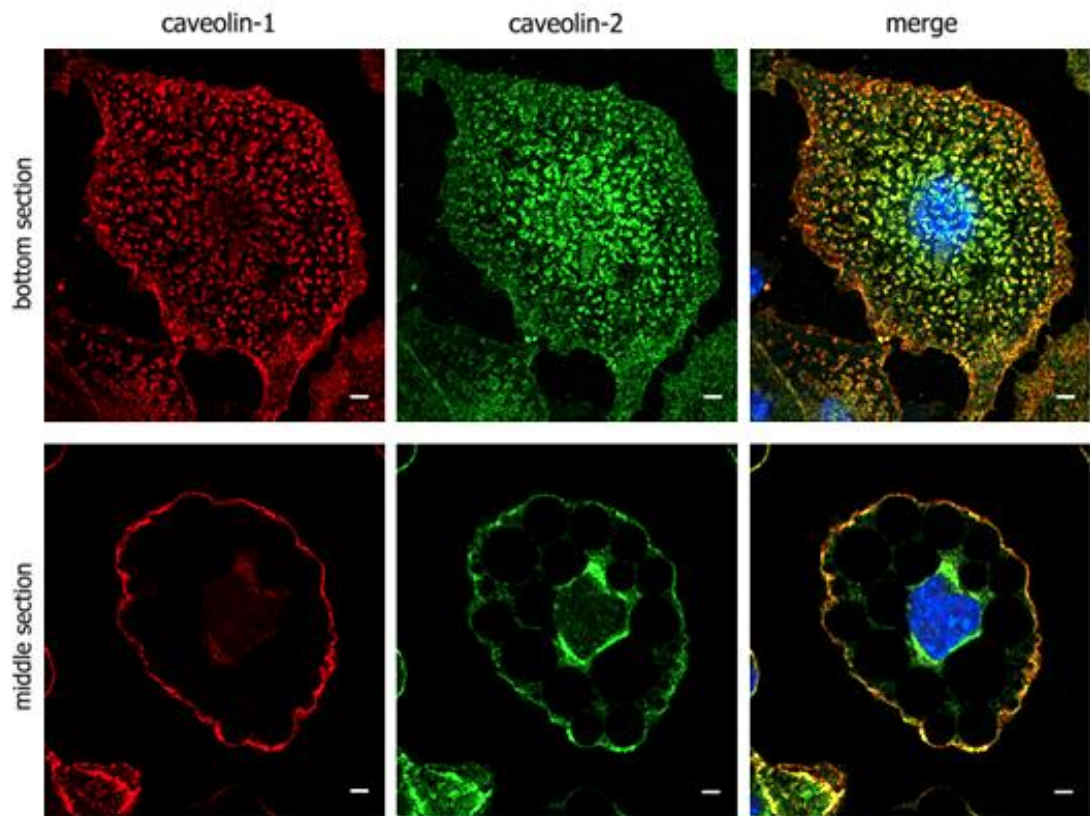


Figure 5.1. Localisation of caveolin-1 and -2 isoforms in mature 3T3-L1 adipocytes. Cells were fixed in 4% formaldehyde 10 days post initiation of differentiation. Subsequently, cells were permeabilised with PBS containing 0.3% (w/v) of bovine serum albumin (PBS/BSA) and 0.25% (v/v) Triton X-100 for 10 minutes at room temperature. Following washing with PBS/BSA, cells were incubated with primary antibodies diluted 1:50 in PBS/BSA for 1 h at room temperature in a humid chamber. Rabbit polyclonal antibody was used for detection of caveolin-1 and mouse polyclonal antibody was used for detection of caveolin-2. After washing with PBS/BSA, the cells were incubated with Alexa Fluor®-conjugated secondary antibodies diluted 1:400 PBS/BSA for 1 h at room temperature. Secondary antibodies used were: Alexa Fluor® 488-conjugated anti-mouse and Alexa Fluor® 647-conjugated anti-rabbit. Cells were mounted in ProLong Gold Antifade mounting medium containing DAPI. Whole cell image stacks were acquired by confocal microscopy and representative sections displayed from the bottom and middle of a typical cell. Separate channels displaying caveolin-1 (red) and caveolin-2 (green) and a merge of both channels including a DAPI staining are shown. Images were deconvolved using Huygen's Essential software. Scale bar = 5 μ m.

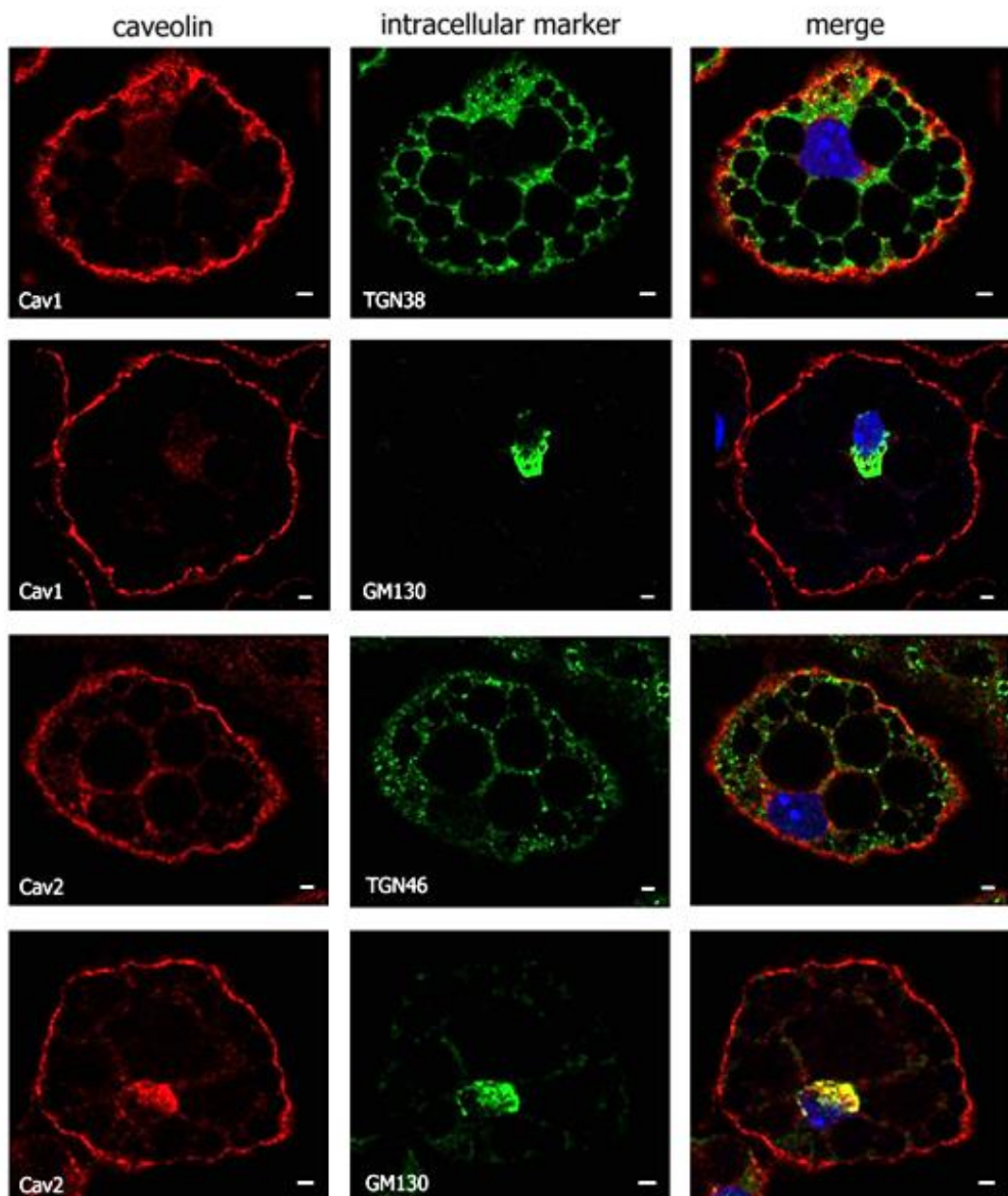


Figure 5.2. Analysis of the co-distribution of caveolin-1 and -2 with Golgi and TGN proteins. 3T3-L1 adipocytes were fixed in 4% formaldehyde 10 days post initiation of differentiation. Subsequently cells were permeabilised with PBS containing 0.3% (w/v) of bovine serum albumin (PBS/BSA) and 0.25% (v/v) Triton X-100 for 10 minutes at room temperature. Following washing with PBS/BSA, the cells were incubated with primary antibodies diluted 1:50 in PBS/BSA for 1 h at room temperature in a humidified chamber. Primary antibodies used were against caveolin-1, caveolin-2, GM130, TGN38 and TGN46. After washing with PBS/BSA, cells were incubated with Alexa Fluor®-conjugated secondary antibodies diluted 1:400 PBS/BSA for 1 h at room temperature. Cells were mounted in ProLong Gold Antifade medium containing DAPI. Whole cell image stacks were acquired by confocal microscopy and representative sections are shown. Separate channels displaying caveolin-1 or caveolin-2 (red) and GM130/TGN38/TGN46 (green) and a merge of both channels including a DAPI staining are shown. Images were deconvolved using Huygen's Essential software. Scale bar = 5 μ m

To investigate the distribution of caveolin-2 further, and specifically to determine the intracellular compartment stained by caveolin-2 antibody, co-labelling with cis-Golgi matrix protein 130 (GM130) and either TGN38 or TGN46 (*trans* Golgi network) antibodies was performed.

As can be seen in Figure 5.2, caveolin-1 displayed little co-localisation with either TGN38 or GM130 (consistent with the lack of an intracellular pool of this protein). In contrast, the intracellular fraction of caveolin-2 was found to overlap with GM130, suggesting a pool of this isoform is localised to the Golgi apparatus.

Collectively the localisation analysis of endogenously expressed caveolin proteins in 3T3-L1 by confocal microscopy has revealed co-localisation of both caveolin-1 and caveolin-2 in caveolar circular-rosette structures at the PM. Caveolin-2 was also readily detected in an intracellular compartment that co-localised with the Golgi marker GM130.

5.3 Palmitoylation of caveolin-2

In Chapter 3, caveolin-1 and caveolin-2 were identified as palmitoylated proteins using acyl-RAC. All three cysteine residues of caveolin-1 have previously been reported to be palmitoylated (Dietzen et al., 1995), whereas palmitoylation of caveolin-2 has not previously been described and hence the sites of modification in this protein are unknown.

Caveolin-2 has 4 cysteine residues at the amino acid positions 72, 109, 122 and 145. Figure 5.3 shows the predicted 2D membrane topology of caveolin-2, illustrating the relative positions of these cysteine residues within the protein. According to this model, all cysteine residues are localised within the cytosolic domains of caveolin-2, of which cysteine-72 resides within the oligomerization domain, whereas cysteine-109 has an intramembrane position. Cysteines-122 and -145 are located in the C-terminus of the protein downstream of the intramembrane domain.

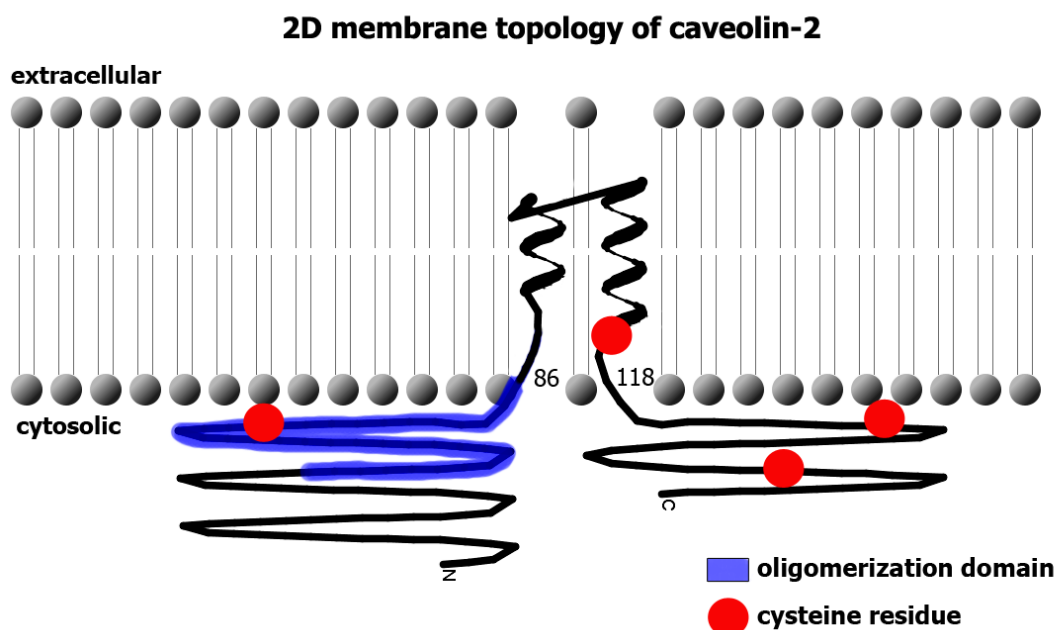


Figure 5.3. 2D membrane topology of caveolin-2. Protein domains are illustrated according to the prediction Lisanti and colleagues (Razani et al., 2002c). Image was created using TMRPres2D software. Oligomerisation domain and cysteine residues are highlighted (see legend). N-terminus and C-terminus are indicated with an N and C. The amino acids at the start and end of the predicted intramembrane domain at the positions 86 and 118 are highlighted.

According to the CSS-Palm prediction for caveolin-2 (shown in Table 5.1) all cysteine residues have the theoretical potential to be palmitoylated. The highest score was obtained for cysteine-109 (13.761) and the lowest for cysteine-145 (1.329).

Table 5.1. CSS-Palm prediction of palmitoylation sites for caveolin-2

Protein	Position	Amino acid sequence	Score	Domain
caveolin-2	72	SFDK V W I CSHALFEI	5.731	Oligomerisation domain
	109	ILFATLS C LHIWILM	13.761	Intramembrane
	122	LMPFVK T CLMVLPSV	12.003	Juxtamembrane
	145	DVVIGPL C TSVGRSF	1.329	Cytosolic

An alignment of all three caveolin isoforms is displayed in Figure 5.4, which highlights the starting methionine, oligomerisation- and intramembrane domain.

Furthermore, palmitoylated cysteine residues of caveolin-1 and caveolin-3 isoforms are highlighted in red. In addition it can be seen that cysteine residues of caveolin-2 which are highlighted in green are not conserved with the cysteine position of the other two caveolin isoforms.

1	MSGGKYVDSEGHLYTVP	IREQ	GNIYK	PNNK	MADEVTEKQ	caveolin-1
1		MGLETEKADVQL	FM	ADDAYSHH		caveolin-2
1			MMTEEHTDLE			caveolin-3
41	---VYDAHTKEIDLV-NRDPKHLNDDVVKIDFEDVIAEPE					caveolin-1
23	SGVDYADPEKYVDSSHDRDPHQLNSHL-KLGFEDLIAEPE					caveolin-2
11	ARI IKDIHCKEIDLV-NRDPKNINEDIVKVDFEDVIAEPE					caveolin-3
77	GTHSFDGIWKASFTTFTVTKYWFYRLLSITIFGIPMALIWG					caveolin-1
62	TTHSFDKVI ^C SHALFEISKYVMYKFLTVFLAIPLAFIAG					caveolin-2
51	GTYSFDGVKVSFTTFTVSKYWCYRLLSITLLGVPLALLWG					caveolin-3
117	IYFAILSFLHIWAVVP ^C IKSFLIEIQ ^C ISRVSIIYVHTFC ^C					caveolin-1
102	ILFATLS ^C LHIWILMPFVKT ^C LMVLPSVQTIWKSVDVVI					caveolin-2
91	FLFACISFCHIWAVVP ^C IKSYLIEIQ ^C ISHIYSLCIRTF ^C					caveolin-3
161	DPLFEAIGKIFSNIRISTQKEI					caveolin-1
142	GPL ^C TSVGRSFSSVSMQLSHD					caveolin-2
131	NPLFAALGQVCSNIKVVLRREG					caveolin-3

Figure 5.4. Alignment of amino acid sequence of the caveolin protein family. Starting methionines are highlighted in blue. Oligomerisation domain is shaded grey and predicted intramembrane domain highlighted in yellow (membrane prediction by Lisanti and colleagues). Palmitoylated cysteines of caveolin-1 and caveolin-3 are highlighted in red. The cysteine residues of caveolin-2 are highlighted in green. Amino acid position is indicated on the left side of the alignment panel.

In order to investigate the palmitoylation sites of caveolin-2 experimentally, incorporation of 17ODYA into both caveolin-2 wild type and cysteine to alanine mutants was examined using click-chemistry in HEK293T cells.

For this, HEK293T cells were transfected with caveolin-2-EGFP constructs, labelled with 17ODYA and incorporated acyl chains were detected using click-chemistry, as described in section 2.4.2. Results of this analysis are displayed in Figure 5.5. The top panel shows an immunoblot using a GFP antibody allowing visualisation of the expression levels of EGFP-tagged caveolin-2 wild type and 4CA mutant constructs. The EGFP-labelled protein bands appear as a doublet at an apparent molecular

weight of approximately 45 kDa. Expression levels of wild type and mutant caveolin-2-EGFP fusion proteins were similar, whereas no signal could be detected in the lanes loaded with non-transfected cell lysates.

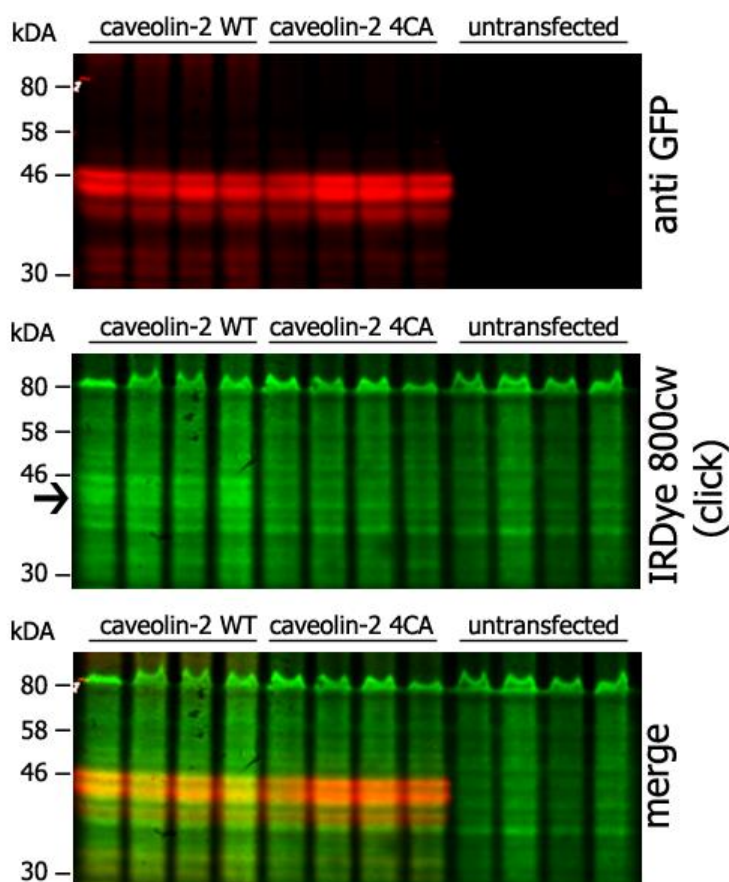


Figure 5.5. Detection of incorporation of 17ODYA into caveolin-2 constructs in HEK293T cells using click-chemistry. HEK293T cells were transfected with the indicated EGFP-tagged plasmid constructs of caveolin-2 cDNA for 24 h. Untransfected cells were used as a control. Cells were then serum starved in DMEM culture medium containing 1% fatty acid free (FAF) BSA for 30 min and metabolically labelled with 15 μ M 17ODYA and 1% FAF BSA in DMEM for 4 h. Incorporation of 17ODYA was detected by reaction with IRDye 800 CW azide (as described in Section 2.4.2). Proteins were transferred onto nitrocellulose membranes and probed with GFP antibody. Antibody binding and IRDye were visualised using the Odyssey[®] infrared imaging system. Each caveolin-2 construct and control was transfected and prepared in quadruplicate. The figure shows a representative result is of an experiment conducted 3 times. Position of molecular weight markers are shown on the left hand side of all panels.

The middle panel of Figure 5.5 shows the signal of the IRDye 800cw in green, which indicates the incorporation of 17ODYA into cellular proteins. Background signal from IRDye 800cw is visible in every lane at all molecular weights, with a prominent

band present at ~ 80 kDa; however, in cells transfected with caveolin-2 wild type, a weak click-signal could be also detected at the size of approximately 40-45 kDa (marked by *arrow*), which overlapped with the bands detected by GFP antibody (merge image, bottom panel Figure 5.5). This signal was not detectable in lysates from cells expressing the caveolin-2 4CA cysteine to alanine mutant, or in lanes loaded with lysates from non-transfected cells.

Although Figure 5.5 indicates that wild type caveolin-2 undergoes incorporation of 17ODYA and that this is reduced in the caveolin-2 4CA mutant, quantification of the click-signal was not possible because of the high background in this experiment. In order to reduce the background signal, click-chemistry was combined with immunoprecipitation of the caveolin-2 proteins using GFP antibody. For this, GFP-tagged caveolin-2 constructs in transfected HEK293T lysates that had been labelled with 17ODYA were captured using anti-GFP MicroBeads (2.4.2.4) and then subjected to the click-reaction. Subsequently, the MicroBeads were captured in a μ column due to the magnetic field, and the immunoprecipitated proteins were eluted using SDS-sample buffer pre-heated to 95 °C; eluates were subsequently analysed by SDS-PAGE and immunoblotting. This approach should theoretically minimize any background signal originating from 17-ODYA bound to other proteins in the cell lysate. The result of such an experiment is shown in Figure 5.6A. The top panel shows a doublet band corresponding to immunoprecipitated EGFP-tagged caveolin-2 constructs detected with an anti-GFP antibody. The intensities of the protein bands are comparable between lanes, although caveolin-2 4CA recovery was slightly higher than caveolin-2 wild type. A click-signal at the apparent molecular weight of approximately 46 kDa could be detected for caveolin-2 wild type (Figure 5.6A middle panel), whereas this signal was greatly reduced in the caveolin-2 4CA mutant (despite higher levels of recovery of this protein). When combining click-chemistry with immunoprecipitation, the detected specific click-signal was clearly distinguishable from the background signal, which enabled its quantification. Quantification was therefore carried out applying densitometry using Image Studio software from LICOR.

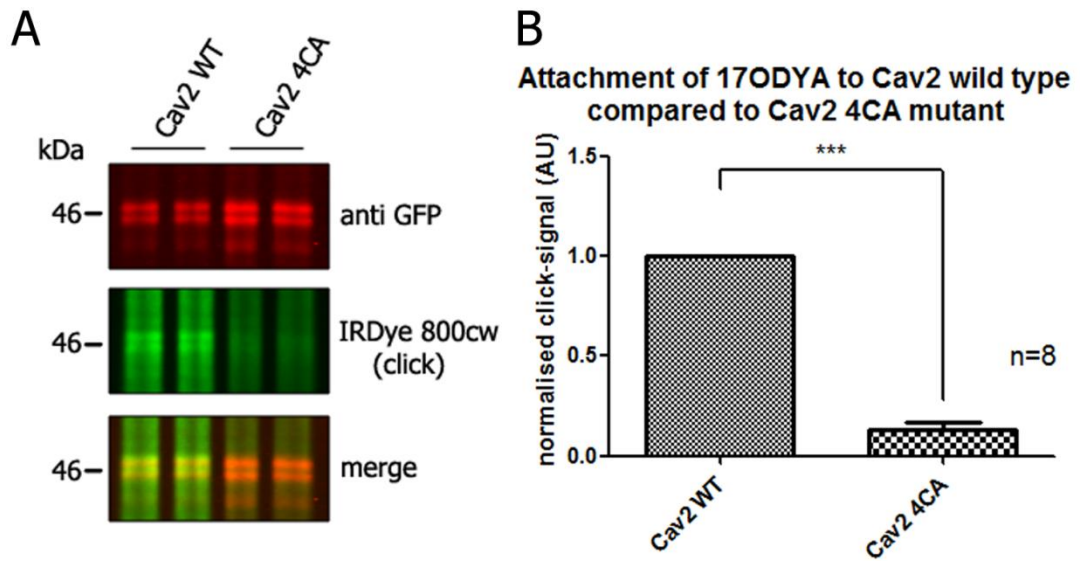


Figure 5.6. Incorporation of 17ODYA into caveolin-2 constructs in HEK293T cells detected by click-chemistry combined with immunoprecipitation. HEK293T cells were transfected with the indicated EGFP-tagged plasmid constructs of caveolin-2 cDNA for 24 h. Cells were then serum starved in DMEM culture medium containing 1% fatty acid free (FAF) BSA for 30 min and metabolically labelled with 50 μ M 17-ODYA and 1% FAF BSA in DMEM for 4 h. Subsequently, cells were lysed, and 5 μ l anti-GFP MicroBeads solution was added and incubated for 30 min on ice. Incorporation of 17ODYA was detected by reaction with IRDye 800 CW azide (as described in Section 2.4.2). GFP-tagged caveolin-2 constructs were isolated using appropriate μ MACS™ Epitope Tag Protein Isolation Kit and analysed by SDS-PAGE with 12% acrylamide followed by immunoblotting with GFP antibody. IRDye 800cw and anti-GFP signals were detected using the Odyssey® infrared imaging system. Samples were loaded in duplicate. **(A)** Representative immunoblot is shown of an experiment conducted 8 times. Position of molecular weight marker is shown on the left hand side of all panels. **(B)** Click-signal and anti-GFP signal quantified by densitometry using Image Studio Software. In order to normalise the click-signal to protein levels of caveolin-2 constructs, the determined value of the click-signal was divided by the value obtained from the immunoblot. n= 8; Statistical analysis using an unpaired Student's *t*-test indicated that there was a significant difference in the incorporation of 17ODYA into wild type and mutant caveolin-2 (***: $p < 0.001$). AU= arbitrary unit.

A bar graph displaying the values of 17ODYA attachment to caveolin-2 wild type and 4CA mutant from 8 separate experiments is shown in Figure 5.6B. The intensity of the click-signal was normalised to the corresponding caveolin-2 protein level. The calculated value for the incorporation of 17-ODYA into the 4CA mutant was ~ 8-fold lower than with the wild type caveolin-2 protein. This difference in 17ODYA incorporation between the wild type and 4CA caveolin proteins was statistically

significant. These results show that the cysteine residues are important for the attachment of 17ODYA to caveolin-2.

5.4 Identification of the palmitoylation sites in caveolin-2

The experiments described above provide further evidence that caveolin-2 is palmitoylated and highlight the importance of its cysteine residues for this modification. In this section, I set out to characterise the palmitoylation sites of caveolin-2 in further detail.

For this, each cysteine was mutated individually to alanine. HEK293T cells were then transfected with these cysteine to alanine mutants of caveolin-2, and subjected to click-chemistry and immunoprecipitation. The result of this experiment is shown in Figure 5.7. The expression level of caveolin-2 wild type was comparable to that of the single cysteine-to-alanine mutants. In contrast the expression level of the caveolin-2 constructs with all four cysteines mutated to alanine is higher when compared to the other caveolin-2 constructs (Figure 5.7A, top panel).

The click-signal shown in the middle panel highlights the incorporation of 17ODYA into the caveolin-2 constructs. By comparison of the relative click-signal intensities (click-signals normalized to GFP signals) among the different caveolin-2 constructs it became clear that the C109A, C122A and C145A mutants were equally palmitoylated. On the contrary, the C72A and the 4CA mutants displayed greatly reduced palmitoylation when compared to the wild type. Quantification of multiple experiments confirmed that mutation of C72A had the greatest effect on 17ODYA labelling of all the single point mutants (Figure 5.7B). In contrast, mutation of the other three cysteines was found to reduce palmitoylation, although this did not reach statistical significance.

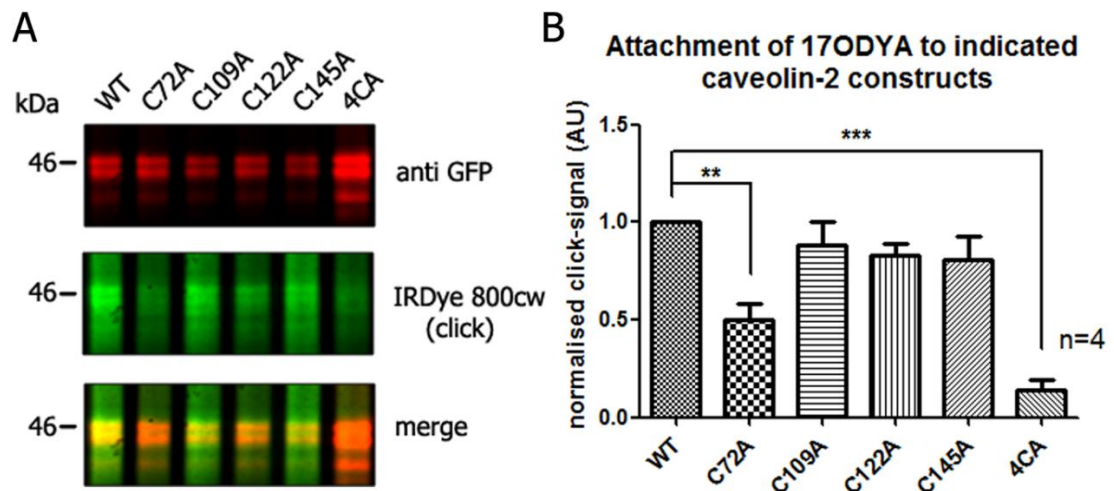


Figure 5.7. Incorporation of 17ODYA into cysteine to alanine mutants of caveolin-2 in HEK293T cells. HEK293T cells were transfected for 24 h with indicated plasmids encoding GFP-tagged caveolin-2 cysteine to alanine mutants. Cells were then serum and metabolically labelled with 50 μ M 17ODYA for 4 h. Subsequently, cells were lysed, and 5 μ l anti-GFP MicroBeads solution was added and incubated for 30 min on ice. Incorporation of 17ODYA was detected by reaction with IRDye 800 CW azide (as described in Section 2.4.2). The GFP-tagged caveolin-2 constructs were isolated using appropriate μ MACS™ Epitope Tag Protein Isolation Kit and analysed by SDS-PAGE with 12% acrylamide followed by immunoblotting with GFP antibody. IRDye 800cw and immunosignal were detected using the Odyssey® infrared imaging system. (A) Representative figure is shown of an experiment conducted four times. Position of molecular weight marker is shown on the left hand side of all panels. (B) Click-signal and signal from immunoblotting from the figure above were quantified by densitometry using Image Studio Software. In order to normalise the click-signal to protein amount of caveolin-2 constructs, the determined value of the click-signal was divided by the value obtained from the immunoblot. Values for caveolin-2 wild type were set to one and all other values are shown as a relative value to caveolin-2 wild type. n=4; One way ANOVA followed by Tukey's multiple comparison test were applied for statistical analysis ** P \leq 0.01; *** P \leq 0.001. AU = arbitrary unit.

5.5 Effect of palmitoylation on caveolin-2 localisation

In previous sections, palmitoylation of caveolin-2 was confirmed and its palmitoylation sites were identified. As palmitoylation frequently affects protein trafficking (Salaun et al., 2010), I investigated whether the palmitoylation of caveolin-2 has an effect on its localisation within the cell, and particularly on its targeting to caveolae and lipid rafts; the latter was assessed by Triton X-100 insolubility, as this has been frequently used as a measure of protein association with caveolae and lipid rafts (London and Brown, 2000; Levental et al., 2010).

It was demonstrated (see Figure 5.7) that mutation of all four cysteines in caveolin-2 resulted in a substantial reduction or complete loss of palmitoylation. Hence, this caveolin-2 4CA mutant represents a non palmitoylated version of caveolin-2 and can be used to examine the role of palmitoylation in regulating caveolin-2 localisation. Before studying the localisation of EGFP-tagged caveolin-2 constructs, the expression levels of endogenous caveolin-1 and -2 in HEK293T cells was compared with expression in 3T3-L1 adipocytes. This is an important consideration as caveolin proteins are known to form homo- and hetero-oligomers, raising the possibility that endogenously expressed caveolins could modulate the trafficking of EGFP-tagged caveolin proteins. Thus, cell lysates of untransfected HEK293T and 3T3-L1 adipocytes were analysed by SDS-PAGE followed by immunoblotting using antibodies against caveolin-1 or caveolin-2. The result of this experiment is displayed in Figure 5.8. Ponceau S staining is shown in the left panel of the figure indicating an approximately equal protein concentration of the cell lysates derived from both cell types. The middle and right panel of the figure show immunoblots probed with either caveolin-1 or caveolin-2 antibodies. Neither caveolin-1 nor caveolin-2 could be detected in lysates derived from HEK293T cells, whereas both proteins were clearly detectable in lysates of 3T3-L1 adipocytes. This result suggests that endogenously expressed caveolin proteins are either absent or expression levels are very low in HEK293T cells. The identified low endogenous expression level of caveolin proteins in HEK293T cells reveal good conditions to study the localisation of overexpressed caveolin-2 EGFP fusion proteins in this cell line.

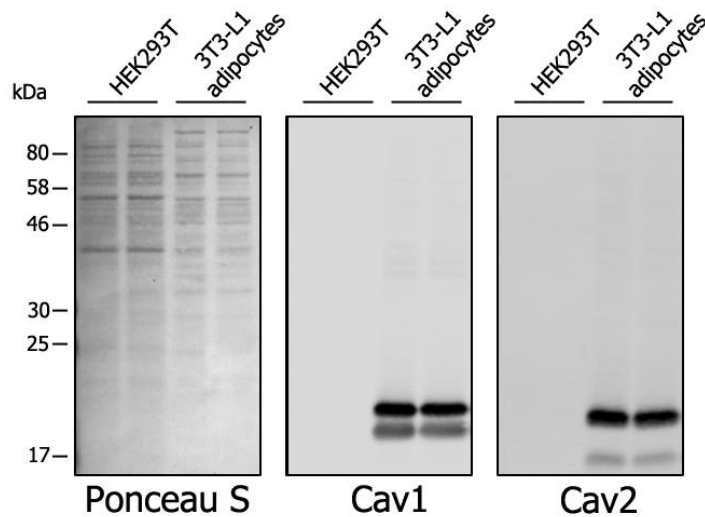


Figure 5.8. Analysis of endogenously expressed caveolin isoforms in HEK293T cells and 3T3-L1 adipocytes. HEK293T cells and mature 3T3-L1 adipocytes were lysed as described in section 2.4.5. Then the protein levels of the lysates were equalised and analysis by SDS-PAGE. Subsequently proteins were transferred to nitrocellulose and stained with Ponceau S, followed by probing the membranes with caveolin-1 and caveolin-2 antibodies. Samples were loaded in duplicate. Position of molecular weight markers are shown on the left hand side of all panels.

To examine how mutation of palmitoylation sites affects localisation of caveolin-2, HEK293T cells were co-transfected with either caveolin-2-EGFP wild type or 4CA mutant together with a caveolin-2-mCherry wild type construct. The localisation of the expressed EGFP-tagged fusion proteins was then analysed relative to caveolin-2-mCherry. Furthermore, co-transfection with caveolin-1-mCherry was carried out, in order to study the localisation of the caveolin-2 constructs relatively to caveolin-1. The top two panels of Figure 5.9 show confocal images from HEK293T cells which were co-transfected with caveolin-2-mCherry wild type and caveolin-2-EGFP constructs. Round intracellular structures with a varying diameter from approximately 0.3 μm to 1.5 μm could be observed. These structures have not previously been described in other studies examining caveolin-2 localisation, and might represent some sort of intracellular inclusions.

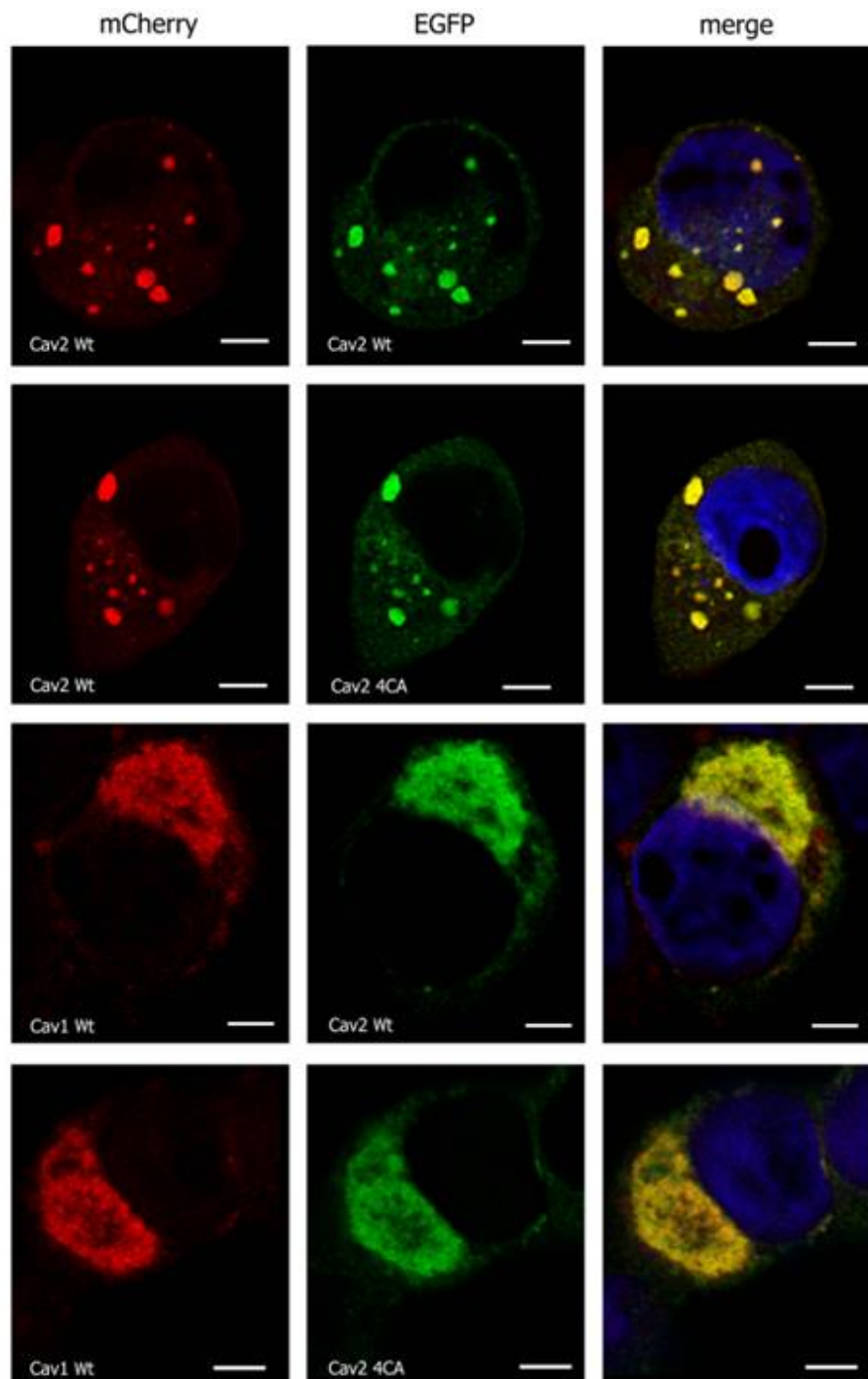


Figure 5.9. Analysis of the localisation of caveolin-2 EGFP fusion proteins in HEK293T cells co-transfected with mCherry caveolin constructs. HEK293T cells were co-transfected with wild type mCherry constructs of caveolin-1 or caveolin-2 together with EGFP constructs of caveolin-2 WT or caveolin-2 4CA as indicated. After 24 h, cells were fixed with 4% formaldehyde for 30 min at room temperature, washed with PBS, and mounted with ProLong Gold Antifade containing DAPI. The left panel shows fusion proteins with mCherry, the middle panel shows EGFP constructs and the right panel shows the merge of both channels including DAPI staining. Images were deconvolved using Huygen's Essential software. Scale bar = 5 μ m.

Neither caveolin-2 mCherry nor caveolin-2 EGFP constructs could be detected at the PM of HEK293T cells, in disagreement with what was previously observed for endogenously expressed caveolin-2 in 3T3-L1 adipocytes (Figure 5.1). Additionally, no difference in the localisation of wild type and 4CA caveolin-2 constructs relative to caveolin-2 mCherry was apparent.

Co-expression of the caveolin-2-EGFP constructs together with caveolin-1-mCherry is displayed in the bottom two panels of Figure 5.9. The pattern of localisation was different compared to co-expression with caveolin-2 mCherry. Most noticeable is the lack of the circular intracellular structures which can be seen in the top two panels. Instead, a strong aggregation in the perinuclear area could be observed. These structures resemble a swollen Golgi apparatus which again could be an effect of protein overexpression. No difference in localisation could be observed for the caveolin-2 4CA mutant when compared to the localisation of caveolin-2 wild type. Both caveolin-2 constructs co-localised with caveolin-1 mCherry intracellularly and specifically in the perinuclear area.

One possibility to explain the unexpected distribution of the caveolin constructs in HEK293T cells shown in Figure 5.9, is that cells with high protein expression levels were selected for analysis. This was necessary for imaging of mCherry constructs using 543 nm laser excitation, as this laser does not maximally excite mCherry fluorescence, and thus the protein is only weakly fluorescent under these conditions. To circumvent this issue, HEK293T cells were transfected with EGFP-tagged caveolin-2 WT or 4CA constructs without co-transfection of mCherry constructs. Furthermore, HeLa cells were transfected in the same way to include an additional type of cell in the analysis. In these experiments, only cells with relative low expression of caveolin constructs were selected for imaging (Figure 5.10).

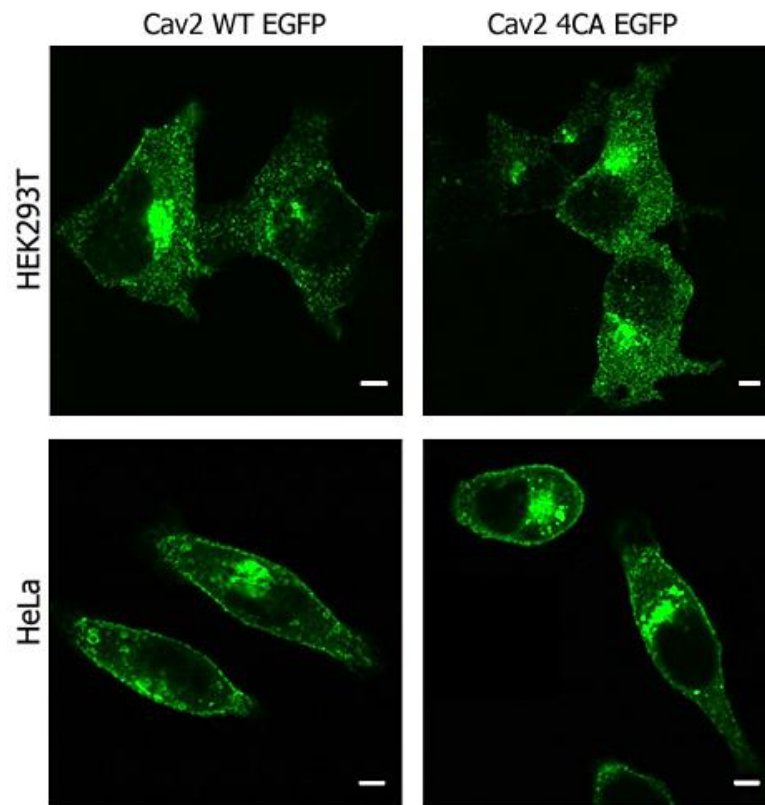


Figure 5.10. Analysis of localisation of caveolin-2-EGFP WT and 4CA mutant in HEK293T and HeLa cells using confocal microscopy. HEK293T and HeLa cells were transfected with EGFP-tagged caveolin-2 WT, or caveolin-2 4CA, as indicated. After 24 h, cells were fixed with 4% formaldehyde for 30 min at room temperature, washed with PBS and mounted with ProLong Gold Antifade with DAPI (not shown). The top panel shows HEK293T cells; bottom panel shows HeLa cells. Scale bar = 5 μ m.

In both cell types the localisation of EGFP-tagged caveolin-2 constructs was similar to that previously reported (Scherer et al., 1997; Mora et al., 1999), and the protein was present in a perinuclear compartment. Furthermore, there was also a punctate distribution throughout the cytoplasm, which was more pronounced in HEK293T cells. Caveolin-2 was also weakly present at the PM in HEK293T cells, and more clearly detectable in the PM of HeLa cells. Furthermore, small (approximately 0.5-2 μ m) round structures could be seen in the cytosol of HeLa cells, which probably originate from caveolin-2 residing at lipid droplets (Fujimoto et al., 2001). In agreement with results from co-expression studies (Figure 5.9.), no difference in caveolin-2 localisation between WT and 4CA mutant was identified, when these were singly transfected in low levels, in either HEK293T cells or HeLa cells. Overall,

these analyses suggest that palmitoylation does not regulate the gross localisation of caveolin-2.

5.5.3 Investigating partitioning of caveolin-1 and caveolin-2 cysteine to alanine mutants into Triton X-100-insoluble membrane microdomains.

As mentioned above, palmitoylation can affect the partitioning of proteins into membrane microdomains, such as caveolae and lipid rafts. Therefore, I have investigated whether palmitoylation plays a role in targeting caveolin-2 into membrane microdomains, by studying Triton X-100-insoluble membrane fractions. In parallel, the localisation of wild type and a cysteine to alanine mutant of caveolin-1 was examined for comparison.

Triton X-100-insoluble membrane fractions are thought to contain cholesterol- and sphingolipid-rich fractions derived from caveolae and lipid rafts (London and Brown, 2000). In order to investigate whether palmitoylation might affect caveola/microdomain association of caveolin-1 or caveolin-2, a Triton X-100-insoluble fraction was isolated from HEK293T cells, which had been transfected with the respective caveolin constructs (caveolin-1-EGFP and caveolin-2-EGFP). The isolated Triton X-100-insoluble fractions were subsequently analysed by SDS-PAGE and immunoblotting.

As shown in Figure 5.11 , wild type and 3CA caveolin-1-EGFP were both present in the Triton X-100-soluble (S) and insoluble (IS) fractions, albeit slightly enriched in the latter. The distribution of flotillin-2 in the recovered fractions (Figure 5.11A, middle panel) was included as control for the equal recovery of Triton X-100-insoluble fractions from different cell transfections (Bickel, 1997; Salzer, 2001).

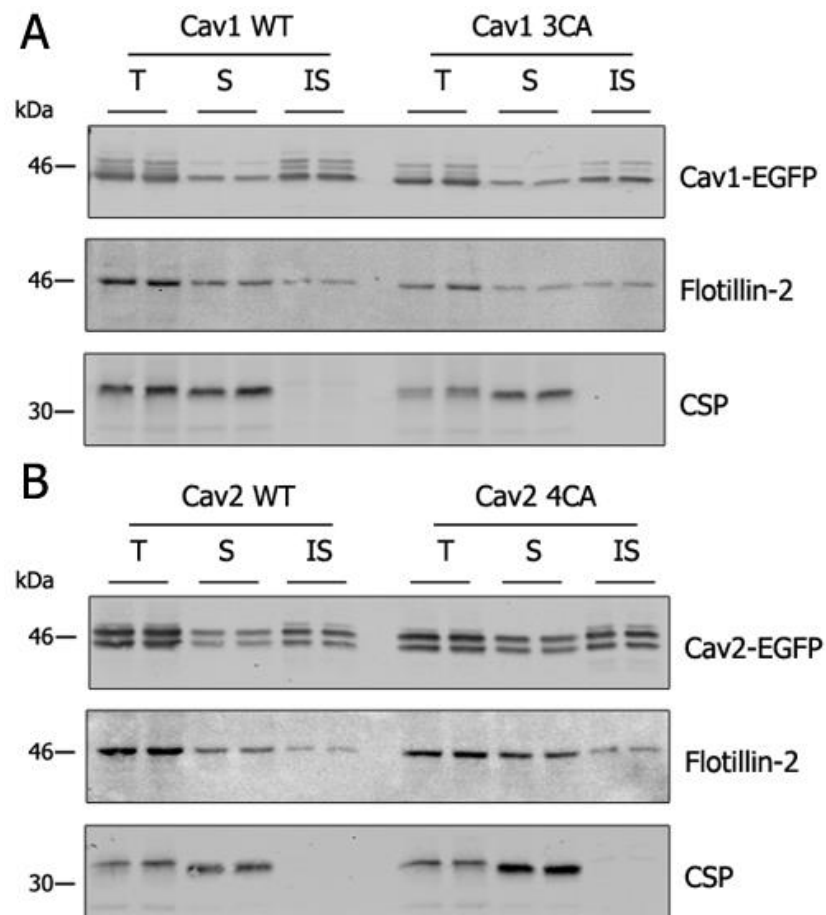


Figure 5.11 Isolation of Triton X-100-insoluble fraction from HEK293T cells transfected with caveolin wild type and cysteine to alanine mutants. Cells were collected 24 h post-transfection and pelleted by centrifugation. Cell pellets were resuspended in PBS containing 1% Triton X-100 and protease inhibitors, and lysed by passing through a 26G needle. After 30 min incubation on ice, the lysate was subjected to centrifugation at 16,400 x g for 20 min at 4°C. At the same time a fraction of the lysate was kept, designated as **T** = Total input. Following the centrifugation, the resulting supernatant was transferred into a fresh reaction tube with the appropriate amount of 4x Laemmli sample buffer (supplemented with 100 mM DTT), designated as **S** = soluble fraction. The pellet, which contains the insoluble fraction = **IS**, was resuspended in 1x Laemmli sample buffer (supplemented with 25 mM DTT). The volume of 1x sample buffer of **IS** fraction was adjusted to the volume of the **S** fraction. All samples were subjected to SDS-PAGE on 12% acrylamide gels, and analysed by immunoblotting with indicated antibodies. Samples were loaded in duplicate. Representative immunoblot of an experiment conducted four times is shown. Position of molecular weight marker is shown on the left hand side of all panels. Panel **A** shows caveolin-1 and panel **B** shows caveolin-2 constructs.

The bottom panel shows the distribution of cysteine-string protein (CSP) at an apparent molecular weight just above 30 kDa. CSP can only be detected in the total and Triton X-100-soluble fraction but not in the Triton X-100-insoluble fraction. CSP has been reported previously to be absent from Triton X-100-insoluble fractions

despite its extensive palmitoylation, and thus serves as a negative control in this experiment (Chamberlain and Gould, 2002).

Similar to caveolin-1 constructs, caveolin-2 wild type and cysteine 4CA mutant were also present in Triton X-100-soluble and -insoluble fractions (Figure 5.11B).

The immunoblots of caveolin-1 and caveolin-2 distribution in Triton X-100-soluble and -insoluble fractions from multiple experiments were quantified using densitometry. For this, the measured values for Triton X-100-insoluble fraction were divided by the values for the soluble fraction (Figure 5.12).

Protein ratio of Triton X-100-insoluble fraction to Triton X-100-soluble fraction

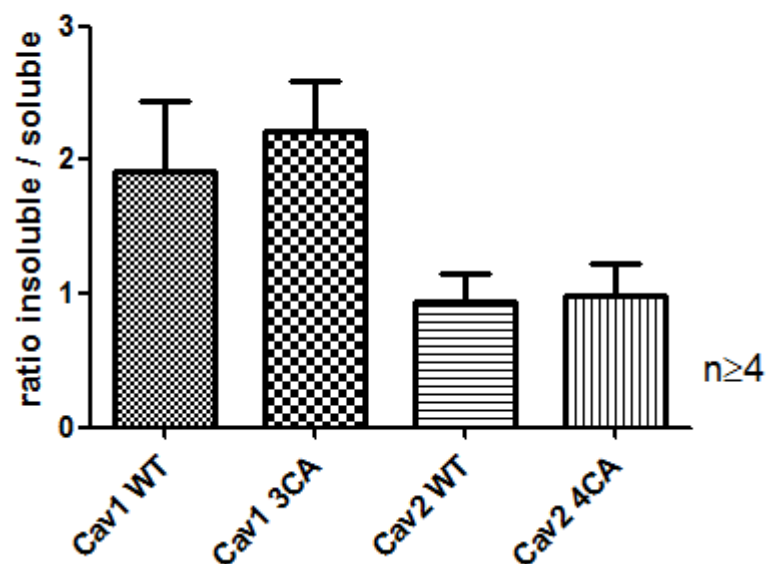


Figure 5.12. Quantification of caveolin-1 and caveolin-2 wild type and cysteine to alanine mutants in Triton X-100-soluble and -insoluble fractions in HEK293T cells. Immunoblots from Figure 5.11 were quantified by densitometry using Image Studio software from LICOR. Measured values for protein bands detected in the Triton X-100-insoluble fraction were divided by the values for Triton X-100-soluble fraction. For statistical analysis an N = 4 for caveolin-1 and an N=5 for caveolin-2 were used. One way ANOVA followed by Tukey's multiple comparison test revealed no significant difference between the wild type and cysteine mutants in association with Triton X-100-insoluble fractions.

The calculated ratios for caveolin-1 wild type and 3CA mutant are approximately 1.9 and 2.2, respectively. The calculated values suggest that the protein amount of both caveolin-1 constructs is approximately twice as high in the Triton X-100-insoluble

fraction than in the soluble fraction. The values calculated for caveolin-2 wild type and 4CA mutant are approximately 0.93 and 0.99 respectively suggesting an equal distribution of the caveolin-2 constructs in both Triton X-100 insoluble and soluble fractions. Although minor differences in the distribution of wild type and cysteine to alanine mutants of caveolin-1 and caveolin-2 could be detected, these differences were not statistically significant ($p=0.372$). Collectively these results demonstrate no effect of palmitoylation on targeting caveolin-1 or caveolin-2 into Triton X-100-insoluble fractions.

5.6 Effect of palmitoylation on oligomerisation of caveolin-2.

Previous studies have shown that caveolin-1 can form homo-oligomers, both *in vitro* and *in vivo* (Monier et al., 1995), which are thought to play a role in the formation of caveolae (Hayer et al., 2010). Furthermore, these oligomers were reported to be stabilised by acylation with long chain fatty acids (Monier et al., 1996). Caveolin-2 has structural similarities with caveolin-1 and has been reported to form oligomers when expressed endogenously or overexpressed in Fisher Rat Thyroid (FRT) cells (Mora et al., 1999). In this section, I set out to confirm and characterise the oligomerisation of caveolin-2 and investigate, whether the loss of palmitoylation at its cysteine residues affects the formation of caveolin-2 oligomers.

5.6.1 Formation of SDS-resistant oligomers of caveolin-2.

In order to investigate whether caveolin-2 forms SDS-resistant oligomers, HEK293T cells were transfected with caveolin-2-EGFP constructs and analysed by SDS-PAGE followed by western blotting. Triton X-100-soluble and -insoluble fractions were isolated to determine if the potentially formed oligomers were present in specific membrane microdomains. In accordance with the experiment shown in Figure 5.11 and Figure 5.12, there was no difference in the distribution of the caveolin-2 proteins between the isolated Triton X-100-soluble and -insoluble fractions (Figure 5.13A).

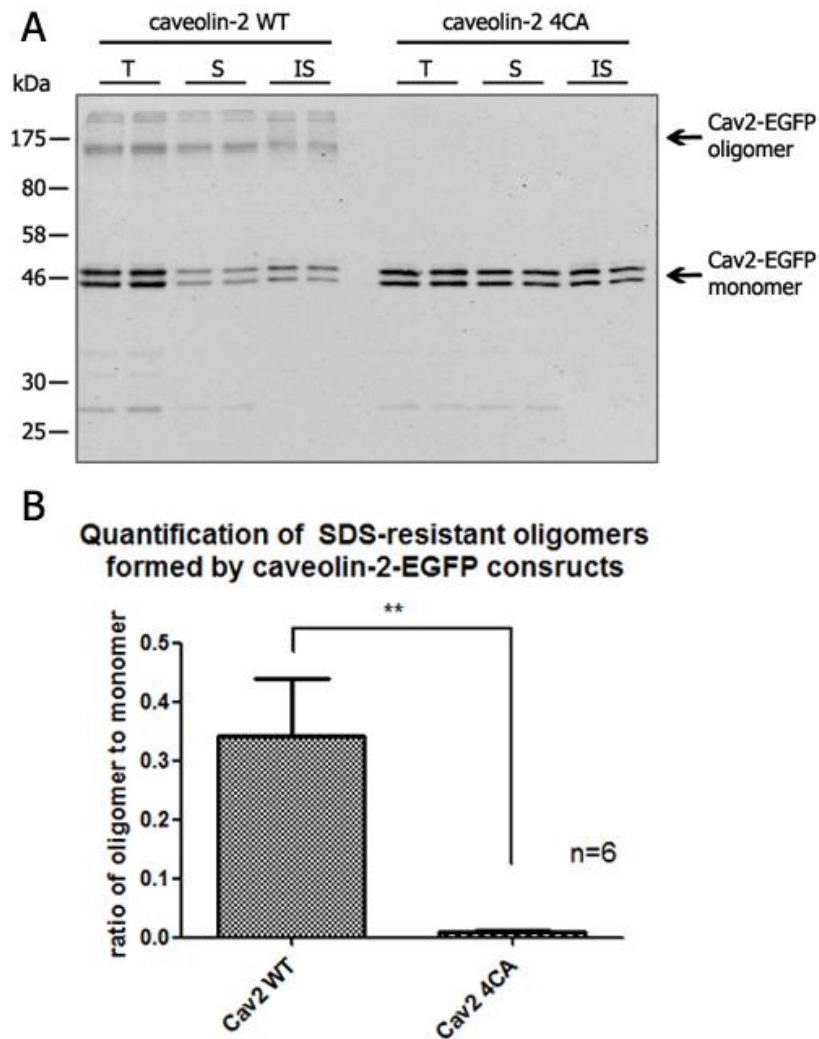


Figure 5.13. SDS-PAGE analysis of Triton X-100-soluble and -insoluble fractions isolated from HEK293T cells transfected with caveolin-2 constructs. Cells were collected 24 h post transfection with the indicated caveolin-2 constructs and pelleted by centrifugation. Cell pellets were resuspended in PBS containing 1% Triton X-100 and protease inhibitors, and lysed by passing through a 26G needle. After 30 min incubation on ice, lysates were subjected to centrifugation at 16400 x g for 20 min at 4°C. A fraction of the lysate before centrifugation was kept as **T** = Total input. Following the centrifugation, the resulting supernatant (soluble fraction = **S**) was transferred into a fresh reaction tube with the appropriate amount of 4x Laemmli sample buffer (supplemented with 100 mM DTT). The pellet was resuspended in 1x Laemmli sample buffer with 25 mM DTT and corresponds to the insoluble fraction = **IS**. The volume of 1x sample buffer of **IS** fraction was adjusted to the volume of the **S** fraction. All samples were subjected to SDS-PAGE with 12% acrylamide gels, and immunoblotting with anti GFP antibody. Samples were loaded in duplicate. **(A)** Representative blot is shown of an experiment carried out six times. Position of molecular weight marker is shown on the left hand side. **(B)** Protein band intensities of caveolin-2-EGFP monomers and the oligomer detected at an apparent molecular weight of 170 kDa, shown in the immunoblot in Figure panel A, were quantified by densitometry using Image Studio from LICOR. The value obtained from the oligomer was divided by the value measured for the caveolin-2 monomer. n=6; ** P ≤ 0.01 (unpaired Student's *t*-test).

However, in fractions prepared from cells transfected with caveolin-2-EGFP wild type, higher molecular weight SDS-resistant bands were clearly visible in both the insoluble and soluble fractions at approximately 170 kDa and 190 kDa. In contrast, no higher molecular weight bands were detected for the 4CA mutant in any isolated fraction.

The protein bands in the total input fraction T, at the apparent molecular weight of approximately 170 kDa, were quantified using densitometry. The calculated intensities of these bands displayed in Figure 5.13B are relative values normalised to the value of the caveolin-2-EGFP monomer. The calculated value for the oligomer is approximately 0.34 when caveolin-2 wild type construct was overexpressed. In contrast, overexpression of caveolin-2 4CA mutant resulted in nearly undetectable levels of the oligomer with a calculated value of 0.008. Collectively, these data suggests that palmitoylation of caveolin-2 is required either for the assembly of caveolin-2 into oligomers or for the stability of these oligomers once formed.

5.6.2 Examination of caveolin-2 oligomer formation using blue native PAGE.

Results in the previous section have demonstrated the formation of SDS-resistant oligomers, when HEK293T cells were transfected with a plasmid encoding caveolin-2 wild type fused with EGFP and were analysed by SDS-PAGE. These observations clearly suggest that there are differences in the oligomeric properties of caveolin-2 wild type and cysteine to alanine mutant. However, this analysis does not indicate if these differences relate to the formation or stability of the oligomers. As SDS disrupts most protein complexes, blue native PAGE was applied to investigate the formation of oligomeric assemblies of caveolin-2 in more detail. In contrast to SDS, the detergent digitonin, which was used to lyse the cells in blue native PAGE, allows proteins to remain in multi-protein complexes.

For examination of homo-oligomerisation of caveolin-2, HEK293T cells were transfected with plasmids encoding caveolin-2-EGFP wild type or the 4CA mutant and subjected to blue native PAGE. Previous studies have also reported hetero-

oligomerisation of caveolin-2 with caveolin-1 (Scherer et al., 1997). Therefore, HEK293T were also co-transfected with caveolin-2-EGFP constructs and a wild type caveolin-1-mCherry fusion protein, to investigate whether caveolin-1 affects the oligomerization of caveolin-2 4CA mutant. Results of this experiment are displayed in Figure 5.14. The left panel of Figure 5.14A displays an immunoblot probed with antibodies against EGFP. In the lane transfected with caveolin-2 wild type, oligomeric assemblies of various sizes could be detected. A protein smear stretching from the apparent molecular weight of over 1236 kDa to 720 kDa is clearly visible including a more distinguished protein band just above 720 kDa. Below the apparent molecular weight of 720 kDa the protein smear continues to be weaker with more distinguishable protein bands at the apparent molecular weight of approximately 480 kDa, 350 kDa and 160 kDa. One additional protein band is visible at the apparent molecular weight of approximately 66 kDa. As the caveolin-2 (predicted molecular mass = 18.2 kDa) is conjugated with EGFP (predicted molecular mass = 26.9 kDa), it is likely that this lower protein band detected at approximately 66 kDa corresponds to a monomeric form of caveolin-2-EGFP. Furthermore, the protein band detected at the apparent molecular weight of approximately 160 kDa is likely to correspond to a homo-dimeric form (or possible trimeric form) of caveolin-2-EGFP; dimers of caveolin-2 have previously been described (Mora et al., 1999; Scherer et al., 1997). The lane loaded with caveolin-4CA mutant shows the same protein smear at high molecular weights as described for caveolin-2 wild type. However, in contrast to the caveolin-2 wild type protein, the protein smear below the apparent molecular weight of 720 kDa is detectable to a substantially lesser degree. At the same time, a noticeable increase in the monomeric form of caveolin-2 4CA when compared to caveolin-2 wild type was apparent, with simultaneous decrease of lower oligomeric bands (160, 350 and 480 kDa). Co-transfection of caveolin-2-EGFP constructs with caveolin-1-mCherry resulted in a loss of the lower oligomeric forms of both wild type and 4CA mutant caveolin-2, as well as monomeric forms (Figure 5.14A). This suggests that the

presence of caveolin-1 facilitates the formation of high molecular weight oligomers of caveolin-2, and that this process is not affected by caveolin-2 palmitoylation.

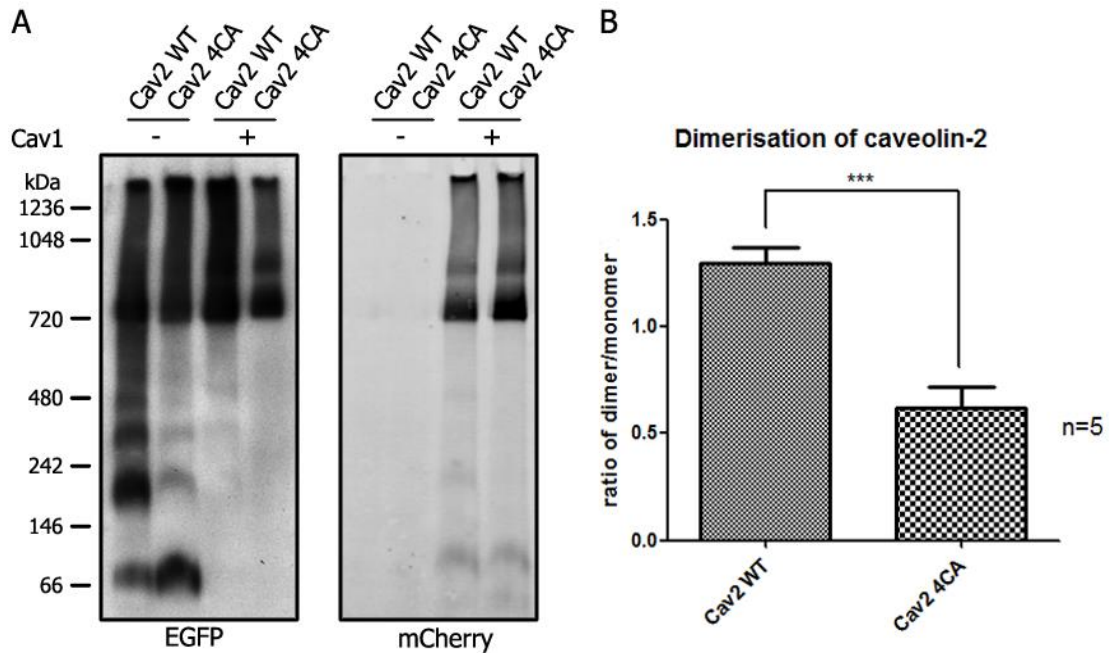


Figure 5.14. Analysis of oligomeric assemblies of caveolin-2 EGFP in HEK293T cells by blue native PAGE. HEK293T cells were transfected with indicated caveolin-2-EGFP and caveolin-1-mCherry constructs for 24 h, lysed by addition of lysis buffer containing 1% (w/v) digitonin, NuPAGE® LDS Sample Buffer (4X) and protease inhibitors, and passage through 26G needle; consequently, lysates were processed as described in methods (section 2.4.4). Samples were resolved on NativePAGE Novex 4-16% Bis-Tris gels, transferred onto PVDF membranes and probed with antibodies against EGFP or mCherry. Signal from EGFP antibodies was visualised with ECL and signal from mCherry was visualised with LI-COR infrared imaging system. **(A)** Representative immunoblots from an experiment conducted 5 times. Position of molecular weight marker is shown on the left hand side. **(B)** Immunoblots resulting from the blue native gels analysis shown in Figure 5.13A were quantified by densitometry. Bands at the apparent molecular weight of approx. 66 kDa and 160 kDa were quantified. A ratio of the value obtained from the dimer to the value obtained from the quantification of the monomer can be seen. P value = 0.0003 calculated by unpaired Student's *t*-test.

The right panel of the Figure 5.14A shows the immunoblot probed with the antibody against mCherry. The majority of caveolin-1-mCherry was detectable as a band at the apparent molecular weight of approximately 720 kDa, and protein smears at higher molecular weights resembled the high molecular weight protein smears described above for caveolin-2. Additionally, weak protein bands

corresponding to monomeric caveolin-1-mCherry were detected at the apparent molecular weight of approximately 66 kDa.

It was consistently noted that the ratio of dimeric and monomeric form of caveolin-2-EGFP wild type and cysteine to alanine constructs were different, and hence these were quantified by densitometry. A ratio of dimer to monomer was calculated and this is displayed in the graph shown in Figure 5.14B. When cells were transfected with caveolin-2-EGFP wild type, a ratio of dimer to monomer of approximately 1.3 was calculated. The calculated value decreased to approximately 0.6 for the caveolin-2 4CA mutant. Hence, there is a two-fold decrease in the ratio of dimer to monomer when caveolin-2 is not able to undergo palmitoylation.

5.7 Discussion

The results in this chapter mainly focus on the characterisation of the palmitoylation of caveolin-2, and how this modification affects protein localisation, detergent-resistance and oligomerisation. Before studying these specific parameters, the distribution of endogenous caveolin-2 was examined in 3T3-L1 adipocytes and compared with caveolin-1. Caveolin-1 and caveolin-2 were found to co-localise at the PM of adipocytes and were present in clustered caveolae with the appearance of circular rosettes. Although the localisation of the two caveolin isoforms was highly similar in adipocytes, caveolin-2 was more enriched than caveolin-1 in an intracellular perinuclear compartment that co-localised with the Golgi marker, GM130. To follow-up the observation made in section 3.3 that caveolin-2 is highly palmitoylated when studied using acyl-RAC, I initially determined, using *in silico* analysis with the CSS-PALM software, which of the four cysteines present in caveolin-2 had potential to be palmitoylated. Although this analysis returned different scores for the four cysteines, it revealed that all four cysteines in caveolin-2 have the potential to be palmitoylated. Thus, palmitoylation was studied experimentally using click-chemistry with 17ODYA. Replacing all four cysteines in caveolin-2 with alanine residues resulted in a loss of palmitoylation. This observation confirms that the modification of caveolin-2 by palmitic acid is via

the conventional attachment of acyl chains onto cysteine residues. Furthermore, cysteine-72 to alanine substitution revealed that this cysteine has the strongest effect on palmitoylation. According to confocal analysis in HEK293T cells, palmitoylation does not alter the gross localisation of caveolin-2 within the cell. Furthermore, biochemical analysis showed that palmitoylation of caveolin-2 is not required for association with Triton X-100-insoluble membrane fractions. Despite the lack of noticeable effects of palmitoylation on the localisation or detergent-resistance of caveolin-2, this modification had clear effects on the oligomerisation properties of this protein, as revealed by analysis using both SDS-PAGE and blue native gel electrophoresis.

Caveolin-1 is an extensively researched protein and a major component of cholesterol-rich membrane microdomains called caveolae (Rothberg et al., 1992). In contrast, caveolin-2, which was identified later than caveolin-1 (Scherer et al., 1996), has been poorly studied compared to caveolin-1. Like caveolin-1, caveolin-2 has also been reported to reside in caveolae (Scherer et al., 1996). Caveolae can form circular grape-shaped rosettes (Parton et al., 1994), which were readily detected by immunostaining of caveolin-1 and caveolin-2 in 3T3-L1 adipocytes (Figure 5.1). A substantial co-localisation of caveolin-1 and caveolin-2 could be seen within caveolar rosette structures, although there were also some differences in staining of the proteins within individual rosettes. Although caveolin-2 has been detected within these circular shapes in membranes sheets of 3T3-L1 adipocytes before (Shigematsu et al., 2001), a direct comparison of caveolin-1 and caveolin-2 has not been undertaken before. Sections taken from the middle of 3T3-L1 adipocytes co-stained with caveolin-1 and caveolin-2 (Figure 5.1) show co-localisation of both caveolin proteins at the PM. This conforms with previously conducted research showing co-localisation of caveolin-1 and caveolin-2, which was shown by immunofluorescence in 3T3-L1 pre-adipocytes (Scherer et al., 1996). Interestingly, caveolin-2 was detected in the perinuclear area co-localising with GM130 to a markedly greater extent when compared to caveolin-1. Additionally caveolin-2 was more readily detected intracellularly throughout the cytoplasm in

adipocytes. These findings indicate a partly differential distribution of caveolin-1 and caveolin-2 at steady state in 3T3-L1 adipocytes. A similar observation was previously made in caveolin-1 and caveolin-2 overexpressing MDCK cells, where caveolin-2 was localised juxtannuclear and caveolin-1 at the PM (Mora et al., 1999). To elucidate the localisation of caveolin-2 in more detail, co-immunostaining with caveolin-2 and Golgi apparatus proteins were performed. Caveolin-2 was found to co-localise with GM130, but not with TGN46 in 3T3-L1 adipocytes, in contrast with previously conducted work in FRT cells, where caveolin-2 partially co-localised with TGN38 (which localises to the TGN, along with TGN46) (Mora et al., 1999).

In Chapter 3 I demonstrated that approximately 80% of caveolin-2 is palmitoylated (see Figure 3.4 and Figure 3.5). Palmitoylation of caveolin-2 was confirmed in this chapter by applying click-chemistry in HEK293T cells overexpressing EGFP-tagged caveolin-2 wild type and cysteine to alanine mutants (Figure 5.5.). It is interesting to note that in all experiments using caveolin-2-EGFP, the protein migrated as a doublet band on immunoblots of SDS gels. At present it is not clear what causes the expression of these two distinct bands. However, similar doublet bands were reported for caveolin-2 when overexpressed in FRT cells (Mora et al., 1999). Endogenous caveolin-2 exists as an α and a (less expressed) β isoform, as demonstrated by work in MDCK cells (Scheiffele et al., 1998). It is speculated that the different isoforms of caveolin-2 are a product from one single gene (Scheiffele et al., 1998) as reported for caveolin-1 (Scherer et al., 1995). Indeed caveolin-2 has a second methionine residue 13 amino acids downstream from its N-terminus, and hence it is possible that there is use of alternative translation initiation sites in the caveolin-2-EGFP construct when expressed in HEK293T cells. Another possibility is that proteolytic cleavage of the overexpressed caveolin-2-EGFP constructs occurs in HEK293T cells. However, both bands of caveolin-2 behave identical in regard to their palmitoylation.

Previous work from our group and other groups have studied palmitoylation of EGFP-SNAP25 or other proteins in HEK293T cells using 3H palmitic acid (e.g. Greaves et al. 2010; Tian et al. 2010). In this study, I implemented the use of click-chemistry

using 17ODYA (Martin and Cravatt, 2009). The application of click-chemistry however resulted in a high amount of background click-signal (Figure 5.5). To resolve this issue, immunoprecipitation with GFP binding beads was incorporated into the protocol, which successfully reduced the background signal and rendered the results quantifiable (Figure 5.6).

As illustrated in Figure 5.3, caveolin-2 has 4 cysteine residues which are predicted to reside in the cytosol. It is noticeable that all four cysteine residues of caveolin-2 differ from the cysteine positions in caveolin-1 (Figure 5.4). *In silico* examination of caveolin-2 using CSS-Palm software revealed that all four cysteines have the potential to be palmitoylated (see Table 5.1). Direct analysis of palmitoylation by click-chemistry revealed that the substitution of cysteine-72 to alanine resulted with 50% reduction of palmitoylation when compared to caveolin-2 wild type. This decrease in palmitoylation could be explained with the assumption that cysteine-72 is the major site of palmitoylation in caveolin-2. Another possible explanation is that the palmitoylation of cysteine-72 is required to facilitate the palmitoylation of the three remaining cysteines. However, the latter is less likely, as cysteine-72 is located 37 amino acids upstream from the next cysteine (cysteine-109) and resides on the opposite side of the intramembrane domain as illustrated in Figure 5.3. Mutation of the remaining cysteine residues also caused a decrease in palmitoylation, but these changes were not statistically significant. These experimental findings differ from the predicted values by CSS palm, where values for the palmitoylation of cysteine-109 and cysteine-122 were higher than for cysteine-72; this emphasises the importance of performing experimental analysis of palmitoylation, rather than relying on the findings of *in silico* analyses. From the conducted experiments it could not be concluded whether all four cysteines of caveolin-2 undergo palmitoylation. Further experiments need to be undertaken to identify the exact number and position of palmitoylation sites. One approach to look at this could include “PEGylation”, where polyethylene glycol is attached to free SH-groups (either before or after chemical removal of acyl chains), and results in a band-shift of the protein on SDS gels dependent on the number of attached PEG groups.

Another possible experiment could be to create mutants with only one of four cysteine residues present at a time and subsequently analyse of palmitoylation by metabolic labelling and click-chemistry.

In order to investigate the effect of palmitoylation on caveolin-2, localisation studies in HEKT293 cells overexpressing caveolin-2 EGFP wild type or 4CA mutant were undertaken. Co-expression of mCherry-tagged caveolin-2 wild type was included to readily highlight any differences in localisation of the mutant caveolin-2 protein relative to the wild type protein. These analyses did not highlight any major differences between the wild type and the cysteine to alanine mutant but were confounded by the requirement to select cells with high expression levels to reliably record mCherry fluorescence. Thus, imaging of mCherry- and EGFP-tagged caveolin-2 constructs in the same cell showed round intracellular inclusions, which did not correspond to any of the major cellular compartments such as Golgi apparatus or ER, and which had not previously been described in the caveolin literature. These structures were not present when caveolin-2 was co-expressed with caveolin-1, but in this case the overexpressed proteins were detected adjacent to the nucleus in a structure which resembled a swollen Golgi apparatus. It is likely that the observed intracellular inclusions result from high level expression of caveolin-2, rather than from natural trafficking events within the cell. Furthermore, the different localisation of caveolin-2, when co-expressed with caveolin-1, should be attributed to the presence of caveolin-1. An effect of caveolin-1 on the localisation of caveolin-2 was reported in previous studies, where caveolin-2 was demonstrated to reside in the Golgi complex and partly redistribute to the PM upon co-expression with caveolin-1 in FRT cells (Mora et al., 1999). Although neither caveolin-1 nor caveolin-2 was detectable at the PM in co-expression experiments described in this chapter, a significant difference in localisation of caveolin-2 could be noted in the presence of caveolin-1. Collectively, the localisation of both caveolin proteins differed from previously reported overexpression studies (Mora et al., 1999; Verma et al., 2010), in which no intracellular inclusions of caveolin-2 were observed and where co-expression of caveolin-1 with caveolin-2 resulted in a partial redistribution of both

proteins at the PM. In order to obtain a more representative localisation study of caveolin-2 wild type and 4CA mutant, HEK293T and HeLa cells were singly transfected with the respective EGFP-tagged constructs, and only cells expressing low protein levels were imaged. This experiment revealed no major difference in caveolin-2 localisation between wild type and 4CA mutant in both cell types; additionally no intracellular inclusions could be observed in these experiments either (Figure 5.10.). Therefore, it can be concluded that palmitoylation of caveolin-2 has no evident effect on its localisation. Furthermore, the localisation of caveolin-2 found in this experiment conformed to the caveolin literature. Nevertheless, it would be worthwhile to investigate further if there are more subtle changes in the distribution of wild type and 4CA caveolin-2. This could be achieved by using a laser with more optimal excitation of mCherry (e.g. 594 nm laser line), allowing cells with lower expression levels to be visualised and hence allowing direct comparison of subcellular localisation between wild type and mutant caveolin-2, within the same cell. Cell fractionation experiments may also be useful to detect any shift in the overall distribution of the proteins between different cellular compartments.

Palmitoylation of some transmembrane and intramembrane proteins was demonstrated to affect their distribution into detergent-resistant domains (Levental et al., 2010). Nevertheless, palmitoylation of caveolin-1 has been reported to be dispensable for its association with Triton X-100-insoluble membrane micro-domains (Dietzen et al., 1995). This finding was confirmed in this thesis, as caveolin-1 wild type and 3CA mutant were detected to the same extent in Triton X-100 insoluble fractions (Figure 5.11). Similarly to caveolin-1, palmitoylation of caveolin-2 did not affect its association with detergent-resistant membrane micro-domains either (Figure 5.11 and Figure 5.12). The observation that, caveolin-1 has a roughly two-fold higher than caveolin-2 level of association with Triton X-100-insoluble membrane domains, supports this conclusion, as caveolin-2 has been shown to be palmitoylated to a higher extent than caveolin-1, at least in 3T3-L1 adipocytes (Figure 3.5, Figure 3.8). If palmitoylation were essential for the distribution into detergent-resistant domains of the caveolin proteins, then caveolin-2 would be

expected to be the more prominent isoform in Triton X-100 insoluble fractions. It should be noted that there is some controversy over the extent to which protein association with detergent-resistant membranes reports on the association with membrane microdomains such as caveolae (Munro, 2003). Thus, it would be useful to examine the association of wild type and mutant caveolin-2 proteins with caveolae directly using immunogold labelling and electron microscopy.

Oligomerisation of caveolin proteins is thought to play a role in the biogenesis of caveolae (Hayer et al., 2010) and caveolin-1 and caveolin-2 were found in oligomeric assemblies in various cell types when overexpressed or expressed endogenously (Monier et al., 1995; Scherer et al., 1997; Mora et al., 1999; Schlegel and Lisanti, 2000). Furthermore, the oligomeric form of caveolin-1 was found to be stabilised by the attachment of long chain fatty acids such as palmitate (Monier et al., 1996). In this thesis, I have demonstrated that SDS-resistant oligomers were formed when HEK293T cells were transfected with caveolin-2-EGFP wild type but not with caveolin-2-EGFP 4CA mutant (Figure 5.13). These oligomers are found in equal amounts in Triton X-100-soluble and -insoluble fractions, and thus might not be directly related to the formation of caveolae. In order to investigate the nature of the oligomeric assemblies of caveolin-2 in more detail, blue native gel electrophoresis with cell lysates from HEK293T cells overexpressing caveolin-2-EGFP constructs was performed. As can be seen in Figure 5.14A, palmitoylation appears to play a role in the assembly of caveolin-2 into oligomers. The migration pattern of caveolin-2 wild type was distinct from caveolin-2 4CA, with the wild type protein forming more oligomers in the range of the apparent molecular weight between 66 and 720 kDa. Since the endogenous expression levels of caveolin proteins are very low in HEK293T cells (Figure 5.8), I theorise that these oligomers are homo-oligomers of caveolin-2 EGFP, rather than hetero-oligomers with endogenous caveolin-1. Additionally quantification of the monomeric and dimeric forms of caveolin-2 EGFP constructs revealed that caveolin-2 wild type was found in the form of dimers twice as much than the 4CA mutant. This is particularly interesting, because the cysteine-72, which was shown to have the biggest impact on

palmitoylation (Figure 5.7), is predicted to reside in the domain of caveolin-2 which is essential for its oligomerisation. It is possible that palmitoylation of caveolin-2 has a subtle effect on the oligomerisation dynamics, as only oligomerisation in lower molecular range is altered upon inhibition of palmitoylation (4CA mutation), but the higher weight oligomers (>720 kDa) are unaffected. It could be hypothesised that lack of palmitoylation slows down the initial steps of oligomerisation. Interestingly, a previous study linked the substantial reduction of caveolin-2 200-500 kDa homo-oligomers with an approximately 9-fold reduction of caveolae formation in MDCK cells (Lahtinen et al., 2003). In that study, expression of a mutant of caveolin-3 (with a truncation of the amino acids 54-151 (cav-DGV)) disturbed the homo-oligomerisation pattern of caveolin-2, similarly to the way caveolin-2 4CA mutant did in this thesis. Additionally, a similar effect on monomer and dimer formation could be observed, as expression of cav-DGV also resulted in the reduction of the dimer to monomer ratio.

The palmitoylation of caveolin-2 did not appear to affect oligomerisation in cells co-expressing caveolin-1. In the presence of caveolin-1, the oligomerisation of caveolin-2 was altered when compared to samples where caveolin-1 was absent. Introduction of caveolin-1 resulted in a substantial reduction of oligomers smaller than 720 kDa and the ablation of the monomeric and dimeric form of caveolin-2. Bands in the right panel of Figure 5.14A showing oligomeric assemblies of mCherry-tagged caveolin-1 strongly resemble the high molecular weight oligomers seen for caveolin-2 suggesting that these oligomeric assemblies are caveolin-1/2 hetero-oligomers. Indeed, hetero-oligomerisation of caveolin-1 and caveolin-2 has been previously reported in NIH3T3 cells too, where down-regulation of caveolin-1 resulted in smaller homo-oligomers of caveolin-2, which were undetectable in the presence of caveolin-1 (Scherer et al., 1997). The stoichiometry of those hetero-oligomers is estimated to be at least 2:1 in favour of caveolin-1 (Scheiffele et al., 1998). It is possible that in presence of caveolin-1, larger caveolin-1/2 hetero-oligomers are formed more efficiently than smaller caveolin-2 homo-oligomers (below the apparent molecular weight of 720 kDa). Another possible explanation is

that caveolin-2 monomers, dimers and oligomers below 720 kDa form first and then these assemble together with caveolin-1 oligomers into larger hetero-oligomers. Involvement of caveolin-2 in the formation of caveolae is controversial. In contrast to caveolin-1, overexpression of caveolin-2 was not sufficient to induce *de novo* formation of caveolae (Fra et al., 1995). Additionally, caveolin-2 knockout mice show normal formation of caveolae in the examined tissues (Razani et al., 2002b). However, there is some evidence suggesting that caveolin-2 is involved in the formation of caveolae. In epithelial and MDCK cells where caveolin-1 is targeted to both apical- and basolateral membranes, caveolae are only detectable at the basolateral surface, where caveolin-1 and caveolin-2 co-reside (Scheiffele et al., 1998). Furthermore, overexpression of caveolin-2 in MDCK cells resulted in an increased number of caveolae (Lahtinen et al., 2003). Research also suggests that caveolin-2 is involved in determining caveolar shape. The formation of deep caveolae was only detectable in the presence of caveolin-2 (Fujimoto et al., 2000). However, it is unclear whether the altered oligomerisation pattern of caveolin-2 upon the loss of palmitoylation is affecting caveolae formation in any way. Further studies would be needed to address this question. For example, overexpression of caveolin-2 4CA mutant and subsequent analysis of caveolae formation by electron microscopy could be conducted. It will also be interesting to examine the oligomerisation pattern of transfected untagged forms on caveolin-2 wild type and 4CA mutant in follow-up studies. This analysis would allow a greater understanding of the exact oligomeric forms of caveolin-2 that are present and would also rule out any effects of the EGFP tag on the formation of caveolae.

Chapter 6: Characterisation of zDHHC enzyme expression profile in the 3T3-L1 cell line and the interaction of zDHHCs with IRAP.

6.1 Introduction

Palmitoylation is mediated by protein acyltransferases (PATs), a protein family consisting of over 20 members in mammals and 7 in yeast (Fukata et al., 2004; Ohno et al., 2006). The defining characteristic of these proteins is a conserved tetrapeptide consisting of the amino acid sequence aspartic acid, histidine, histidine, cysteine (DHHC) within a 51-amino acid cysteine-rich, zinc finger domain (Mitchell et al., 2006; Fukata et al., 2004). Because of this characteristic feature, these PATs are referred to as “zDHHC” proteins. Palmitoylation mediated by zDHHC enzymes is thought to be a two-step process which is initiated by the auto-palmitoylation of the zDHHC enzyme, followed by the transfer of the attached palmitate onto a cysteine residue of its substrate (Mitchell et al., 2010). The cysteine within the DHHC motif was demonstrated to be essential for the PAT activity of zDHHC enzymes, as deletion of this cysteine residue resulted in a lack of both auto-palmitoylation and the palmitoylation of substrates (Roth et al., 2002). The tissue distribution, cell-specific expression and subcellular localisation of mammalian zDHHC enzymes is versatile and a comprehensive study addressing this subject was conducted by Ohno and colleagues (Ohno et al., 2006). This study revealed that the majority of zDHHC enzymes reside either in the ER or the Golgi apparatus and only a few exceptions reside elsewhere in the cell. However, subsequent studies challenged the identified subcellular localisation of a few zDHHCs, for example zDHHC2, which was identified to reside in ER and Golgi apparatus by Ohno but later found to be localised at the PM (Greaves et al., 2011; Fukata et al., 2013).

All zDHHC enzymes are integral membrane proteins with 4-6 membrane-spanning domains with the DHHC motif facing the cytosol in a cytoplasmic loop (Mitchell et

al., 2006). Hence, palmitoylation mediated by zDHHC enzymes is catalysed in the cytosol adjacent to membranes of cellular compartments such as the ER or Golgi apparatus or the PM. Yet, only little is known about how zDHHC enzyme substrate interaction and specificity is regulated. One theory is that zDHHC enzyme interaction with their substrates is regulated by the overlapping co-existence of zDHHCs enzymes and their substrates within the same cellular compartment. Another discussed theory is that zDHHCs which reside in the Golgi apparatus palmitoylate their substrates non-specifically and that the Golgi apparatus functions as a palmitoylation hub for peripheral membrane proteins (Rocks et al., 2010). In contrast, there is also evidence for more specific interactions between zDHHC enzymes and their substrates, as shown for zDHHC13 and zDHHC17, which use an ankyrin-repeat domain to recruit selected substrate proteins (Huang et al., 2009; Lemonidis et al., 2014).

The aim of this chapter was to characterise the expression profile of the zDHHC enzyme family in the 3T3-L1 cell line, with a view to identifying potentially important enzymes for adipocyte physiology. In addition, the role of zDHHC enzymes in regulating palmitoylation of IRAP was also investigated.

6.2 Characterisation of zDHHC enzyme expression in the 3T3-L1 cell line

Some proteins are expressed in a cell type-specific manner. In 3T3-L1 adipocytes, for example, GLUT4 expression is only detected after initiating the differentiation of 3T3-L1 pre-adipocytes into adipocytes (Wu et al. 1998; See Figure 3.1). In order to investigate the potential physiological importance of zDHHC proteins in adipocytes, a characterisation of the expression profile of these enzymes in cultured 3T3-L1 adipocytes was undertaken. Additionally, I aimed to examine whether differentiation of 3T3-L1 pre-adipocytes into mature adipocytes elicits the expression of a specific set of palmitoylation enzymes.

There is currently a lack of suitable antibodies that would facilitate the analysis of zDHHC protein expression in adipocytes, and thus the expression profile of these

Having confirmed that the isolated RNA was of a sufficient quality, the next step was to identify a control gene for which the mRNA expression level would remain constant throughout the process of differentiation. This is important to enable a quantitative comparison of the relative zDHHC mRNA expression levels between pre-adipocytes and adipocytes. Previous work has suggested that F-box and leucine-rich repeat protein-10 (Fbox), importin 8 (IPO8) (Hurtado del Pozo et al., 2010) or peptidylprolyl isomerase A (Ppia) (Pei et al., 2011) may serve as reliable reference genes for this analysis. qPCR analysis using primers for these mRNAs was carried out on cDNA synthesised by reverse transcription from the recovered total RNA obtained from pre-adipocytes and adipocytes. As can be seen in Figure 6.2, the difference in mRNA levels between pre-adipocytes and adipocytes is the least for IPO8, indicated by the lowest values of ΔCt when compared to the other control genes. Based on this analysis, IPO8 was used as the control gene for the following qPCR analysis of zDHHC enzyme expression.

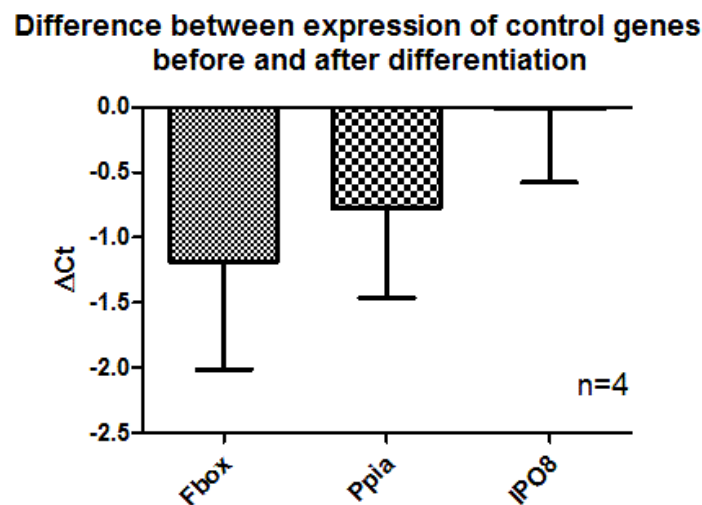


Figure 6.2. Difference in mRNA expression of possible reference genes in 3T3-L1 pre-adipocytes and adipocytes. SYBR Green-based qPCR with cDNA obtained from pre-adipocytes and corresponding adipocytes was carried out as described in the methods section 2.3.16 using primers for the indicated control genes. ΔCt was calculated by subtraction of the Ct values obtained from adipocytes from the Ct values obtained from pre-adipocytes. N=4.

As the RNA integrity was confirmed and a control gene with stable mRNA expression throughout the differentiation process was identified, the prerequisites were set for analysis of the zDHHC expression profile in the 3T3-L1 cell line.

First, the zDHHC enzyme expression profile in adipocytes was examined by qPCR. Primers for the 24 zDHHC enzymes were used to amplify a gene-specific product from the cDNA template. Figure 6.3 displays the results of this qPCR analysis. The Ct values of the zDHHC enzymes were normalised to the Ct value of zDHHC6 (lowest Ct value), in order to visualise the relative expression levels of the zDHHC protein family in cultured adipocytes. The expression analysis suggests that the mRNA levels for zDHHC6 are the highest, followed by zDHHCs 1, 3, 16, 18 and 20. The mRNA expression levels of zDHHC 7, 8, 12, 13, 17, 21, and 24 were lower than a third of the mRNA expression level of zDHHC6. The mRNAs coding for the remainder of the zDHHCs were barely expressed or below the level of detection.

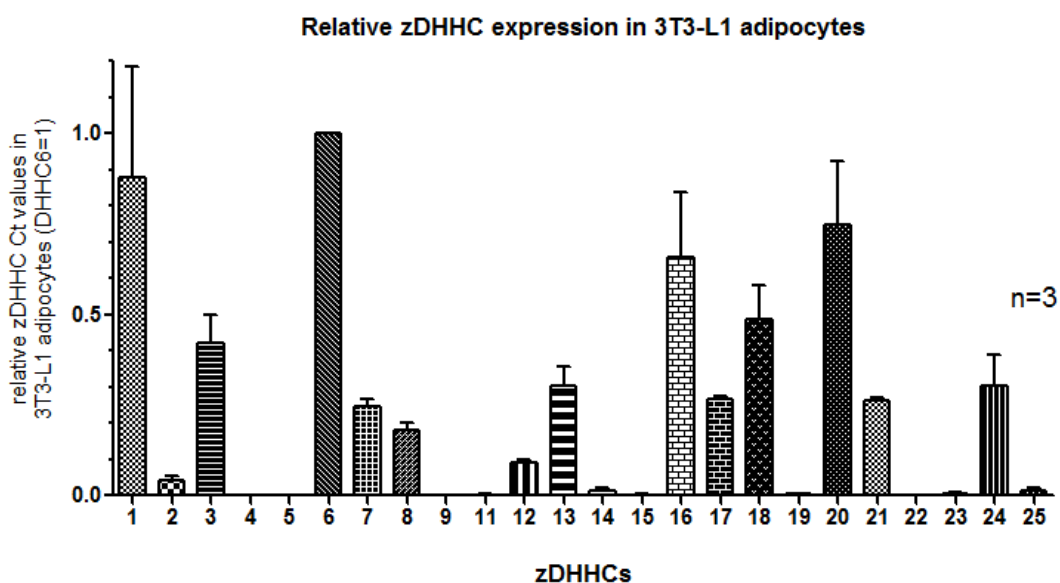


Figure 6.3. zDHHC mRNA expression profile of 3T3-L1 adipocytes. SYBR Green based qPCR was performed using cDNA from 3T3-L1 adipocytes. Validated primers for each zDHHC were used. zDHHC enzyme Ct values are shown relative to the Ct value of zDHHC6 (Ct value = 20.4), which was normalised to the value 1. N=3.

During the differentiation from 3T3-L1 pre-adipocytes to adipocytes, major morphological changes could be observed (see Chapter 3, Figure 3.1). In contrast to pre-adipocytes, adipocytes respond to an insulin stimulus with the translocation of

GLUT4 transporters from intracellular storage vesicles to the PM. It is possible that the morphological changes that occur during adipocyte differentiation and the capability to respond to insulin with GLUT4 translocation are accompanied by a change of zDHHC expression profile. To investigate if there are any changes in mRNA expression levels between zDHHCs enzymes in pre-adipocytes and adipocytes, a qPCR analysis was performed. For this, pre-adipocyte cDNA and the corresponding adipocyte cDNA were amplified using zDHHC primers and expression levels were compared by applying the $2^{-\Delta\Delta CT}$ method (Livak and Schmittgen, 2001). Supplementary investigation of changes in expression levels of GLUT4 and the enzymes which catalyse depalmitoylation (acyl-protein thioesterase) APT1, APT2 and APT3 were included. All results of this experiment are included in Figure 6.4.

zDHC expression in 3T3-L1 adipocytes relative to 3T3-L1 pre-adipocytes

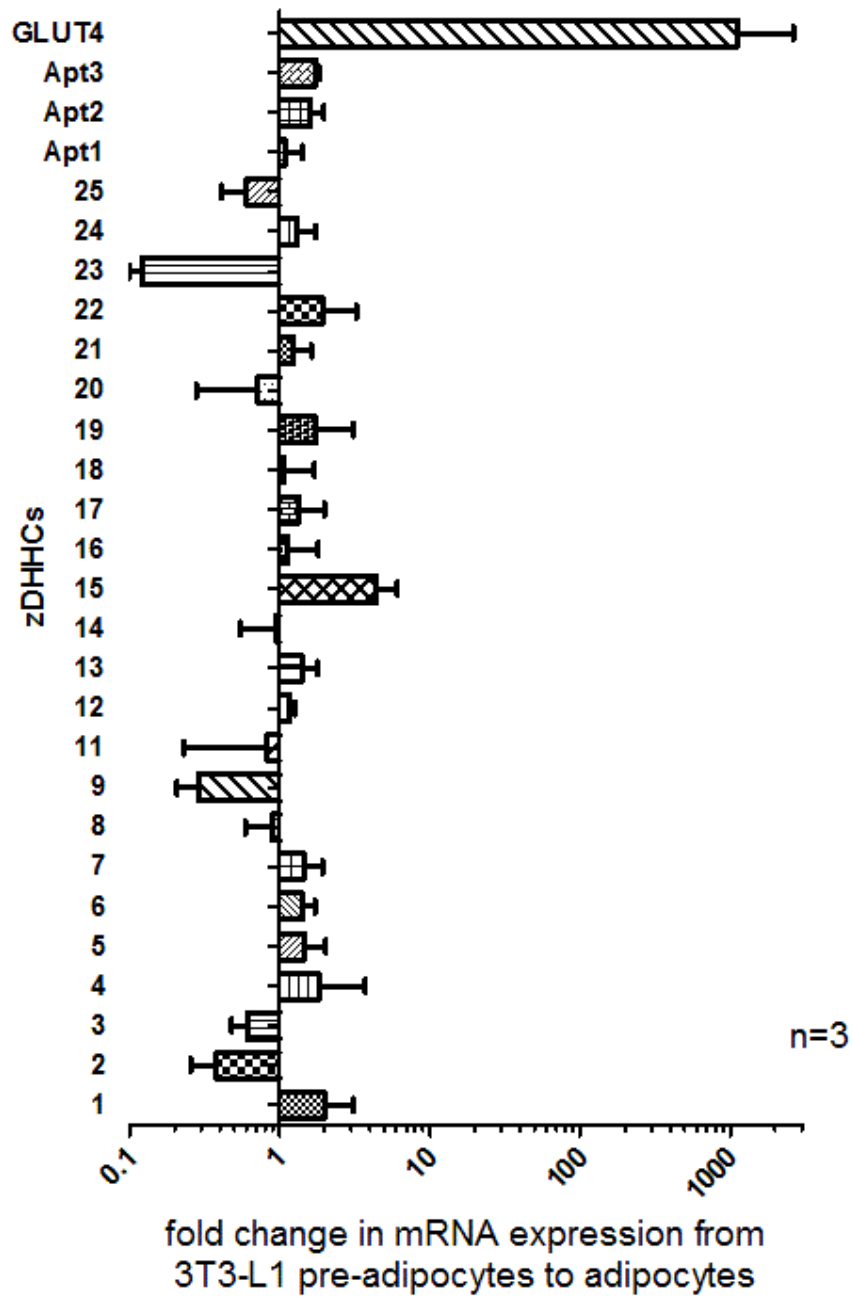


Figure 6.4. zDHC and APT mRNA expression in 3T3-L1 adipocytes relative to 3T3-L1 pre-adipocytes. SYBR Green based qPCR was performed using cDNA from 3T3-L1 pre-adipocytes and corresponding adipocytes. Validated primers for each zDHC and APT 1-3 and GLUT4 were used. Fold changes in mRNA expression from 3T3-L1 pre-adipocytes to adipocytes are shown and were calculated as described in the Methods section (2.3.16). All quantified data were from three experimental repeats.

The relative expression profile comparing zDHHC mRNA expression levels in pre-adipocytes and adipocytes is displayed in Figure 6.4. No major differences in mRNA expression levels could be detected for the zDHHC family, at least at the mRNA level, when 3T3-L1 pre-adipocytes were differentiated into adipocytes. Although some zDHHC enzymes did display marked changes in expression (e.g. zDHHC-15 and -23), the low expression of these enzymes (see Figure 6.3) makes these detected differences unreliable. The mRNA levels for APT2 and APT3 increased approximately 1.5 fold, whereas almost no change could be detected for APT1. The mRNA levels of GLUT4 are approximately 1300 times higher in adipocytes than in pre-adipocytes as previously shown in Chapter 3.

6.3 Effect of zDHHC family proteins on IRAP palmitoylation

In previous sections (Chapter 3 and Chapter 4), palmitoylation of IRAP was demonstrated and quantified, and its palmitoylation sites were identified. Yet, it is unknown which member(s) of the zDHHC protein family are involved in the palmitoylation of IRAP. zDHHC enzymes exhibit compartment-specific localisations, with most isoforms enriched on ER or Golgi membranes (Ohno et al., 2006). IRAP is an integral membrane protein, which is initially translocated across the ER membrane during its synthesis and folding, and transiently passes through the Golgi apparatus before being inserted into the PM or intracellular storage vesicles. Hence, during its biosynthesis and trafficking, IRAP transits through several cellular compartments expressing most of the zDHHC enzymes. In this section, I set out to elucidate which zDHHC enzymes might be involved in the palmitoylation of IRAP.

For this, HA-tagged members of the zDHHC protein family were co-expressed with N-terminally HA-tagged IRAP in HEK293T cells. Subsequently, incorporation of 17ODYA into IRAP and zDHHCs was quantified using click-chemistry. Application of this method allowed an analysis of whether specific members of the zDHHC family modify the incorporation of 17ODYA into IRAP. The result of this experiment is displayed in Figure 6.5. The top panel shows immunoblots probed with an antibody

against the HA-tag. At an apparent molecular weight of approximately 175 kDa, protein bands corresponding to IRAP can be detected; the intensity of these protein bands is comparable between all lanes.

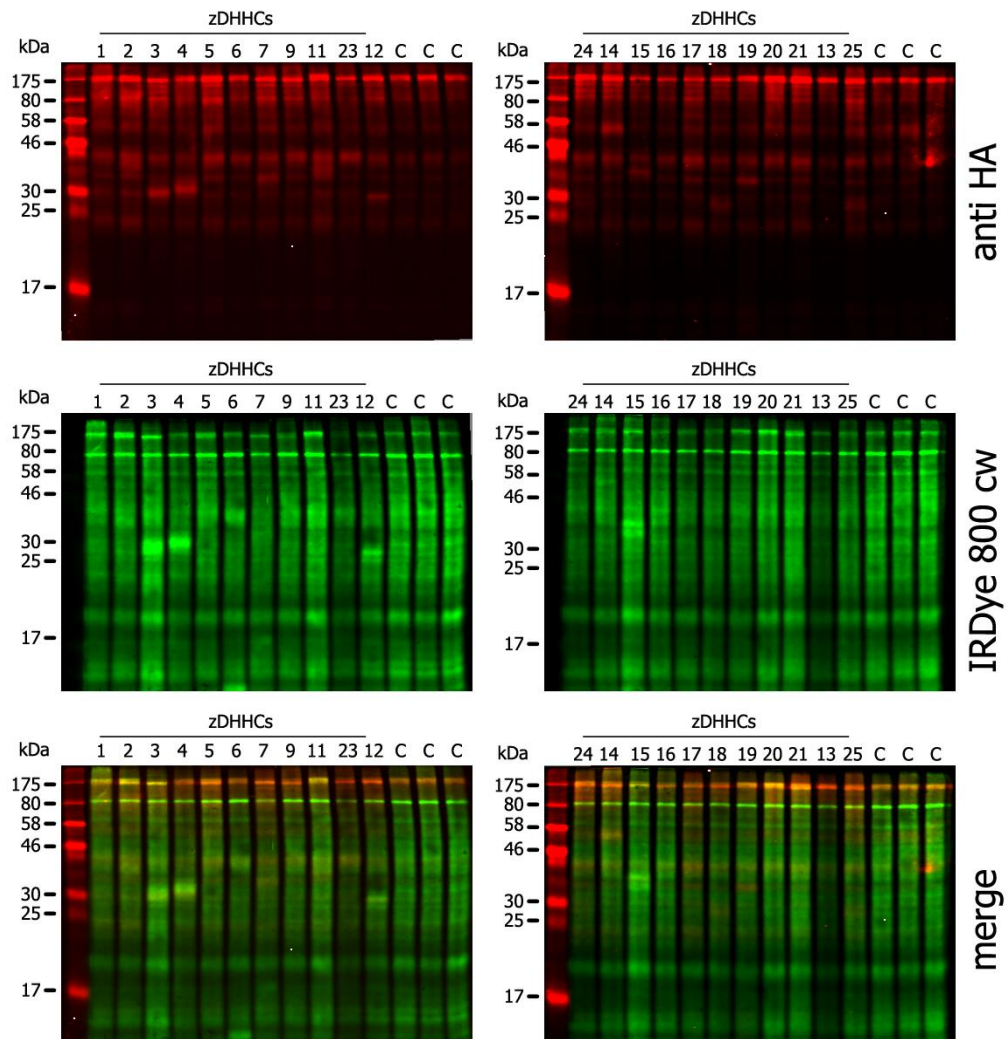


Figure 6.5. Effect of zDHC enzyme co-expression on the incorporation of 17ODYA into IRAP. HEK293T cells were co-transfected with plasmids encoding the indicated HA-tagged members of zDHC family and HA-tagged IRAP for 24 h. Cells were then serum starved in DMEM culture medium containing 1% fatty acid free (FAF) BSA for 30 min and metabolically labelled with 15 μ M 17ODYA in DMEM with 1% FAF BSA for 4 h. Subsequently, incorporation of 17ODYA was detected using IRDye as described in section 2.4.2. Proteins were precipitated using acetone and resuspended in 1x Laemmli buffer containing 25 mM DTT and subjected to SDS-PAGE on 12% acrylamide gels. Subsequently, proteins were transferred onto nitrocellulose membranes and probed with HA antibody. The lanes labelled with C indicate control samples derived from cells transfected with IRAP only. Antibody binding and IRDye were visualised using the Odyssey[®] infrared imaging system. Representative result is shown of an experiments conducted at least four times. Position of the molecular weight marker is indicated on the left hand side of each panel.

Furthermore, protein bands could be detected corresponding to zDHHC 2, 3, 4, 7, 10, 12, 14, 15, 19 and 25 at the approximate apparent molecular weight of each zDHHC protein (see Table 6.1 for molecular mass of zDHHC proteins).

Table 6.1. zDHHC enzyme molecular mass sizes according to UniProt. The columns labelled “Protein” indicate members of mouse zDHHC protein family. The predicted molecular mass in kDa according to UniProt can be seen in the columns indicated with “Protein mass”.

Predicted molecular mass for zDHHC enzyme family members			
Protein	Protein mass [kDa]	Protein	Protein mass [kDa]
zDHHC1	54.8	zDHHC14	53.8
zDHHC2	42.0	zDHHC15	39.3
zDHHC3	34.0	zDHHC16	43.6
zDHHC4	39.5	zDHHC17	72.6
zDHHC5	77.5	zDHHC18	42.0
zDHHC6	47.5	zDHHC19	34.2
zDHHC7	35.1	zDHHC20	42.2
zDHHC9	40.9	zDHHC21	31.3
zDHHC11	45.9	zDHHC23	48.1
zDHHC12	30.8	zDHHC24	30.4
zDHHC13	70.9	zDHHC25	30.8

The middle panel of Figure 6.5 shows the incorporation of 17ODYA. Protein bands at the apparent molecular weight of approximately 175 kDa highlight the attachment of 17ODYA to IRAP. The intensities of these bands vary, and are the strongest for lanes with zDHHC1, 2, 3, 5, 11, 15, 20 and 21. Furthermore, incorporation of 17ODYA into zDHHC3, 4, 12, and 15 is detectable at the corresponding molecular weight for each zDHHC enzyme. This signal is likely to originate from the auto-palmitoylation of the zDHHC proteins. A background signal, resulting from attachment of the IRDye to other cellular proteins is visible in each lane, particularly at an apparent molecular weight of approximately 80 kDa; this background signal presumably reflects the palmitoylation of other cellular proteins. The bottom panel shows a merge of signals obtained from the HA antibody and the IRDye 800cw.

In order to display the differences in incorporation of 17ODYA into IRAP, fluorescence images from Figure 6.5 were quantified using Image Studio software

and attachment of 17ODYA to IRAP was calculated as described in Chapter 4 section 4.2. The calculated values for the attachment of 17ODYA to IRAP in cells co-transfected with the indicated zDHC proteins are illustrated in Figure 6.6.

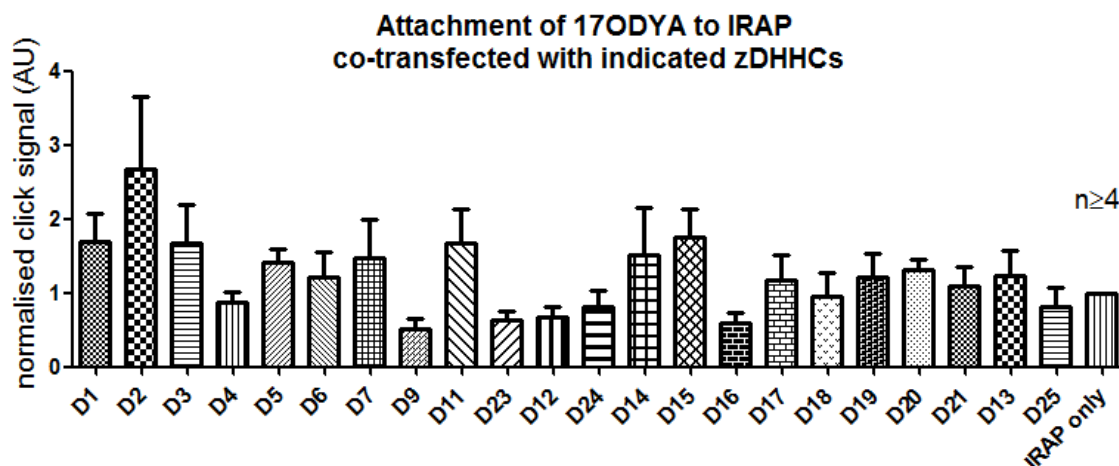


Figure 6.6. Quantification of incorporation of 17ODYA into IRAP co-expressed with the indicated zDHCs in HEK293T cells. Incorporation of 17ODYA into IRAP was measured by quantification of the click-signal from images shown in Figure 6.5 and additional experimental repeats using Image Studio software. Quantified values of click-signal from IRAP were normalised to corresponding value for the HA-tagged IRAP constructs. The value for 17ODYA incorporation into IRAP obtained from cells without co-transfected zDHCs was set to 1. Statistical One way ANOVA analysis followed by Tukey's multiple comparison test revealed no significant differences in 17ODYA incorporation in the presence of any zDHC enzyme. All quantified data was from a minimum of four experimental repeats.

As a control, IRAP wild type cDNA was transfected alone into HEK293T cells and the determined value for attachment of 17ODYA was set to the value one. Co-expression of IRAP with zDHC1, 2, 3, 5, 7, 11, 14 or 15 resulted in a somewhat increased incorporation of 17ODYA into IRAP when compared to control samples. Calculated values varied between approximately 2.6 for co-expression with zDHC2 and approximately 1.4 for co-expression with zDHC5. When IRAP was co-transfected with zDHC4, 6, 13 17, 18, 19, 20, 21, 24 and 25, comparable values for attachment of 17ODYA to the control samples were obtained. A reduction of 17ODYA attachment to IRAP could be observed when IRAP was co-expressed with zDHC9, 12, 16 and 23. Despite the differences in determined values for attachment of 17ODYA to IRAP ranging from 2.6 to 0.5, there was no statistical

significance when compared to the control condition (i.e. no co-expression of zDHHC enzymes).

6.4 Interaction of IRAP with selected zDHHC enzymes.

In section 6.3, it was found that although co-expression with certain members of the zDHHC protein family (e.g. zDHHC2) had an effect on IRAP palmitoylation, none of the detected changes were statistically significant. Interestingly, however, co-expression of specific zDHHC enzymes appeared to cause a downward shift in the apparent molecular weight of IRAP (e.g. zDHHC 3, 7 and 9 in Figure 6.5 top and middle panels). This shift in migration was a consistent observation and was specific to IRAP, as the major band labelled with 17ODYA (Figure 6.5, middle panel) at ~ 80 kDa did not show a similar band-shift. According to the protein database UniProt and previous publications, IRAP is predicted to undergo other PTMs, such as glycosylation and phosphorylation (Keller et al., 1995). IRAP is a protein comprising 1025 amino acids and has a predicted molecular mass of approximately 117 kDa. In accordance with previous studies, IRAP was detected in this study at the apparent molecular weight of approximately 140 kDa in brain and at approximately 175 kDa in 3T3-L1 adipocytes and HEK293T cells (Keller et al., 1995; Hashiramoto and James, 2000; Albiston et al., 2001). The discrepancy between the predicted molecular mass and the apparent molecular mass of IRAP is likely to originate from cell-specific variations in PTM processing, most notably glycosylation (Keller et al., 1995). Glycosylation of proteins begins in the ER, with further trimming and modification of sugar groups taking place in the Golgi apparatus (Lodish et al., 2000). Thus, it is possible that the Golgi-localised enzymes zDHHC3, 7 and 9 are somehow interfering with the trafficking of IRAP, resulting in changes in its glycosylation profile and in a visible band-shift on SDS gels.

To further examine the effect of specific zDHHC enzymes on the migration of IRAP on SDS gels, IRAP was co-expressed with either wild type zDHHC7 or a catalytically-inactive form containing a mutation of the cysteine within the DHHC motif (zDHHC7-C160S). Lysates from transfected cells were prepared and analysed by

SDS-PAGE on 8% acrylamide gels. A low percentage of acrylamide was chosen to obtain a better resolution of higher molecular weights, which was important to be able to detect potential changes in the molecular weight of IRAP. The result of this experiment is shown in Figure 6.7. The top panel of the figure shows the detection of protein bands corresponding to IRAP. When IRAP was transfected without zDHHHC7, it appeared as a doublet band stretching from the apparent molecular weight of approximately 170 kDa to just over 175 kDa. This is also the case for the palmitoylation-deficient mutant (3CA) of IRAP. In contrast, IRAP appeared predominantly as a single protein band at the apparent molecular weight of approximately 170 kDa when it was co-expressed together with both zDHHHC7 constructs (wild type and catalytically-inactive). In the bottom panel of the Figure 6.7, zDHHHC7 expression is indicated.

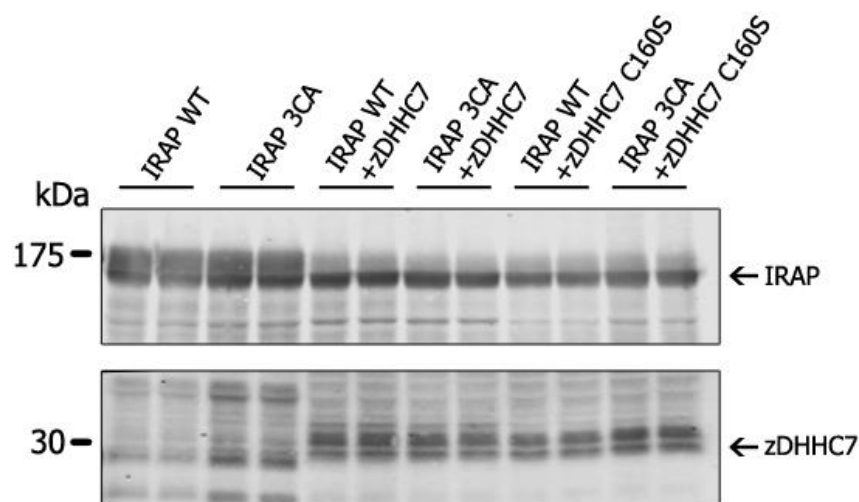


Figure 6.7. SDS-PAGE analysis of HEK293T cells co-transfected with HA-tagged IRAP constructs and HA-tagged zDHHHC7 constructs. HEK293T cells were co-transfected with plasmids encoding the indicated HA-tagged IRAP constructs and HA-tagged constructs of zDHHHC7 for 24 h. Cells were then lysed in 200 μ l lysis buffer (50 mM Tris; 17 mM SDS; pH 8.0 containing protease inhibitors) and subjected to SDS-PAGE on 8% polyacrylamide gels. Subsequently, immunoblotting was performed using an anti-HA antibody. Samples were loaded in duplicate. Lanes indicating: zDHHHC7= zDHHHC7 wild type; zDHHHC7 C160S= zDHHHC7 with cysteine-160 mutated to serine within DHHHC-motif.

6.5 Discussion

Many proteins are expressed in a cell-type specific manner, and can contribute to the determination of physiological properties, such as cellular metabolism, morphology or function. This chapter focused on the expression profile of zDHHC enzymes in the 3T3-L1 cell line. Furthermore, interaction of zDHHC enzymes with the previously identified palmitoylation substrate IRAP was examined. qPCR was applied to measure differences in zDHHC mRNA levels of 3T3-L1 pre-adipocytes and adipocytes. This analysis revealed similar mRNA copy numbers for all the examined zDHHCs when 3T3-L1 pre-adipocytes and adipocytes were compared (Figure 6.4); any expression changes detected were for enzymes with very low levels of mRNA, and hence these results were considered unreliable. In contrast, comparing qPCR Ct values in mature 3T3-L1 adipocytes demonstrated potential differential expression levels of zDHHC isoforms in this cell type. Furthermore, I attempted to identify which of the zDHHC enzymes are involved in the palmitoylation of the protein IRAP, using click-chemistry experiments in HEK293T co-expressing this protein and each of the zDHHC enzyme isoforms. This approach showed that, despite elevated zDHHC protein levels, the incorporation of 17ODYA into IRAP remained largely unchanged (Figure 6.5 and Figure 6.6). However, co-expression of some zDHHC enzymes (e.g. zDHHC3, 7 and 9) was found to change the migration profile of IRAP on SDS gels. This effect was demonstrated to be independent of IRAP palmitoylation status and on the palmitoyl transferase activity of the zDHHC enzyme indicating that high copy numbers of certain zDHHC enzymes potentially affects the processing of IRAP.

The composition of cellular proteins and their distribution ultimately determines the physiological and morphological properties of each cell type. The 3T3-L1 cell line is derived from a subset of embryonic mouse fibroblasts, also referred to as pre-adipocytes, which can differentiate into cells with adipocyte physiology (Green and Kehinde, 1972, 1975). The differentiation process whereby these pre-adipocytes mature into adipocytes includes the up-regulation of the expression of several proteins which are important for structural and physiological changes

accompanying this process. Many proteins have been established to play a role in adipocyte differentiation or to exhibit changes in expression during this process, such as GLUT4, caveolin-1 and peroxisome proliferator-activated receptor (PPAR) gamma (Scherer et al., 1994; Wu et al., 1998; Chawla et al., 1994). Hence, it was possible that changes in the expression of certain zDHHC proteins might indicate an important role in adipocyte differentiation or physiology. In order to examine whether changes in expression takes place, mRNA levels of the zDHHC proteins were measured by qPCR before and after differentiation of 3T3-L1 cells. The purification of RNA from 3T3-L1 pre-adipocytes and corresponding adipocytes was the basis of this analysis and the quality of purified RNA is an essential factor determining the success of any qPCR analysis (Fleige and Pfaffl, 2006). The quality of the purified RNA was assessed by resolving the RNA with electrophoresis. A typical band pattern with an intensity ratio of 2:1 for bands corresponding to 28S and 18S indicated that the isolated RNA was mostly intact (see Figure 6.1) (Sambrook et al., 1989). In order to be able to compare expression levels of proteins between different cells, stably expressed reference genes are needed. As mentioned above, the differentiation of 3T3-L1 pre-adipocytes to adipocytes is accompanied by severe morphological (see Chapter 3 Figure 3.1) and physiological changes, and expression of many proteins is altered after differentiation is completed. Commonly used control genes for qPCR such as β -actin or glyceraldehyde 3-phosphate dehydrogenase (GAPDH) were not suitable, as their expression varied during differentiation (data not shown). Therefore in this thesis, Fbox, IPO8 or Ppia were considered as reference genes. These proteins were previously reported to function as reference genes for qPCR analysis (Hurtado del Pozo et al., 2010; Pei et al., 2011), and indeed changes in mRNA expression of IPO8 between pre-adipocytes and adipocytes were suitably low as indicated by a low value of Δ Ct, and this gene was chosen as the reference gene for the qPCR analysis (Figure 6.2). The comparison of Ct values of zDHHCs in mature 3T3-L1 adipocytes revealed that the mRNA of zDHHC6, zDHHC1, zDHHC16 and zDHHC21 were potentially expressed at the highest levels. This comparison was based on the obtained Ct values of the qPCR analysis.

Although the efficiency of the primers for each zDHHC isoform was validated, the copy number of mRNA which corresponded to Ct values was not calibrated. Hence, this analysis serves only as an approximate estimation of the actual mRNA copy numbers of the examined zDHHCs in adipocytes, and thus direct comparison of expression levels between different zDHHC isoforms is only semi-quantitative. The established $2^{-\Delta\Delta CT}$ method was applied to compare relative mRNA expression levels of each zDHHC isoform between 3T3-L1 pre-adipocytes and adipocytes. This analysis revealed that no major changes were observed in the expression of zDHHC mRNA linked to the maturation of 3T3-L1 adipocytes. The highest changes in mRNA expression were registered for zDHHC23, zDHHC15 and zDHHC9. Although the determined differences in expression reached an almost 10-fold increase (zDHHC15) or decrease (zDHHC23), it is not clear whether these observations are reliable. The reason for this is that the zDHHC isoforms with the greatest registered changes in mRNA expression were simultaneously shown to have the highest Ct values as can be seen in Figure 6.3. The precision of qPCR analysis in high ranges of Ct values is not as precise as analysis with low Ct values, hence these observed differences in expression could have originated from inaccurate analysis due to low copy numbers of mRNA. Nevertheless, the validity of this qPCR analysis was confirmed by the high increase of GLUT4 mRNA upon differentiation, which was reported in previous publications (Wu et al., 1998). Although differentiation into adipocytes was not accompanied by detectable changes of mRNA copy numbers of the zDHHC enzymes, it was possible that the regulation of their mRNA translation into proteins has changed. An altered translation rate could result in increased or decreased protein levels without a change in the copy numbers of the mRNA itself. Protein levels of the zDHHC enzymes were not examined because suitable antibodies against zDHHC proteins were not available. Furthermore, it was possible that the activity of these enzymes could have changed upon differentiation. However, zDHHC enzyme activity has been not examined in this study.

Substrate specificity of zDHHC enzymes and the regulation of it is an extensively studied subject of the palmitoylation field. There is evidence that palmitoylation by

zDHHC enzymes is promiscuous and not substrate-specific. For example, loss of palmitoylation of VAC8, which followed the depletion of 5 out of 7 PATs in yeast, was compensated by the over-expression of any single one of the five depleted zDHHCs (Hou et al., 2009). Furthermore, palmitoylation by zDHHC enzymes localised in the Golgi apparatus was shown to occur in the absence of conserved structural features or evident consensus sequences (Rocks et al., 2010). Hence, it is possible that substrate specificity is regulated only by an overlapping localisation of substrates and zDHHC enzymes in the same intracellular compartment. However, a few studies have demonstrated substrate specificity of zDHHC enzymes and identified some specific features of both enzyme and substrate that regulate the interaction (Greaves and Chamberlain, 2011a). The majority of insights into zDHHC substrate specificity have been obtained from either co-expression or depletion experiments. Co-expression of zDHHC17 or zDHHC3 with SNAP25, glutamate receptor subunit 1 or stress-regulated exon (STREX) domain of large conductance potassium (BK) channels resulted in an increase of palmitoylation of those substrates and complementary depletion of these zDHHC proteins also led to a reduction of palmitoylation the same substrates (Huang et al., 2009; Tian et al., 2010). Here, I attempted to identify zDHHC proteins that are involved in the palmitoylation of IRAP. For this, IRAP was co-expressed together with zDHHC proteins in HEK293T cells and subsequently palmitoylation of IRAP was measured by click-chemistry. Albeit, some minor increases and decreases in 17ODYA incorporation after co-expression were registered, however no statistical significance of these changes was found. Assuming that zDHHC proteins catalyse the palmitoylation of IRAP without a specific preference, it would have been predicted that an increase in 17ODYA attachment onto IRAP would have been most evident in cells expressing zDHHC enzymes at the highest levels (with the caveat that localisation of zDHHC enzymes is also likely to be important for IRAP palmitoylation). This was not the case, as zDHHC 3, 4, 12 and 15 were found to be the most clearly detectable zDHHCs by immunoblotting, but co-expression with these enzymes did not consistently result in an increased palmitoylation of IRAP

(Figure 6.5 and Figure 6.6). Although an increase in 17ODYA incorporation into IRAP was observed when IRAP was co-expressed with zDHHC 3 and 15, a decrease in palmitoylation was observed when zDHHC4 and 12 were co-expressed. Furthermore, it could be concluded that the level of auto-palmitoylation of zDHHC proteins did not correlate with highest incorporation of 17 ODYA onto IRAP. zDHHCs 3, 4, 12 and 15 had clearly detectable auto-palmitoylation, but as mentioned above, co-expression with these DHHCs was not linked to a consistent change in IRAP palmitoylation. Expression of IRAP without co-expression of any zDHHC resulted in clearly detectable 17ODYA incorporation into IRAP. This observation indicates that HEK293T cells endogenously express PATs which are capable of palmitoylating IRAP. zDHHC2, 4, 13 and 16 might be involved in the palmitoylation of IRAP as the mRNA levels of these zDHHC enzymes are the highest in HEK293T cells (Tian et al., 2010). It would be interesting to co-express zDHHCs with IRAP in a cell line, which lacks efficient palmitoylation by endogenously expressed PATs. Furthermore, depletion of zDHHCs in HEK293T cells might be an approach that is potentially more likely to identify the enzymes involved in IRAP palmitoylation. A similar siRNA (small interfering ribonucleic acid) approach successfully identified zDHHCs that modulate the palmitoylation of the STREX variant of the BK channel in HEK293 cells (Tian et al., 2010).

Within some proteins the ankyrin-repeat domain mediates protein-protein interaction (Li et al., 2006). The cytosolic fragment from amino acids 96 to 101 of IRAP was identified as an ankyrin-repeat binding domain (Sbodio and Chi, 2002). Interestingly the protein tankyrase, contains an ankyrin-repeat domain and was shown to interact with IRAP. This interaction is thought to be mediated by the ankyrin-repeat motif of tankyrase (Chi and Lodish, 2000). Furthermore, the ankyrin-repeat domain is also thought to play a role in the enzyme substrate interaction of zDHHC17 and zDHHC13, which have an N-terminal ankyrin-repeat domain and were demonstrated to palmitoylate huntingtin (Huang et al., 2009). In contrast, zDHHC3 has no ankyrin-repeat domain and is not able to palmitoylate huntingtin. The importance of the ankyrin-repeat in huntingtin recognition by zDHHC17/13 was

demonstrated, as a chimeric form of zDHHC3 with the N-terminal ankyrin-repeat domain from zDHHC17 gained palmitoylation activity towards huntingtin (Huang et al., 2009). Furthermore, the ankyrin-repeat domain of zDHHC17 was also shown to be important for recognition and palmitoylation of both SNAP25 and CSP (Lemonidis et al., 2014). Despite the putative ankyrin-repeat domain recognition site of IRAP, its palmitoylation was not affected by the co-expression of either zDHHC13 or zDHHC17 (Figure 6.6). More research is clearly needed to elucidate the interaction of IRAP with zDHHC enzymes, especially with zDHHC13 and zDHHC17. This could be done by classic protein-protein interaction studies like co-immunoprecipitation, or more recent methods such as the mating based split-ubiquitin system, which was successfully applied to identify interaction of zDHHC proteins with their substrates (Lemonidis et al., 2014). Attempts to study IRAP interaction with zDHHC enzymes in this yeast system were hampered by an inability to successfully express IRAP in yeast (data not shown).

The compartments of the Golgi apparatus with its residing zDHHCs were suggested to function as hub for palmitoylation of peripheral membrane proteins in the cell (Rocks et al., 2010). IRAP undergoes various PTMs, most notably glycosylation in the Golgi apparatus before trafficking to the PM or intracellular storage vesicle (Keller et al., 1995). Co-expression of Golgi apparatus residing zDHHC enzymes such as DHHC3, 7 or 9 with IRAP (Figure 6.5) resulted in a somewhat different band migration pattern of IRAP on SDS gels. These subtle changes are difficult to notice in Figure 6.5, as the resolution of high molecular weight proteins is limited on 12% acrylamide gels, but these differences were readily apparent on 8% acrylamide gels. In order to investigate this effect in more detail, IRAP constructs were co-transfected with zDHHC7 wild type and catalytically inactive mutant and analysed on 8% polyacrylamide gels (Figure 6.7). Co-expression of zDHHC7 resulted in loss of the upper band of the IRAP doublet. Involvement of palmitoylation of IRAP in this phenomenon could be excluded as transfection of a palmitoylation-deficient IRAP 3CA mutant (without co-transfection of zDHHC7) resulted in the same band pattern as seen for the wild type IRAP. Additionally, the

band shift could be still observed when both IRAP constructs were transfected with a mutant form of zDHHC7 that lacked the cysteine within the DHHC motif. It is possible that the increased presence of zDHHC7 perturbed the normal processing of IRAP. Interestingly, over-expression of zDHHCs localised at the Golgi apparatus (zDHHC3, 7 and 17) was previously shown to affect the secretion of proteins via both regulated and constitutive secretory pathways (Huang et al., 2004; Fukata et al., 2004; Greaves et al., 2010). Hence, the effects of zDHHC expression on IRAP migration on SDS gels could reflect a disruption of the secretory pathway. It is not clear how over-expression of certain zDHHC enzymes would cause this effect but this is not likely to be linked to the palmitoylation activity of these enzymes. It will be interesting in future work to examine how zDHHC over-expression affects the trafficking of other cargo proteins through the Golgi apparatus, such as the G protein of vesicular stomatitis virus (VSV-G), which has been used as a general marker protein for trafficking process in the secretory pathway.

Further research needs to be conducted to understand the nature of zDHHC interaction with IRAP and to identify zDHHCs which are involved in IRAP palmitoylation.

Chapter 7: General discussion

7.1 ACYL-RAC AND THE IDENTIFICATION OF PALMITOYLATED PROTEINS

The main focus of this study was to examine protein palmitoylation in 3T3-L1 adipocytes, with the goal of identifying new roles for this post-translational modification within the insulin signalling and GLUT4 trafficking pathways. To address this question, the relatively new “acyl-RAC” technique was applied to isolate the palmitoylome of 3T3-L1 adipocytes. The initial plan was to employ both a candidate-based approach and also a wider proteomics approach to identify novel palmitoylated proteins captured in the adipocyte palmitoylome. However, the 3T3-L1 adipocyte palmitoylome was reported in a separate study that was published during the course of this work (Ren et al., 2013b). This, combined with the success of the candidate-based approach in identifying novel palmitoylated proteins of interest (IRAP and caveolin-2), led to the decision to focus subsequent analysis on the characterisation of these two novel palmitoylated proteins.

IRAP resides in GSVs of muscle and adipocytes, and shows extensive overlap with GLUT4 in these cells (Martinez-Arca et al., 2000). Furthermore, there is evidence that IRAP regulates sorting of GLUT4 in these cell types (Waters, 1997; Yeh et al., 2007). Both IRAP and GLUT4 were found to be palmitoylated in adipocytes, albeit at markedly different levels. The finding that these proteins are palmitoylated was a novel observation when this work was initiated, however palmitoylation of IRAP and GLUT4 was confirmed in a recent proteomics-based study (Ren et al., 2013b). Although other proteins that were investigated, such as caveolin-1, flotillin1/2, SNAP23, IR β and IGF receptor β were already known to be palmitoylated, the level of palmitoylation of these proteins was not known until the results of the quantitative analysis that was performed in this study (Dietzen et al., 1995; Vogel and Roche, 1999; Magee and Siddle, 1988; Morrow et al., 2002; Neumann-Giesen et al., 2004).

Albeit the acyl-RAC method was established a few years ago (Forrester et al., 2011), the present study (to my knowledge) is the first time this technique has been used

to determine the steady state palmitoylated fractions of various proteins within the same cells. Quantification of relative differences in the extent of palmitoylation of individual proteins has been reported in numerous studies using metabolic labelling with ^3H -palmitic acid (e.g. Fernández-Hernando et al. 2006; Abrami et al. 2008). In these studies, cells are typically labelled with ^3H -palmitic acid and proteins of interest recovered by immunoprecipitation. Incorporation of ^3H -palmitic acid into specific proteins is then detected by fluorography. For quantification, the fluorographic signal is then normalised to the total protein amount estimated by immunoblotting. Although this approach gives information about changes in palmitoylation levels, assessment of the absolute palmitoylation states is not possible, as two separate detection systems are used (fluorography and immunoblotting), which are not comparable with each other. Thus, quantifying the palmitoylated pool of proteins of interest is a major strength of the acyl-RAC technique, which is not yet being fully exploited in the literature.

With the application of acyl-RAC, where the total palmitoylated pool of a protein is directly related to the level of capture of that protein by a thio reactive matrix, approximately 80% of the soluble proteins SNAP23 and flotillin1/2 were found to be palmitoylated. Previous work has demonstrated that palmitoylation of multiple cysteines regulates membrane attachment of these proteins (Vogel and Roche, 1999; Neumann-Giesen et al., 2004). In contrast to the uniformly high palmitoylation values of the soluble proteins that were examined in this work, the percentage of palmitoylation of integral membrane proteins varied and was the highest for caveolin-2 (~80%) and lowest for GLUT4 (~14%) and IGF receptor β (~7%). Although acyl-RAC provides direct information on the palmitoylated and non-palmitoylated pool sizes of proteins of interest, it cannot determine how highly palmitoylated an individual protein molecule is. Theoretically, the attachment of only one palmitate per molecule is sufficient for the capture of a protein within the palmitoylated fraction. Hence, it is not possible to distinguish whether one, or multiple cysteines are palmitoylated on a protein with this method. However, this could be addressed by including a PEGylation labelling step (Roberts et al., 2002; Yu

et al., 2006), and this type of modification has potential to further increase the strength of acyl-RAC-based approaches.

PALMITOYLATION OF PROTEINS INVOLVED IN INSULIN SIGNALLING/GLUT4 TRANSLOCATION

When this work was initiated, very little was known about the impact of palmitoylation on the insulin signalling and GLUT4 trafficking pathways. Palmitoylation was already established to regulate membrane binding of the SNARE protein SNAP23 (Veit et al., 1996; Vogel and Roche, 1999), and TC10 and lotillin-1/2 (Morrow et al., 2002; Watson et al., 2003), which are involved in the PI3-kinase-independent insulin signalling pathway. In addition, work published over 25 years ago reported palmitoylation of the IR (Magee and Siddle, 1988). The identification of caveolin-2 and IRAP as novel palmitoylated proteins further adds to the overall picture of where palmitoylation might be most important in these insulin-regulated pathways. Furthermore, the novel observations that a pool of GLUT4 is palmitoylated, and that palmitoylation of the IR is limited to a small pool of the protein also add to our understanding of the links between this post-translational modification and insulin signalling/GLUT4 trafficking. Thus, it would be interesting to investigate if the palmitoylated pools of these proteins correspond to specific intracellular locations of the proteins, or whether there are regulated changes in the palmitoylation state of these key proteins occurring under specific conditions. Interestingly, a recent study also demonstrated a further role of palmitoylation in the insulin-dependent GLUT4 translocation pathway. Silencing of the PAT zDHHC17 was shown to impair insulin-stimulated GLUT4 translocation to the PM, which was linked to reduced palmitoylation of the zDHHC17 substrate clipR-59, a protein that regulates compartmentalisation of AKT protein kinase (Ren et al., 2013a).

The findings made in this study are supported by a recent study that also reported palmitoylation of IRAP and GLUT4, and additionally identified novel palmitoylated proteins in adipocytes such as mammalian homolog of Unc (Munc) 18c or AS160 (Ren et al., 2013b). However, the palmitoylated fraction of AS160 and Munc18c was

not quantified either by Ren *et al.* or in our study; in the work reported here, detection of these proteins in acyl-RAC fractions was inconsistent, most likely due to issues with the antibodies that were used.

EFFECTS OF PALMITOYLATION ON INSULIN SIGNALLING/GLUT4 TRAFFICKING PROTEINS

Previously conducted studies demonstrated that palmitoylation is capable of modifying protein-protein interactions (Delandre et al., 2009). Hence it is possible that palmitoylation is involved in regulating the interaction between components of the insulin signalling and GLUT4 translocation pathways. In support of this notion, the interaction of IRAP with AS160 and GLUT4 has been reported in previous studies, and all three are palmitoylated proteins (Peck et al., 2006; Shi et al., 2008). However, interaction of IRAP and GLUT4 is unlikely to be mediated by palmitoylation, as I found that the major palmitoylation sites of IRAP are the cytosolic cysteine residues cysteine-103 and cysteine-114 but GLUT4 and IRAP are thought to interact through the luminal domain of IRAP (Shi and Kandror, 2005). Furthermore, co-transfection of a palmitoylation-deficient mutant of IRAP or the wild type IRAP together with GLUT4 in HEK293T cells resulted in the same localisation in respect to GLUT4 for both IRAP constructs (see Figure 4.6). In contrast to the IRAP-GLUT4 interaction, the interaction of IRAP with AS160 has more potential to be affected by palmitoylation as it is thought to be mediated through the cytoplasmic domain of IRAP (Peck et al., 2006), where the palmitoylation sites of IRAP are present. However, the palmitoylation sites and the extent of palmitoylation of AS160 have not been identified. Further work needs to be conducted to elucidate the role of palmitoylation in the interaction of components of the GLUT4 translocation pathway. For example, it would be interesting to test if wild type and palmitoylation-deficient mutants of IRAP and GLUT4/AS160 co-immunoprecipitate to the same extent.

The assembly of GSVs is another potential process that might involve palmitoylation. Interestingly, the major components of GSVs, which are GLUT4,

IRAP and sortilin, have all been reported to be palmitoylated either in the present study or in other studies (McCormick et al., 2008; Ren et al., 2013b). Sortilin is thought to play an important role in the assembly of the GLUT4 containing vesicles, as it is believed that sortilin is required for the recruitment of GLUT4 into GSVs (Shi and Kandror, 2005). Palmitoylation of sortilin was found to affect its stability and is essential for its correct trafficking within the cell (McCormick et al., 2008; Dumaresq-Doiron et al., 2013), which in turn would be important for its function in the assembly of GSVs. However, the effect of palmitoylation on GLUT4 is not known and palmitoylation of IRAP was demonstrated in this study to have no effect on either localisation or protein stability. Hence, without further investigation, it cannot be concluded how palmitoylation of the major components of GSVs impacts on the assembly of the insulin responsive, GLUT4 containing storage vesicles.

As previously reported and demonstrated by the application of acyl-RAC, the IR β subunit of the IR, caveolin-1 and caveolin-2 are also modified by palmitoylation (Magee and Siddle, 1988; Dietzen et al., 1995). The IR was reported to predominantly reside in caveolae at the PM of adipocytes (Gustavsson et al., 1999; Foti et al., 2007). Interestingly, there are a few studies suggesting that insulin stimulated internalisation of the IR is mediated by caveolae. The IR and caveolin-1 were also shown to interact with each other, and caveolin-1 has been identified as a target of the receptor tyrosine kinase (Kimura et al., 2002). Moreover, both proteins were co-immunopurified together from endosomal vesicles using antibodies against the IR or tyrosine(14)-phosphorylated caveolin-1 respectively (Fagerholm et al., 2009). Finally, a clathrin independent endocytosis pathway of GLUT4 is suggested to be mediated by caveolae (Montesano et al., 1982; Shigematsu et al., 2003; Blot and McGraw, 2006).

In the present study, there is evidence suggesting that a specific intracellular pool of caveolin-1 and the IR β subunit might be a particular target for palmitoylation. Before isolation of the palmitoylome from 3T3-L1 adipocytes by acyl-RAC, the cell membrane fraction was purified in one of two different ways: in one experiment the starting membrane fraction consisted mainly of the PM, mitochondria,

lysosomes and peroxisomes and was purified by centrifugation at a speed of 16,000 x g; in the other experiment, membrane purification was conducted by centrifugation at a higher speed (136,000 x g), which also isolates membranes from the ER, Golgi apparatus, endosomes and small vesicles (including GSVs) (Lodish et al., 2007). Out of the panel of examined proteins, only the calculated palmitoylated fraction of caveolin-1 and the IR varied when acyl-RAC was conducted using the two different membrane fractions. The percentage of palmitoylation increased to similar levels (50-60%) for both proteins when centrifugation with the higher speed was used for the membrane purification. For caveolin-1 a nearly two-fold increase was observed and the palmitoylation of the IR increased approximately 4-fold. One possible explanation is that palmitoylated molecules of caveolin-1 and the IR are enriched in low density membranes, which are only purified by high speed centrifugation. These low density vesicle membranes could potentially be endosomes, which originate from caveolae-mediated endocytosis of the IR. Another possibility is that the palmitoylated molecules of both proteins were purified from low density vesicles that carry newly synthesised IR and caveolin-1 from the ER to the PM. In summary, this result might suggest a potential involvement of palmitoylation in the trafficking of newly synthesised IR and caveolin-1, or in the endocytic recycling-pathway of these proteins. This idea warrants investigation in subsequent studies. A potential way to demonstrate co-localisation of palmitoylated IR and caveolin-1, might be the application of a recent technique, whereby palmitoylated proteins can be localised within cells with the help of click-chemistry and a proximity ligation signal, as demonstrated for the proteins sonic Hedgehog, tubulin and H-RAS (Gao and Hannoush, 2014).

Palmitoylation is known to have a major effect on the intracellular trafficking of proteins (Greaves and Chamberlain, 2007). However, analysis of the localisation of EGFP-tagged caveolin-2 or HA-tagged IRAP constructs in HEK293T cells by confocal microscopy or biochemical methods did not reveal any effect of palmitoylation on the localisation of either protein. Caveolin-2 and IRAP both contain a membrane-spanning domain (Keller et al., 1995; Das et al., 1999), thus loss of membrane

attachment by palmitoylation site mutation was not expected, however even subtle changes in localisation were not apparent. In addition, palmitoylation of caveolin-2 was found to not be important for the partitioning of caveolin-2 into Triton X-100 resistant membrane domains, as has been previously demonstrated for the isoform caveolin-1 (Dietzen et al., 1995). Furthermore, although palmitoylation has been demonstrated to affect the stability of proteins (Linder and Deschenes, 2007; McCormick et al., 2008), no difference in the stability of a cysteine deficient mutant of IRAP was noted in this study.

Caveolin-1 and caveolin-2 were found to be major components of caveolae and form homo-oligomers and hetero-oligomers. Furthermore, these oligomeric assemblies were reported to be important for the biogenesis of caveolae (Monier et al., 1995; Scherer et al., 1997; Mora et al., 1999; Schlegel and Lisanti, 2000). In this study, the presence of both caveolin isoforms has been confirmed in caveolae, as caveolin-1 and caveolin-2 were identified to co-localise in “circular rosette” structures formed by caveolae at the PM of 3T3-L1 adipocytes. Additionally, the formation of caveolin-2 homo-oligomers and caveolin-2 hetero-oligomeric assemblies together with caveolin-1 was demonstrated in HEK293T cells that transiently expressed EGFP-tagged caveolin constructs. Interestingly, analysis by both SDS and blue native PAGE revealed that the palmitoylation of caveolin-2 affected the formation of homo-oligomeric assemblies of caveolin-2. These analyses suggest that palmitoylation of caveolin-2 is required for the formation of SDS-resistant aggregates of caveolin-2 and also favours the formation of caveolin-2 homo-dimers and homo-oligomers with an apparent molecular weight lower than 720 kDa. A similar effect has been previously reported for caveolin-1, where the attachment of long chain fatty acids and cholesterol was demonstrated to stabilise caveolin-1 oligomers (Monier et al., 1996). Albeit, it is known that the formation of large oligomeric assemblies of these proteins is important for the biogenesis of caveolae, the direct effect of palmitoylation on caveolae remains unknown and requires further examination. In particular, it will be interesting to knockdown caveolin-1/-2 expression in 3T3-L1 adipocytes and examine the ability of

palmitoylation-deficient mutants to rescue insulin signalling and GLUT4 trafficking pathways.

PALMITOYLATION AND INSULIN RESISTANCE

At present, it is too early to say if changes in palmitoylation might be linked to insulin resistant states or if targeting palmitoylation might be a therapeutic strategy to treat insulin resistance/diabetes. Clearly, many important players in the insulin signalling and GLUT4 trafficking pathways are palmitoylated but at present we lack a clear picture of how these proteins are regulated by this modification. One would predict that blocking palmitoylation of caveolin proteins might have effects on the assembly of caveolae, which could affect trafficking of both the IR and GLUT4.

Chronic insulin treatment or varying extracellular glucose concentrations did not have any effect on the extent of palmitoylation of the proteins studied here. Chronic insulin treatment was demonstrated to cause insulin resistance in 3T3-L1 adipocytes (Knutson et al., 1982) and hence change the signalling properties of this cell type. Low (5 mM) or high glucose (25 mM) conditions were included in this study to create similar glucose concentrations as the adipocytes of non-diabetic or type 2 diabetic patients are exposed to (Alberti and Zimmet, 1998). An increased palmitoylation (although not quantified) was observed for IRAP when 3T3-L1 adipocytes were cultured with 22.5 mM extracellular glucose or in adipocytes of obese mice (Ren et al., 2013b). However, in contrast to the study of Ren *et al.*, neither chronic insulin treatment nor varying extracellular glucose concentrations resulted in changes of palmitoylation of the proteins examined in this study including IRAP. This suggests that the extent of palmitoylation of these proteins probably does not play a major role in insulin resistance of 3T3-L1 adipocytes. Although this result does not exclude the role of palmitoylation in the development of insulin resistance, as palmitoylation levels in this assay were only examined after 24 h of treatment, when the cells have already acquired the condition. It is possible that insulin or elevated extracellular glucose concentration have transient effects on palmitoylation which were not picked up with this method.

It will be interesting in future work to examine how knockdown of specific zDHHC PAT enzymes affects insulin-stimulated GLUT4 trafficking; this would offer valuable information on whether the palmitoylation machinery is a potential new target for the modulation of insulin signalling and insulin resistance states. A major hurdle in the palmitoylation field is the lack of selective inhibitors. The development of such tools is likely to lead to rapid progress in our understanding of the importance of palmitoylation for insulin action, and these inhibitors might also offer translational development as new treatments to modulate insulin signalling.

Chapter 8: References

- Abel, E.D., O. Peroni, J.K. Kim, Y.B. Kim, O. Boss, E. Hadro, T. Minnemann, G.I. Shulman, and B.B. Kahn. 2001. Adipose-selective targeting of the GLUT4 gene impairs insulin action in muscle and liver. *Nature*. 409:729–733. doi:10.1038/35055575.
- Abrami, L., B. Kunz, I. Iacovache, and F.G. van der Goot. 2008. Palmitoylation and ubiquitination regulate exit of the Wnt signaling protein LRP6 from the endoplasmic reticulum. *Proc Natl Acad Sci U S A*. 105:5384–5389. doi:0710389105 [pii] 10.1073/pnas.0710389105.
- Abrami, L., S.H. Leppla, and F.G. van der Goot. 2006. Receptor palmitoylation and ubiquitination regulate anthrax toxin endocytosis. *J. Cell Biol.* 172:309–20. doi:10.1083/jcb.200507067.
- Alberti, K.G., and P.Z. Zimmet. 1998. Definition, diagnosis and classification of diabetes mellitus and its complications. Part 1: diagnosis and classification of diabetes mellitus provisional report of a WHO consultation. *Diabet. Med.* 15:539–53. doi:10.1002/(SICI)1096-9136(199807)15:7<539::AID-DIA668>3.0.CO;2-S.
- Albiston, a L., S.G. McDowall, D. Matsacos, P. Sim, E. Clune, T. Mustafa, J. Lee, F. a Mendelsohn, R.J. Simpson, L.M. Connolly, and S.Y. Chai. 2001. Evidence that the angiotensin IV (AT(4)) receptor is the enzyme insulin-regulated aminopeptidase. *J. Biol. Chem.* 276:48623–6. doi:10.1074/jbc.C100512200.
- Albiston, A.L., R.N. Fernando, H.R. Yeatman, P. Burns, L. Ng, D. Daswani, S. Diwakarla, V. Pham, and S.Y. Chai. 2010. Gene knockout of insulin-regulated aminopeptidase: loss of the specific binding site for angiotensin IV and age-related deficit in spatial memory. *Neurobiol. Learn. Mem.* 93:19–30. doi:10.1016/j.nlm.2009.07.011.
- Alessi, D.R., M. Andjelkovic, B. Caudwell, P. Cron, N. Morrice, P. Cohen, and B.A. Hemmings. 1996. Mechanism of activation of protein kinase B by insulin and IGF-1. *EMBO J.* 15:6541–6551.
- American Diabetes Association. 2004. Diagnosis and classification of diabetes mellitus. *Diabetes Care*. 27 Suppl 1:S5–S10. doi:10.2337/dc12-s064.
- American Diabetes Association. 2008. Diagnosis and classification of diabetes mellitus. *Diabetes Care*. 31 Suppl 1:S55–60. doi:10.2337/dc08-S055.
- Antonescu, C.N., M. Díaz, G. Femia, J. V Planas, and A. Klip. 2008. Clathrin-dependent and independent endocytosis of glucose transporter 4 (GLUT4) in

myoblasts: regulation by mitochondrial uncoupling. *Traffic*. 9:1173–90.
doi:10.1111/j.1600-0854.2008.00755.x.

Antonescu, C.N., M. Foti, N. Sauvonnnet, and A. Klip. 2009. Ready, set, internalize: mechanisms and regulation of GLUT4 endocytosis. *Biosci. Rep.* 29:1–11.
doi:10.1042/BSR20080105.

Antonny, B., D. Madden, S. Hamamoto, L. Orci, and R. Schekman. 2001. Dynamics of the COPII coat with GTP and stable analogues. *Nat Cell Biol.* 3:531–537.
doi:10.1038/35078500 35078500 [pii].

Aronoff, S.L., K. Berkowitz, B. Shreiner, and L. Want. 2004. Glucose Metabolism and Regulation: Beyond Insulin and Glucagon. *Diabetes Spectr.* 17:183–190.
doi:10.2337/diaspect.17.3.183.

Augustin, R. 2010. The protein family of glucose transport facilitators: It's not only about glucose after all. *IUBMB Life.* 62:315–33. doi:10.1002/iub.315.

Baker, E.N., T.L. Blundell, J.F. Cutfield, S.M. Cutfield, E.J. Dodson, G.G. Dodson, D.M. Hodgkin, R.E. Hubbard, N.W. Isaacs, C.D. Reynolds, and et al. 1988. The structure of 2Zn pig insulin crystals at 1.5 Å resolution. *Philos Trans R Soc L. B Biol Sci.* 319:369–456.

Baker, T.L., H. Zheng, J. Walker, J.L. Coloff, and J.E. Buss. 2003. Distinct rates of palmitate turnover on membrane-bound cellular and oncogenic H-ras. *J. Biol. Chem.* 278:19292–300. doi:10.1074/jbc.M206956200.

Balbis, A., G. Baquiran, C. Mounier, and B.I. Posner. 2004. Effect of insulin on caveolin-enriched membrane domains in rat liver. *J. Biol. Chem.* 279:39348–57.
doi:10.1074/jbc.M404280200.

Barlowe, C., L. Orci, T. Yeung, M. Hosobuchi, S. Hamamoto, N. Salama, M.F. Rexach, M. Ravazzola, M. Amherdt, and R. Schekman. 1994. COPII: a membrane coat formed by Sec proteins that drive vesicle budding from the endoplasmic reticulum. *Cell.* 77:895–907.

Bass, J., G. Chiu, Y. Argon, and D.F. Steiner. 1998. Folding of insulin receptor monomers is facilitated by the molecular chaperones calnexin and calreticulin and impaired by rapid dimerization. *J. Cell Biol.* 141:637–46.

Bastiani, M., L. Liu, M.M. Hill, M.P. Jedrychowski, S.J. Nixon, H.P. Lo, D. Abankwa, R. Luetterforst, M. Fernandez-Rojo, M.R. Breen, S.P. Gygi, J. Vinten, P.J. Walser, K.N. North, J.F. Hancock, P.F. Pilch, and R.G. Parton. 2009. MURC/Cavin-4 and cavin family members form tissue-specific caveolar complexes. *J. Cell Biol.* 185:1259–73. doi:10.1083/jcb.200903053.

- Bhattacharyya, R., C. Barren, and D.M. Kovacs. 2013. Palmitoylation of amyloid precursor protein regulates amyloidogenic processing in lipid rafts. *J. Neurosci.* 33:11169–83. doi:10.1523/JNEUROSCI.4704-12.2013.
- Bi, X., R.A. Corpina, and J. Goldberg. 2002. Structure of the Sec23/24-Sar1 pre-budding complex of the COPII vesicle coat. *Nature.* 419:271–7. doi:10.1038/nature01040.
- Bickel, P.E. 1997. Flotillin and Epidermal Surface Antigen Define a New Family of Caveolae-associated Integral Membrane Proteins. *J. Biol. Chem.* 272:13793–13802. doi:10.1074/jbc.272.21.13793.
- Blot, V., and T.E. McGraw. 2006. GLUT4 is internalized by a cholesterol-dependent nystatin-sensitive mechanism inhibited by insulin. *EMBO J.* 25:5648–58. doi:10.1038/sj.emboj.7601462.
- Boettner, D.R., R.J. Chi, and S.K. Lemmon. 2011. Lessons from yeast for clathrin-mediated endocytosis. *Nat Cell Biol.* 14:2–10. doi:10.1038/ncb2403 ncb2403 [pii].
- Bonifacino, J.S., and B.S. Glick. 2004. The mechanisms of vesicle budding and fusion. *Cell.* 116:153–166. doi:S0092867403010791 [pii].
- Bonifacino, J.S., and J. Lippincott-Schwartz. 2003. Coat proteins: shaping membrane transport. *Nat Rev Mol Cell Biol.* 4:409–414. doi:10.1038/nrm1099.
- Briand, N., I. Dugail, and S. Le Lay. 2011. Cavin proteins: New players in the caveolae field. *Biochimie.* 93:71–7. doi:10.1016/j.biochi.2010.03.022.
- Brown, D.A., and E. London. 1998. Functions of lipid rafts in biological membranes. *Annu. Rev. Cell Dev. Biol.* 14:111–36. doi:10.1146/annurev.cellbio.14.1.111.
- Brownlee, M. 2005. The pathobiology of diabetic complications: a unifying mechanism. *Diabetes.* 54:1615–25.
- Brunetti, A., G. Manfioletti, E. Chiefari, I.D. Goldfine, and D. Foti. 2001. Transcriptional regulation of human insulin receptor gene by the high-mobility group protein HMGI(Y). *FASEB J.* 15:492–500. doi:10.1096/fj.00-0190com.
- Bryant, N.J., R. Govers, and D.E. James. 2002. Regulated transport of the glucose transporter GLUT4. *Nat Rev Mol Cell Biol.* 3:267–277. doi:10.1038/nrm782.
- Burgener, R., M. Wolf, T. Ganz, and M. Baggiolini. 1990. Purification and characterization of a major phosphatidylserine-binding phosphoprotein from human platelets.

- Capozza, F., T.P. Combs, A.W. Cohen, Y.-R. Cho, S.-Y. Park, W. Schubert, T.M. Williams, D.L. Brasaemle, L. a Jelicks, P.E. Scherer, J.K. Kim, and M.P. Lisanti. 2005. Caveolin-3 knockout mice show increased adiposity and whole body insulin resistance, with ligand-induced insulin receptor instability in skeletal muscle. *Am. J. Physiol. Cell Physiol.* 288:C1317–31. doi:10.1152/ajpcell.00489.2004.
- Chai, S.Y., R. Fernando, G. Peck, S.-Y. Ye, F. a O. Mendelsohn, T. a Jenkins, and a L. Albiston. 2004. The angiotensin IV/AT4 receptor. *Cell. Mol. Life Sci.* 61:2728–37. doi:10.1007/s00018-004-4246-1.
- Chamberlain, L.H., and G.W. Gould. 2002. The vesicle- and target-SNARE proteins that mediate Glut4 vesicle fusion are localized in detergent-insoluble lipid rafts present on distinct intracellular membranes. *J. Biol. Chem.* 277:49750–4. doi:10.1074/jbc.M206936200.
- Chang, T.H., and S.E. Polakis. 1978. Differentiation of 3T3-L1 fibroblasts to adipocytes. Effect of insulin and indomethacin on the levels of insulin receptors. *J. Biol. Chem.* 253:4693–6.
- Chawla, A., E.J. Schwarz, D.D. Dimaculangan, M.A. Lazar, and A. Lazar. 1994. Peroxisome proliferator-activated receptor (PPAR) gamma: adipose-predominant expression and induction early in adipocyte differentiation. *Endocrinology.* 135:798–800. doi:10.1210/endo.135.2.8033830.
- Chen, J., F. Capozza, A. Wu, T. Deangelis, H. Sun, M. Lisanti, and R. Baserga. 2008. Regulation of insulin receptor substrate-1 expression levels by caveolin-1. *J. Cell. Physiol.* 217:281–9. doi:10.1002/jcp.21498.
- Chen, Y.A., and R.H. Scheller. 2001. SNARE-mediated membrane fusion. *Nat Rev Mol Cell Biol.* 2:98–106. doi:10.1038/35052017.
- Chi, N.W., and H.F. Lodish. 2000. Tankyrase is a golgi-associated mitogen-activated protein kinase substrate that interacts with IRAP in GLUT4 vesicles. *J. Biol. Chem.* 275:38437–44. doi:10.1074/jbc.M007635200.
- Chiang, S.H., C.A. Baumann, M. Kanzaki, D.C. Thurmond, R.T. Watson, C.L. Neudauer, I.G. Macara, J.E. Pessin, and A.R. Saltiel. 2001. Insulin-stimulated GLUT4 translocation requires the CAP-dependent activation of TC10. *Nature.* 410:944–8. doi:10.1038/35073608.
- Choudhury, A., D.L. Marks, K.M. Proctor, G.W. Gould, and R.E. Pagano. 2006. Regulation of caveolar endocytosis by syntaxin 6-dependent delivery of membrane components to the cell surface. *Nat. Cell Biol.* 8:317–28. doi:10.1038/ncb1380.

- Clausen, T. 2008. Regulatory role of translocation of Na⁺-K⁺ pumps in skeletal muscle: hypothesis or reality? *Am. J. Physiol. Endocrinol. Metab.* 295:E727–728. doi:10.1152/ajpendo.90494.2008.
- Cohen, A.W., B. Razani, X.B. Wang, T.P. Combs, T.M. Williams, P.E. Scherer, and M.P. Lisanti. 2003. Caveolin-1-deficient mice show insulin resistance and defective insulin receptor protein expression in adipose tissue. *Am. J. Physiol. Cell Physiol.* 285:C222–35. doi:10.1152/ajpcell.00006.2003.
- Collins, K.M., and W.T. Wickner. 2007. Trans-SNARE complex assembly and yeast vacuole membrane fusion. *Proc Natl Acad Sci U S A.* 104:8755–8760. doi:0702290104 [pii] 10.1073/pnas.0702290104.
- Cook, B.D., J.N. Dynek, W. Chang, G. Shostak, and S. Smith. 2002. Role for the Related Poly(ADP-Ribose) Polymerases Tankyrase 1 and 2 at Human Telomeres. *Mol. Cell. Biol.* 22:332–342. doi:10.1128/MCB.22.1.332-342.2002.
- Couet, J., M.M. Belanger, E. Roussel, and M.-C. Drolet. 2001. Cell biology of caveolae and caveolin. *Adv. Drug Deliv. Rev.* 49:223–235. doi:10.1016/S0169-409X(01)00139-9.
- Czech, M.P., and J.M. Buxton. 1993. Insulin action on the internalization of the GLUT4 glucose transporter in isolated rat adipocytes. *J. Biol. Chem.* 268:9187–90.
- Czech, M.P., M. Tencerova, D.J. Pedersen, and M. Aouadi. 2013. Insulin signalling mechanisms for triacylglycerol storage. *Diabetologia.* 56:949–64. doi:10.1007/s00125-013-2869-1.
- Das, K., R.Y. Lewis, P.E. Scherer, and M.P. Lisanti. 1999. The Membrane-spanning Domains of Caveolins-1 and -2 Mediate the Formation of Caveolin Hetero-oligomers: IMPLICATIONS FOR THE ASSEMBLY OF CAVEOLAE MEMBRANES IN VIVO. *J. Biol. Chem.* 274:18721–18728. doi:10.1074/jbc.274.26.18721.
- Delandre, C., T.R. Penabaz, a L. Passarelli, S.K. Chapes, and R.J. Clem. 2009. Mutation of juxtamembrane cysteines in the tetraspanin CD81 affects palmitoylation and alters interaction with other proteins at the cell surface. *Exp. Cell Res.* 315:1953–63. doi:10.1016/j.yexcr.2009.03.013.
- Dietzen, D.J., W.R. Hastings, and D.M. Lublin. 1995. Caveolin is palmitoylated on multiple cysteine residues. Palmitoylation is not necessary for localization of caveolin to caveolae. *J Biol Chem.* 270:6838–6842.
- Ding, J., and K. Du. 2009. ClipR-59 interacts with Akt and regulates Akt cellular compartmentalization. *Mol. Cell. Biol.* 29:1459–71. doi:10.1128/MCB.00754-08.

- Dodson, G.G., and J.L. Whittingham. 2002. Insulin: Sequence, structure and function - A story of surprises. *Insul. Relat. Proteins - Struct. to Funct. Pharmacol.* 29–39.
- Dumaresq-Doiron, K., F. Jules, and S. Lefrancois. 2013. Sortilin turnover is mediated by ubiquitination. *Biochem. Biophys. Res. Commun.* 433:90–5. doi:10.1016/j.bbrc.2013.02.059.
- Duncan, J.A., and A.G. Gilman. 1998. A cytoplasmic acyl-protein thioesterase that removes palmitate from G protein alpha subunits and p21(RAS). *J. Biol. Chem.* 273:15830–7.
- Dupree, P., R.G. Parton, G. Raposo, T. V Kurzchalia, and K. Simons. 1993. Caveolae and sorting in the trans-Golgi network of epithelial cells. *EMBO J.* 12:1597–605.
- El-Husseini Ael, D., E. Schnell, S. Dakoji, N. Sweeney, Q. Zhou, O. Prange, C. Gauthier-Campbell, A. Aguilera-Moreno, R.A. Nicoll, and D.S. Bredt. 2002. Synaptic strength regulated by palmitate cycling on PSD-95. *Cell.* 108:849–863. doi:S0092867402006839 [pii].
- Fagerholm, S., U. Ortegren, M. Karlsson, I. Ruishalme, and P. Strålfors. 2009. Rapid insulin-dependent endocytosis of the insulin receptor by caveolae in primary adipocytes. *PLoS One.* 4:e5985. doi:10.1371/journal.pone.0005985.
- Fan, J.Y., J.L. Carpentier, E. van Obberghen, C. Grunfeld, P. Gorden, and L. Orci. 1983. Morphological changes of the 3T3-L1 fibroblast plasma membrane upon differentiation to the adipocyte form. *J. Cell Sci.* 61:219–30.
- Fernandez, I., Y. Ying, J. Albanesi, and R.G.W. Anderson. 2002. Mechanism of caveolin filament assembly. *Proc. Natl. Acad. Sci. U. S. A.* 99:11193–8. doi:10.1073/pnas.172196599.
- Fernández-Hernando, C., M. Fukata, P.N. Bernatchez, Y. Fukata, M.I. Lin, D.S. Bredt, and W.C. Sessa. 2006. Identification of Golgi-localized acyl transferases that palmitoylate and regulate endothelial nitric oxide synthase. *J. Cell Biol.* 174:369–77. doi:10.1083/jcb.200601051.
- Feron, O., L. Belhassen, L. Kobzik, T.W. Smith, R.A. Kelly, and T. Micheal. 1996. Endothelial Nitric Oxide Synthase Targeting to Caveolae. SPECIFIC INTERACTIONS WITH CAVEOLIN ISOFORMS IN CARDIAC MYOCYTES AND ENDOTHELIAL CELLS. *J. Biol. Chem.* 271:22810–22814. doi:10.1074/jbc.271.37.22810.
- Fielding, P.E., P. Chau, D. Liu, T. a Spencer, and C.J. Fielding. 2004. Mechanism of platelet-derived growth factor-dependent caveolin-1 phosphorylation: relationship to sterol binding and the role of serine-80. *Biochemistry.* 43:2578–86. doi:10.1021/bi035442c.

- Fielding, P.E., and C.J. Fielding. 1995. Plasma membrane caveolae mediate the efflux of cellular free cholesterol. *Biochemistry*. 34:14288–92.
- Fleige, S., and M.W. Pfaffl. 2006. RNA integrity and the effect on the real-time qRT-PCR performance. *Mol. Aspects Med.* 27:126–39. doi:10.1016/j.mam.2005.12.003.
- Fletcher, L.M., G.I. Welsh, P.B. Oatey, and J.M. Tavaré. 2000. Role for the microtubule cytoskeleton in GLUT4 vesicle trafficking and in the regulation of insulin-stimulated glucose uptake. *Biochem J.* 352 Pt 2:267–276.
- Forrester, M.T., D.T. Hess, J.W. Thompson, R. Hultman, M.A. Moseley, J.S. Stamler, and P.J. Casey. 2011. Site-specific analysis of protein S-acylation by resin-assisted capture. *J Lipid Res.* 52:393–398. doi:10.1194/jlr.D011106 [pii] 10.1194/jlr.D011106.
- Foti, M., G. Porcheron, M. Fournier, C. Maeder, and J.-L. Carpentier. 2007. The neck of caveolae is a distinct plasma membrane subdomain that concentrates insulin receptors in 3T3-L1 adipocytes. *Proc. Natl. Acad. Sci. U. S. A.* 104:1242–7. doi:10.1073/pnas.0610523104.
- Fra, a M., E. Williamson, K. Simons, and R.G. Parton. 1995. De novo formation of caveolae in lymphocytes by expression of VIP21-caveolin. *Proc. Natl. Acad. Sci. U. S. A.* 92:8655–9.
- Fujimoto, T., H. Kogo, K. Ishiguro, K. Tauchi, and R. Nomura. 2001. Caveolin-2 is targeted to lipid droplets, a new “membrane domain” in the cell. *J. Cell Biol.* 152:1079–85.
- Fujimoto, T., H. Kogo, R. Nomura, and T. Une. 2000. Isoforms of caveolin-1 and caveolar structure. *J. Cell Sci.* 113 Pt 19:3509–17.
- Fukata, M., Y. Fukata, H. Adesnik, R.A. Nicoll, D.S. Bredt, and S. Francisco. 2004. Identification of PSD-95 palmitoylating enzymes. *Neuron.* 44:987–996. doi:S0896627304007937 [pii] 10.1016/j.neuron.2004.12.005.
- Fukata, Y., A. Dimitrov, G. Boncompain, O. Vielemeyer, F. Perez, and M. Fukata. 2013. Local palmitoylation cycles define activity-regulated postsynaptic subdomains. *J. Cell Biol.* 202:145–61. doi:10.1083/jcb.201302071.
- Fukumoto, H., T. Kayano, J.B. Buse, Y. Edwards, P.F. Pilch, G.I. Bell, and S. Seino. 1989. Cloning and characterization of the major insulin-responsive glucose transporter expressed in human skeletal muscle and other insulin-responsive tissues. *J. Biol. Chem.* 264:7776–9.

- Gabella, G. 1976. Quantitative morphological study of smooth muscle cells of the guinea-pig taenia coli. *Cell Tissue Res.* 170. doi:10.1007/BF00224297.
- Galbiati, F., D. Volonté, C. Minetti, J.B. Chu, and M.P. Lisanti. 1999. Phenotypic Behavior of Caveolin-3 Mutations That Cause Autosomal Dominant Limb Girdle Muscular Dystrophy (LGMD-1C). RETENTION OF LGMD-1C CAVEOLIN-3 MUTANTS WITHIN THE GOLGI COMPLEX. *J. Biol. Chem.* 274:25632–25641. doi:10.1074/jbc.274.36.25632.
- Gammeltoft, S., and E. Vanobberghen. 1986. Protein-Kinase Activity of the Insulin-Receptor. *Biochem. J.* 235:1–11.
- Gao, X., and R.N. Hannoush. 2014. Method for cellular imaging of palmitoylated proteins with clickable probes and proximity ligation applied to Hedgehog, tubulin, and Ras. *J. Am. Chem. Soc.* 136:4544–50. doi:10.1021/ja410068g.
- Garvey, W.T., L. Maianu, T.P. Huecksteadt, M.J. Birnbaum, J.M. Molina, and T.P. Ciaraldi. 1991. Pretranslational Suppression of a Glucose Transporter Protein Causes Insulin Resistance in Adipocytes from Patients with Non-Insulin-Dependent Diabetes-Mellitus and Obesity. *J. Clin. Invest.* 87:1072–1081.
- Gedulin, B.R., T.J. Rink, and A.A. Young. 1997. Dose-response for glucagonostatic effect of amylin in rats. *Metabolism.* 46:67–70.
- Gil, J. 1983. Number and distribution of plasmalemmal vesicles in the lung. *Fed. Proc.* 42:2414–8.
- Glenney, J.R. 1989. Novel tyrosine kinase substrates from Rous sarcoma virus-transformed cells are present in the membrane skeleton. *J. Cell Biol.* 108:2401–2408. doi:10.1083/jcb.108.6.2401.
- Glenney, J.R. 1992. The sequence of human caveolin reveals identity with VIP21, a component of transport vesicles. *FEBS Lett.* 314:45–8.
- Gómez-Ruiz, A., F.I. Milagro, J. Campión, J.A. Martínez, and C. de Miguel. 2011. High-fat diet feeding alters metabolic response to fasting/non fasting conditions. Effect on caveolin expression and insulin signalling. *Lipids Health Dis.* 10:55. doi:10.1186/1476-511X-10-55.
- González-Muñoz, E., C. López-Iglesias, M. Calvo, M. Palacín, A. Zorzano, and M. Camps. 2009. Caveolin-1 loss of function accelerates glucose transporter 4 and insulin receptor degradation in 3T3-L1 adipocytes. *Endocrinology.* 150:3493–502. doi:10.1210/en.2008-1520.
- Gorleku, O.A., A.-M. Barns, G.R. Prescott, J. Greaves, and L.H. Chamberlain. 2011. Endoplasmic reticulum localization of DHHC palmitoyltransferases mediated by

- lysine-based sorting signals. *J. Biol. Chem.* 286:39573–84.
doi:10.1074/jbc.M111.272369.
- Gould, G.W., and G.D. Holmant. 1993. The glucose transporter family : structure ,
function and tissue-specific expression. 341:329–341.
- Govers, R., A.C.F. Coster, and D.E. James. 2004. Insulin increases cell surface GLUT4
levels by dose dependently discharging GLUT4 into a cell surface recycling
pathway. *Mol. Cell. Biol.* 24:6456–6466. doi:Doi 10.1128/Mcb.24.14.6456-
6466.2004.
- Greaves, J., J. a Carmichael, and L.H. Chamberlain. 2011. The palmitoyl transferase
DHHC2 targets a dynamic membrane cycling pathway: regulation by a C-
terminal domain. *Mol. Biol. Cell.* 22:1887–95. doi:10.1091/mbc.E10-11-0924.
- Greaves, J., and L.H. Chamberlain. 2006. Dual role of the cysteine-string domain in
membrane binding and palmitoylation-dependent sorting of the molecular
chaperone cysteine-string protein. *Mol. Biol. Cell.* 17:4748–59.
doi:10.1091/mbc.E06-03-0183.
- Greaves, J., and L.H. Chamberlain. 2007. Palmitoylation-dependent protein sorting. *J*
Cell Biol. 176:249–254. doi:jcb.200610151 [pii] 10.1083/jcb.200610151.
- Greaves, J., and L.H. Chamberlain. 2011a. DHHC palmitoyl transferases: substrate
interactions and (patho)physiology. *Trends Biochem Sci.* 36:245–253.
doi:S0968-0004(11)00014-4 [pii] 10.1016/j.tibs.2011.01.003.
- Greaves, J., and L.H. Chamberlain. 2011b. Differential palmitoylation regulates
intracellular patterning of SNAP25. *J. Cell Sci.* 124:1351–60.
doi:10.1242/jcs.079095.
- Greaves, J., O.A. Gorleku, C. Salaun, and L.H. Chamberlain. 2010. Palmitoylation of
the SNAP25 protein family: specificity and regulation by DHHC palmitoyl
transferases. *J Biol Chem.* 285:24629–24638. doi:M110.119289 [pii]
10.1074/jbc.M110.119289.
- Green, H., and O. Kehinde. 1972. Sublines of Mouse 3T3 Cells That Accumulate
Lipid.
- Green, H., and O. Kehinde. 1975. An established preadipose cell line and its
differentiation in culture. II. Factors affecting the adipose conversion. *Cell.*
5:19–27. doi:0092-8674(75)90087-2 [pii].
- Guariguata, L., D.R. Whiting, I. Hambleton, J. Beagley, U. Linnenkamp, and J.E. Shaw.
2014. Global estimates of diabetes prevalence for 2013 and projections for

2035. *Diabetes Res. Clin. Pract.* 103:137–49.
doi:10.1016/j.diabres.2013.11.002.

Gundersen, C.B., A. Mastrogiacomo, K. Faull, and J.A. Umbach. 1994. Extensive lipidation of a Torpedo cysteine string protein. *J. Biol. Chem.* 269:19197–9.

Gupta, A.K., R. V. Clark, and K.A. Kirchner. 1992. Effects of insulin on renal sodium excretion. *Hypertension.* 19:178–178. doi:10.1161/01.HYP.19.1_Suppl.178.

Gustavsson, J., S. Parpal, M. Karlsson, C. Ramsing, H. Thorn, M. Borg, M. Lindroth, K.H. Peterson, K.E. Magnusson, and P. Stralfors. 1999. Localization of the insulin receptor in caveolae of adipocyte plasma membrane. *FASEB J.* 13:1961–1971.

Gustavsson, J., S. Parpal, and P. Strålfors. 1996. Insulin-stimulated glucose uptake involves the transition of glucose transporters to a caveolae-rich fraction within the plasma membrane: implications for type II diabetes. *Mol. Med.* 2:367–72.

Haney, P.M., J.W. Slot, R.C. Piper, D.E. James, and M. Mueckler. 1991. Intracellular targeting of the insulin-regulatable glucose transporter (GLUT4) is isoform specific and independent of cell type. *J. Cell Biol.* 114:689–699.
doi:10.1083/jcb.114.4.689.

Hansen, C.G., N.A. Bright, G. Howard, and B.J. Nichols. 2009. SDPR induces membrane curvature and functions in the formation of caveolae. *Nat. Cell Biol.* 11:807–14. doi:10.1038/ncb1887.

Hashiramoto, M., and D.E. James. 2000. Characterization of insulin-responsive GLUT4 storage vesicles isolated from 3T3-L1 adipocytes. *Mol. Cell. Biol.* 20:416–27.

Hayashi, T., G. Rumbaugh, and R.L. Huganir. 2005. Differential regulation of AMPA receptor subunit trafficking by palmitoylation of two distinct sites. *Neuron.* 47:709–723. doi:S0896-6273(05)00645-8 [pii] 10.1016/j.neuron.2005.06.035.

Hayashi, T., G.M. Thomas, and R.L. Huganir. 2009. Dual palmitoylation of NR2 subunits regulates NMDA receptor trafficking. *Neuron.* 64:213–26.
doi:10.1016/j.neuron.2009.08.017.

Hayer, A., M. Stoeber, C. Bissig, and A. Helenius. 2010. Biogenesis of caveolae: stepwise assembly of large caveolin and cavin complexes. *Traffic.* 11:361–82.
doi:10.1111/j.1600-0854.2009.01023.x.

Henley, J.R., E.W.A. Krueger, B.J. Oswald, and M.A. Mcniven. 1998. Dynamin-mediated Internalization of Caveolae. 141:85–99.

- Herbst, J.J., S.A. Ross, H.M. Scott, S.A. Bobin, N.J. Morris, G.E. Lienhard, and S.R. Keller. 1997. Insulin stimulates cell surface aminopeptidase activity toward vasopressin in adipocytes. *Am. J. Physiol. Endocrinol. Metab.* 35:E600–E606.
- Hill, M.M., M. Bastiani, R. Luetterforst, M. Kirkham, A. Kirkham, S.J. Nixon, P. Walser, D. Abankwa, V.M.J. Oorschot, S. Martin, J.F. Hancock, and R.G. Parton. 2008. PTRF-Cavin, a conserved cytoplasmic protein required for caveola formation and function. *Cell.* 132:113–24. doi:10.1016/j.cell.2007.11.042.
- Ho, G.P.H., B. Selvakumar, J. Mukai, L.D. Hester, Y. Wang, J.A. Gogos, and S.H. Snyder. 2011. S-nitrosylation and S-palmitoylation reciprocally regulate synaptic targeting of PSD-95. *Neuron.* 71:131–41. doi:10.1016/j.neuron.2011.05.033.
- Hosaka, T., C.C. Brooks, E. Presman, S.-K. Kim, Z. Zhang, M. Breen, D.N. Gross, E. Sztul, and P.F. Pilch. 2005. p115 Interacts with the GLUT4 vesicle protein, IRAP, and plays a critical role in insulin-stimulated GLUT4 translocation. *Mol. Biol. Cell.* 16:2882–90. doi:10.1091/mbc.E05-01-0072.
- Hou, H., A.T. John Peter, C. Meiringer, K. Subramanian, and C. Ungermann. 2009. Analysis of DHHC acyltransferases implies overlapping substrate specificity and a two-step reaction mechanism. *Traffic.* 10:1061–73. doi:10.1111/j.1600-0854.2009.00925.x.
- Houssay, B.A., V.G. Foglia, F.S. Smyth, C.T. Rietti, and A.B. Houssay. 1942. THE HYPOPHYSIS AND SECRETION OF INSULIN. *J. Exp. Med.* 75:547–66.
- Hruz, P.W., and M.M. Mueckler. 2001. Structural analysis of the GLUT1 facilitative glucose transporter (review). *Mol Membr Biol.* 18:183–193.
- Hu, J., J. Liu, R. Ghirlando, A.R. Saltiel, S.R. Hubbard, and A. Arbor. 2003. Structural Basis for Recruitment of the Adaptor Protein APS to the Activated Insulin Receptor. *Mol. Cell.* 12:1379–1389.
- Huang, J., T. Imamura, and J.M. Olefsky. 2001. Insulin can regulate GLUT4 internalization by signaling to Rab5 and the motor protein dynein. *Proc. Natl. Acad. Sci. U. S. A.* 98:13084–9. doi:10.1073/pnas.241368698.
- Huang, K., S. Sanders, R. Singaraja, P. Orban, T. Cijssouw, P. Arstikaitis, A. Yanai, M.R. Hayden, and A. El-Husseini. 2009. Neuronal palmitoyl acyl transferases exhibit distinct substrate specificity. *FASEB J.* 23:2605–15. doi:10.1096/fj.08-127399.
- Huang, K., A. Yanai, R. Kang, P. Arstikaitis, R.R. Singaraja, M. Metzler, A. Mullard, B. Haigh, C. Gauthier-Campbell, C.-A. Gutekunst, M.R. Hayden, and A. El-Husseini. 2004. Huntingtin-interacting protein HIP14 is a palmitoyl transferase involved

- in palmitoylation and trafficking of multiple neuronal proteins. *Neuron*. 44:977–86. doi:10.1016/j.neuron.2004.11.027.
- Huang, S., L.M. Lifshitz, C. Jones, K.D. Bellve, C. Standley, S. Fonseca, S. Corvera, K.E. Fogarty, and M.P. Czech. 2007. Insulin stimulates membrane fusion and GLUT4 accumulation in clathrin coats on adipocyte plasma membranes. *Mol. Cell. Biol.* 27:3456–69. doi:10.1128/MCB.01719-06.
- Huang, S.H., and M.P. Czech. 2007. The GLUT4 glucose transporter. *Cell Metab.* 5:237–252. doi:DOI 10.1016/j.cmet.2007.03.006.
- Hubbard, S.R., L. Wei, L. Ellis, and W.A. Hendrickson. 1994. Crystal structure of the tyrosine kinase domain of the human insulin receptor. *Nature*. 372:746–754. doi:10.1038/372746a0.
- Hurtado del Pozo, C., R.M. Calvo, G. Vesperinas-García, J. Gómez-Ambrosi, G. Frühbeck, R. Corripio-Sánchez, M. a Rubio, and M.-J. Obregon. 2010. IPO8 and FBXL10: new reference genes for gene expression studies in human adipose tissue. *Obesity (Silver Spring)*. 18:897–903. doi:10.1038/oby.2009.374.
- Hurtley, S.M., and A. Helenius. 1989. Protein oligomerization in the endoplasmic reticulum. *Annu. Rev. Cell Biol.* 5:277–307. doi:10.1146/annurev.cb.05.110189.001425.
- Inoue, M., L. Chang, J. Hwang, S.-H. Chiang, and A.R. Saltiel. 2003. The exocyst complex is required for targeting of Glut4 to the plasma membrane by insulin. *Nature*. 422:629–33. doi:10.1038/nature01533.
- Ishikura, S., a Koshkina, and a Klip. 2008. Small G proteins in insulin action: Rab and Rho families at the crossroads of signal transduction and GLUT4 vesicle traffic. *Acta Physiol. (Oxf)*. 192:61–74. doi:10.1111/j.1748-1716.2007.01778.x.
- Iwanishi, M., T. Haruta, Y. Takata, O. Ishibashi, T. Sasaoka, K. Egawa, T. Imamura, K. Naitou, T. Itazu, and M. Kobayashi. 1993. A mutation (Trp1193?Leu1193) in the tyrosine kinase domain of the insulin receptor associated with type A syndrome of insulin resistance. *Diabetologia*. 36:414–422. doi:10.1007/BF00402277.
- Izumi, T., Y. Shibatas, and T. Yamamoto. 1989. The Cytoplasmic Surface Structures of Uncoated Vesicles in Various Tissues of Rat as Revealed by Quick-Freeze, Deep-Etching Replicas. *Microsc.* 38:47–53.
- Jahn, R., T. Lang, and T.C. Sudhof. 2003. Membrane fusion. *Cell*. 112:519–533.

- James, D.E., K.M. Burleigh, and E.W. Kraegen. 1985. Time dependence of insulin action in muscle and adipose tissue in the rat in vivo. An increasing response in adipose tissue with time. *Diabetes*. 34:1049–1054.
- Jansa, P., S.W. Mason, U. Hoffmann-Rohrer, and I. Grummt. 1998. Cloning and functional characterization of PTRF, a novel protein which induces dissociation of paused ternary transcription complexes. *EMBO J*. 17:2855–64. doi:10.1093/emboj/17.10.2855.
- JeBailey, L., A. Rudich, X. Huang, C. Di Ciano-Oliveira, A. Kapus, and A. Klip. 2004. Skeletal muscle cells and adipocytes differ in their reliance on TC10 and Rac for insulin-induced actin remodeling. *Mol. Endocrinol*. 18:359–72. doi:10.1210/me.2003-0294.
- Jiang, Z.Y., A. Chawla, A. Bose, M. Way, and M.P. Czech. 2002. A phosphatidylinositol 3-kinase-independent insulin signaling pathway to N-WASP/Arp2/3/F-actin required for GLUT4 glucose transporter recycling. *J. Biol. Chem*. 277:509–15. doi:10.1074/jbc.M108280200.
- Johnson, a O., M. a Lampson, and T.E. McGraw. 2001. A di-leucine sequence and a cluster of acidic amino acids are required for dynamic retention in the endosomal recycling compartment of fibroblasts. *Mol. Biol. Cell*. 12:367–81.
- Jordan, S.D., A.C. Konner, and J.C. Bruning. 2010. Sensing the fuels: glucose and lipid signaling in the CNS controlling energy homeostasis. *Cell Mol Life Sci*. 67:3255–3273. doi:10.1007/s00018-010-0414-7.
- Jordens, I., D. Molle, W. Xiong, S.R. Keller, and T.E. McGraw. 2010. Insulin-regulated aminopeptidase is a key regulator of GLUT4 trafficking by controlling the sorting of GLUT4 from endosomes to specialized insulin-regulated vesicles. *Mol. Biol. Cell*. 21:2034–44. doi:10.1091/mbc.E10-02-0158.
- Kahn, S.E., R.L. Hull, and K.M. Utzschneider. 2006. Mechanisms linking obesity to insulin resistance and type 2 diabetes. *Nature*. 444:840–6. doi:10.1038/nature05482.
- Kaiser, N., S. Sasson, E.P. Feener, N. Boukobza-Vardi, S. Higashi, D.E. Moller, S. Davidheiser, R.J. Przybylski, and G.L. King. 1993. Differential regulation of glucose transport and transporters by glucose in vascular endothelial and smooth muscle cells. *Diabetes*. 42:80–9.
- Kandror, K. V, J.M. Stephens, and P.E. Pilch. 1995. Expression and Compartmentalization of Caveolin in Adipose Cells : Coordinate Regulation with and Structural Segregation from GLUT4 Fractionation of Intracellular Microsomes. 129.

- Kandror, K. V, L. Yu, and P.F. Pilch. 1994. The major protein of GLUT4-containing vesicles, gp160, has aminopeptidase activity. *J. Biol. Chem.* 269:30777–30780.
- Kane, S., H. Sano, S.C.H. Liu, J.M. Asara, W.S. Lane, C.C. Garner, and G.E. Lienhard. 2002. A method to identify serine kinase substrates. Akt phosphorylates a novel adipocyte protein with a Rab GTPase-activating protein (GAP) domain. *J. Biol. Chem.* 277:22115–8. doi:10.1074/jbc.C200198200.
- Kang, R., J. Wan, P. Arstikaitis, H. Takahashi, K. Huang, A.O. Bailey, J.X. Thompson, A.F. Roth, R.C. Drisdell, R. Mastro, W.N. Green, J.R. Yates, N.G. Davis, and A. El-Husseini. 2008. Neural palmitoyl-proteomics reveals dynamic synaptic palmitoylation. *Nature.* 456:904–9. doi:10.1038/nature07605.
- Karlsson, M., H. Thorn, A. Danielsson, K.G. Stenkula, A. Ost, J. Gustavsson, F.H. Nystrom, and P. Strålfors. 2004. Colocalization of insulin receptor and insulin receptor substrate-1 to caveolae in primary human adipocytes. Cholesterol depletion blocks insulin signalling for metabolic and mitogenic control. *Eur. J. Biochem.* 271:2471–9. doi:10.1111/j.1432-1033.2004.04177.x.
- Karlsson, M., H. Thorn, S. Parpal, P. Strålfors, and J. Gustavsson. 2002. Insulin induces translocation of glucose transporter GLUT4 to plasma membrane caveolae in adipocytes. *FASEB J.* 16:249–51. doi:10.1096/fj.01-0646fje.
- Karylowski, O., A. Zeigerer, A. Cohen, and T.E. McGraw. 2004. GLUT4 is retained by an intracellular cycle of vesicle formation and fusion with endosomes. *Mol. Biol. Cell.* 15:870–882. doi:10.1091/mbc.E03-07-0517 E03-07-0517 [pii].
- Katz, E.B., A.E. Stenbit, K. Hatton, R. DePinho, and M.J. Charron. 1995a. Cardiac and adipose tissue abnormalities but not diabetes in mice deficient in GLUT4. *Nature.* 377:151–5. doi:10.1038/377151a0.
- Katz, J.D., C. Benoist, and D. Mathis. 1995b. T helper cell subsets in insulin-dependent diabetes. *Science (80-).* 268:1185–1188.
- Keller, P., and K. Simons. 1997. Post-Golgi biosynthetic trafficking. *J. Cell Sci.* 110:3001–3009.
- Keller, S.R., H.M. Scott, C.C. Mastick, R. Aebersold, and G.E. Lienhard. 1995. Cloning and characterization of a novel insulin-regulated membrane aminopeptidase from Glut4 vesicles. *J. Biol. Chem.* 270:23612–8.
- Kellett, G.L., and P.A. Helliwell. 2000. The diffusive component of intestinal glucose absorption is mediated by the glucose-induced recruitment of GLUT2 to the brush-border membrane. *Biochem. J.* 350 Pt 1:155–62.

- Kimura, A., S. Mora, S. Shigematsu, J.E. Pessin, and A.R. Saltiel. 2002. The insulin receptor catalyzes the tyrosine phosphorylation of caveolin-1. *J. Biol. Chem.* 277:30153–8. doi:10.1074/jbc.M203375200.
- Knutson, V.P., G. V Ronnett, and M.D. Lane. 1982. Control . of insulin receptor level in 3T3 cells : Effect of insulin- induced down-regulation and dexamethasone-induced up-regulation on rate of receptor inactivation *Biochemistry* : 79:2822–2826.
- Kokkola, T., C. Kruse, E.-M. Roy-Pogodzik, J. Pekkinen, C. Bauch, H.-H. Hönck, H. Hennemann, and H.-J. Kreienkamp. 2011. Somatostatin receptor 5 is palmitoylated by the interacting ZDHHC5 palmitoyltransferase. *FEBS Lett.* 585:2665–70. doi:10.1016/j.febslet.2011.07.028.
- Kurzchalia, T. V, P. Dupree, R.G. Parton, R. Kellner, H. Virta, M. Lehnert, and K. Simons. 1992. VIP21, a 21-kD membrane protein is an integral component of trans-Golgi-network-derived transport vesicles. *J. Cell Biol.* 118:1003–14.
- Laemmli, U.K. 1970. Cleavage of structural proteins during the assembly of the head of bacteriophage T4. *Nature.* 227:680–685.
- Lahtinen, U., M. Honsho, R.G. Parton, K. Simons, and P. Verkade. 2003. Involvement of caveolin-2 in caveolar biogenesis in MDCK cells. *FEBS Lett.* 538:85–88. doi:10.1016/S0014-5793(03)00135-2.
- Lajoie, P., and I.R. Nabi. 2010. Lipid rafts, caveolae, and their endocytosis. *Int. Rev. Cell Mol. Biol.* 282:135–63. doi:10.1016/S1937-6448(10)82003-9.
- Lampson, M.A., J. Schmoranzler, A. Zeigerer, S.M. Simon, and T.E. McGraw. 2001. Insulin-regulated Release from the Endosomal Recycling Compartment Is Regulated by Budding of Specialized Vesicles. *Mol. Biol. Cell.* 12:3489–3501.
- Lederkremer, G.Z., Y. Cheng, B.M. Petre, E. Vogan, S. Springer, R. Schekman, T. Walz, and T. Kirchhausen. 2001. Structure of the Sec23p/24p and Sec13p/31p complexes of COPII. *Proc. Natl. Acad. Sci. U. S. A.* 98:10704–9. doi:10.1073/pnas.191359398.
- Lee, H., D.S. Park, X.B. Wang, P.E. Scherer, P.E. Schwartz, and M.P. Lisanti. 2002. Src-induced phosphorylation of caveolin-2 on tyrosine 19. Phospho-caveolin-2 (Tyr(P)19) is localized near focal adhesions, remains associated with lipid rafts/caveolae, but no longer forms a high molecular mass hetero-oligomer with caveolin-1. *J. Biol. Chem.* 277:34556–67. doi:10.1074/jbc.M204367200.
- Lemonidis, K., O.A. Gorleku, M.C. Sanchez-Perez, C. Grefen, and L.H. Chamberlain. 2014. The Golgi S-acylation machinery is comprised of zDHHC enzymes with

- major differences in substrate affinity and S-acylation activity. *Mol. Biol. Cell*. doi:10.1091/mbc.E14-06-1169.
- Leto, D., and A.R. Saltiel. 2012. Regulation of glucose transport by insulin: traffic control of GLUT4. *Nat Rev Mol Cell Biol*. 13:383–396. doi:10.1038/nrm3351 nrm3351 [pii].
- Letourneur, F., E.C. Gaynor, S. Hennecke, C. Demolliere, R. Duden, S.D. Emr, H. Riezman, and P. Cosson. 1994. Coatamer is essential for retrieval of dilysine-tagged proteins to the endoplasmic reticulum. *Cell*. 79:1199–1207.
- Levental, I., D. Lingwood, M. Grzybek, U. Coskun, and K. Simons. 2010. Palmitoylation regulates raft affinity for the majority of integral raft proteins. *Proc. Natl. Acad. Sci. U. S. A.* 107:22050–4. doi:10.1073/pnas.1016184107.
- Levine, R. 1981. Insulin action: 1948-80. *Diabetes Care*. 4:38–44.
- Li, J., A. Mahajan, and M. Tsai. 2006. Ankyrin Repeat : A Unique Motif Mediating Protein - Protein Interactions †. 15168–15178.
- Li, W.P., P. Liu, B.K. Pilcher, and R.G. Anderson. 2001. Cell-specific targeting of caveolin-1 to caveolae, secretory vesicles, cytoplasm or mitochondria. *J. Cell Sci*. 114:1397–408.
- Lin, R.C., and R.H. Scheller. 2000. Mechanisms of synaptic vesicle exocytosis. *Annu. Rev. Cell Dev. Biol*. 16:19–49. doi:10.1146/annurev.cellbio.16.1.19.
- Linder, M., F. Tamanoi, and D.S. Sigman. 2000. The Enzymes, 3rd ed, Volume XXII: Protein Lipidation. Academic Press.
- Linder, M.E., and R.J. Deschenes. 2007. Palmitoylation: policing protein stability and traffic. *Nat Rev Mol Cell Biol*. 8:74–84. doi:nrm2084 [pii] 10.1038/nrm2084.
- Lisanti, M.P., P.E. Scherer, Z. Tang, and M. Sargiacomo. 1994. Caveolae, caveolin and caveolin-rich membrane domains: a signalling hypothesis. *Trends Cell Biol*. 4:231–235. doi:10.1016/0962-8924(94)90114-7.
- Liu, J., A. Kimura, C.A. Baumann, and A.R. Saltiel. 2002. APS facilitates c-Cbl tyrosine phosphorylation and GLUT4 translocation in response to insulin in 3T3-L1 adipocytes. *Mol. Cell. Biol*. 22:3599–609.
- Liu, J., P. Oh, T. Horner, R.A. Rogers, and J.E. Schnitzer. 1997. Organized Endothelial Cell Surface Signal Transduction in Caveolae Distinct from Glycosylphosphatidylinositol-anchored Protein Microdomains. *J. Biol. Chem*. 272:7211–7222. doi:10.1074/jbc.272.11.7211.

- Liu, L., D. Brown, M. McKee, N.K. Lebrasseur, D. Yang, K.H. Albrecht, K. Ravid, and P.F. Pilch. 2008. Deletion of Cavin/PTRF causes global loss of caveolae, dyslipidemia, and glucose intolerance. *Cell Metab.* 8:310–7. doi:10.1016/j.cmet.2008.07.008.
- Liu, L., and P.F. Pilch. 2008. A critical role of cavin (polymerase I and transcript release factor) in caveolae formation and organization. *J. Biol. Chem.* 283:4314–22. doi:10.1074/jbc.M707890200.
- Liu, M.L., A.L. Olson, W.S. Moye-Rowley, J.B. Buse, G.I. Bell, and J.E. Pessin. 1992. Expression and regulation of the human GLUT4/muscle-fat facilitative glucose transporter gene in transgenic mice. *J Biol Chem.* 267:11673–11676.
- Livak, K.J., and T.D. Schmittgen. 2001. Analysis of relative gene expression data using real-time quantitative PCR and the 2(-Delta Delta C(T)) Method. *Methods.* 25:402–8. doi:10.1006/meth.2001.1262.
- Lobo, S., W.K. Greentree, M.E. Linder, and R.J. Deschenes. 2002. Identification of a Ras palmitoyltransferase in *Saccharomyces cerevisiae*. *J. Biol. Chem.* 277:41268–73. doi:10.1074/jbc.M206573200.
- Lodish, H., A. Berk, C.A. Kaiser, M. Krieger, M.P. Scott, A. Bretscher, H. Ploegh, and P. Matsudaira. 2007. Purification of Cells and Their Parts. *In* Molecular Cell Biology. 6th edition. W. H. Freeman. 392–394.
- Lodish, H., A. Berk, S.L. Zipursky, P. Matsudaira, D. Baltimore, and J. Darnell. 2000. Protein Glycosylation in the ER and Golgi Complex. W. H. Freeman.
- London, E., and D. a Brown. 2000. Insolubility of lipids in triton X-100: physical origin and relationship to sphingolipid/cholesterol membrane domains (rafts). *Biochim. Biophys. Acta.* 1508:182–95.
- Lopez, J.A., J.G. Burchfield, D.H. Blair, K. Mele, Y. Ng, P. Vallotton, D.E. James, and W.E. Hughes. 2009. Identification of a distal GLUT4 trafficking event controlled by actin polymerization. *Mol. Biol. Cell.* 20:3918–3929. doi:E09-03-0187 [pii] 10.1091/mbc.E09-03-0187.
- Lugari, R., A. Dei Cas, D. Ugolotti, L. Finardi, A.L. Barilli, C. Ognibene, A. Luciani, R. Zandomenighi, and A. Gnudi. 2002. Evidence for early impairment of glucagon-like peptide 1-induced insulin secretion in human type 2 (non insulin-dependent) diabetes. *Horm. Metab. Res.* 34:150–4. doi:10.1055/s-2002-23199.
- Madeira, V.M. 2012. Overview of mitochondrial bioenergetics. *Methods Mol Biol.* 810:1–6. doi:10.1007/978-1-61779-382-0_1.

- Magee, A.I., L. Gutierrez, I.A. McKay, C.J. Marshall, and A. Hall. 1987. Dynamic fatty acylation of p21N-ras. *EMBO J.* 6:3353–3357.
- Magee, A.I., and K. Siddle. 1988. Insulin and IGF-1 receptors contain covalently bound palmitic acid. *J Cell Biochem.* 37:347–357. doi:10.1002/jcb.240370403.
- Mahfouz, R., R. Khoury, A. Blachnio-Zabielska, S. Turban, N. Loiseau, C. Lipina, C. Stretton, O. Bourron, P. Ferré, F. Foufelle, H.S. Hundal, and E. Hajduch. 2014. Characterising the Inhibitory Actions of Ceramide upon Insulin Signaling in Different Skeletal Muscle Cell Models: A Mechanistic Insight. *PLoS One.* 9:e101865. doi:10.1371/journal.pone.0101865.
- Martin, B.R., and B.F. Cravatt. 2009. Large-scale profiling of protein palmitoylation in mammalian cells. 6:135–138. doi:10.1038/NMETH.1293.
- Martin, S., J. Tellam, C. Livingstone, J.W. Slot, G.W. Gould, and D.E. James. 1996. The glucose transporter (GLUT-4) and vesicle-associated membrane protein-2 (VAMP-2) are segregated from recycling endosomes in insulin-sensitive cells. *J. Cell Biol.* 134:625–35.
- Martinez-Arca, S., V.S. Lalioti, and I. V Sandoval. 2000. Intracellular targeting and retention of the glucose transporter GLUT4 by the perinuclear storage compartment involves distinct carboxyl-tail motifs. *J Cell Sci.* 113 (Pt 1:1705–1715.
- Mastick, C.C., R. Aebersold, and G.E. Lienhard. 1994. Characterization of a major protein in GLUT4 vesicles. Concentration in the vesicles and insulin-stimulated translocation to the plasma membrane. *J. Biol. Chem.* 269:6089–92.
- Matsuyama, T., R. Komatsu, M. Namba, N. Watanabe, H. Itoh, and S. Tarui. 1988. Glucagon-like peptide-1 (7-36 amide): a potent glucagonostatic and insulinotropic hormone. *Diabetes Res. Clin. Pract.* 5:281–4.
- McCormick, P.J., K. Dumaresq-Doiron, A.-S. Pluviose, V. Pichette, G. Tosato, and S. Lefrancois. 2008. Palmitoylation controls recycling in lysosomal sorting and trafficking. *Traffic.* 9:1984–97. doi:10.1111/j.1600-0854.2008.00814.x.
- McMahon, K.-A., H. Zajicek, W.-P. Li, M.J. Peyton, J.D. Minna, V.J. Hernandez, K. Luby-Phelps, and R.G.W. Anderson. 2009. SRBC/cavin-3 is a caveolin adapter protein that regulates caveolae function. *EMBO J.* 28:1001–15. doi:10.1038/emboj.2009.46.
- Meshulam, T., J.R. Simard, J. Wharton, J. a Hamilton, and P.F. Pilch. 2006. Role of caveolin-1 and cholesterol in transmembrane fatty acid movement. *Biochemistry.* 45:2882–93. doi:10.1021/bi051999b.

- Mettlen, M., T. Pucadyil, R. Ramachandran, and S.L. Schmid. 2009. Dissecting dynamin's role in clathrin-mediated endocytosis. *Biochem. Soc. Trans.* 37:1022–6. doi:10.1042/BST0371022.
- De Meyts, P. 2004. Insulin and its receptor: structure, function and evolution. *Bioessays.* 26:1351–62. doi:10.1002/bies.20151.
- De Meyts, P., and J. Whittaker. 2002. Structural biology of insulin and IGF1 receptors: implications for drug design. *Nat. Rev. Drug Discov.* 1:769–83. doi:10.1038/nrd917.
- Mîineea, C.P., H. Sano, S. Kane, E. Sano, M. Fukuda, J. Peränen, W.S. Lane, and G.E. Lienhard. 2005. AS160, the Akt substrate regulating GLUT4 translocation, has a functional Rab GTPase-activating protein domain. *Biochem. J.* 391:87–93. doi:10.1042/BJ20050887.
- Mineo, C., Y.S. Ying, C. Chapline, S. Jaken, and R.G. Anderson. 1998. Targeting of Protein Kinase Calpha to Caveolae. *J. Cell Biol.* 141:601–610. doi:10.1083/jcb.141.3.601.
- Mitchell, D. a, G. Mitchell, Y. Ling, C. Budde, and R.J. Deschenes. 2010. Mutational analysis of *Saccharomyces cerevisiae* Erf2 reveals a two-step reaction mechanism for protein palmitoylation by DHHC enzymes. *J. Biol. Chem.* 285:38104–14. doi:10.1074/jbc.M110.169102.
- Mitchell, D. a, A. Vasudevan, M.E. Linder, and R.J. Deschenes. 2006. Protein palmitoylation by a family of DHHC protein S-acyltransferases. *J. Lipid Res.* 47:1118–27. doi:10.1194/jlr.R600007-JLR200.
- Mobley, B.A. 1975. Sizes of components in frog skeletal muscle measured by methods of stereology. *J. Gen. Physiol.* 66:31–45. doi:10.1085/jgp.66.1.31.
- Moffett, S., L. Adam, H. Bonin, T.P. Loisel, M. Bouvier, and B. Mouillac. 1996. Palmitoylated cysteine 341 modulates phosphorylation of the beta2-adrenergic receptor by the cAMP-dependent protein kinase. *J. Biol. Chem.* 271:21490–7.
- Moffett, S., B. Mouillac, H. Bonin, and M. Bouvier. 1993. Altered phosphorylation and desensitization patterns of a human beta 2-adrenergic receptor lacking the palmitoylated Cys341. *EMBO J.* 12:349–356.
- Monier, S., D.J. Dietzen, W.R. Hastings, D.M. Lublin, and T. V Kurzchalia. 1996. Oligomerization of VIP21-caveolin in vitro is stabilized by long chain fatty acylation or cholesterol. *FEBS Lett.* 388:143–9.

- Monier, S., R.G. Parton, F. Vogel, J. Behlke, a Henske, and T. V Kurzchalia. 1995. VIP21-caveolin, a membrane protein constituent of the caveolar coat, oligomerizes in vivo and in vitro. *Mol. Biol. Cell.* 6:911–27.
- Montesano, R., J. Roth, A. Robert, and L. Orci. 1982. Non-coated membrane invaginations are involved in binding and internalization of cholera and tetanus toxins. *Nature.* 296:651–653. doi:10.1038/296651a0.
- Moore, C.X., and G.J. Cooper. 1991. Co-secretion of amylin and insulin from cultured islet beta-cells: modulation by nutrient secretagogues, islet hormones and hypoglycemic agents. *Biochem. Biophys. Res. Commun.* 179:1–9.
- Mora, R., V.L. Bonilha, A. Mamorstein, P.E. Scherer, D. Brown, M.P. Lisanti, and E. Rodriguez-Boulan. 1999. Caveolin-2 Localizes to the Golgi Complex but Redistributes to Plasma Membrane, Caveolae, and Rafts when Co-expressed with Caveolin-1. *J. Biol. Chem.* 274:25708–25717. doi:10.1074/jbc.274.36.25708.
- Morrow, I.C., S. Rea, S. Martin, I.A. Prior, R. Prohaska, J.F. Hancock, D.E. James, and R.G. Parton. 2002. Flotillin-1/reggie-2 traffics to surface raft domains via a novel golgi-independent pathway. Identification of a novel membrane targeting domain and a role for palmitoylation. *J. Biol. Chem.* 277:48834–41. doi:10.1074/jbc.M209082200.
- Mueckler, M., C. Caruso, S.A. Baldwin, M. Panico, I. Blench, H.R. Morris, W.J. Allard, G.E. Lienhard, and H.F. Lodish. 1985. Sequence and structure of a human glucose transporter. *Science (80-).* 229:941–945.
- Mueckler, M.M. 1992. The molecular biology of mammalian glucose transporters. *Curr Opin Nephrol Hypertens.* 1:12–20.
- Munro, S. 2003. Lipid rafts: elusive or illusive? *Cell.* 115:377–88.
- Murata, M., J. Peränen, R. Schreiner, F. Wieland, T. V Kurzchalia, and K. Simons. 1995. VIP21/caveolin is a cholesterol-binding protein. *Proc. Natl. Acad. Sci. U. S. A.* 92:10339–43.
- Nakayama, K. 1997. Furin: a mammalian subtilisin/Kex2p-like endoprotease involved in processing of a wide variety of precursor proteins. *Biochem. J.* 327 (Pt 3:625–35.
- Napolitano, L. 1963. the Differentiation of White Adipose Cells. an Electron Microscope Study. *J. Cell Biol.* 18:663–79.
- Neumann-Giesen, C., B. Falkenbach, P. Beicht, S. Claasen, G.L. Uers, N.-G. C, F. B, B. P, C. S, L. G, S. C, H. V, T. R, G. Lüers, C.A.O. Stuermer, V. Herzog, and R.

- Tikkanen. 2004. Membrane and raft association of reggie-1/flotillin-2: role of myristoylation, palmitoylation and oligomerization and induction of filopodia by overexpression. *Biochem. J.* 378:509–18. doi:10.1042/BJ20031100.
- Ng, Y., G. Ramm, J. a Lopez, and D.E. James. 2008. Rapid activation of Akt2 is sufficient to stimulate GLUT4 translocation in 3T3-L1 adipocytes. *Cell Metab.* 7:348–356. doi:10.1016/j.cmet.2008.02.008.
- Nilsson, L.H., and E. Hultman. 1974. Liver and muscle glycogen in man after glucose and fructose infusion. *Scand. J. Clin. Lab. Invest.* 33:5–10.
- O’Rahilly, S., I. Barroso, and N.J. Wareham. 2005. Genetic factors in type 2 diabetes: the end of the beginning? *Science.* 307:370–3. doi:10.1126/science.1104346.
- Ohno, Y., A. Kihara, T. Sano, and Y. Igarashi. 2006. Intracellular localization and tissue-specific distribution of human and yeast DHHC cysteine-rich domain-containing proteins. *Biochim. Biophys. Acta.* 1761:474–83. doi:10.1016/j.bbali.2006.03.010.
- Oomura, Y., and H. Yoshimatsu. 1984. Neural network of glucose monitoring system. *J Aut. Nerv Syst.* 10:359–372.
- Palade, G.E. 1953. Fine structure of blood capillaries. *J Appl Phys.* 24:1224–1236. doi:10.1161/01.RES.27.3.482.
- Parat, M.O., and P.L. Fox. 2001. Palmitoylation of caveolin-1 in endothelial cells is post-translational but irreversible. *J Biol Chem.* 276:15776–15782. doi:10.1074/jbc.M006722200 M006722200 [pii].
- Pardridge, W.M., R.J. Boado, and C.R. Farrell. 1990. Brain-type glucose transporter (GLUT-1) is selectively localized to the blood-brain barrier. Studies with quantitative western blotting and in situ hybridization. *J Biol Chem.* 265:18035–18040.
- Parpal, S., M. Karlsson, H. Thorn, and P. Strålfors. 2001. Cholesterol depletion disrupts caveolae and insulin receptor signaling for metabolic control via insulin receptor substrate-1, but not for mitogen-activated protein kinase control. *J. Biol. Chem.* 276:9670–8. doi:10.1074/jbc.M007454200.
- Parton, R.G. 1997. Caveolin-3 Associates with Developing T-tubules during Muscle Differentiation. *J. Cell Biol.* 136:137–154. doi:10.1083/jcb.136.1.137.
- Parton, R.G., B. Joggerst, and K. Simons. 1994. Regulated internalization of caveolae. *J. Cell Biol.* 127:1199–215.

- Peck, G.R., S. Ye, V. Pham, R.N. Fernando, S.L. Macaulay, S.Y. Chai, and A.L. Albiston. 2006. Interaction of the Akt substrate, AS160, with the glucose transporter 4 vesicle marker protein, insulin-regulated aminopeptidase. *Mol. Endocrinol.* 20:2576–83. doi:10.1210/me.2005-0476.
- Peer, W., A. Murphy, and B. Schulz. 2011. *The Plant Plasma Membrane*. 19. A.S. Murphy, B. Schulz, and W. Peer, editors. Springer Berlin Heidelberg, Berlin, Heidelberg.
- Pei, H., Y. Yao, Y. Yang, K. Liao, and J.-R. Wu. 2011. Krüppel-like factor KLF9 regulates PPAR γ transactivation at the middle stage of adipogenesis. *Cell Death Differ.* 18:315–27. doi:10.1038/cdd.2010.100.
- Pelkmans, L., and M. Zerial. 2005. Kinase-regulated quantal assemblies and kiss-and-run recycling of caveolae. *Nature.* 436:128–33. doi:10.1038/nature03866.
- Pol, A., S. Martin, M.A. Ferna, M. Ingelmo-torres, C. Ferguson, C. Enrich, and R.G. Parton. 2005. Cholesterol and Fatty Acids Regulate Dynamic Caveolin Cell Surface and Lipid Bodies \square . 16:2091–2105. doi:10.1091/mbc.E04.
- Ponnambalam, S., and S.A. Baldwin. 2003. Constitutive protein secretion from the trans-Golgi network to the plasma membrane. *Mol. Membr. Biol.* 20:129–39. doi:10.1080/0968768031000084172.
- Prescott, G.R., O. a Gorleku, J. Greaves, and L.H. Chamberlain. 2009. Palmitoylation of the synaptic vesicle fusion machinery. *J. Neurochem.* 110:1135–49. doi:10.1111/j.1471-4159.2009.06205.x.
- Prior, I., A. Harding, J. Yan, and J. Sluimer. 2001. GTP-dependent segregation of H-ras from lipid rafts is required for biological activity. *Nat. Cell* 3:368 – 375.
- Randle, P.J., P.B. Garland, C.N. Hales, and E.A. Newsholme. 1963. THE GLUCOSE FATTY-ACID CYCLE ITS ROLE IN INSULIN SENSITIVITY AND THE METABOLIC DISTURBANCES OF DIABETES MELLITUS. *Lancet.* 281:785–789. doi:10.1016/S0140-6736(63)91500-9.
- Razani, B., T.P. Combs, X.B. Wang, P.G. Frank, D.S. Park, R.G. Russell, M. Li, B. Tang, L.A. Jelicks, P.E. Scherer, and M.P. Lisanti. 2002a. Caveolin-1-deficient mice are lean, resistant to diet-induced obesity, and show hypertriglyceridemia with adipocyte abnormalities. *J. Biol. Chem.* 277:8635–47. doi:10.1074/jbc.M110970200.
- Razani, B., X.B. Wang, J.A. Engelman, G. Lagaud, X.L. Zhang, B. Kneitz, H.H. Jr, G.J. Christ, W. Edelmann, M.P. Lisanti, M. Battista, and H. Hou. 2002b. Caveolin-2-Deficient Mice Show Evidence of Severe Pulmonary Dysfunction without Disruption of Caveolae Caveolin-2-Deficient Mice Show Evidence of Severe

Pulmonary Dysfunction without Disruption of Caveolae.
doi:10.1128/MCB.22.7.2329.

- Razani, B., S.E. Woodman, and M.P. Lisanti. 2002c. Caveolae: from cell biology to animal physiology. *Pharmacol. Rev.* 54:431–67.
- Reaven, G.M., C. Hollenbeck, C.Y. Jeng, M.S. Wu, and Y.D. Chen. 1988. Measurement of plasma glucose, free fatty acid, lactate, and insulin for 24 h in patients with NIDDM. *Diabetes.* 37:1020–4.
- Ren, J., L. Wen, X. Gao, C. Jin, Y. Xue, and X. Yao. 2008. CSS-Palm 2.0: an updated software for palmitoylation sites prediction. *Protein Eng. Des. Sel.* 21:639–44. doi:10.1093/protein/gzn039.
- Ren, W., Y. Sun, and K. Du. 2013a. DHHC17 palmitoylates ClipR-59 and modulates ClipR-59 association with the plasma membrane. *Mol. Cell. Biol.* 33:4255–65. doi:10.1128/MCB.00527-13.
- Ren, W., J.S. Ulupi, and K. Du. 2013b. Proteomic analysis of protein palmitoylation in adipocytes. *Adipocyte.* 2:17–28.
- Rice, L.M., and A.T. Brunger. 1999. Crystal structure of the vesicular transport protein Sec17: implications for SNAP function in SNARE complex disassembly. *Mol Cell.* 4:85–95.
- Rickman, C., and R.R. Duncan. 2010. Munc18/Syntaxin interaction kinetics control secretory vesicle dynamics. *J Biol Chem.* 285:3965–3972. doi:M109.040402 [pii] 10.1074/jbc.M109.040402.
- Roberts, M.J., M.D. Bentley, and J.M. Harris. 2002. Chemistry for peptide and protein PEGylation. *Adv. Drug Deliv. Rev.* 54:459–76.
- Rocks, O., M. Gerauer, N. Vartak, S. Koch, Z.-P. Huang, M. Pechlivanis, J. Kuhlmann, L. Brunsveld, A. Chandra, B. Ellinger, H. Waldmann, and P.I.H. Bastiaens. 2010. The palmitoylation machinery is a spatially organizing system for peripheral membrane proteins. *Cell.* 141:458–71. doi:10.1016/j.cell.2010.04.007.
- Rocks, O., A. Peyker, M. Kahms, P.J. Verveer, C. Koerner, M. Lumbierres, J. Kuhlmann, H. Waldmann, A. Wittinghofer, and P.I.H. Bastiaens. 2005. An acylation cycle regulates localization and activity of palmitoylated Ras isoforms. *Science.* 307:1746–52. doi:10.1126/science.1105654.
- Rogi, T., M. Tsujimoto, H. Nakazato, S. Mizutani, and Y. Tomoda. 1996. Human placental leucine aminopeptidase/oxytocinase. A new member of type II membrane-spanning zinc metallopeptidase family. *J. Biol. Chem.* 271:56–61.

- Ronnett, G., V. Knutson, and M. Lane. 1982. Insulin-induced down-regulation of insulin receptors in 3T3-L1 adipocytes. Altered rate of receptor inactivation. *J. Biol. Chem.* 257:4285–4291.
- Ros-Baro, A., C. Lopez-Iglesias, S. Peiro, D. Bellido, M. Palacin, A. Zorzano, and M. Camps. 2001. Lipid rafts are required for GLUT4 internalization in adipose cells. *Proc. Natl. Acad. Sci. U. S. A.* 98:12050–5. doi:10.1073/pnas.211341698.
- Ross, S. a, J.J. Herbst, S.R. Keller, and G.E. Lienhard. 1997. Trafficking kinetics of the insulin-regulated membrane aminopeptidase in 3T3-L1 adipocytes. *Biochem. Biophys. Res. Commun.* 239:247–51. doi:10.1006/bbrc.1997.7459.
- Ross, S.A., S.R. Keller, and G.E. Lienhard. 1998. Increased intracellular sequestration of the insulin-regulated aminopeptidase upon differentiation of 3T3-L1 cells. *Biochem. J.* 330 (Pt 2:1003–8.
- Roth, A.F., Y. Feng, L. Chen, and N.G. Davis. 2002. The yeast DHHC cysteine-rich domain protein Akr1p is a palmitoyl transferase. *J. Cell Biol.* 159:23–8. doi:10.1083/jcb.200206120.
- Roth, A.F., J. Wan, A.O. Bailey, B. Sun, J.A. Kuchar, N. Green, B.S. Phinney, J.R.Y. Iii, and N.G. Davis. 2006. Global Analysis of Protein Palmitoylation in Yeast. *Cell.* 125:1003–1013.
- Rothberg, K.G., J.E. Heuser, W.C. Donzell, Y.S. Ying, J.R. Glenney, and R.G. Anderson. 1992. Caveolin, a protein component of caveolae membrane coats. *Cell.* 68:673–82.
- Russell, T.R., and R. Ho. 1976. Conversion of 3T3 fibroblasts into adipose cells: triggering of differentiation by prostaglandin F₂alpha and 1-methyl-3-isobutyl xanthine. *Proc Natl Acad Sci U S A.* 73:4516–4520.
- Ryle, A.P., F. Sanger, L.F. Smith, and R. Kitai. 1955. The disulphide bonds of insulin. *Biochem. J.* 60:541–56.
- Sakamoto, K., and G.D. Holman. 2008. Emerging role for AS160/TBC1D4 and TBC1D1 in the regulation of GLUT4 traffic. *Am J Physiol Endocrinol Metab.* 295:E29–37. doi:10.1152/ajpendo.90331.2008.
- Salaun, C., J. Greaves, and L.H. Chamberlain. 2010. The intracellular dynamic of protein palmitoylation. *J Cell Biol.* 191:1229–1238. doi:jcb.201008160 [pii] 10.1083/jcb.201008160.
- Saltiel, A.R., and C.R. Kahn. 2001. glucose and lipid metabolism. 414:799–806.

- Saltiel, A.R., and J.E. Pessin. 2002. Insulin signaling pathways in time and space. *Trends Cell Biol.* 12:65–71. doi:S0962892401022073 [pii].
- Salzer, U. 2001. Stomatin, flotillin-1, and flotillin-2 are major integral proteins of erythrocyte lipid rafts. *Blood.* 97:1141–1143. doi:10.1182/blood.V97.4.1141.
- Sambrook, J., E.F. Fritsch, and T. Maniatis. 1989. Molecular cloning: a laboratory manual.
- Sansom, M., L.A. Szarka, M. Camilleri, A. Vella, A.R. Zinsmeister, and R.A. Rizza. 2000. Pramlintide, an amylin analog, selectively delays gastric emptying: potential role of vagal inhibition. *Am. J. Physiol. Gastrointest. Liver Physiol.* 278:G946–51.
- Sarbassov, D.D., D.A. Guertin, S.M. Ali, and D.M. Sabatini. 2005. Phosphorylation and regulation of Akt/PKB by the rictor-mTOR complex. *Science.* 307:1098–101. doi:10.1126/science.1106148.
- Sargiacomo, M., P.E. Scherer, Z. Tang, E. Kübler, K.S. Song, M.C. Sanders, and M.P. Lisanti. 1995. Oligomeric structure of caveolin: implications for caveolae membrane organization. *Proc. Natl. Acad. Sci. U. S. A.* 92:9407–11.
- Sbodio, J.I., and N.-W. Chi. 2002. Identification of a tankyrase-binding motif shared by IRAP, TAB182, and human TRF1 but not mouse TRF1. NuMA contains this RXXPDG motif and is a novel tankyrase partner. *J. Biol. Chem.* 277:31887–92. doi:10.1074/jbc.M203916200.
- Scheiffele, P., P. Verkade, A.M. Fra, H. Virta, K. Simons, and E. Ikonen. 1998. Caveolin-1 and -2 in the exocytic pathway of MDCK cells. *J. Cell Biol.* 140:795–806.
- Scherer, P.E., R.Y. Lewis, D. Volonte, J. a. Engelman, F. Galbiati, J. Couet, D.S. Kohtz, E. van Donselaar, P. Peters, and M.P. Lisanti. 1997. Cell-type and Tissue-specific Expression of Caveolin-2: CAVEOLINS 1 AND 2 CO-LOCALIZE AND FORM A STABLE HETERO-OLIGOMERIC COMPLEX IN VIVO. *J. Biol. Chem.* 272:29337–29346. doi:10.1074/jbc.272.46.29337.
- Scherer, P.E., M.P. Lisanti, G. Baldini, M. Sargiacomo, C.C. Mastick, and H.F. Lodish. 1994. Induction of caveolin during adipogenesis and association of GLUT4 with caveolin-rich vesicles. *J. Cell Biol.* 127:1233–43.
- Scherer, P.E., T. Okamoto, M. Chun, I. Nishimoto, H.F. Lodish, and M.P. Lisanti. 1996. Identification, sequence, and expression of caveolin-2 defines a caveolin gene family. *Proc. Natl. Acad. Sci. U. S. A.* 93:131–5.

- Scherer, P.E., Z. Tang, M. Chun, M. Sargiacomo, H.F. Lodish, and M.P. Lisanti. 1995. Caveolin isoforms differ in their N-terminal protein sequence and subcellular distribution. Identification and epitope mapping of an isoform-specific monoclonal antibody probe. *J. Biol. Chem.* 270:16395–16401. doi:10.1074/jbc.270.27.16395.
- Schlegel, a, and M.P. Lisanti. 2000. A molecular dissection of caveolin-1 membrane attachment and oligomerization. Two separate regions of the caveolin-1 C-terminal domain mediate membrane binding and oligomer/oligomer interactions in vivo. *J. Biol. Chem.* 275:21605–17. doi:10.1074/jbc.M002558200.
- Schloegl, H., R. Percik, A. Horstmann, A. Villringer, and M. Stumvoll. 2011. Peptide hormones regulating appetite--focus on neuroimaging studies in humans. *Diabetes. Metab. Res. Rev.* 27:104–12. doi:10.1002/dmrr.1154.
- Schnitzer, J.E. 2001. Caveolae: from basic trafficking mechanisms to targeting transcytosis for tissue-specific drug and gene delivery in vivo. *Adv. Drug Deliv. Rev.* 49:265–80.
- Seino, S., and G.I. Bell. 1989. Alternative splicing of human insulin receptor messenger RNA. *Biochem. Biophys. Res. Commun.* 159:312–6.
- Seino, S., M. Seino, S. Nishi, and G.I. Bell. 1989. Structure of the human insulin receptor gene and characterization of its promoter. *Proc. Natl. Acad. Sci. U. S. A.* 86:114–8.
- Seitz, R. 1996. Phosphorylation of Caveolin by Src Tyrosine Kinases. *J. Biol. Chem.* 271:3863–3868. doi:10.1074/jbc.271.7.3863.
- Shahinian, S., and J.R. Silvius. 1995. Doubly-lipid-modified protein sequence motifs exhibit long-lived anchorage to lipid bilayer membranes. *Biochemistry.* 34:3813–3822.
- Shengwen, L., F. Galbiati, D. Volonte, M. Sargiacomo, J.A. Engelman, K. Das, P.E. Scherer, M.P. Lisanti, and M.P. Lisanti. 1998. Mutational analysis of caveolin-induced vesicle formation. Expression of caveolin-1 recruits caveolin-2 to caveolae membranes. *FEBS Lett.* 434:127–34.
- Shi, J., G. Huang, and K. V Kandror. 2008. Self-assembly of Glut4 storage vesicles during differentiation of 3T3-L1 adipocytes. *J. Biol. Chem.* 283:30311–21. doi:10.1074/jbc.M805182200.
- Shi, J., and K. V Kandror. 2005. Sortilin is essential and sufficient for the formation of Glut4 storage vesicles in 3T3-L1 adipocytes. *Dev. Cell.* 9:99–108. doi:10.1016/j.devcel.2005.04.004.

- Shigematsu, S., S.L. Miller, and J.E. Pessin. 2001. Differentiated 3T3L1 adipocytes are composed of heterogenous cell populations with distinct receptor tyrosine kinase signaling properties. *J. Biol. Chem.* 276:15292–7. doi:10.1074/jbc.M009684200.
- Shigematsu, S., R.T. Watson, A.H. Khan, and J.E. Pessin. 2003. The adipocyte plasma membrane caveolin functional/structural organization is necessary for the efficient endocytosis of GLUT4. *J. Biol. Chem.* 278:10683–90. doi:10.1074/jbc.M208563200.
- Shulman, G.I. 2000. Cellular mechanisms of insulin resistance. *J. Clin. Invest.* 106:171–6. doi:10.1172/JCI10583.
- Simionescu, N., M. Simionescu, and G.E. Palade. 1975. Permeability of muscle capillaries to small heme-peptides. Evidence for the existence of patent transendothelial channels. *J. Cell Biol.* 64:586–607.
- Sinha, M.K., C. Raineri-Maldonado, C. Buchanan, W.J. Pories, C. Carter-Su, P.F. Pilch, and J.F. Caro. 1991. Adipose tissue glucose transporters in NIDDM. Decreased levels of muscle/fat isoform. *Diabetes.* 40:472–477.
- Song, K.S., P.E. Scherer, Z. Tang, T. Okamoto, S. Li, M. Chafel, C. Chu, D.S. Kohtz, and M.P. Lisanti. 1996. Expression of caveolin-3 in skeletal, cardiac, and smooth muscle cells: Caveolin-3 is a component of the sarcolemma and co-fractionates with dystrophin and dystrophin-associated glycoproteins. *J. Biol. Chem.* 271:15160–15165.
- Song, K.S., Z. Tang, S. Li, and M.P. Lisanti. 1997. Mutational Analysis of the Properties of Caveolin-1: A NOVEL ROLE FOR THE C-TERMINAL DOMAIN IN MEDIATING HOMO-TYPIC CAVEOLIN-CAVEOLIN INTERACTIONS. *J. Biol. Chem.* 272:4398–4403. doi:10.1074/jbc.272.7.4398.
- Sowa, G., M. Pypaert, D. Fulton, and W.C. Sessa. 2003. The phosphorylation of caveolin-2 on serines 23 and 36 modulates caveolin-1-dependent caveolae formation. *Proc. Natl. Acad. Sci. U. S. A.* 100:6511–6. doi:10.1073/pnas.1031672100.
- Stenbit, A.E., T.S. Tsao, J. Li, R. Burcelin, D.L. Geenen, S.M. Factor, K. Houseknecht, E.B. Katz, and M.J. Charron. 1997. GLUT4 heterozygous knockout mice develop muscle insulin resistance and diabetes. *Nat. Med.* 3:1096–101.
- Strålfors, P. 2012. Caveolins and caveolae, roles in insulin signalling and diabetes. *Adv. Exp. Med. Biol.* 729:111–26. doi:10.1007/978-1-4614-1222-9_8.
- Stuart, C.A., D. Yin, M.E. Howell, R.J. Dykes, J.J. Laffan, and A.A. Ferrando. 2006. Hexose transporter mRNAs for GLUT4, GLUT5, and GLUT12 predominate in

- human muscle. *Am J Physiol Endocrinol Metab.* 291:E1067–73. doi:00250.2006 [pii] 10.1152/ajpendo.00250.2006.
- Tang, Z., P.E. Scherer, T. Okamoto, K. Song, C. Chu, D.S. Kohtz, I. Nishimoto, H.F. Lodish, and M.P. Lisanti. 1996. Molecular Cloning of Caveolin-3, a Novel Member of the Caveolin Gene Family Expressed Predominantly in Muscle. *J. Biol. Chem.* 271:2255–2261. doi:10.1074/jbc.271.4.2255.
- Taylor, S.I. 1992. Lilly Lecture: Molecular Mechanisms of Insulin Resistance Lessons From Patients With Mutations in the Insulin-Receptor Gene. *Diabetes.* 41:1473–1490.
- Thoidis, G., and K. V. Kandror. 2001. A Glut4-Vesicle Marker Protein, Insulin-Responsive Aminopeptidase, is Localized in a Novel Vesicular Compartment in PC12 Cells. *Traffic.* 2:577–587. doi:10.1034/j.1600-0854.2001.20807.x.
- Thomson, M.J., M.G. Williams, and S.C. Frost. 1997. Development of Insulin Resistance in 3T3-L1 Adipocytes. *J. Biol. Chem.* 272:7759–7764. doi:10.1074/jbc.272.12.7759.
- Thorn, H., K.G. Stenkula, M. Karlsson, O. Unn, F.H. Nystrom, J. Gustavsson, and P. Strålfors. 2003. Cell Surface Orifices of Caveolae and Localization of Caveolin to the Necks of Caveolae in Adipocytes □. 14:3967–3976. doi:10.1091/mbc.E03.
- Tian, L., O. Jeffries, H. McClafferty, A. Molyvdas, I.C.M. Rowe, F. Saleem, L. Chen, J. Greaves, L.H. Chamberlain, H.-G. Knaus, P. Ruth, and M.J. Shipston. 2008. Palmitoylation gates phosphorylation-dependent regulation of BK potassium channels. *Proc. Natl. Acad. Sci. U. S. A.* 105:21006–11. doi:10.1073/pnas.0806700106.
- Tian, L., H. McClafferty, O. Jeffries, and M.J. Shipston. 2010. Multiple palmitoyltransferases are required for palmitoylation-dependent regulation of large conductance calcium- and voltage-activated potassium channels. *J Biol Chem.* 285:23954–23962. doi:M110.137802 [pii] 10.1074/jbc.M110.137802.
- Tiwari, S., V.K.M. Halagappa, S. Riaz, X. Hu, and C.A. Ecelbarger. 2007. Reduced expression of insulin receptors in the kidneys of insulin-resistant rats. *J. Am. Soc. Nephrol.* 18:2661–71. doi:10.1681/ASN.2006121410.
- Valdez-Taubas, J., and H. Pelham. 2005. Swf1-dependent palmitoylation of the SNARE Tlg1 prevents its ubiquitination and degradation. *EMBO J.* 24:2524–32. doi:10.1038/sj.emboj.7600724.
- Vanitallie, T.B., and T.H. Nufert. 1967. Ketones : Metabolism ' s Ugly Duckling. 61. doi:10.131/nr.2003.oct.327.

- Veit, M. 2000. Palmitoylation of the 25-kDa synaptosomal protein (SNAP-25) in vitro occurs in the absence of an enzyme, but is stimulated by binding to syntaxin. *Biochem. J.* 345 Pt 1:145–51.
- Veit, M., A. Becher, and G. Ahnert-Hilger. 2000. Synaptobrevin 2 is palmitoylated in synaptic vesicles prepared from adult, but not from embryonic brain. *Mol. Cell. Neurosci.* 15:408–16. doi:10.1006/mcne.1999.0830.
- Veit, M., K. Sachs, M. Heckelmann, D. Maretzki, K.P. Hofmann, and M.F. Schmidt. 1998. Palmitoylation of rhodopsin with S-protein acyltransferase: enzyme catalyzed reaction versus autocatalytic acylation. *Biochim. Biophys. Acta.* 1394:90–8.
- Veit, M., T.H. Söllner, and J.E. Rothman. 1996. Multiple palmitoylation of synaptotagmin and the t-SNARE SNAP-25. *FEBS Lett.* 385:119–23.
- Venkatesan, N., and M.B. Davidson. 1995. Insulin resistance in rats harboring growth hormone-secreting tumors: decreased receptor number but increased kinase activity in liver. *Metabolism.* 44:75–84.
- Verma, P., A.G. Ostermeyer-Fay, and D. a Brown. 2010. Caveolin-1 induces formation of membrane tubules that sense actomyosin tension and are inhibited by polymerase I and transcript release factor/cavin-1. *Mol. Biol. Cell.* 21:2226–40. doi:10.1091/mbc.E09-05-0417.
- Vinten, J., A.H. Johnsen, P. Roepstorff, J. Harpøth, and J. Tranum-Jensen. 2005. Identification of a major protein on the cytosolic face of caveolae. *Biochim. Biophys. Acta.* 1717:34–40. doi:10.1016/j.bbamem.2005.09.013.
- Vogel, K., and P.A. Roche. 1999. SNAP-23 and SNAP-25 are palmitoylated in vivo. *Biochem Biophys Res Commun.* 258:407–410. doi:S0006-291X(99)90652-6 [pii] 10.1006/bbrc.1999.0652.
- Wang, X.B., H. Lee, F. Capozza, S. Marmon, F. Sotgia, J.W. Brooks, R. Campos-Gonzalez, and M.P. Lisanti. 2004. Tyrosine phosphorylation of caveolin-2 at residue 27: differences in the spatial and temporal behavior of phospho-Cav-2 (pY19 and pY27). *Biochemistry.* 43:13694–706. doi:10.1021/bi049295+.
- Watanabe, M., H. Hayasaki, T. Tamayama, and M. Shimada. 1998. Histologic distribution of insulin and glucagon receptors. *Braz. J. Med. Biol. Res.* 31:243–56.
- Waters, S.B. 1997. The Amino Terminus of Insulin-responsive Aminopeptidase Causes Glut4 Translocation in 3T3-L1 Adipocytes. *J. Biol. Chem.* 272:23323–23327. doi:10.1074/jbc.272.37.23323.

- Watson, R.T., M. Furukawa, S.-H. Chiang, D. Boeglin, M. Kanzaki, A.R. Saltiel, and J.E. Pessin. 2003. The Exocytotic Trafficking of TC10 Occurs through both Classical and Nonclassical Secretory Transport Pathways in 3T3L1 Adipocytes. *Mol. Cell. Biol.* 23:961–974. doi:10.1128/MCB.23.3.961-974.2003.
- Watson, R.T., S. Shigematsu, S.H. Chiang, S. Mora, M. Kanzaki, I.G. Macara, A.R. Saltiel, and J.E. Pessin. 2001. Lipid raft microdomain compartmentalization of TC10 is required for insulin signaling and GLUT4 translocation. *J Cell Biol.* 154:829–840. doi:10.1083/jcb.200102078 jcb.200102078 [pii].
- Weir, G.C., S.D. Knowlton, and D.B. Martin. 1974. Glucagon secretion from the perfused rat pancreas. Studies with glucose and catecholamines. *J. Clin. Invest.* 54:1403–12. doi:10.1172/JCI107887.
- Wild, S., G. Roglic, A. Green, R. Sicree, and H. King. 2004. Global prevalence of diabetes: estimates for the year 2000 and projections for 2030. *Diabetes Care.* 27:1047–53.
- Wilden, P.A., C.R. Kahn, K. Siddle, and M.F. White. 1992. Insulin receptor kinase domain autophosphorylation regulates receptor enzymatic function. *J. Biol. Chem.* 267:16660–8.
- Wolven, A., H. Okamura, Y. Rosenblatt, and M.D. Resh. 1997. Palmitoylation of p59fyn is reversible and sufficient for plasma membrane association. *Mol. Biol. Cell.* 8:1159–73.
- Wood, I.S., L. Hunter, and P. Trayhurn. 2003. Expression of Class III facilitative glucose transporter genes (GLUT-10 and GLUT-12) in mouse and human adipose tissues. *Biochem Biophys Res Commun.* 308:43–49. doi:S0006291X03013226 [pii].
- Wu, Z., Y. Xie, R.F. Morrison, N.L.R. Bucher, and S.R. Farmer. 1998. PPARgamma induces the insulin-dependent glucose transporter GLUT4 in the absence of C/EBPalpha during the conversion of 3T3 fibroblasts into adipocytes. *J. Clin. Invest.* 101:22–32. doi:10.1172/JCI1244.
- Xie, X., Z. Gong, V. Mansuy-Aubert, Q.L. Zhou, S.A. Tatulian, D. Sehrt, F. Gnad, L.M. Brill, K. Motamedchaboki, Y. Chen, M.P. Czech, M. Mann, M. Krüger, and Z.Y. Jiang. 2011. C2 domain-containing phosphoprotein CDP138 regulates GLUT4 insertion into the plasma membrane. *Cell Metab.* 14:378–89. doi:10.1016/j.cmet.2011.06.015.
- Yamada, E. 1955. The fine structure of the gall bladder epithelium of the mouse. *J. Biophys. Biochem. Cytol.* 1:445–58.

- Yamada, E., S. Okada, T. Saito, K. Ohshima, M. Sato, T. Tsuchiya, Y. Uehara, H. Shimizu, and M. Mori. 2005. Akt2 phosphorylates Synip to regulate docking and fusion of GLUT4-containing vesicles. *J Cell Biol.* 168:921–928. doi:jcb.200408182 [pii] 10.1083/jcb.200408182.
- Yamamoto, M., Y. Toya, C. Schwencke, M.P. Lisanti, M.G. Myers, and Y. Ishikawa. 1998. Caveolin Is an Activator of Insulin Receptor Signaling. *J. Biol. Chem.* 273:26962–26968. doi:10.1074/jbc.273.41.26962.
- Yaney, G.C., and B.E. Corkey. 2003. Fatty acid metabolism and insulin secretion in pancreatic beta cells. *Diabetologia.* 46:1297–312. doi:10.1007/s00125-003-1207-4.
- Yeh, T.-Y.J., J.I. Sbdio, Z.-Y. Tsun, B. Luo, and N.-W. Chi. 2007. Insulin-stimulated exocytosis of GLUT4 is enhanced by IRAP and its partner tankyrase. *Biochem. J.* 402:279–90. doi:10.1042/BJ20060793.
- Yip, M.F., G. Ramm, M. Larance, K.L. Hoehn, M.C. Wagner, M. Guilhaus, and D.E. James. 2008. CaMKII-mediated phosphorylation of the myosin motor Myo1c is required for insulin-stimulated GLUT4 translocation in adipocytes. *Cell Metab.* 8:384–398. doi:S1550-4131(08)00296-9 [pii] 10.1016/j.cmet.2008.09.011.
- Yip, R.G., and M.M. Wolfe. 2000. GIP biology and fat metabolism. *Life Sci.* 66:91–103. doi:S0024320599003148 [pii].
- Yoshimasa, Y., S. Seino, J. Whittaker, T. Takechi, A. Kosaki, H. Kuzuya, H. Imura, G.I. Bell, D.F. Steiner, J.R. Napier, B. Mus, N. Hist, E.S. Vrba, J.T. Robinson, A.T. Mus, J. Whrrraker, and A. Kosaiu. 1988. Insulin-resistant diabetes due to a point mutation that prevents insulin proreceptor processing. *Science.* 240:784–7.
- Young, A. 1997. Amylin's physiology and its role in diabetes. *Curr. Opin. Endocrinol. Diabetes* 4.
- Yount, J.S., B. Moltedo, Y.-Y. Yang, G. Charron, T.M. Moran, C.B. López, and H.C. Hang. 2010. Palmitoylome profiling reveals S-palmitoylation-dependent antiviral activity of IFITM3. *Nat. Chem. Biol.* 6:610–4. doi:10.1038/nchembio.405.
- Yu, G.-Y., K.-J. Lee, L. Gao, and M.M.C. Lai. 2006. Palmitoylation and polymerization of hepatitis C virus NS4B protein. *J. Virol.* 80:6013–23. doi:10.1128/JVI.00053-06.
- Zaarour, N., M. Berenguer, Y. Le Marchand-Brustel, and R. Govers. 2012. Deciphering the role of GLUT4 N-glycosylation in adipocyte and muscle cell models. *Biochem. J.* 445:265–73. doi:10.1042/BJ20120232.

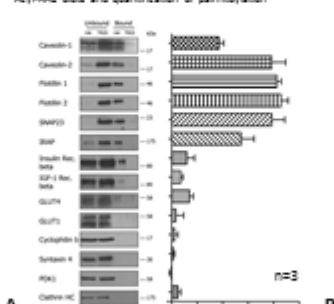
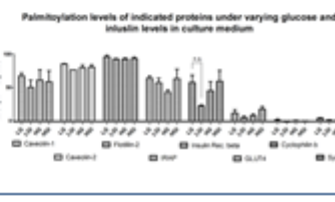
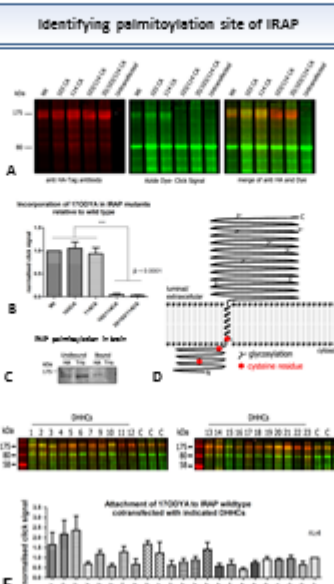
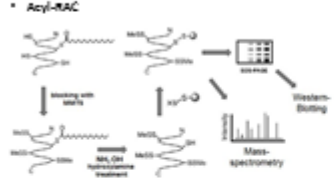
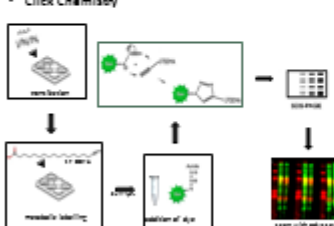
- Zeidman, R., C.S. Jackson, and A.I. Magee. 2009. Protein acyl thioesterases (Review). *Mol. Membr. Biol.* 26:32–41. doi:10.1080/09687680802629329.
- Zimmet, P., K.G.M.M. Alberti, and J. Shaw. 2001. Global and societal implications of the diabetes epidemic. *Nature*. 414:782–7. doi:10.1038/414782a.
- Zisman, A., O.D. Peroni, E.D. Abel, M.D. Michael, F. Mauvais-Jarvis, B.B. Lowell, J.F. Wojtaszewski, M.F. Hirshman, A. Virkamaki, L.J. Goodyear, C.R. Kahn, and B.B. Kahn. 2000. Targeted disruption of the glucose transporter 4 selectively in muscle causes insulin resistance and glucose intolerance. *Nat. Med.* 6:924–8. doi:10.1038/78693.

Appendix II

Investigating the Role of Palmitoylation in Insulin Action

Martin W. Werno and Luke H. Chamberlain

Strathclyde Institute of Pharmacy and Biomedical Sciences (SIPBS) 161 Cathedral Street, University of Strathclyde, Glasgow, G4 0RE, Scotland, UK

Introduction	Results																																										
<p>Insulin signaling and the trafficking of the facilitative glucose transporter GLUT4 are crucial components of glucose homeostasis, and defects in these processes are linked to insulin resistance, Type 2 Diabetes and obesity (1). Components of the Insulin signaling and GLUT4 trafficking pathways are regulated by post-translational modifications (PTMs), most notably phosphorylation. S-palmitoylation is an important reversible PTM involving the attachment of palmitate onto cysteine residues, and can regulate membrane binding, protein-protein interaction, protein stability and lipid raft partitioning. There is already some evidence that palmitoylation may play a role in the Insulin signaling cascade, as earlier studies have shown that key components of the signaling pathway (like the Shc family GTPase TC10), the Insulin receptor and the vesicle fusing proteins SNAP23 and CSP are palmitoylated (2,3,4,5). However, in general very little is known about how palmitoylation regulates components of the GLUT4 trafficking and Insulin pathways. In this study we are undertaking a more detailed analysis of palmitoylation in 3T3-L1 adipocytes with the aims of: (1) Identifying novel palmitoylated components of the Insulin signaling/GLUT4 trafficking pathway; (2) Investigating whether Insulin treatment alters palmitoylation levels; (3) Mapping and characterising palmitoylation sites of IRAP.</p>	<p>Screening for palmitoylated proteins</p>																																										
<p>Insulin induced GLUT4 trafficking</p> 	<p>Acyl-RAC blots and quantification of palmitoylation</p>  <p>Prediction of palmitoylation with GPS-Palm</p> <table border="1" data-bbox="1021 504 1356 806"> <thead> <tr> <th>Protein</th> <th>Protein Size</th> <th>GPS-Palm Score</th> <th>GPS-Palm Score</th> <th>GPS-Palm Score</th> <th>Example</th> </tr> </thead> <tbody> <tr> <td>Cavell-1</td> <td>142</td> <td>0.00000000</td> <td>0.000</td> <td>0.000</td> <td>Palmitoylated</td> </tr> <tr> <td>FcγR2</td> <td>132</td> <td>0.00000000</td> <td>0.000</td> <td>0.000</td> <td>Palmitoylated</td> </tr> <tr> <td>IRAP</td> <td>70</td> <td>0.00000000</td> <td>0.000</td> <td>0.000</td> <td>Palmitoylated</td> </tr> <tr> <td>Insulin Receptor</td> <td>132</td> <td>0.00000000</td> <td>0.000</td> <td>0.000</td> <td>Palmitoylated</td> </tr> <tr> <td>GLUT4</td> <td>132</td> <td>0.00000000</td> <td>0.000</td> <td>0.000</td> <td>Palmitoylated</td> </tr> <tr> <td>Synaptobrevin 2</td> <td>132</td> <td>0.00000000</td> <td>0.000</td> <td>0.000</td> <td>Palmitoylated</td> </tr> </tbody> </table> <p>Palmitoylation levels of indicated proteins under varying glucose and insulin levels in culture medium</p> 	Protein	Protein Size	GPS-Palm Score	GPS-Palm Score	GPS-Palm Score	Example	Cavell-1	142	0.00000000	0.000	0.000	Palmitoylated	FcγR2	132	0.00000000	0.000	0.000	Palmitoylated	IRAP	70	0.00000000	0.000	0.000	Palmitoylated	Insulin Receptor	132	0.00000000	0.000	0.000	Palmitoylated	GLUT4	132	0.00000000	0.000	0.000	Palmitoylated	Synaptobrevin 2	132	0.00000000	0.000	0.000	Palmitoylated
Protein	Protein Size	GPS-Palm Score	GPS-Palm Score	GPS-Palm Score	Example																																						
Cavell-1	142	0.00000000	0.000	0.000	Palmitoylated																																						
FcγR2	132	0.00000000	0.000	0.000	Palmitoylated																																						
IRAP	70	0.00000000	0.000	0.000	Palmitoylated																																						
Insulin Receptor	132	0.00000000	0.000	0.000	Palmitoylated																																						
GLUT4	132	0.00000000	0.000	0.000	Palmitoylated																																						
Synaptobrevin 2	132	0.00000000	0.000	0.000	Palmitoylated																																						
<p>Methods</p>	<p>Identifying palmitoylation site of IRAP</p> 																																										
<p>Acyl-RAC</p>  <p>Click Chemistry</p> 	<p>Conclusions</p> <ul style="list-style-type: none"> The method to capture palmitoylated proteins "acyl-RAC" has been applied successfully and novel palmitoylated proteins such as Cavell-1, GLUT4 and IRAP were identified. Importantly, this technique also allows an estimate of the extent of palmitoylation of these proteins. This revealed that the majority of SNAP23, cavellin and FcγR2 molecules were palmitoylated, whereas much smaller pools of the Insulin receptor and GLUT4 were modified. Insulin induced Insulin resistance and varying glucose concentration in cell culture medium do not alter the extent of palmitoylation of investigated proteins. Application of Click Chemistry with cells over-expressing cysteine to alanine mutants of IRAP revealed that the cysteine at position 103 and 114 are important for palmitoylation. Mutation of both cysteines to alanine resulted in a substantial loss of palmitoylation. Overexpression of IRAP and D4HGs show differential ability of D4HGs to palmitate IRAP with D4HG1, 2, 3, 10 and 15 having the highest ability. 																																										
<p>References</p> <ol style="list-style-type: none"> Boden, G. (2001) <i>Endocr Pract</i> 7(1): 44-51. Leto, D. and A. R. Saltiel (2012). <i>Nat Rev Mol Cell Biol</i> 13(3): 262-269. Watson, et al. (2001) <i>J Cell Biol</i> 154(4): 829-840. Vogel, K. and R. A. Roche (1999). <i>Biochem Biophys Res Commun</i> 258(2): 407-410. Magee, A. J. and K. Stele (1998). <i>J Cell Biochem</i> 71(4): 247-257. Fornace, M. T. et al. (2011). <i>J Lipid Res</i> 52(2): 292-299. 	<p>Acknowledgements</p> <p>We would like to thank Maria Sanchez-Perez for providing us with the expertise in the acyl-RAC. This work has been funded by a studentship award from Diabetes UK.</p>																																										

Appendix III

Investigating the Role of Palmitoylation in Insulin Action

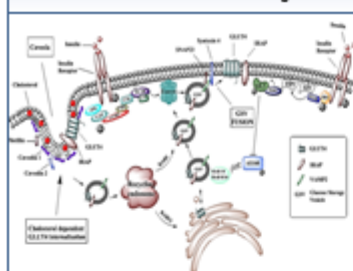
Martin W. Werno¹, Kimon Lemonidis¹, Heather McClafferty², Michael J. Shipston² and Luke H. Chamberlain¹

¹ Strathclyde Institute of Pharmacy and Biomedical Sciences (SIPBS) 161 Cathedral Street, University of Strathclyde, Glasgow, G4 0RE, Scotland, UK
² Centre for Integrative Physiology College of Medicine and Veterinary Medicine, University of Edinburgh, Edinburgh EH8 9XD, Scotland, UK

Introduction

Insulin signalling and the trafficking of the facilitative glucose transporter GLUT4 are crucial components of glucose homeostasis, and defects in these processes are linked to insulin resistance, Type 2 Diabetes and obesity (1). Components of the insulin signalling and GLUT4 trafficking pathways are regulated by post-translational modifications (PTMs), most notably phosphorylation. S-palmitoylation is an important reversible PTM involving the attachment of palmitate onto cysteine residues, and can regulate membrane binding, protein-protein interaction, protein stability and lipid raft partitioning. There is already some evidence that palmitoylation may play a role in the insulin signalling cascade, as earlier studies have shown that key components of the signalling pathway like the Rho family GTPase TC10, the Insulin receptor and the vesicle fusion protein SNAP25 are palmitoylated (2,3,4,5). However in general very little is known about how palmitoylation regulates components of the GLUT4 trafficking and insulin pathways. In this study we are undertaking a more detailed analysis of palmitoylation in 3T3-L1 adipocytes with the aim of: (i) identifying novel palmitoylated components of the insulin signalling/GLUT4 trafficking pathways; (ii) profiling the expression of DHHC palmitoyl transferase; and (iii) studying DHHC-substrate interactions.

Insulin induced GLUT4 trafficking



Methods

Acyl-RAC

Meting Based Split Ubiquitin System

The meting Based Split Ubiquitin System (mBSUS) is an assay to investigate protein-protein interaction and is based on the ubiquitin-degradation pathway in yeast (7). bait (3') and prey (5') proteins are fused to C-terminal and N-terminal part of ubiquitin, respectively. The Gal (10) - on the prey (Ugapanase mediated ubiquitin) and release the transcription reporter sample (YU (Practin-Ind-1712)). The interaction could be then measured on minimal media.

Quantitative real time PCR

Results

Screening for palmitoylated proteins

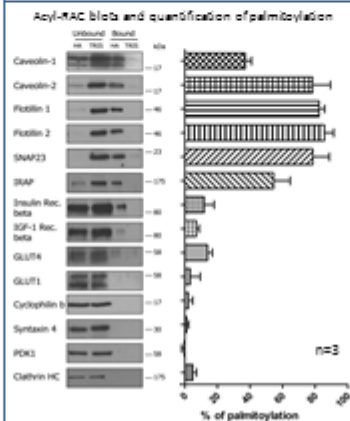


Figure 1. Acyl-RAC with 3T3-L1 adipocytes. Cells were seeded on day 10 post-differentiation. Insulin treatment was initiated on differential centrifugation and proteins were precipitated with acetone. Following a treatment with NEMO (1.25 μg/ml) the isolated proteins were incubated with either D-2 or hydrocortisone or D-2 in the presence of free thiol groups binding beads. Proteins were eluted from the beads using 1 μg/ml sample buffer with 10 mM DTT. The **left** image shows Western blots with indicated antibodies. The **right** image shows palmitoylation levels of indicated proteins measured by densitometry of the Western blots shown in the left figure.

Protein interaction with DHHCs

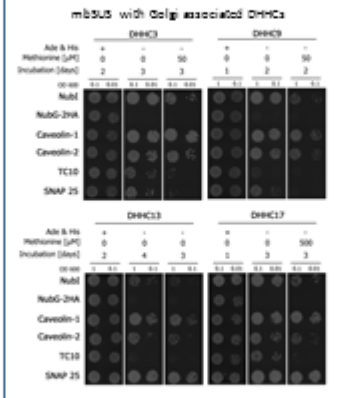


Figure 2. Meting Based Split Ubiquitin System with Golgi associated DHHCs. C-terminal ubiquitin (Cub) was fused with indicated DHHCs (Bait) and transformed into yeast strain TH1215. N-terminal ubiquitin (Nubi) was fused to prey proteins (Caveolin-1, Caveolin-2, TC10 and SNAP 25) and transformed into yeast strain TH1215. The transformed yeast strains were mated on yeast and after 48 hours in mating media. Subsequently 3 μl of mated strains were dropped onto plates with protein interaction selective media using different ubiquitin (Cub or Nubi). Growth on these plates indicate protein-protein interaction of bait/prey on prey protein. Methionine mBSUS expression of the bait and prey used as indicated. Yeast strains were incubated at 30°C for up to 2 days.

DHHC Expression profile in 3T3-L1 adipocytes

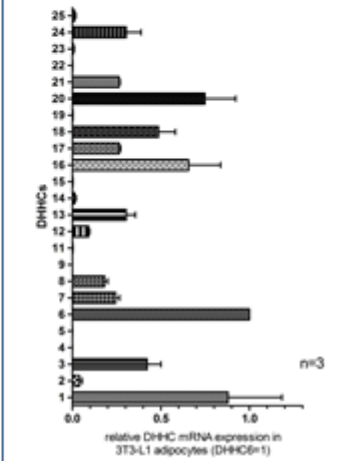


Figure 3. DHHC expression profile. 28kT Green Bead quantitative real-time PCR was performed using qPCR from 3T3-L1 adipocytes. PCRs were used to determine gene DHHC mRNA expression levels were normalized to DHHCβ.

Conclusions

- The method to capture palmitoylated proteins (Acyl-RAC) has been applied successfully and novel palmitoylated proteins such as Caveolin-2, GLUT4 and IRAP were identified. Importantly, this technique also allows an estimate of the extent of palmitoylation of these proteins. This revealed that the majority of SNAP25, caveolin in a not lot in molecules were palmitoylated, whereas much smaller pools of the Insulin receptor and GLUT4 were modified.
- Palmitoylated proteins involved in insulin signalling such as TC10, SNAP 25, Caveolin-1 and Caveolin-2 were shown to interact with Golgi localized DHHCs in the Golgi.
- Quantitative real-time PCR revealed the DHHC expression profile in 3T3-L1 adipocytes with the highest mRNA levels for DHHC 1, 2, 6, 16, 18, 20. The expression levels of DHHCs 7, 8, 12, 17, 21 and 24 were lower but still in a detectable range.

Acknowledgements

We would like to thank Maria Sanchez-Perez for providing us with the expertise in the acyl-RAC and Christopher Grafen who provided us with DNA constructs for mBSUS. This work has been funded by a studentship award from Diabetes UK.

References

- Soden, G. (2001) *Endocr Pract* 7(1): 44-51.
- Lehto, D. and A. R. Salonen (2012). *Nat Rev Mol Cell Biol* 13(5): 242-256.
- Watson, et al. (2001). *J Cell Biol* 154(4): 829-840.
- Vogel, K. and R. A. Roche (1999). *Glycochim Glycoprote Res Commun* 258(2): 407-410.
- Vilgase, A. J. and K. Sidde (1998). *J Cell Biochem* 71(4): 247-257.
- Fornatar, M. T. et al. (2011). *J Lipid Res* 52(2): 292-298.
- Grafen, C., R. Cordell, et al. (2009) *Methods Mol Biol* 479: 217-232.

Investigating the Role of Palmitoylation in Insulin Action

Martin Werno¹, Heather McClafferty², Michael J. Shipston² and Luke H. Chamberlain¹

¹Strathclyde Institute of Pharmacy and Biomedical Sciences (SIPBS) 161 Cathedral Street, University of Strathclyde, Glasgow, G4 0RE, Scotland, UK
²Centre for Integrative Physiology, College of Medicine and Veterinary Medicine, University of Edinburgh, Edinburgh EH8 9XD, Scotland, UK



Prediction of palmitoylation sites

Protein	Accession	Length (aa)	Palmitoylation sites
GLUT4	U01483	322	19
INSR	U01483	1100	10
SH2B1	U01483	1000	10
SH2B2	U01483	1000	10
SH2B3	U01483	1000	10
SH2B4	U01483	1000	10
SH2B5	U01483	1000	10
SH2B6	U01483	1000	10
SH2B7	U01483	1000	10
SH2B8	U01483	1000	10
SH2B9	U01483	1000	10
SH2B10	U01483	1000	10
SH2B11	U01483	1000	10
SH2B12	U01483	1000	10
SH2B13	U01483	1000	10
SH2B14	U01483	1000	10
SH2B15	U01483	1000	10
SH2B16	U01483	1000	10
SH2B17	U01483	1000	10
SH2B18	U01483	1000	10
SH2B19	U01483	1000	10
SH2B20	U01483	1000	10
SH2B21	U01483	1000	10
SH2B22	U01483	1000	10
SH2B23	U01483	1000	10
SH2B24	U01483	1000	10
SH2B25	U01483	1000	10
SH2B26	U01483	1000	10
SH2B27	U01483	1000	10
SH2B28	U01483	1000	10
SH2B29	U01483	1000	10
SH2B30	U01483	1000	10
SH2B31	U01483	1000	10
SH2B32	U01483	1000	10
SH2B33	U01483	1000	10
SH2B34	U01483	1000	10
SH2B35	U01483	1000	10
SH2B36	U01483	1000	10
SH2B37	U01483	1000	10
SH2B38	U01483	1000	10
SH2B39	U01483	1000	10
SH2B40	U01483	1000	10
SH2B41	U01483	1000	10
SH2B42	U01483	1000	10
SH2B43	U01483	1000	10
SH2B44	U01483	1000	10
SH2B45	U01483	1000	10
SH2B46	U01483	1000	10
SH2B47	U01483	1000	10
SH2B48	U01483	1000	10
SH2B49	U01483	1000	10
SH2B50	U01483	1000	10
SH2B51	U01483	1000	10
SH2B52	U01483	1000	10
SH2B53	U01483	1000	10
SH2B54	U01483	1000	10
SH2B55	U01483	1000	10
SH2B56	U01483	1000	10
SH2B57	U01483	1000	10
SH2B58	U01483	1000	10
SH2B59	U01483	1000	10
SH2B60	U01483	1000	10
SH2B61	U01483	1000	10
SH2B62	U01483	1000	10
SH2B63	U01483	1000	10
SH2B64	U01483	1000	10
SH2B65	U01483	1000	10
SH2B66	U01483	1000	10
SH2B67	U01483	1000	10
SH2B68	U01483	1000	10
SH2B69	U01483	1000	10
SH2B70	U01483	1000	10
SH2B71	U01483	1000	10
SH2B72	U01483	1000	10
SH2B73	U01483	1000	10
SH2B74	U01483	1000	10
SH2B75	U01483	1000	10
SH2B76	U01483	1000	10
SH2B77	U01483	1000	10
SH2B78	U01483	1000	10
SH2B79	U01483	1000	10
SH2B80	U01483	1000	10
SH2B81	U01483	1000	10
SH2B82	U01483	1000	10
SH2B83	U01483	1000	10
SH2B84	U01483	1000	10
SH2B85	U01483	1000	10
SH2B86	U01483	1000	10
SH2B87	U01483	1000	10
SH2B88	U01483	1000	10
SH2B89	U01483	1000	10
SH2B90	U01483	1000	10
SH2B91	U01483	1000	10
SH2B92	U01483	1000	10
SH2B93	U01483	1000	10
SH2B94	U01483	1000	10
SH2B95	U01483	1000	10
SH2B96	U01483	1000	10
SH2B97	U01483	1000	10
SH2B98	U01483	1000	10
SH2B99	U01483	1000	10
SH2B100	U01483	1000	10

Screening for palmitoylated proteins

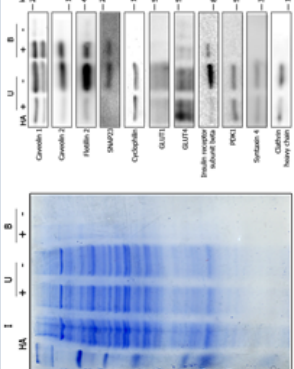


Figure 1. *Acyl-SH* with 370-413. *Acyl-SH* was isolated on day 10 post-differentiation medium. Membrane fraction was isolated by differential centrifugation and proteins were probed with antibodies following a treatment with NEMO (1, 10, 50, 100, 200, 400, 800, 1600, 3200, 6400, 12800, 25600, 51200, 102400, 204800, 409600, 819200, 1638400, 3276800, 6553600, 13107200, 26214400, 52428800, 104857600, 209715200, 419430400, 838860800, 1677721600, 3355443200, 6710886400, 13421772800, 26843545600, 53687091200, 107374182400, 214748364800, 429496729600, 858993459200, 1717986918400, 3435973836800, 6871947673600, 13743895347200, 27487790694400, 54975581388800, 109951162777600, 219902325555200, 439804651110400, 879609302220800, 1759218604441600, 3518437208883200, 7036874417766400, 14073748035532800, 28147496071065600, 56294992142131200, 112589984284262400, 225179968568524800, 450359937137049600, 900719874274099200, 1801439748548198400, 3602879497096396800, 7205758994192793600, 14411517988385587200, 28823035976771174400, 57646071953542348800, 115292143907084697600, 230584287814169395200, 461168575628338790400, 922337151256677580800, 1844674302513355161600, 3689348605026710323200, 7378697210053420646400, 14757394420106841292800, 29514788840213682585600, 59029577680427365171200, 118059155360854730342400, 236118310721709460684800, 472236621443418921369600, 944473242886837842739200, 1888946485773675685478400, 3777892971547351370956800, 7555785943094702741913600, 15111571886189404883827200, 30223143772378809767654400, 60446287544757619535308800, 120892575089515239070617600, 241785150179030478141235200, 483570300358060956282470400, 967140600716121912564940800, 1934281201432243825129881600, 3868562402864487650259763200, 7737124805728975300519526400, 1547424961145795060103952000, 3094849922291590120207904000, 6189699844583180240415808000, 12379399689166360480831616000, 24758799378332720961663232000, 49517598756665441923326464000, 99035197513330883846652928000, 198070395026661776933305856000, 396140790053323553866611712000, 792281580106647107733223424000, 1584563160213294215466446848000, 3169126320426588431692893792000, 6338252640853176863385787584000, 12676505281706353726771575168000, 25353010563412707453543150336000, 50706021126825414907086300672000, 101412042253650829814172601344000, 202824084507301659628345202688000, 405648169014603319256690405376000, 811296338029206638513380810752000, 1622592676058413277026761621504000, 3245185352116826554053523243008000, 6490370704233653108107046486016000, 12980741408467306216214092972032000, 25961482816934612432428185444064000, 51922965633869224864856370888128000, 103845931267738449729712741776256000, 207691862535476899459425483552512000, 415383725070953798918848867105024000, 830767450141907597837777734210048000, 1661534900283815195675555468420096000, 3323069800567630391351110936840192000, 6646139601135260782702221873680384000, 13292279202270521565404443747360768000, 26584558404541043130808887494721536000, 5316911680908208626161777498944288000, 10633823361816417252323554997888576000, 21267646723632834504647109955771552000, 42535293447265669009294219911543104000, 85070586894531338018588439823086208000, 170141173789062676037176879646172416000, 340282347578125352074353759292344832000, 680564695156250704148687518584689664000, 1361129390312501408297375037169379328000, 2722258780625002816594750074338746656000, 5444517561250005633189500148675133312000, 10889035122500011266378999297341466624000, 21778070245000022532757998594683332512000, 43556140490000045065515997189666664000, 87112280980000090131031994379333328000, 174224571960000180262061986758666656000, 348449143920000360524123373517333312000, 696898287840000721048246747024666624000, 139379657568000144209649349404933328000, 278759315136000288419298698809866656000, 557518630272000576838597397619733312000, 1115037260544001153677194795239466624000, 2230074521088002307354389590478933328000, 446014904217600461470877918095866656000, 892029808435200922941755836191733312000, 1784059616870401845883511712383466624000, 356811923374083691776702342476693328000, 713623846748167383553404684953366656000, 1427247693496334767106809369906733312000, 2854495386992669534213618739813466624000, 570899077398533906842723747962693328000, 1141798154797067813685447495925366656000, 2283596309594135637090894991850733312000, 4567192619188271274181789983701466624000, 913438523837654254836357996740293328000, 182687704767530850967271593348066656000, 365375409535061701934543186696133312000, 730750819070123403869086373392266624000, 1461501638140246807738172646784533328000, 292300327628049361547634529356906656000, 5846006552560987230952690587138133312000, 1169201310512197446190538117546266624000, 233840262102439489238107623109253328000, 4676805242048789784762152462185066656000, 935361048409757956952430492430133312000, 1870722096819515913904860984860266624000, 374144419363903182780972196972053328000, 7482888387278063655619443939441066656000, 14965776774556127311238887878882133312000, 29931553549112254622477775757764266624000, 5986310709822450844495555151552853328000, 1197262141964490168899111103030566656000, 2394524283928980337798222206061133312000, 4789048567857960675596444412122266624000, 957809713571592135119288882424453328000, 1915619427143184270238577744488866656000, 3831238854286368540477155488977733312000, 76624777085727370809543097797566624000, 153249551371454741619086195595133328000, 306499102742909483238172391190266656000, 612998205485818966476344782380533312000, 1225996410971637932952689564761066624000, 2451992821943275865905379129522133312000, 4903985643886551731810758259044266656000, 980797128777310346362151651808853328000, 1961594257554620692724303303617666656000, 392318851510924138544860660723533312000, 784637703021848277089721321447066624000, 1569275406043696554179542422894133312000, 3138550812087393108359084845788266656000, 6277101624174786216718169691576533328000, 12554203248349572433436339383551066656000, 2510840649669914486687267876710133312000, 5021681299339828973374535753420266624000, 1004336259867965794674907150684053328000, 2008672519735931589349814213768066656000, 4017345039471863178699628427536133312000, 8034690078943726357399256455072266624000, 1606938015788745271479851291014533328000, 3213876031577490542959702582029066656000, 6427752063154981085919405164058133312000, 128555041263099621718388102881176